

Annual progress report of the Department of Solid State Physics 1 January - 31 December 1994

Lindgård, Per-Anker; Bechgaard, Klaus; Clausen, Kurt Nørgaard; Feidenhans'l, Robert Krarup; Johannsen, Ib

Publication date:
1995

Document Version
Publisher's PDF, also known as Version of record

[Link back to DTU Orbit](#)

Citation (APA):
Lindgård, P-A., Bechgaard, K., Clausen, K. N., Feidenhans'l, R., & Johannsen, I. (1995). Annual progress report of the Department of Solid State Physics 1 January - 31 December 1994. (Denmark. Forskningscenter Risoe. Risoe-R; No. 779(EN)).

DTU Library

Technical Information Center of Denmark

General rights

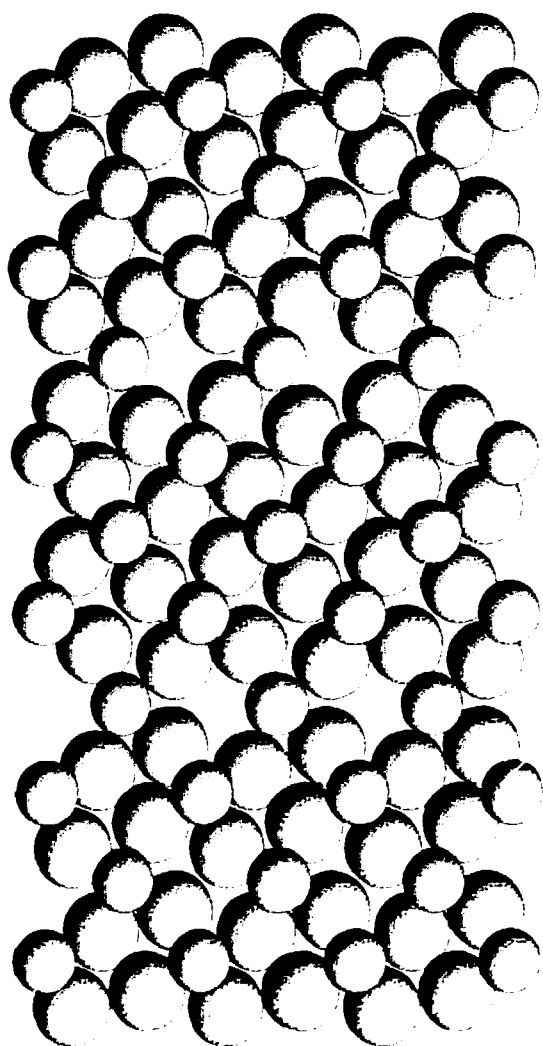
Copyright and moral rights for the publications made accessible in the public portal are retained by the authors and/or other copyright owners and it is a condition of accessing publications that users recognise and abide by the legal requirements associated with these rights.

- Users may download and print one copy of any publication from the public portal for the purpose of private study or research.
- You may not further distribute the material or use it for any profit-making activity or commercial gain
- You may freely distribute the URL identifying the publication in the public portal

If you believe that this document breaches copyright please contact us providing details, and we will remove access to the work immediately and investigate your claim.

Annual Progress Report of the Department of Solid State Physics 1 January – 31 December 1994

edited by P-A. Lindgård, K. Bechgaard, K.N. Clausen, R. Feidenhans'l,
and I. Johansen



Annual Progress Report of the Department of Solid State Physics 1 January – 31 December 1994

Risø-R-779(EN)

**edited by P.-A. Lindgård, K. Bechgaard, K.N. Clausen, R. Feidenhans'l,
and I. Johannsen**

**Risø National Laboratory, Roskilde, Denmark
January 1995**

Abstract Research in the department is concerned with "Materials with Distinct Physical and Chemical Properties". The principal activities of the department in the period from 1 January to 31 December, 1994, are presented in this Progress Report.

Neutron and x-ray diffraction techniques are used to study a wide variety of problems in condensed matter physics and include: two- and three-dimensional structures, magnetic ordering, heavy fermions, high T_c superconductivity, phase transitions in model systems, precipitation phenomena, and nano-scale structures in various materials. The research in chemistry includes chemical synthesis and physico-chemical investigation of small molecules and polymers, with emphasis on polymers with new optical properties, block copolymers, surface modified polymers, and supramolecular structures. Related to these problems there is work going on in theory, Monte Carlo simulations, and methods of data analysis.

This report contains unpublished results and should not be quoted without permission from the authors.

Frontpage illustration:
Reconstruction of a Ni(111) surface
due to sulphur add-atoms

ISBN 87-550-2026-7
ISSN 0106-2840
ISSN 0907-0249

Grafisk Service · Risø · 1995

Contents

1	Introduction	9
2	Research Projects in the Department	11
2.1	Theory, Monte Carlo Simulations, and Methods of Data Analysis	12
2.1.1	Classification of the Folding of Protein Polymers	12
2.1.2	Theory for a Degenerate Blume-Emery-Griffiths Model of an Entropy Stabilized Phase	13
2.1.3	Theory and Computer Simulation of Diffuse Scattering from Lattice Gas Models	14
2.1.4	Mean-field and Monte Carlo Calculations of the Three-Dimensional Structure Factor for $\text{YBa}_2\text{Cu}_3\text{O}_{6+x}$	15
2.1.5	Theory of the Transition Temperatures for Lattice Gas Models	16
2.1.6	Strain Effects in a Lattice-Gas Model	17
2.1.7	Effect of the Fermionic Degrees of Freedom on the Phase Diagram and the Structure Factor for $\text{YBa}_2\text{Cu}_3\text{O}_{6+x}$	18
2.1.8	Monte Carlo Simulation Studies of Semi-flexible Polymers with Excluded Volume Interactions	19
2.1.9	Relationship Between the Roton Minimum and T_λ in ^4He	20
2.1.10	Reverse Monte Carlo Analysis of Powder Patterns	21
2.1.11	Instrumental Smearing Effects in Radially Symmetric Small-Angle Neutron Scattering by Numerical and Analytical Methods	22
2.2	Magnetic Structures, Magnetic Phase Transitions, and Spin Dynamics	23
2.2.1	Nuclear Magnetic Ordering in ^{109}Ag	23
2.2.2	Magnetic Phase Diagram of MnSi	24
2.2.3	Commensurate-Commensurate Magnetic Phase Transitions in CeSb	25
2.2.4	Magnetic Structures of NdCu_2 in Finite Magnetic Fields	26
2.2.5	Absence of AF Reordering at Low Temperature in Pure $\text{YBa}_2\text{Cu}_3\text{O}_{6+x}$	27
2.2.6	High Pressure Neutron Diffraction Studies of the Magnetic Structures of Er	28
2.2.7	Trigonal Interactions in Holmium	29
2.2.8	The Magnetic Structure of Ho/Pr Alloys	30
2.2.9	The Magnetic Structure of Ho/Lu Superlattices and Alloys	31
2.2.10	Novel Magnetic Structures of Epitaxial Nd/Y Systems	32
2.2.11	Resonant X-Ray Magnetic Scattering from Ho/Pr Alloys	33
2.2.12	Structural and Magnetic Properties of $\text{Ni}_{1.3}\text{Fe}_{1.8}\text{O}_4$	34
2.2.13	Effect of Al Doping on the Magnetism of $\text{YBa}_2\text{Cu}_3\text{O}_{6+x}$ Single Crystals	35
2.2.14	Crystal Fields and Conduction Electrons in Pr	36
2.2.15	Energy-gap of Magnetic Fluctuations in UPd_2Al_3	37
2.2.16	Quadrupolar Order in UPd_3	38
2.2.17	Structural and Magnetic Small-Angle Neutron Scattering Study of $\text{Fe}_{90-x}\text{Zr}_{10+x}$ Amorphous Ribbons	39

2.3	Superconducting Materials and Phenomena	40
2.3.1	Random-Field Structural Transition in $\text{YBa}_2\text{Cu}_3\text{O}_{6+x}$	40
2.3.2	Observation of Ortho-III Correlations by Neutron and Hard X-Ray Diffraction in an Untwinned $\text{YBa}_2\text{Cu}_3\text{O}_{6.77}$ Single Crystal	41
2.3.3	Structural Phase Transitions in $\text{YBa}_2\text{Cu}_3\text{O}_{6.37}$ Studied by Hard X-ray Diffraction	42
2.3.4	Influence of Al Doping on the Structural Properties of Al Doped $\text{YBa}_2\text{Cu}_3\text{O}_{6+x}$ Single Crystals	43
2.3.5	Oxidation Kinetics of $\text{YBa}_2\text{Cu}_3\text{O}_{6+x}$ at Relatively Low Temperature	44
2.3.6	Investigations of the New $\text{RNi}_2\text{B}_2\text{C}$ (R = Rare Earth) Compounds	45
2.3.7	Structural and Physical Modifications Induced by Chemical Oxidation of the High- T_c Superconductor $\text{La}_{2-x}\text{Ba}_x\text{CuO}_4$ ($x = 0.115, 0.125, 0.135$)	46
2.3.8	Structural Study of $\text{LnBaCuFeO}_{5+\delta}$, (Ln = Y, Pr)	47
2.3.9	Flux Lattice in the Superconducting Phases of UPt_3	48
2.3.10	Small-Angle Neutron Scattering Studies of Pinned and Flowing Magnetic Flux Lattices in 2H-NbSe_2	49
2.3.11	Flux-Lattice in BSCCO-2212 Studied by Small-Angle Neutron Scattering	50
2.4	Structures and Defects	51
2.4.1	Critical Scattering from Rb_2ZnCl_4	51
2.4.2	Neutron Diffraction on Ternary Alkali - Metal Platinum Deuterides	52
2.4.3	Site Preferences for Deuterium in Zr_2NiD_x	53
2.4.4	Neutron Diffraction Investigation of the Atomic Defect Structure of Y-doped SrCeO_3	54
2.4.5	Neutron Powder Diffraction on the $\text{K}_2\text{S}_2\text{O}_7$ KHSO_4 System	55
2.4.6	Crystal Structure Refinement of RECoO_3 (RE = La, Pr and Tb)	56
2.4.7	Small-Angle Neutron Scattering on Al-3 at.% Ag	57
2.4.8	Precipitation in Supersaturated Solid Solution Thin Al(Ti) Films Studied by Small-Angle Neutron Scattering	58
2.5	Surfaces and Interfaces	59
2.5.1	Growth of Ag on Ni(111) Studied by X-Ray Diffraction	59
2.5.2	X-Ray Diffraction from Ag Clusters on Ni(110)	60
2.5.3	Preliminary Investigations of the Close-packed Pb Structures on Ge(111) by Surface X-Ray Diffraction	61
2.5.4	Hutclusters on the Ge(100) Surface Studied by Surface X-Ray Diffraction	62
2.5.5	X-Ray Diffraction from Incommensurate Surface Structures on In/Ge(111)	63
2.5.6	Atomic Structure of the $\text{Ge}(111)\sqrt{3} \times \sqrt{3}$ -Ag Surface	64
2.5.7	Surface X-Ray Diffraction Studies of the Ag and Na Induced $\text{Si}(111)3 \times 1$ Reconstructions	65
2.5.8	Relaxation Mechanism of Epitaxial Ge on Si(001) Studied by X-Ray Diffraction	66
2.5.9	Coverage-Dependent Structures of Bismuth on Cu(110) Determined by Surface X-Ray Diffraction.	67

2.5.10	Sulphur Induced Reconstructions of the Ni(111) and Cu(111) Surfaces	68
2.5.11	The $c(8 \times 2)$ Reconstruction of the In-rich InSb(001) Surface	69
2.5.12	X-Ray Structure Analysis of the (1×2) -Phases of Bi/GaSb(110)	70
2.5.13	Metallic Thin Films and Superlattices	71
2.5.14	Epitaxy of HTC Films on SrTiO ₃ Substrates	72
2.5.15	X-Ray Scattering from a SrTiO ₃ Bicrystal Interface	73
2.5.16	In-situ X-Ray Characterization of the GaAs(001)-H ₂ SO ₄ (:Cu) Interface	74
2.5.17	X-Ray Diffraction Study of Polymer Films on Graphite and H-Si(111) Surfaces	75
2.5.18	Surfaces of an Organic Crystal: β -Alanine	76
2.5.19	Molecular Structure within Self-Assembled Hexakis(hexylthio)-triphenylene Monolayers	77
2.5.20	X-ray Diffraction Study of Cr/Mn Superlattices	78
2.6	Langmuir Films	79
2.6.1	X-Ray 2D-Powder Diffraction Methods for Films at Liquid Surfaces	79
2.6.2	Tilted Monolayer Phases of Diol Derivatives Studied by Grazing Incidence X-Ray Diffraction	80
2.6.3	Structure of Monolayer Phases of a Simple n-alkane-1,2-diol.	81
2.6.4	Correlation between Domain Shapes and Monolayer Structures of Triple-chain Phospholipids on Water	82
2.6.5	Highly Compressed Phases of C ₂₂ H ₄₅ OH	83
2.6.6	Influence of a Hydrophilic Spacer on the Structure of a Phospholipid Monolayer	84
2.6.7	Grazing-Incidence Synchrotron X-Ray Studies of Phase-Separated Mixtures of Amphiphilic Monolayers on the Surface of Water	85
2.6.8	Self-Aggregated 2D Crystal Structure of Mixed Monolayers of Triacontanoic Acid and Nonacosylamine. Evidence in Favour of an Ordered Arrangement of the Ionized Headgroups	86
2.6.9	Formation of a Copper Complex of Docosanoyl-(S)-Lysine, as Determined by GID at the Monolayer- Solution Interface	87
2.6.10	Dynamics of Chiral Microseparation in Amphiphilic Monolayers on the Surface of Water	88
2.6.11	Influence of Handedness of Water-Soluble Additives on the Formation of Two-Dimensional Chiral and Racemic Amphiphilic Crystallites on Water Surfaces	89
2.6.12	Self-Assembled Crystalline Multilayers and Monolayers of n-Paraffins on Water Surfaces	90
2.6.13	N-Methyl Amides as Model Compounds for Understanding Monolayer and Multilayer Formation in Amphiphiles and Alkanes	91
2.6.14	Two-Dimensional Crystalline Order at the Surface of Homogeneous Solutions	92
2.7	Microemulsions, Surfactants and Biological Systems	93
2.7.1	Aggregation of Zinc-free Native Insulin and an Insulin Mutant Studied by Small-Angle Neutron Scattering	93
2.7.2	Structure of Casein Micelles Studied by Small-Angle Neutron Scattering	94

2.7.3	Cross-Section Structure of Polymer-like Lecithin Reverse Micelles	95
2.7.4	Formation of Polymer-like Mixed Micelles and Vesicles in Lecithin-Bile Salt Solutions	96
2.7.5	Structural Studies of a Micellar System with Cation Complexing Potential	97
2.7.6	Carbon Black Dispersion in Non-ionic Surfactant Water Solutions	98
2.7.7	The Cross-over from Meanfield to 3D-Ising Critical Behavior in a 3-Component Microemulsion	99
2.7.8	Micelles of Mixed Short-Chain Lecithin Molecules	100
2.7.9	Macrostructural Studies of Bile Salts by Small-Angle Neutron Scattering	101
2.7.10	Small-Angle Neutron Scattering Studies of DNA Complexes with RecA Protein	102
2.8	Polymers	103
2.8.1	On the N-scaling of the Ginzburg Number of Polymer Blends	103
2.8.2	Spinodal Decomposition of Poly(styrene)-Poly(Cyclohexyl Acrylate-stat-Butyl Methacrylate) Blends	104
2.8.3	Epitaxial Growth and Shearing of the Body Centered Cubic Phase in Diblock Copolymer Melts	105
2.8.4	Scattering Study on the Transamidation of Poly(Amide-4.6)	106
2.8.5	Stretching Induced Correlations in Triblock Copolymer Gels of PS-PEP-PS	107
2.8.6	Lamellar Meso-phase of PEO-PPO-PEO Melts and Water-swollen Mixtures	108
2.8.7	Interaction of PEO-PPO-PEO Block Copolymers with Ionic Surfactants	109
2.8.8	Phase Behavior of Triblock Copolymers Melt and Aqueous Solutions of Poly(Propylene Oxide)-Poly(Ethylene Oxide)-Poly(Propylene Oxide)	110
2.8.9	Epitaxial Growth and Shearing of the Body Centered Cubic Phase in Diblock Copolymer Melts	111
2.8.10	Influence of Shear on the Hexagonal-to-Disorder Transition in a Diblock Copolymer Melt	112
2.8.11	Investigation of the Surface Induced Ordering of P85 on Quartz	113
2.8.12	Butterfly Effect in Randomly Cross-Linked PDMS Gels. Classical Deformation at Large Scales	114
2.9	Molecular Science	115
2.9.1	Self-Assembling Molecular Wires	115
2.9.2	Synthesis of New Non-linear Organic Materials	116
2.9.3	Novel Peptide Nucleic Acids	117
2.9.4	New Solid Supports and Linkers for Peptide Synthesis	118
2.9.5	Side-Chain Liquid Crystalline Polyesters for Optical Information Storage	119
2.9.6	New Azobenzene Based Polyesters for Optical Storage	120
2.9.7	The Influence of Spacer Length and Substituents on the Orientational Behaviour of Novel Azobenzene Side-Chain Polyesters	121

2.10 Instrument Development	122
2.10.1 First Test of the RITA Analyser System	122
2.10.2 Characterization of an Image-Plate Detector used for Small-Angle X-Ray Scattering	123
2.10.3 A Pin-Hole Small-Angle X-Ray Scattering Instrument	124
2.10.4 Performance Test of the BW2 Beamline.	125
2.10.5 AFM of Insulating Surfaces	126
2.10.6 Calculation of the Performance of the New RITA Cold-plug	127
2.11 LIP - CEC Large Installation Programme at Risø	128
3 Publications, Educational and Organizational Activities, Colloquia	131
3.1 Publications	131
3.2 Other Publications	139
3.3 Conferences	139
3.4 Lectures	149
3.5 Organization of Meetings and Courses	150
3.6 Membership of Committees and Boards	153
3.7 Colloquia	154
4 Participants in the Work in the Department	155
4.1 Staff	155
4.2 Short Time Visitors	157
4.3 Short Time Visitors under the CEC Large Installation Programme	159

1 Introduction

The Department of Solid State Physics carries out research within Risø's long term program "Materials with distinct physical and chemical properties". Until 1994 the Department of Solid State Physics was organised in sections centred around scientific methods - neutron scattering, x-ray scattering and polymer chemistry. During 1994 the department was organised in three research programs: Macromolecular Chemistry, Magnetism and Superconductivity, and Surfaces and Interfaces. In addition the Department of Solid State Physics is in charge of a special program under the Commission of the European Community (CEC) Large Installations Program (LIP).

Macromolecular Chemistry

In 1994 the Macromolecular chemistry group was expanded and now (together with the Department of Chemical Engineering at the Technical University of Denmark) it forms the core of the "Danish Polymer Centre", which has received a four-year contract with the national authorities within the Danish Materials Technology Programme (MUP-2). The centre has four major areas of emphasis: (1) Structure and phase properties of polymer systems, (2) Polymer Rheology and processing, (3) Functional polymers for sensing and separation, and (4) Liquid crystalline polymers for optical applications. In connection with the formation of the centre and two smaller MUP-2 programmes, collaboration with some of the major Danish polymer-related industries has been established. In 1994 the chemistry facilities have been improved, several laboratories have been completely renewed, and new equipment, including an XPS dedicated for surface analysis of polymers, has been installed.

Some of the scientific highlights during 1994 are:

- A new highly symmetrical phase occurring around the order-disorder transition in block-copolymer systems has been identified. This result, which gives new information on intermolecular forces in polymers, has resulted in the revision of a widely accepted model for block copolymer phase behaviour.
- Peptide synthesis relies on highly controlled conditions for the stepwise growth of the peptide on solid supports. New methods including synthesis in tubes and peptide synthesis under mild chemical conditions have been developed.
- Molecular ordering of electroactive molecules open possibilities for obtaining new phenomena like molecular ferromagnets, molecular wires, etc. Self-assembling of linear molecular aggregates based on bis-arborol-tetrathiafulvalene have been demonstrated, showing the potential for forming molecular wires.
- Laser induced anisotropy and holographic optical storage in a series of newly synthesized azobenzene side-chains have been investigated. High efficiency is found in cyano- and unsubstituted azobenzene polyesters.

Magnetism and Superconductivity

In the program for Magnetism and Superconductivity, extensive use has been made of neutron scattering, but in 1994 we have also seen the results of a stronger emphasis on complementary methods. New theoretical models, simulations and the use of hard x-rays have all made substantial contributions to the progress reported here. A new laboratory with an

AC susceptometer in a dilplex cryostat and an AC/DC 5T magnetometer/susceptometer (Lake shore model 7125) has been finished. The gas volumetric equipment used to prepare High T_c superconductors with specific oxygen content has been upgraded to high vacuum accuracy.

Some of the scientific highlights during 1994 are:

- Silver is a spin 1/2 nuclear antiferromagnet. The fcc structure and the weak antiferromagnetic interactions make it an ideal model for the study of frustrated antiferromagnets. The first neutron scattering observations of ordering, which occurs at 500 pK, have been performed at the BER2 reactor in Berlin in collaboration with Helsinki Technical University, the University of Copenhagen and the Hahn-Meitner institute in Berlin.
- Hard x-rays (about 100 keV) from the synchrotron at HASYLAB in Hamburg were used to complement neutron studies of the oxygen ordering in the superconductor $YBa_2Cu_3O_{6+x}$ as a function of temperature and oxygen content.
- Theory and extensive Monte Carlo simulations were performed in order to understand the oxygen ordering phenomena and the corresponding scattering patterns.

Surfaces and Interfaces

The programme for Surfaces and Interfaces is concentrated on the study of atomic and molecular structure and magnetism of surfaces, interfaces and thin films. Nearly all work is performed by using x-ray scattering at the synchrotron radiation laboratories HASYLAB in Hamburg, ESRF in Grenoble and NSLS in Brookhaven, and neutron scattering at Rise's DR3 reactor.

Some of the scientific highlights during 1994 are:

- A number of rare-earth magnetic multilayers grown at the MBE plant at the Clarendon Laboratory has been investigated, mainly using neutron scattering at the TASI and TAS6 instruments. The work includes the first investigations of superlattices and thin films fabricated from light rare earth elements. The first magnetic x-ray scattering measurements on these systems at the BW2 beamline at HASYLAB were also conducted.
- At beamline BW1 in HASYLAB, in collaboration with the University of Mainz and with the Weizmann Institute in Israel, the structures of mono- and multilayers of long organic molecules on liquid surfaces have been studied by x-ray specular reflection and grazing-incidence diffraction. The types of compounds investigated include phospholipids (as encountered in biological membranes), other amphiphilic molecules, as well as non-amphiphilic alkanes. The types of problems addressed comprise (lack of) symmetry in monolayer phases, relation between molecular and 2D-crystalline structure, monolayer- to multilayer transformation and influence thereupon of additive molecules, microseparation of left- and right-handed molecules, and surface excess of water soluble amphiphilics.
- Complex surface/interface phenomena problems have been attacked. This consists of metal on metal growth, epitaxial clusters on surfaces and metal induced superstructures on semiconductor surfaces. An effort has also been made to start investigating

interfaces. This includes ceramic interfaces, surfaces of organic crystals and semiconductor/electrolyte interfaces.

- The use of positrons at the DORIS III storage ring in Hamburg has provided a much more stable and intense beam than previously and a count rate of 10^5 counts/sec was achieved from a surface reflection on a Ge(100)2x1 surface in an experiment performed at the BW2 beamline. This is similar to counts rates obtained at third generation synchrotron radiation sources. The first experiments at ESRF were also conducted in the new user mode operation.

Neutron Facilities

The cold neutron facilities at DR3 have been included in the CEC Large Installations Program (LIP) since early 1992. In 1994 the first contract expired. It was renewed and in 1994 more than 90 scientists from 7 different European countries used about 25% of the available beam time. The remaining beam time was allocated for internal use by the Department of Solid State Physics, the Department of Materials Science and their respective national and international collaborators.

The design of a new triple axis spectrometer (RITA) with area sensitive detectors, state of the art optical elements and modern computer facilities was started in 1994. The instrument will be constructed during 1995 and be operational in January 1996.

2 Research Projects in the Department

The work is divided into the following subject categories:

1. Theory, Monte Carlo Simulations, and Methods of Data Analysis
2. Magnetic Structures, Magnetic Phase Transitions, and Spin Dynamics
3. Superconducting Materials and Phenomena
4. Structures and Defects
5. Surfaces and Interfaces
6. Langmuir Films
7. Microemulsions, Surfactants and Biological Systems
8. Polymers
9. Molecular Science
10. Instrument Development
11. LIP - CEC Large Installation Programme at Risø

2.1 Theory, Monte Carlo Simulations, and Methods of Data Analysis

2.1.1 Classification of the Folding of Protein Polymers

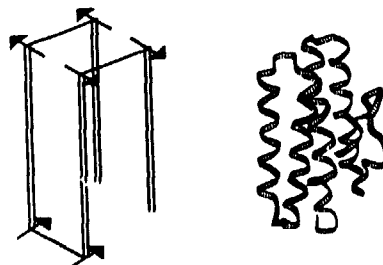
P.-A. Lindgård, *Department of Solid State Physics, Risø National Laboratory, Denmark*, and H. Bohr, *CBCA, Department of Physical Chemistry, The Technical University of Denmark*

Proteins consist of long chains of almost equally many hydrophilic and hydrophobic monomers. Nature's polymers are much more complex than most man made polymers - but the physics is the same. In water, proteins tend to form very closed packed structures, called their *native* structure. It has been conjectured that the structure is intimately related to the information content in the monomer sequence. It would therefore be of great interest to be able to classify the protein folds, which would allow a prediction of how many new classes, one may expect, will eventually be stored under the *GENOME PROJECT* in the Brookhaven data bank. Another interesting question is how are the natural proteins with typically 200 monomers able to fold up in a matter of seconds. Levinthal¹⁾ pointed out that if all $3^{200} \approx 10^{95}$ individual turn possibilities were to be tested it would last something like 10^{74} years! However, proteins fold in building blocks of secondary structures, the most important of which are the α -helices and β -sheets. We consider the problem at this level and want to define a unique name to each fold. The proteins are rather twisted, and irregular folds of different length secondary structures, which are connected by wiggly strands of monomer chains. To simplify the problem to the principal features, we consider a local angular description which translates the sequence of three consecutive elements into directions in a cubic lattice. There is a close analogy with this simplification and the cubic phase in the complicated *Martensitic materials*. We can now form a Hamiltonian of the form

$$\mathcal{H} = - \sum_{P=2n+1} (J_P \mathcal{S}_P \cdot \mathcal{S}_{P+1} + K_P \mathcal{S}_P \times \mathcal{S}_{P+1} \cdot \hat{\mathbf{e}}_\alpha^P) - \sum_{p=2n} (j_p \mathcal{S}_p \cdot \mathcal{S}_{p+1} + k_p \mathcal{S}_p \times \mathcal{S}_{p+1} \cdot \hat{\mathbf{e}}_\alpha^p), \quad (1)$$

where the parameter sequence gives a unique description of a fold, including the chirality. A unique, systematic name is the first requirement towards a classification. It allows us to study the fold by Monte Carlo simulations. We have estimated by scaling arguments, and directly computed the total number of fold classes to be ~ 4000 , which is close to the empiric estimate by Chotia²⁾ ~ 1000 . It would in fact be interesting if nature in the course of the evolution has not used all the possibilities. The number is much smaller than the astronomic numbers mentioned above and also smaller than any so far published.

Fig. 1. This figure demonstrates that the unique name given by the parameter sequence $\uparrow j \uparrow -K \uparrow j \uparrow K \uparrow j \uparrow$ represents the well known compact fold called a 4- α -helix bundle. It is easy to see that the name is identical for any rotations of the object, as it should of course.



¹⁾ C. J. Levinthal, *Chem. Phys.* **65**, 99 (1968).

²⁾ C. Chothia, *Nature*, **357**, 543 (1992).

2.1.2 Theory for a Degenerate Blume-Emery-Griffiths Model of an Entropy Stabilized Phase

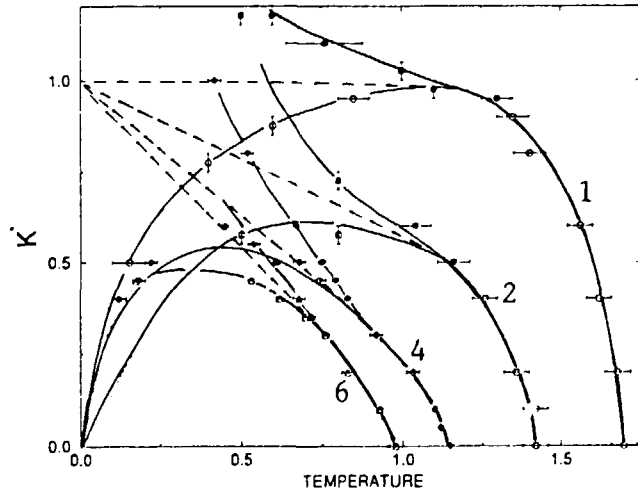
P.-A. Lindgård, *Department of Solid State Physics, Risø National Laboratory, Denmark*, and Eduard Vives and Teresa Castán, *Department d'Estructura i Constituents de la Matèria, Universitat de Barcelona, Diagonal 647, E-08028 Barcelona, Catalonia, Spain*

The Blume-Emery-Griffiths (BEG) model is a well known model in statistical physics, useful for describing a system having three states of which two are identical. However, for the phase transition in for example the *Martensitic* materials or in soft condensed matter the high temperature phase is often stabilized by "entropic forces". That means that there are so many available configurations that a system prefers a volatile state over a low energy state. To describe the essential physics of this by the simplest possible model we have simplified the Lindgård Mouritsen model¹⁾, which was first used to study the *Martensitic* transformation in a magnetic language. The model was later studied in details with respect to the domain formation kinetics after a quench²⁾. The basic form is

$$\mathcal{H} = - \sum_{\langle ij \rangle} \{ K S_{iz} S_{jz} + J S_{ix} S_{jx} \} , \quad (2)$$

where the first term with $S_{iz} = 1$, stabilizes the open *bcc* structure (*z*-phase), and the last term, with $S_{ix} = \pm 1$, the closed packed *hcp* structure (*x*-phase). However, in order to have a transition at a given temperature for a fixed ratio of the parameters $K/J = K^*$ it was needed to include higher order spin terms, which essentially are energy terms. This is unsatisfactory because the *bcc* phase is stabilized by a higher degeneracy of phases than a given domain of the *hcp* (*z*)-phase. A very simple solution is to postulate that the variables S_{iz} can assume a higher degeneracy $p > 1$ of identical states. One can show that Eq. (1) is exactly equivalent to the BEG-model for $p = 1$. Allowing the degeneracy to be $p > 1$ a new model is constructed which we call the DEG-BEG model. It is shown to have several interesting properties of relevance for the entropy stabilized phase transition problem. We have studied this DEG-BEG model by means of mean field theory and Monte Carlo simulations. It is now easy within the simple model to obtain a first order transition at a fixed ratio K^* with a large range of coexistence regions. This is shown in Fig. 1.

Fig. 1. The phase diagram for the DEG-BEG model for the degeneracy values $p = 1, 2, 4, 6$. The solid lines represent continuous phase transitions or spinodal stability lines, whereas the dashed lines are discontinuous phase transition lines.



¹⁾ P.-A. Lindgård and O. G. Mouritsen, *Phys. Rev. Lett.* **50**, 690 (1986).

²⁾ T. Castán and P.-A. Lindgård, *Phys. Rev. B* **40**, 5069 (1989).

2.1.3 Theory and Computer Simulation of Diffuse Scattering from Lattice Gas Models

T. Fiiig, N.H. Andersen, P.-A. Lindgård, *Department of Solid State Physics, Riso National Laboratory, Denmark*, and G. Uimin *Landau Institute for Theoretical Physics, Russia*

For one-dimensional ordered structures the relation between the structure factor $S(q)$ and the cluster size distribution $\mathcal{D}(n)$ is discussed. For a number of one-dimensional models the problem of excluded volume related to densely packed ordered structures is treated exactly and the corresponding line shapes are found. In table 1, $S_{\text{dif}}(q)$ has been calculated for different pertinent cluster size distributions $\mathcal{D}(n)$. The long lasting problem where there is a strong correlation between particles and vacancies has also been solved. Comparing the δ -function distribution (iv) with the Poisson distribution (vi), we see that due to the variation of cluster lengths around ℓa , the intensity does not vanish at any q -vector. For small particle concentration $x \leq x_{\text{Poisson}} \approx 0.33$, $S_{\text{dif}}(q)$ has a maximum at $q = 0$. The line shape depends on the particular value of ℓ . In (v) we see that an exponential distribution gives rise to a cosine form for $S_{\text{dif}}(q)$, which is exactly equal to an infinite sum over Lorentzian line shapes. However, the excluded volume effect gives rise to a broadening of the peaks, where the FWHM is increased from κ to $\kappa/(1-x)$. Neglecting this effect in an experimental fit may drastically underestimate the correlation length.

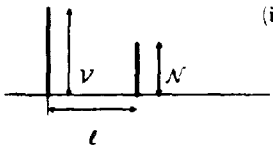
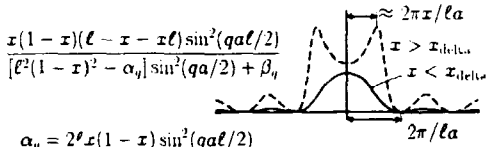
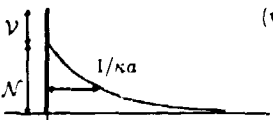
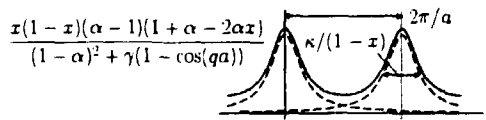
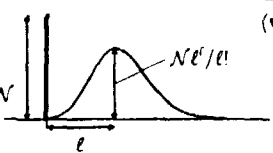
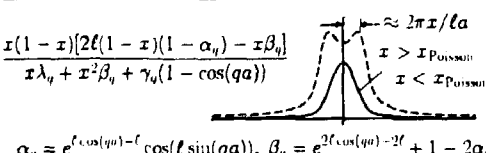
$\mathcal{D}(n)$	$S_{\text{dif}}(q)/b^2$ $\left[S_{\text{dif}}(q)/b^2 = \frac{(1-x)(1-u^2)}{1+u^2-2u \cos(\phi)}, \right.$ $\left. ue^{i\phi} = \frac{1}{1-x} \sum_{n=0}^{\infty} \mathcal{D}(n) e^{iq(n+1)a} \right]$
<p>(iv)</p> <p>$\mathcal{V}\delta_{n,0} + \mathcal{N}\delta_{n,\ell}$</p>  <p>$\mathcal{N} = x/\ell, \mathcal{V} = 1 - x(1 + 1/\ell)$</p>	 <p>$\alpha_q = 2^\ell x(1-x) \sin^2(qa\ell/2)$ $\beta_q = \ell x(1-x) \sin(qa) \sin(qa\ell/2) + x^2 \sin^2(qa\ell/2)$</p>
<p>(v)</p> <p>$\mathcal{V}\delta_{n,0} + \mathcal{N} \exp(-\kappa na)$</p>  <p>$\mathcal{N} = x[e^{\kappa a} - 1]^2 / e^{\kappa a}, \mathcal{V} = 1 - xe^{\kappa a}$</p>	 <p>$\alpha = e^{\kappa a}, \gamma = 2\alpha(1-x)^2 - 2x(1-x)\alpha(\alpha-1)$</p>
<p>(vi)</p> <p>$\mathcal{V}\delta_{n,0} + \mathcal{N}\ell^n/n!$</p>  <p>$\mathcal{N} = (x/\ell)e^{-\ell}, \mathcal{V} = 1 - x(1 + 1/\ell)$</p>	 <p>$\alpha_q = e^{\ell \cos(qa) - \ell} \cos(\ell \sin(qa)), \beta_q = e^{2\ell \cos(qa) - 2\ell} + 1 - 2\alpha_q$ $\gamma_q = 2\ell(1-x)(\ell - \ell x - x) + 2\ell x(1-x)\alpha_q$ $\lambda_q = 2\ell(1-x)e^{\ell \cos(qa) - \ell} \sin(qa) \sin(\ell \sin(qa))$</p>

Table 1. Cluster size distribution $\mathcal{D}(n)$ and corresponding structure factor $S_{\text{dif}}(q)$. The distributions are: (iv) δ -function distribution; (v) exponential distribution; (vi) Poisson distribution.

¹⁾ T. Fiiig, N.H. Andersen, P.-A. Lindgård, and J. Berlin. *Phys. Rev. B*, *submitted*.

2.1.4 Mean-field and Monte Carlo Calculations of the Three-Dimensional Structure Factor for $\text{YBa}_2\text{Cu}_3\text{O}_{6+x}$

T. Fiig, N.H. Andersen P.-A. Lindgård, *Department of Solid State Physics, Risø National Laboratory, Denmark*, and J. Berlin, *Thinking Machines Corporation, 45 First Street, Cambridge, Massachusetts, USA*

We have developed a general mean-field matrix theory for calculating phase boundaries and structure factors of a broad class of lattice gas Hamiltonians, which allow for any finite range interactions. We investigated the oxygen order in $\text{YBa}_2\text{Cu}_3\text{O}_{6+x}$ by applying our mean field theory and by Monte Carlo simulation using an extension to three dimensions of the well known two-dimensional Anisotropic Next Nearest Neighbor Interaction lattice gas model (the ASYNNNI model). The calculation of the structure factor in three spatial dimensions on a $256 \times 256 \times 16$ system has been implemented on a massively parallel computer, the Connection Machine CM2. This allows for an extremely accurate determination of the line shape of the structure factor for all scans in reciprocal space. We report on the results for an oxygen stoichiometry of $x = 0.4$, $x = 0.5$, and $x = 0.6$ for temperatures between $T = 450\text{K}$ and $T = 800\text{K}$. Our results for the line shapes of the structure factor at the $(\frac{1}{2}, 0, 0)$ superstructure reflection have been compared with mean-field predictions in Fig. 1 and with recent neutron and synchrotron X-ray diffraction measurements. The result for our mean-field calculation for the structurefactor yields:

$$S_{\text{dif}}(\mathbf{q}) = k_B T b^2 \frac{\frac{1}{2} \{ \chi_{14}^{-1}(\dot{\chi}_a, \mathbf{q}) + \chi_{14}^{-1}(\dot{\chi}_d, \hat{\mathbf{q}}) \} + 4V_1 \cos(\frac{qx}{2}) \cos(\frac{qy}{2})}{\chi_{14}^{-1}(\dot{\chi}_a, \mathbf{q}) \chi_{14}^{-1}(\dot{\chi}_d, \hat{\mathbf{q}}) - 16V_1^2 \cos^2(\frac{qx}{2}) \cos^2(\frac{qy}{2})}, \text{ where} \quad (3)$$

$$\chi_{14}(\dot{\chi}, \mathbf{q}) = \frac{1}{(\dot{\chi})^{-1} - 2V_3 \cos(q_x) - 2V_2 \cos(q_y) - 2V_4 \cos(q_z)}, \quad (4)$$

and $\dot{\chi}_a, \dot{\chi}_d$ are the local susceptibilities on the two interpenetrating sublattices, which constitute the CuO_x planes, and V_n the ASYNNNI interaction parameters.

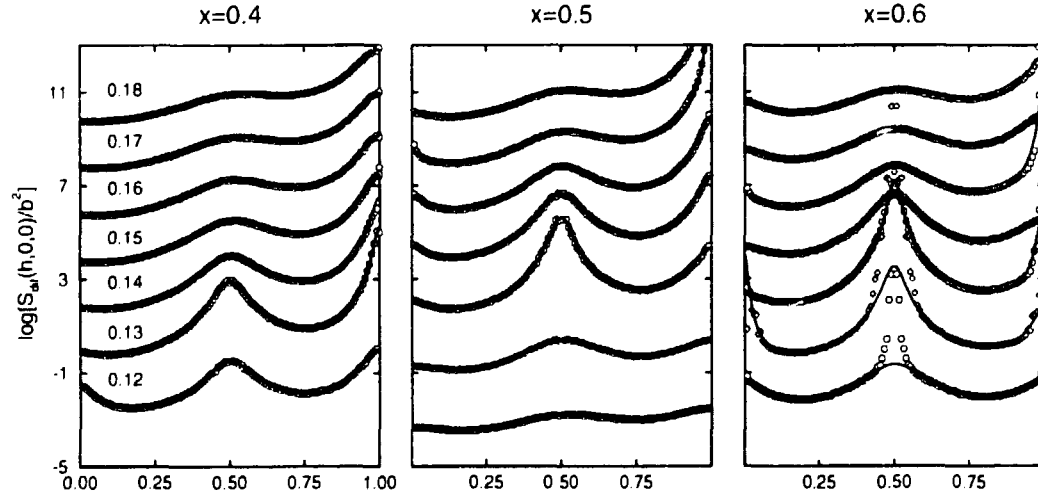


Fig 1. The lineshapes of the $(\frac{1}{2}, 0, 0)$ superstructure reflection $S_{\text{dif}}(q)$ along the a -axis (h -scan) is shown on a (natural)logarithmic scale for $x = 0.4$, $x = 0.5$, and $x = 0.6$ from $T = 0.12$ (450K) to $T = 0.18$ (800K). The open circles are the actual data points, while the solid curves represent the best fit to Eq. (3) plus a diffuse peak centered around $(1, 0, 0)$ for the ortho-I phase. Deviations indicate non-equilibrium domain formations. This is in particular evident at $x = 0.6$ due to the increased relaxation time.

2.1.5 Theory of the Transition Temperatures for Lattice Gas Models

T. Füg, P.-A. Lindgård, *Department of Solid State Physics, Riso National Laboratory, Denmark*

Lattice gas (LG) models are of importance for describing the statistical properties of many materials, from alloys to polymers. For the high T_c material $\text{YBa}_2\text{Cu}_3\text{O}_{6+x}$, the ASYNNNI model has recently been studied extensively by means of Monte Carlo (MC) simulations. MC is very time consuming and in order to get an analytic understanding of the dependence of a phase diagram on both interaction parameters and oxygen concentration x , it is important to have a basic theory. We have developed a general mean field theory for any LG model and shown that the non-trivial line shape for the susceptibility function $\chi(\mathbf{q})$ is in agreement with MC data in all q -space (in this case $\chi(\mathbf{q}) = \chi_{14}(\mathbf{q})$). This allows us to utilize the sum rule which relates $\sum_{\mathbf{q}} k_B T \chi(\mathbf{q})$ to the occupation probability $\sim x(1-x)$. From this we can analytically determine the transition temperature T_c which includes fluctuation corrections very well. The application of the sum rule method is a new generalization of the so called spherical method previously only used in context with continuous models like the Heisenberg model - with good results. In this theory we have had to solve a generalized Watson-type integral yielding

$$G(t) = \int_0^{2\pi} \int_0^{2\pi} \int_0^{2\pi} dx dy dz \frac{1}{t - \alpha \cos x - \beta \cos y - \gamma \cos z} = \frac{8\pi}{\sqrt{\beta\gamma}} \int_0^\pi dx k K(k^2), \quad (5)$$

where $k = \{4\beta\gamma/[(t - \alpha \cos x)^2 - (\beta - \gamma)^2]\}^{1/2}$ and $K(k)$ is the complete elliptic integral of the first kind. Here t is related to T_c and α, β, γ to the interaction parameters in the x, y, z directions. Using this theory we have first calculated the influence on T_c of introducing a coupling parameter V_4 in the third dimension for the ASYNNNI model. Because of the change of dimensionality from 2D to 3D the influence is very dramatic as shown on Fig. 1. We have also calculated the transition temperatures as a function of x for both 2D and 3D. The results are shown in Fig. 2. in comparison with the MC results. A remarkable feature is that the theory correctly predicts a shift in the maximum for the 3D case. This is due to the complicated multi-sublattice interactions in the ASYNNNI model and in particular the strong interaction V_1 which deters simultaneous occupation on subsystems with perpendicular oxygen chains.

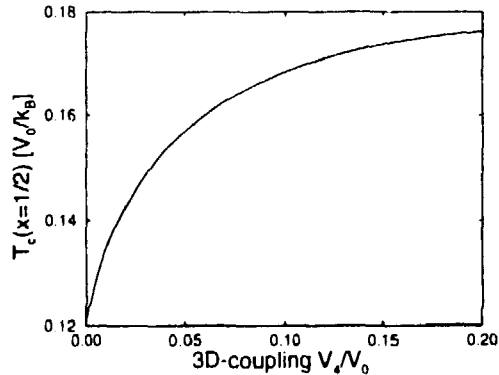


Fig. 1. The dependence of the transition temperature as a function of the interaction parameter V_4 in the third dimension for the ASYNNNI model.

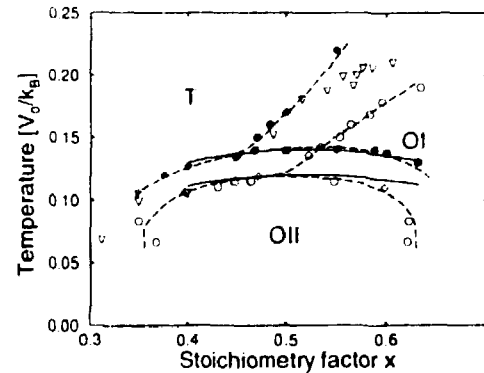


Fig. 2. The theoretical prediction for $T_c(x)$ for the 2D and 3D ASYNNNI models, valid for $x \approx 0.5$. ∇ , are experimental data, full symbols are 3D, and \circ 2D MC simulation data, respectively.

2.1.6 Strain Effects in a Lattice-Gas Model

S. Mannstaedt^a, G. S. Pawley, *Department of Physics and Astronomy, The University of Edinburgh, Scotland*, N. H. Andersen, T. Fiig, P.-A. Lindgård, *Department of Solid State Physics, Risø National Laboratory, Denmark*, and O. G. Mouritsen ^a*Department of Physical Chemistry, The Technical University of Denmark, Denmark*

Strain effects are included in the ASYNNNI lattice gas model, which is used to describe the oxygen ordering of the $\text{YBa}_2\text{Cu}_3\text{O}_{6+x}$ high- T_c superconductor. The geometry of the twin-domains rules that the oxygen forms Cu-O chains in mutually perpendicular directions in different domains. In reality this causes distortions which in the lattice gas model may be simulated by shifting the metal ions to intermediate sites. The strain is added to the lattice gas model by introducing a spring energy that increases with the oxygen chain lengths, and it is assumed that the strain may be released by the creation of defects in the structure and allowing the metal ions to shift to the intermediate sites. Because the spring energy is generated by the distortion of the lattice, which the oxygen ordering forces onto the crystal, it has to be calculated along both the a and b axes. The strain can take account for twin domains in both the Ortho-I and the Ortho-II phase, see Fig. 1. The strain-energy is calculated by use of two terms: 1) A long-distance term which is the accumulation of the strain in the lattice. Similar to Hooks law, the energy is calculated by a spring constant (K^{\parallel} along the oxygen chains, and K^{\perp} perpendicular to the oxygen chains) times the spring length squared. 2) A local term (K_{NNN}) which accounts for the energy barrier for making a deformation of the unit-cell configuration. The Hamiltonian for the system therefore becomes:

$$\mathcal{H} = \mathcal{H}_{\text{ASYNNNI}} - K^{\parallel} \sum_{\parallel} |f_{\parallel}(+)^2 - f_{\parallel}(-)^2| - K^{\perp} \sum_{\perp} |f_{\perp}(+)^2 - f_{\perp}(-)^2| - K_{\text{NNN}} \sum_{i,j} m_i m_j, \quad (6)$$

where $\mathcal{H}_{\text{ASYNNNI}}$ is the ASYNNNI model Hamiltonian, and $m_i = 1, 0$ is the metal ion occupation variables. The function f is gives the length of a perfect unit cell arrangement, either up ($f(+)$) or down ($f(-)$) an axis, to the point where the chain is broken by a defect in the lattice.

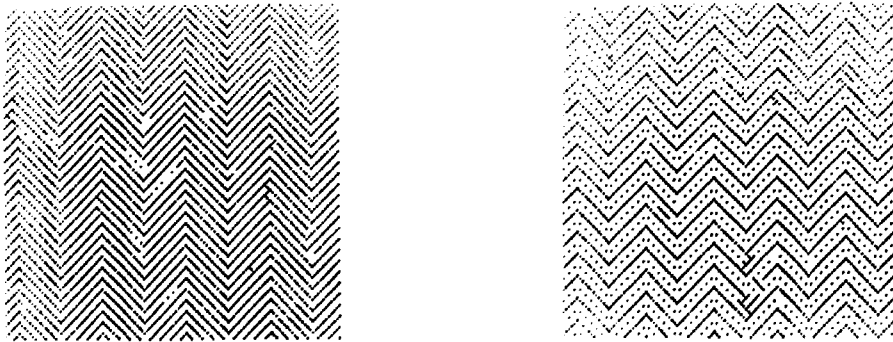


Fig. 1. Twin domains for a very strong spring constant. A weak spring constant gives rise to larger twin domains. (a) twin domains in the Ortho-I phase. (b) twin domains in the Ortho-II phase.

2.1.7 Effect of the Fermionic Degrees of Freedom on the Phase Diagram and the Structure Factor for $\text{YBa}_2\text{Cu}_3\text{O}_{6+x}$

T. Fiig, N.H. Andersen, P. Schleger, P.-A. Lindgård, *Department of Solid State Physics, Risø National Laboratory, Denmark*, and G. Uimin, *Landau Institute for Theoretical Physics, Russia*

It is now well-established that the superconducting properties of the $\text{YBa}_2\text{Cu}_3\text{O}_{6+x}$ type high T_c superconductors are strongly dependent on the details of the oxygen ordering in the CuO_x plane of the structure. It is therefore important to establish models that may be used to describe these oxygen ordering phenomena. The concentration of oxygen holes in the CuO_x planes has experimentally been estimated to be 30%. A charge transfer mechanism has therefore been proposed¹⁾, which calculates the free energy $f(n, m)$ per oxygen site of a copper-oxygen chain fragment containing n O atoms, m O^{2-} and $(n - m)$ O^- , based on a Kondo like model. The free energy $\phi(n)$ of a copper-oxygen chain fragment of length n , is calculated from

$$e^{-n\phi(n)/k_B T} = \sum_{m=0}^n e^{-nf(n,m)/k_B T}, \quad (7)$$

where $f(n, m)$ only depends on the ratio $\xi = m/n$, and may be approximated very well by a parabola with minimum around $\xi = 0.7$. We have included this free energy term $\phi(n)$ in addition to the traditional 2D-ASYNNNI model Hamiltonian. The result of such a phenomenological incorporation of fermionic degrees of freedom causes an additional degree of disorder, favoring formation of copper-oxygen chain fragments of finite lengths. Through a change in the lengths distribution of the copper-oxygen chain, a renormalization of the absolute temperature scale is observed in Fig. 1. In addition a splitting in the structure factor along the k -direction arises as a result of a predominant length scale, as shown in Fig. 2.

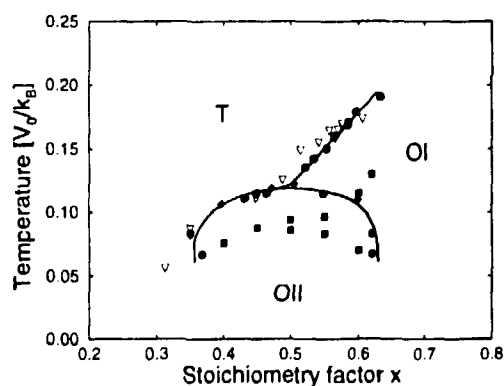


Fig. 1. The structural phase diagram of $\text{YBa}_2\text{Cu}_3\text{O}_{6+x}$. Triangles are experimental data, solid circles, diamonds and full line are results of a Monte Carlo simulation on the ASYNNNI model. Solid squares includes the fermionic degrees of freedom.

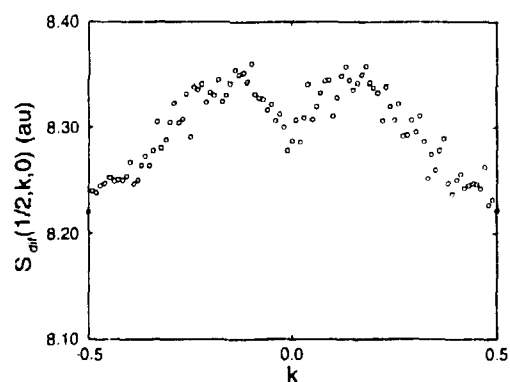


Fig. 2. The simulated $(\frac{1}{2}, 0, 0)$ Ortho-II superstructure peak at $x = 0.8$ and $k_B T = 0.46$. The inclusion of the fermionic degrees of freedom gives rise to a splitting along the k -axis.

¹⁾ G. Uimin, Phys. Rev. B **50**, 9531 (1994).

2.1.8 Monte Carlo Simulation Studies of Semi-flexible Polymers with Excluded Volume Interactions

J. Skov Pedersen, *Department of Solid State Physics, Risø National Laboratory, Denmark*,
M. Laso, and P. Schurtenberger, *Institut für Polymere, ETH Zürich, Switzerland*

Long flexible cylindrical micelles display a behavior which can be described by polymer models. While atomistically detailed models for polymers usually take into account the hindrance to torsion along the backbone by means of a suitable torsional potential, the polymer-like micelles can be accurately described by an extrapolation of the freely rotating chain model. In this model, the valence angle and the number of segments on the chain approach zero and infinity, respectively, in such a way that constant-torsion, freely rotating continuous worm-like chains is obtained for which the ratio of the contour length, L , to the statistical segment length, b , is constant¹⁾. We have performed Monte Carlo simulation on this model both with and without excluded volume interactions. For the excluded volume interactions a finite thickness of the chain was modeled by placing spheres of radius $R = 0.1b$ at each point on the chain. Check for excluded volume effects were done for points separated by more than $b/3$ along the contour. The smallest radius of the spheres was 0.6 times the distance between neighboring points. The number of points on the chain was chosen so that the finite size effects are less than 0.05% for the radius of gyration, R_g , and the end-to-end distance, D_{ee} . We have performed simulation for length from $L/b = 0.25$ up to 8196. For the latter case the number of points on the chain is 49153. For the shortest chains we have used a simple rejection algorithm in which chains with overlap were rejected and a new sample was grown. For the longer chains ($L/b \geq 64$) this procedure becomes too inefficient due to the small acceptance fraction. For the longer chains we have therefore used the pivot algorithm and made an implementation based on the extremely efficient approach developed by Stellman and Gans²⁾. The simulations by this approach have been checked by comparisons with more sophisticated methods which are used for denser polymer systems³⁾. The typical ensemble sizes for the rejection method and the pivot method were 10^5 and 5×10^5 , respectively. We have determined R_g , D_{ee} , and the distance between end and middle, D_{em} , and the distance, D_{ii} , between two inner points at $L/4b$ and $3L/4b$. For these parameters we have calculated expansion factors of the chains with excluded volume interaction as compared to those without. There is a large cross-over region between $L/b = 1$ and $L/b = 100$, where the asymptotic behavior for large values of L/b is reached. We have further determined the distribution function of D_{ee} , D_{em} , and D_{ii} , and are currently analyzing these using the function suggested by Mazur⁴⁾. Our preliminary results show good agreement with the results of renormalization group calculations⁵⁾ with $\epsilon = 0.175$ in the scaling law $R_g^2 \propto (L/b)^\epsilon$. Finally, we have determined scattering functions which we will aim at parameterizing so that experimental small-angle scattering data for polymer-like micelles can be analyzed.

¹⁾ O. Kratky and G. Porod, *Rev. Trav. Chim. Pay-Bas* **68**, 1105 (1947).

²⁾ S.D. Stellman and P.J. Gans, *Macromolecules* **5**, 516 (1972).

³⁾ E. Leontidis, J.J. de Pablo, M. Laso, and U.W. Suter, *Advances in Polymer Science* **116**, 285 (1994).

⁴⁾ J. Mazur, *J. Res. Nat. Bur. Stand.* **A69**, 355 (1965).

⁵⁾ J. des Cloizeaux, *J. Physique* **41**, 223 (1980).

2.1.9 Relationship Between the Roton Minimum and T_λ in ^4He

W. Montfrooij, *Department of Solid State Physics, Risø National Laboratory, Denmark,*
and I.M de Schepper, *IRI, Delft University of Technology, Delft, the Netherlands*

Liquid ^4He under saturated vapor pressure (SVP) undergoes a second order phase transition at $T_\lambda = 2.172$ K from a normal fluid state to a superfluid state, known as the λ -transition. The superfluid state is marked by sharp excitations, the so-called phonon-roton curve, directly observable by inelastic neutron scattering. The dispersion $\epsilon(q)$ of these excitations is plotted in Fig. 1 for $p=\text{SVP}$, where the region around $q=2 \text{ \AA}^{-1}$ is the region of the roton minimum. In the superfluid state, the fluid can sustain macroscopic frictionless flow provided no internal excitations are created. We have applied this concept to the atomic level in order to derive a relationship between the roton minimum and T_λ . As is the case in describing electrons in a metal, a moving atom in a liquid can be viewed as a stable excitation with an effective mass m^* (due to large scale hydrodynamic backflow). This atom moving at velocity v can emit a quasiparticle of volume V^* if the following two conservation laws are satisfied

$$m^*u^2/2 = \epsilon(q) + pV^*, \quad (8)$$

$$m^*u = \hbar q, \quad (9)$$

where u is the change in velocity and p the pressure of the fluid. Dividing the two equations we find the minimum requirement on v for emitting a quasiparticle, independent of m^* as

$$v_m(p) \geq u = 2\epsilon(q)/\hbar q + 2pV^*/\hbar q. \quad (10)$$

The minimum of the r.h.s. can directly be determined by graphical differentiation (solid line in Fig. 1). Finally, equating the average velocity v to the temperature by $\frac{3}{2}k_B T = \frac{1}{2}mv^2$, with m the bare atomic mass, and substituting the minimum of the r.h.s. of eq. (3) for v (as a function of pressure), we find the temperature at which a moving atom has sufficient thermal energy to emit a quasiparticle, and thus the fluid ceases to be a superfluid. We plot this temperature against the measured transition temperatures $T_\lambda(p)$ in Fig. 2, with $V^* \approx 8\text{\AA}^3$. We note that for $p=0$ there is no adjustable parameter. Thus the macroscopic transition temperature can be directly related to the microscopic excitation curve, just as is the case in superconductors.

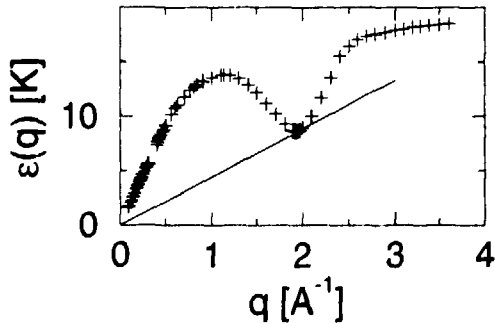


Fig. 1. Phonon-roton dispersion curve (+) adapted from Donnelly et al.¹⁾ The solid line tangent to the dispersion is given by eq. (3).

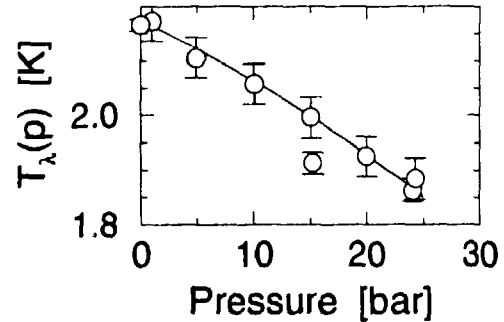


Fig. 2. T_λ vs. pressure as measured (solid line), and as calculated from eq. (3) (circles)

¹⁾ R.J. Donnelly, J.A. Donnelly and R.N. Hills, *J. Low. Temp. Phys.* **44**, 471 (1981).

2.1.10 Reverse Monte Carlo Analysis of Powder Patterns

W. Montfrooij, R. Hadfield, N.H. Andersen, *Department of Solid State Physics, Risø National Laboratory, Denmark*, and R.L. McGreevy, *Studsvik Research Laboratory, University of Nyköping, Sweden*

In traditional neutron powder diffraction analysis using the Rietveld method of refinement, the part of the background corresponding to diffuse scattering from the system is fitted to a functional form independent of the actual properties of the sample under investigation. This background, containing information on the Debye-Waller factors, is then subtracted, resulting in a final determination of the Debye-Waller factors which is no longer self-consistent. To overcome this problem, we have developed a Reverse Monte Carlo¹⁾ analysis technique (RMC) which models the diffuse background and the intensities of the Bragg peaks simultaneously, yielding Debye-Waller factors based upon using a maximum amount of information in the full powder pattern, under a minimum amount of assumptions. The new technique does not rely on any particular functional form of the Debye-Waller factors, and should therefore be most useful in cases where one expects highly anisotropic Debye-Waller factors, or even split sites in the unit cell.

As an illustration, we plot the calculated RMC powder pattern for $\text{YBa}_2\text{Cu}_3\text{O}_{6.93}$ measured on TAS3 in Fig. 1. This pattern was calculated using 1008 atoms (72 unit cells) in the simulation, while the lineshapes were corrected for asymmetry effects due to finite sample and detector heights. Also plotted in this figure is the part representing the diffusive background, as directly calculated from the simulation (slightly sloping solid line in the figure). We find that the oxygen distribution on the basal plane oxygen site O(1) is rather asymmetric, but we do not see any evidence for this site being a split site.

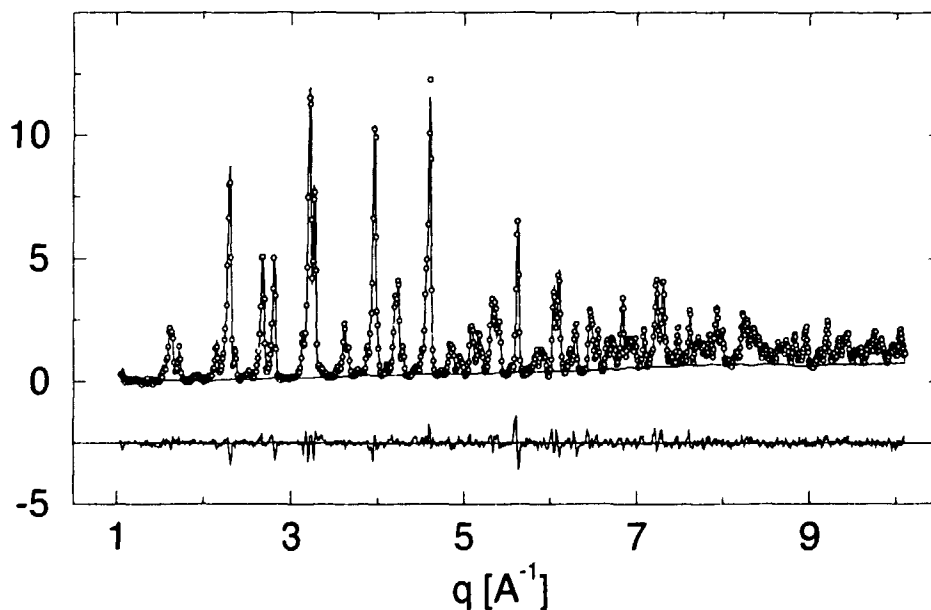


Fig. 1. Powder pattern (points) and RMC fit (solid line) for $\text{YBa}_2\text{Cu}_3\text{O}_{6.93}$, together with the difference profile (lower curve). The sloping background curve is calculated directly from the unit cell contents.

¹⁾ R.L. McGreevy and L. Pusztai, *Mol. Simulation* **1**, 359 (1988).

2.1.11 Instrumental Smearing Effects in Radially Symmetric Small-Angle Neutron Scattering by Numerical and Analytical Methods

J.G. Barker, *National Institute of Science and Technology, Gaithersburg, Maryland, USA*, and J. Skov Pedersen, *Department of Solid State Physics, Risø National Laboratory, Denmark*

A numerical calculation method for determining the resolution functions for radially symmetric collimation and scattering is described. In the present approach the total number of integrations are reduced to four by use of the radial symmetry of the geometry. Furthermore, the beamstop shadowing effect is included exactly. A typical calculation can be completed in minutes on current personal computers. An interactive computer program allows the user to enter the experimental parameters such as aperture size and wavelength spread, allowing smearing calculations to be handled routinely as a 'black box' operation. The exact smearing treatment is compared both to an improved technique involving Gaussian resolution functions where corrections for the beamstop are included and with results from Monte Carlo simulations. An example calculation is shown in the figure, where the detector pixel is located 3 cm from the center of a beam with a 2.5 cm radius beam stop. Within statistics the simulation and numerical results agree perfectly. Note also that the Gaussian approximation agrees very well with the numerical and simulation results except in the tails of the distribution. The error in the Gaussian representation can be mitigated if the distribution is truncated to $\pm 2.5\sigma$. In most experiments, the use of a truncated Gaussian distribution to approximate the resolution is preferred on account of its ease of calculation. But in a few cases, such as Porod scattering, the present more extensive numerical calculation or inclusion of the developed beamstop shadowing correction factors into a Gaussian scheme are needed for an adequate prediction of the smearing effects.

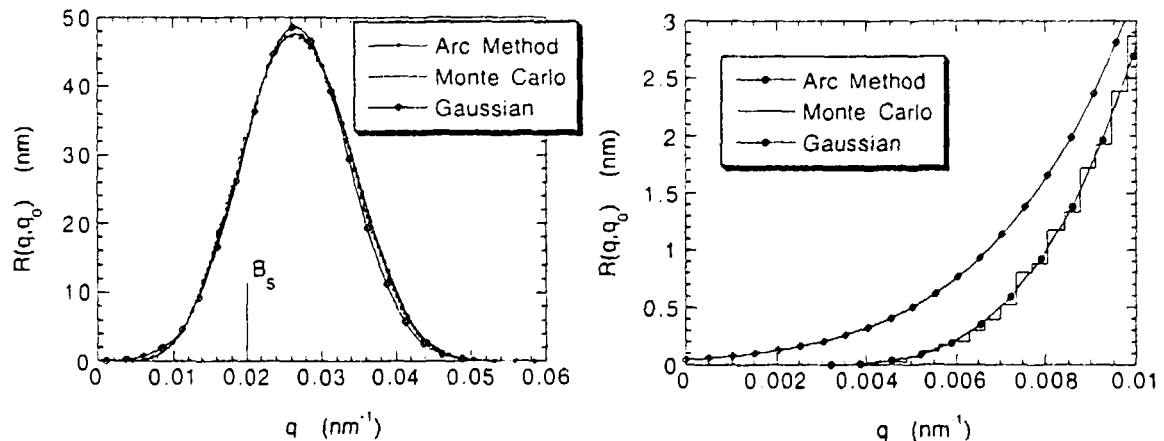


Fig. 1. The resolution function calculated for a detector annulus centered at $r_0 = 3$ cm close to the beamstop. Solid circle symbols are calculated by arc method, the solid line is the result of the Monte Carlo simulation, and diamond symbols are calculated by Gaussian approximation. The bottom figure expands the small q tail to highlight the Gaussian over-estimation.

2.2 Magnetic Structures, Magnetic Phase Transitions, and Spin Dynamics

2.2.1 Nuclear Magnetic Ordering in ^{109}Ag

K. Lefmann, K.N. Clausen, *Department of Solid State Physics, Risø National Laboratory, Denmark*, K. K. Nummila, J. T. Tuoriniemi, R. Vuorinen, O. V. Lounasmaa, *Low Temperature Laboratory, Helsinki Technical University, Finland*, F. B. Rasnussen, *Ørsted Laboratory, Niels Bohr Institute, University of Copenhagen, Denmark*, A. Metz, K. Siemensmeyer, M. Steiner, *Hahn-Meitner Institut, Berlin, Germany*.

When the temperature of a solid reaches the sub-mK range, all degrees of freedom are frozen out, except for the orientation of the nuclear moments. Eventually, when the temperature is comparable to the magnetic interaction between the nuclei, a nuclear magnetic ordered state may be reached. Producing nuclear ordered states in metals is an extremely difficult experimental task, as the necessary temperatures are in the nK range. For Ag, recent NMR measurements from Helsinki¹⁾ shows nuclear ordering below 560 pK. The study of nuclear magnetism is a testing ground for different kinds of theoretical many-body models, that have been calculated from first principles²⁾. The nuclear magnetic structure of Cu were studied by neutron diffraction at Risø, and a rich magnetic phase diagram in the (B, T) plane was found³⁾. The nuclear spin of Cu is $I = 3/2$. Ag has spin $I = 1/2$, promising more quantum-like behaviour.

At Hahn-Meitner Institut in Berlin an experiment for studying the nuclear magnetic ordering of ^{109}Ag has been set up. The project is a collaboration between researchers from Finland, Germany and Denmark, and was started in April, 1992. The cryostat is situated at a permanent beam hole in the neutron guide hall at HMI. In October 1994, the first trace of the nuclear ordered state was seen, and the results has been reproduced several times. We have observed an (001) peak at $B = 0$, when the final demagnetization is made along the [001] direction. The peak was observed by a position sensitive detector, and is resolution limited. This indicates a true long range ordered (001) phase.

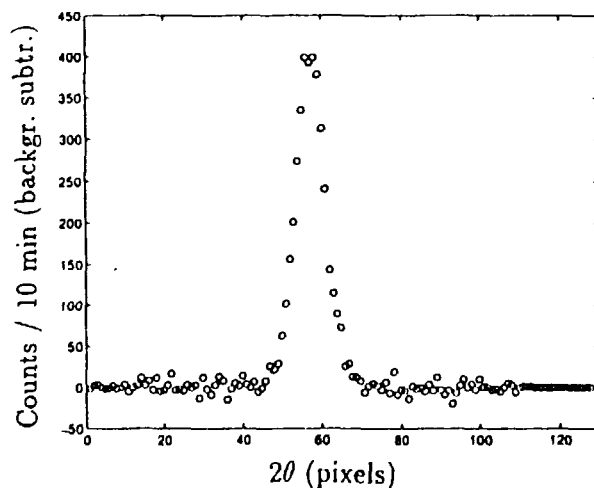


Fig. 1. (001) peak produced by the nuclear ordered state in ^{109}Ag . The full 2θ scan is produced by a position sensitive detector, each pixel representing 0.075° . The counting time is 10 minutes, starting right after entering the ordered state.

¹⁾ P.J. Hakonen, S. Yin and K.K. Nummila, *Europhys. Lett.* **15**, 677 (1991).

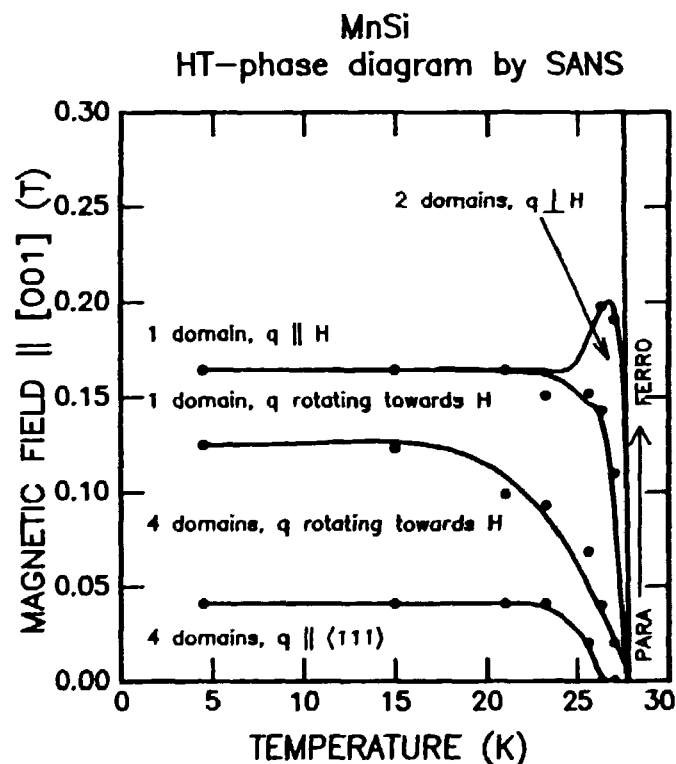
²⁾ M. Heinilä and A. Oja, *Phys. Rev. B.* **48**, 7227 (1993). B.N. Harmon, X.-W. Wang and P.-A. Lindgård, *J. Magn. Magn. Mat.* **104**, 2113 (1992).

³⁾ T. Jyrkkiö *et. al.*, *Phys. Rev. Lett.* **60**, 2418 (1988).

2.2.2 Magnetic Phase Diagram of MnSi

B. Lebech, P. Harris, J. Skov Pedersen, K. Mortensen, S. Aa. Sørensen, *Department of Solid State Physics, Risø National Laboratory, Denmark*, Hae Seop Shim, *Korea Atomic Energy Research Institute, Taejon, Korea*, M. Jermy, and J. Wingfield, *School of Physics and Space Research, University of Birmingham, Birmingham, UK*, N.R. Bernhoeft, C.I. Gregory, *Department of Physics, University of Durham, UK*, S.A. Brown, *The Cavendish Laboratory, University of Cambridge, Cambridge, UK*

The magnetic phase diagram of MnSi with the cubic B20 crystal structure ($P2_13$) was determined using Small Angle Neutron Scattering (SANS). The diffraction data were analysed using the three dimensional resolution function and the scattering cross section to model the diffraction data^{1,2}. The method of analysis allows us to extract physical parameters related to the magnetic order, such as intensity, direction and length of the modulation vector, and the transverse correlation width from the SANS data. A small phase pocket (phase 'A') just below T_N is found to be a modulated antiferromagnet. The field-temperature phase diagram for MnSi determined from a series of field sweeps ($\mathbf{H} \parallel [001]$) at constant temperature is shown in Fig. 1. The field sweeps were done as follows: (1) heat the sample to 35 K at maximum field, (2) remove the field, (3) cool the sample to 4.2 K. (4) heat to the relevant temperature, (5) sweep the field from zero to maximum and measure at relevant field settings. The sample was allowed time to equilibrate between each step.



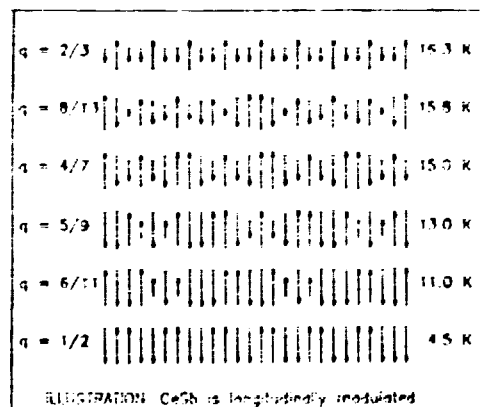
¹)P. Harris, Risø-R-747 (1994).

²)P. Harris, B. Lebech and J. Skov Pedersen (1994). *J. Appl. Crystallography*, *accepted*.

2.2.3 Commensurate-Commensurate Magnetic Phase Transitions in CeSb

Hae Seop Shim, *Korea Atomic Energy Research Institute, Taejon, Korea*, and B. Lebech, *Department of Solid State Physics, Riso National Laboratory, Denmark*

The rare earth monopnictide CeSb with the rocksalt crystal structure ($Fm\bar{3}m$), orders magnetically at T_N 16.5 K via a first order transition and the crystal structure transforms to the corresponding tetragonal structure ($I4/mmm$) at T_N . The magnetic order is to a longitudinal commensurately modulated structure with modulation vector along $[0\ 0\ 1]$ of length $q = 2/3$. Below T_N , there are several first order magnetic phase transitions between commensurately modulated structures with $q < 2/3$. The first transition is a few tenth of a degree below T_N , the last type IA antiferromagnetic structure ($q \sim 1/2$) is at 9 K. Previous neutron diffraction studies¹⁻³⁾ were interpreted in terms of longitudinally modulated commensurate magnetic structures ($\mathbf{q} \parallel \mathbf{c}_t$) built up of ferromagnetic and paramagnetic layers of Ce atoms, where the latter layer type originally were introduced in order to generate a commensurate magnetic structure in which the free ion moment was not exceeded on any Ce atom. Inspired by the recent investigations of the magnetic ordering in NdCu₂⁴⁾ we reinvestigated the magnetic ordering in CeSb. In the high and low temperature phases ($q = 2/3$ and $q \sim 1/2$) only one harmonic component is observed in the diffraction patterns, while higher order harmonic components are observed in all the intermediate phases. These were indexed as odd harmonics of the first harmonic components ($q = 6/11$, $q = 5/9$, $q = 4/7$, $q = 8/13$) and their amplitudes were used in an analysis similar to that applied in Ref. 5. With an appropriate choice of phases, the diffraction data is consistent with squared up commensurate structures where the c_t -axis moment component varies very little, i.e., as illustrated in the figure, there are no paramagnetic planes in these structures. The maximum moment component in any Ce layer remains almost independent of temperature between 1.5 K and 15 K. Between 15 K and T_N , the maximum c_t -axis moment component and the degree of squaring up decreases rapidly with increasing temperature.



¹⁾ J. Rossat-Mignod, P. Burlet, J. Villain, H. Bartholin, Wang Tchong-Si, D. Florence and O. Vogt, *Phys. Rev.* **B16**, 444 (1977).

²⁾ P. Fischer, B. Lebech, G. Meier, B.D. Rainford and O. Vogt, *J. Phys. C: Solid State Phys.* **11**, 345 (1978).

³⁾ P. Burlet, J. Rossat-Mignod, H. Bartholin and O. Vogt, *J. Physique* **40**, 47 (1979).

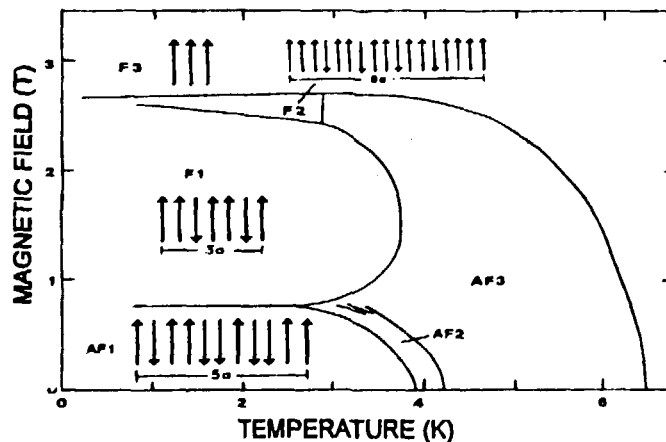
⁴⁾ M. Loewenhaupt, Th. Reif, R.R. Arons, E. Gratz, M. Potter and B. Lebech (1995). *Z. Physik B: Cond. Matter*, *accepted*.

⁵⁾ S. Kawano, B. Lebech and N. Achiwa, *J. Phys.: Condens. Matter* **5**, 1535 (1993).

2.2.4 Magnetic Structures of NdCu₂ in Finite Magnetic Fields

M. Loewenhaupt, Th. Reif, *Institut für Festkörperforschung, Forschungszentrum Jülich, Germany*, P. Svoboda, *Department of Metal Physics, Charles University, Prague, Czech Republic*, and B. Lebech, *Department of Solid State Physics, Risø National Laboratory, Denmark*

NdCu₂ shows a very rich magnetic field-temperature phase diagram (especially for $\mathbf{H} \parallel b$) with commensurate and incommensurate magnetic structures and first and second order phase transitions. The magnetic structures of NdCu₂ have been determined from powder¹⁾ and single crystal²⁾ neutron diffraction data in zero external field. In the low-temperature phase AF1, the magnetic structure is commensurate with progressing squaring-up for decreasing temperatures and modulation vectors $n\mathbf{q}$, where $\mathbf{q} = (3/5\ 0\ 0)$ and $n = 1, 3$ and 5 . In the high-temperature phase AF3, the magnetic structure is incommensurate sinusoidally modulated with wave vector $\mathbf{q} = (0.62\ 0.044\ 0)$. The AF1 magnetic structure consists of ferromagnetic (bc)-planes stacked in a complicated, antiferromagnetic order along the a -direction comprising five crystallographic unit cells (10 bc -planes). The ordered moment is $1.8\ \mu_B$ per Nd atom at 1.2 K. In both phases the Nd moments are oriented along the b -direction. Within a narrow temperature region, between the commensurate AF1 and the incommensurate AF3 phase there exists one more phase, AF2. In a recent experiment we have investigated the AF2 phase in more detail using the same NdCu₂ crystal as in ref. 2. The magnetic Bragg reflections were determined in the a^*c^* and a^*b^* planes. The temperature was controlled within 0.003 K. The magnetic structure of AF2 is similar to that of AF1. We observe magnetic reflections belonging to a fundamental wave vector \mathbf{q}' and its higher harmonics $3\mathbf{q}'$ and $5\mathbf{q}'$. In AF2, $\mathbf{q}' = \mathbf{q} + \epsilon$ with $\mathbf{q} = (3/5\ 0\ 0)$, as in AF1, and $\epsilon = (0.003\ 0.003\ 0)$. We have also performed neutron diffraction experiments in finite external fields up to 3 T using the NdCu₂ single crystal with its b -axis and the field vertical. A phase diagram (including the results of other measurements like magnetization³⁾, thermal expansion and specific heat is shown in the figure. The arrows indicate the stacking of the ferromagnetic bc -planes along the a -direction in the commensurate phases.



¹⁾R. R. Arons, M. Loewenhaupt, Th. Reif and E. Gratz, *J. Phys.: Condensed Matter* **6** 6789 (1994).

²⁾M. Loewenhaupt, Th. Reif, R. R. Arons, E. Gratz, M. Rotter and B. Lebech (1995). *Z. Physik B: Cond. Matter*, *accepted*.

³⁾S. W. Zochowski, M. Rotter, E. Gratz and K. A. McEwen (1995), *ICM 1994*, *accepted*.

2.2.5 Absence of AF Reordering at Low Temperature in Pure $\text{YBa}_2\text{Cu}_3\text{O}_{6+x}$

H. Casalta, P. Schleger, W. Montfrooij, N.H. Andersen, B. Lebech, *Department of Solid State Physics, Risø National Laboratory, Denmark* E. Brecht, W.W. Schmahl, H. Fuess *Fachbereich Materialwissenschaft, TH Darmstadt, Germany*, Ruixing Liang, W.N. Hardy *Dept. of Physics, UBC, Vancouver, Canada*, Th. Wolf, *Institut für Technische Physik, Kernforschungszentrum Karlsruhe, Germany*

Conflicting results have been reported about the existence^{1,2)} or not^{3,4,5)} of an antiferromagnetic reordering (AFII) in pure $\text{YBa}_2\text{Cu}_3\text{O}_{6+x}$ at low temperature, corresponding to a doubling of the magnetic unit cell along the c-axis. In here, we investigate the magnetic ordering in an $\text{YBa}_2\text{Cu}_3\text{O}_{6+x}$ crystal ($x=0.1$ and $x=0.18$) and in an $\text{YBa}_2(\text{Cu}_{2.86}\text{Al}_{0.14})\text{O}_{6.25}$ crystal doped with non magnetic Al impurities. Note that the pure $\text{YBa}_2\text{Cu}_3\text{O}_{6+x}$ crystal was grown in a zirconia crucible to avoid aluminum contamination (this contamination is common due to the use of alumina crucibles).

The neutron scattering measurements were performed on both the cold source triple-axis spectrometer TAS1 and the 4-circle diffractometer TAS2. A standard ^4He -cryostat and a furnace were used at TAS1 to measure from 2 K to 450 K. TAS2 was used to determine the oxygen and aluminum contents.

T_N was deduced from the onset of the $(\frac{1}{2} \frac{1}{2} 2)$ peak associated with the AFI phase and found to be equal to 410(1) K, 368(1) K, and 411(1) K for $\text{YBa}_2\text{Cu}_3\text{O}_{6.1}$, $\text{YBa}_2\text{Cu}_3\text{O}_{6.18}$ and $\text{YBa}_2(\text{Cu}_{2.86}\text{Al}_{0.14})\text{O}_{6.25}$ respectively (Figs. 1 and 2). For the 14% Al doped sample, a $T_2=8(1)$ K was found (inset Fig. 2) by following the $(\frac{1}{2} \frac{1}{2} \frac{3}{2})$ peak associated with the AFII. The absence of the AFII phase in a pure $\text{YBa}_2\text{Cu}_3\text{O}_{6+x}$ crystal, together with its appearance in an Al doped one, shows the extreme sensitivity of this transition to impurities in the basal plane, and explains the lack of consensus concerning its existence in $\text{YBa}_2\text{Cu}_3\text{O}_{6+x}$.

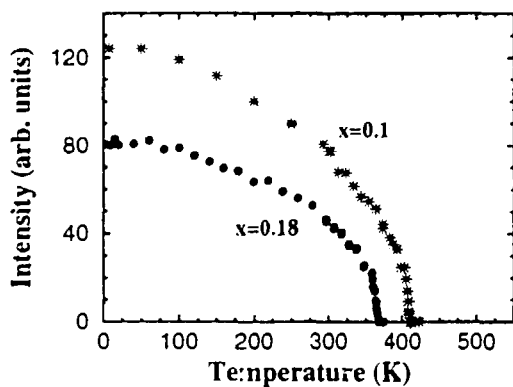


Fig1: Determination of T_N in $\text{YBa}_2\text{Cu}_3\text{O}_{6+x}$ by following the $(\frac{1}{2} \frac{1}{2} 2)$ peak vs temperature.

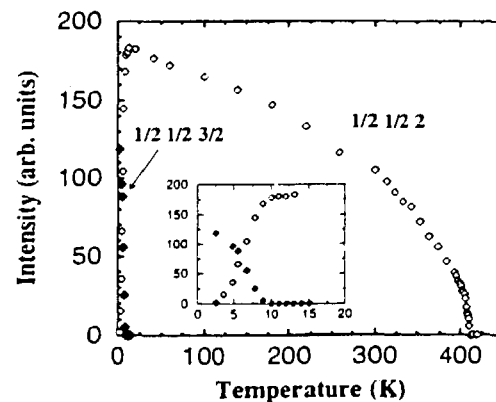


Fig2: Magnetic ordering in $\text{YBa}_2(\text{Cu}_{2.86}\text{Al}_{0.14})\text{O}_{6.25}$. Two transitions are observed at $T_N=411$ K and $T_2=8$ K by monitoring the $(\frac{1}{2} \frac{1}{2} 2)$ and the $(\frac{1}{2} \frac{1}{2} \frac{3}{2})$ reflections vs temperature.

- 1) H. Kadowaki *et al.*, Phys. Rev. B **37**, 7932 (1988).
- 2) S. Shamato *et al.*, Phys. Rev. B **48**, 13817 (1993).
- 3) P. Burlet *et al.*, Physica C **153-155**, 1115 (1988).
- 4) J. M. Tranquada *et al.*, Phys. Rev. B **38**, 2477 (1988).
- 5) H. Casalta *et al.*, Phys. Rev. B **50**, 9688 (1994).

2.2.6 High Pressure Neutron Diffraction Studies of the Magnetic Structures of Er

S. Aa. Sørensen and B. Lebech, *Department of Solid State Physics, Risø National Laboratory, Denmark*

A neutron diffraction study of the magnetic structure of single crystal Erbium at 14 kbar was carried out at the research reactor DR3, Risø National Laboratory using an improved McWhan type pressure cell mounted in a Duplex closed cycle refrigerator.

The magnetic structures of Er at ambient pressure are described in ¹⁾ and ²⁾. Briefly three distinct magnetically ordered phases are observed : (i) for $T_N \approx 84 \text{ K} > T > T_{CY} \approx 52 \text{ K}$ the c -axis moments are sinusoidal ordered with the modulation vector parallel to the c -axis and higher order harmonics develop with decreasing temperature; (ii) for $T_{CY} \approx 52 \text{ K} > T > T_C \approx 18 \text{ K}$ the structure changes to a cycloidal in the ac -plane and (iii) for $T < T_C \approx 18 \text{ K}$ a c -axis cone appears with a period close to eight atomic layers.

With the combination of the pressure cell and the closed cycle refrigerator, it was possible to control the temperature in the range between 8 K and 120 K. The temperature was measured by a set of Ge and Pt thermometers in the top and the bottom of the pressure cell. The typical temperature stability was 0.25 K and the temperature difference from top to bottom of the cell was below 0.5 K. The cool-down time from room temperature to 8 K was approximately 15 hours.

Figure 1 shows the temperature dependence of the intensities of the first order satellites along the $[11l]$ and the $[00l]$ directions (normalized to 9 K) at 14 kbar hydrostatic pressure. As the $(002^{\pm q})$ satellites disappear at a temperature $T_{CY}^P = (46 \pm 1) \text{ K}$, one concludes that the basal plane component of the magnetic moment becomes disordered above T_{CY}^P . The c -axis moment remains ordered up to $T_N^P = (82 \pm 1) \text{ K}$. Figure 2 shows the length of the modulation vector, Q (in units of c^*) as a function of temperature. Below $\sim 30 \text{ K}$ Q locks in to the commensurate value $2/7 \times c^*$.

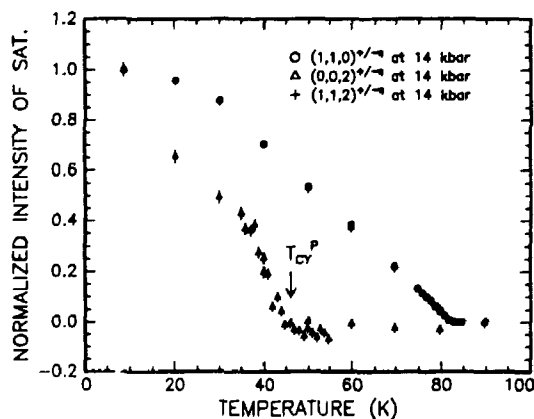


Fig. 1. The temperature dependence at 14 kbar hydrostatic pressure of the magnetic satellite intensities along the $[00l]$ and $[11l]$ directions.

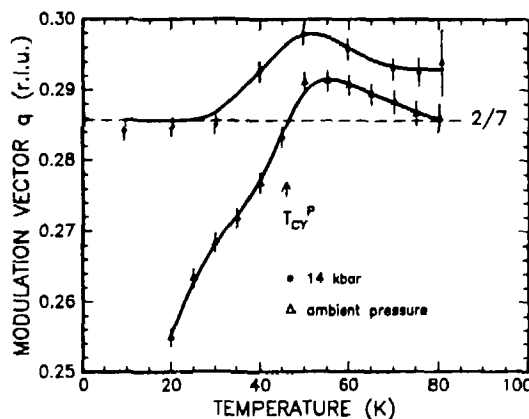


Fig. 2. The temperature dependence of the modulation vector Q in units of $2\pi/c$ obtained from the displacement between the $(11l \pm q)$ satellites. The full curves are guides to the eye

¹⁾ M. Habenschuss, C. Stassis, S. K. Sinha, H. W. Deckman and F. H. Spedding, *Phys. Rev. B* **10**, 1020 (1974).

²⁾ S. Kawano, B. Lebech and N. Achiwa, *J. Phys. Cond. Mat.* **5**, 1535 (1993).

2.2.7 Trigonal Interactions in Holmium

J.A. Simpson, R.A. Cowley, and D.A. Jehan, *Oxford Physics, Clarendon Laboratory, UK*, and D.F. McMorrow, *Department of Solid State Physics, Risø National Laboratory, Denmark*

The low temperature magnetic properties of Ho have been re-examined in order to search for evidence of couplings of trigonal symmetry, which have been shown to have an important influence on the magnetic properties of other heavy rare-earth elements such as Er¹⁾. Our study concentrated on the cone phase, which develops below ≈ 20 K.

The experiments were performed using TAS7, with scans made along $[00\ell]$ and $[10\ell]$ at 10 K, a temperature well below the transition to the cone structure. The previously accepted picture of this phase is one in which pairs of moments bunch about easy axes and each cants out of the basal plane slightly. Due to the hexagonal symmetry, the period is twelve atomic planes.

From Fig. 1, peaks are observed at (100) and (101) due to nuclear scattering, and the first harmonics of the spiral at $(10\frac{1}{6})$ and $(10\frac{5}{6})$. Additional features are also observed, marked by the arrows, which are not expected from the simple picture of this phase and indicate that the cone structure is distorted.

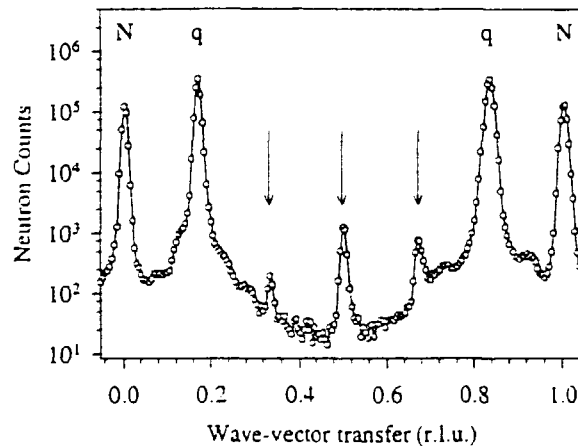


Fig. 1. $[10\ell]$ scattering data at 10 K. Peaks marked by N arise from nuclear scattering processes, and the first harmonics of the spiral are labelled q. Additional features, marked by the arrows, can be seen at $(10\frac{1}{3})$, $(10\frac{1}{2})$ and $(10\frac{2}{3})$.

Our observations are consistent with the structure being one where in any group of four moments, two have a large tilt out of the basal plane, but the adjacent two have a smaller value. The basal-plane projections also vary in this manner, as the total moment length is constant. This has been modelled using a mean field calculation, and the data is well described by including terms in the Hamiltonian which are of trigonal symmetry, similar to that found for Er¹⁾. This will be described more fully elsewhere²⁾, where we also discuss the detailed nature of the transition into the cone phase.

¹⁾ R.A. Cowley, and J. Jensen, *J. Phys.:Condens. Matter* **4**, 9673 (1992).

²⁾ J.A. Simpson, D.F. McMorrow, R.A. Cowley, and D.A. Jehan, *Phys. Rev. B*, *submitted*.

2.2.8 The Magnetic Structure of Ho/Pr Alloys

J.P. Goff, J.A. Simpson, R.A. Cowley, *Oxford Physics, Clarendon Laboratory, UK*, and D.F. McMorrow, *Department of Solid State Physics, Risø National Laboratory, Denmark*

Holmium adopts a helical magnetic structure below $T_N \sim 132$ K with the moments in the basal planes and the wave vector of the helix along the hexagonal c -axis. In contrast, the exchange interaction between magnetic ions in praseodymium is just insufficient to induce magnetic ordering and instead magnetic order is established below ~ 50 mK via the hyperfine interaction. $\text{Ho}_x\text{Pr}_{1-x}$ alloys may be formed over the entire composition range with a crystal structure dependent on concentration x . The aim of the experiment was to determine how the ordering in Ho is affected by dilution with Pr and by the concomitant changes in crystal structure.

Random thin-film alloys of composition $x = 0.8, 0.6, 0.5, 0.4$ and 0.2 were grown at Oxford by molecular beam epitaxy. Neutron diffraction measurements were performed down to $T=1.8$ K using TAS1. Ambient temperature scans along $[0\ 0\ L]$ and $[1\ 0\ L]$ revealed the following crystal structures: hcp $x = 0.8$ and 0.6 ; Sm $x = 0.5$ and 0.4 ; dhcp $x = 0.2$.

In the two hcp samples a basal plane helix modulated along c is observed. The temperature dependence of the ordering wave vector is compared with that of bulk Ho in Fig. 1. At low temperatures the magnetic structures become commensurate with wave vectors $5/23c^*$ ($x=0.8$) and $2/9c^*$ ($x=0.6$). The Néel temperatures $T_N = 100$ and 70 K for $x = 0.8$ and 0.6 respectively, are rather lower than might be expected for simple dilution of the magnetic ion.

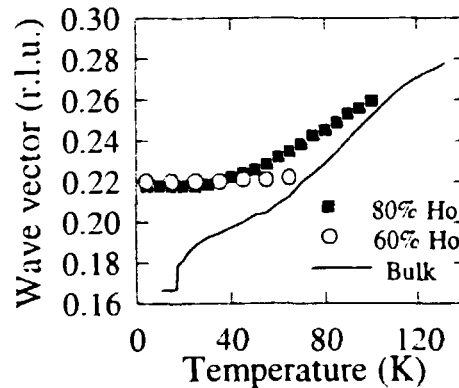


Fig. 1. The temperature dependence of the magnetic wave vector in a series of Ho/Pr alloys.

For the samples with the Sm crystal structure magnetic peaks are detected at $(0,0,5/3)$, $(1,0,1/9)$, $(1,0,5/9)$, and $(1,0,7/9)$ using hcp notation. There is no temperature dependence of the wave vectors, and these features are consistent with a magnetic structure comprising ferromagnetic c -planes in the sequence $0 + + 0 - - 0 + + \dots$. This is therefore very similar to the magnetic ordering of the hexagonal sites in Sm, except that in the case of Ho the moments are confined to the basal plane. The Néel temperatures were found to be $T_N = 40$ and 30 K for $x = 0.5$ and 0.4 respectively. Despite exhaustive searches in a variety of scans along $[0\ 0\ 1]$, $[1\ 0\ 0]$ and $[\bar{1}\ 2\ 0]$ directions no magnetic ordering could be detected down to $T=1.8$ K in the dhcp ($x=0.2$) sample. This suggests that Ho may have a singlet ground state.

2.2.9 The Magnetic Structure of Ho/Lu Superlattices and Alloys

P.P. Swaddling, R.A. Cowley, R.C.C. Ward, M.R. Wells, *Oxford Physics, Clarendon Laboratory, UK*, and D.F. McMorrow, *Department of Solid State Physics, Risø National Laboratory, Denmark*

The study of the Ho/Lu system represents the next step in our systematic study of the magnetism of rare-earth superlattices. In our previous neutron scattering study of Ho/Y¹⁾ we observed that the magnetic helix found in bulk Ho was able to propagate coherently through non-magnetic Y spacer layers for spacers as thick as 150 Å, in agreement with earlier observations on the Dy/Y system²⁾. In addition, at low-temperatures the Ho magnetic moments were found to adopt spin-slip structures not found in the bulk. It was natural to extend this work to Ho/Lu, as epitaxy of the two materials requires that the Ho undergoes a compressive rather than tensile distortion in the basal plane, and Lu has been shown to have a weaker peak in its conduction electron susceptibility than Y.

When interpreting the data from such studies it is essential to be able to compare the behaviour of the superlattice with the corresponding alloy system, and hence we also performed neutron scattering measurements on the Ho/Lu system. All of the samples used in this work were produced using the MBE facilities in the Clarendon Laboratory, Oxford. The neutron scattering experiments were performed using the TAS1 and TAS6 spectrometers at DR3.

One of the main findings of this work is the observation of a novel ferromagnetic phase of Ho at low temperatures in samples with twenty atomic planes or fewer of Ho. This is illustrated in Fig. 1 which shows the neutron scattering from a Ho₂₀Lu₁₅ superlattice. Above 25 K the scattering can be accounted for by a model in which the Ho moments form a coherent spiral (as shown by the solid line in the left panel), but below this temperature the scattering changes dramatically. The intensity in the helical sidebands drops and a new peak appears near $Q=2.2 \text{ \AA}^{-1}$. Subtraction of the high temperature data reveals that the Ho moments within a single block are ferromagnetically coupled, and that adjacent blocks couple into a complex four block antiferromagnetic structure.

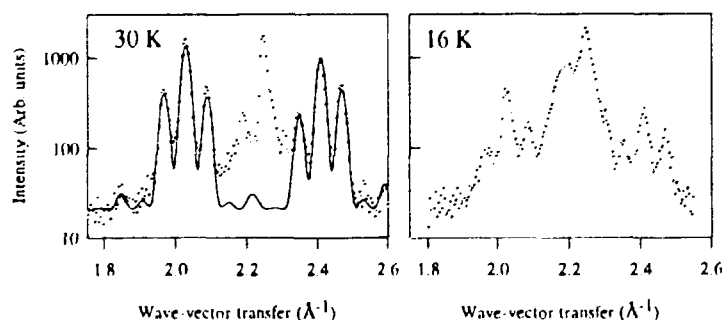


Fig. 1. The neutron diffraction observed from a Ho₂₀Lu₁₅ superlattice at 30 K and 16 K. Note the increase of the scattering near $Q=2.2 \text{ \AA}^{-1}$ on cooling.

¹⁾ D.A. Jehan *et al.*, Phys. Rev. B **48**, 5594 (1993).

²⁾ M.B. Salamon *et al.*, Phys. Rev. Lett. **56**, 259 (1986).

2.2.10 Novel Magnetic Structures of Epitaxial Nd/Y Systems

B.A. Everitt, M.B. Salamon, B.J. Park, C.P. Flynn, *U. of Illinois at U.-C., USA*, J.A. Borchers, R.W. Erwin, *NIST, Gaithersburg, MD, USA*, D. F. McMorrow, *Department of Solid State Physics, Risø National Laboratory, Denmark*, J.J. Rhyne, *MURR, Columbia, MO, USA*

We report new results for an epitaxial superlattice and an alloy consisting of the light rare earth Nd and non-magnetic Y. Bulk Nd exhibits complex magnetic order below ≈ 20 K in zero-field¹⁾; the moments are in the basal-plane and undergo a full sinusoidal modulation which is described by up to four wave vectors and exhibits at least four magnetic phases. The Nd in epitaxial Nd/Y superlattices orders strikingly differently from that of bulk.

We have studied the superlattice $[\text{Nd}(115\text{\AA})|\text{Y}(20\text{\AA})]_{80}$ using the Risø TAS1 spectrometer in the scattering geometry $a^* - b^*$, which affords good resolution throughout the basal-plane. Neutron diffraction scans about (100) revealed that the hexagonal-site ordering is single- q at 5K, instead of the multi- q magnetic structure found in bulk Nd. The magnitude of q varies from $0.128a^*$ at 2K to $0.145a^*$ at 20K, which is somewhat larger than that of the bulk. $T_N \approx 25$ K and is slightly enhanced over that of bulk. Previous studies of epitaxial Nd/Y superlattices performed in the $a^* - c^*$ scattering geometry have shown other differences from bulk behaviour²⁾. Briefly, instead of undergoing a full modulation, the basal-plane moment has a large ferromagnetic component with a small sinusoidal modulation superposed. The multilayers exhibit Néel temperatures which are up to ≈ 40 K larger than the bulk. In addition, the multilayers do not couple through the Y spacer layers along the c -axis, even for Y interlayers as thin as 11 Å. We attribute the differences from bulk behaviour to epitaxial strain rather than the multilayer nature of the samples.

We have also studied a $\text{Nd}_{0.75}\text{Y}_{0.25}$ epitaxial alloy film using the Risø TAS-6 spectrometer. The alloy orders as a simple basal-plane c -axis helimagnet below ≈ 35 K with a temperature-independent turn angle of approximately 60° per atomic layer. No additional or bulk-like ordering was observed at temperatures to 5K. In contrast, previous studies of a series of Nd/Y alloys by Sharif and Coles³⁾ exhibited three anomalies for concentrations in the range 55-100% Nd; the first was above the bulk T_N at temperatures comparable to our observation; two additional lower-temperature anomalies, corresponding to hexagonal and cubic-site ordering, were also observed. While differences are likely due to sample preparation, these results suggest that further study of a series of epitaxial Nd/Y alloys, especially for larger Nd concentrations, would be interesting as well as complimentary to our Nd/Y multilayer work.

¹⁾ B. Lebech, J. Wolny, R.M. Moon, *J. Phys. Condens. Matter* **6**, 5201 (1994).

²⁾ B.A. Everitt, J.A. Borchers, M.B. Salamon, J.J. Rhyne, R.W. Erwin, B.J. Park, C.P. Flynn, *J. Magn. Magn. Mater.*, *accepted*.

³⁾ B. Sharif and B.R. Coles, *J. L. Comm. Met.* **62**, 295 (1978).

2.2.11 Resonant X-Ray Magnetic Scattering from Ho/Pr Alloys

D.F. McMorrow, M. Christensen, S.Aa. Sørensen, R. Feidenhans'l, *Department of Solid State Physics, Risø National Laboratory, Denmark*, M.R. Wells, R.C.C. Ward, *Oxford Physics, Clarendon Laboratory, UK*, G. Helgesen, *IFE, Norway*, A. Vigliante, J. Hill, Doon Gibbs, *Department of Physics, Brookhaven National Laboratory, USA*, and J. Bohr, *Department of Physics, DTU, Denmark*

The x-ray magnetic scattering cross-section has well-defined resonances at atomic absorption edges, and this allows element-specific diffraction experiments to be performed that, in principle, should yield more information than neutron scattering. The rare-earths are particularly well suited to this type of study as their L edges occur around 1-2 Å and produce an \approx fifty-fold enhancement of the magnetic scattering. For the study of thin films the higher resolution offered by x-ray scattering provides a more powerful probe of the chemical structure, and its interaction with the magnetism.

Here we report preliminary results on the $\text{Ho}_x\text{Pr}_{1-x}$ system. Elemental Ho crystallises in the hcp structure and the magnetic moments order into a helix below $T_N=132$ K, whereas Pr adopts the dhcp structure, and as a result of its singlet ground state, does not order until $T_N=50$ mK. There have been few, if any, systematic studies of the interaction between the chemical and magnetic structure of random alloys formed between the heavy and light rare earths. The samples for this study were all grown as thin films using the MBE facilities in the Clarendon Laboratory, Oxford.

To date three alloys have been studied in total, one ($\text{Ho}_{0.6}\text{Pr}_{0.4}$) at beamline X22C, NSLS, and two others ($\text{Ho}_{0.4}\text{Pr}_{0.6}$ and $\text{Ho}_{0.8}\text{Pr}_{0.2}$) at beamline BW2, Hasylab. (A neutron scattering study was also undertaken and is reported elsewhere in the Annual Report.) The preliminary phase diagram is shown in Fig. 1.

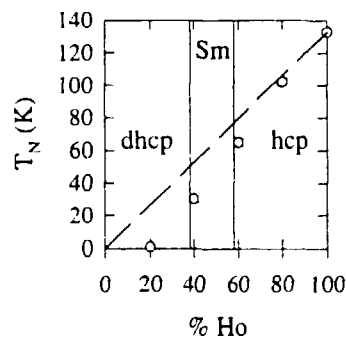


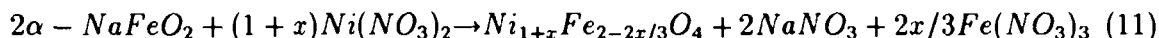
Fig. 1. The phase diagram of $\text{Ho}_x\text{Pr}_{1-x}$ alloys.

The $x=0.8$ sample exhibited an hcp chemical structure, and magnetic scattering at the $L_{III}(\text{Ho})$ edge below ≈ 102 K; we did not find any magnetic scattering at any of the $L(\text{Pr})$ edges down to ≈ 13 K. The $x=0.6$ sample also adopted the hcp structure, and magnetic scattering was observed at both the $L_{III}(\text{Ho})$ and $L_{II}(\text{Pr})$ edges. It appears that the order parameter at $L_{III}(\text{Ho})$ is significantly different from that at $L_{II}(\text{Pr})$. Finally, the $x=0.4$ Ho sample was found to adopt the same crystal structure as Sm, a complex nine-layer stacking sequence, and a similar magnetic structure; q at both $L_{III}(\text{Ho})$ and $L_{III}(\text{Pr})$ was locked to $1/3$ at all temperatures below $T_N=30$ K.

2.2.12 Structural and Magnetic Properties of Ni_{1.3}Fe_{1.8}O₄

M.C. Blesa, U. Amador, E. Morán, *Depto. Q. Inorgánica, Universidad Complutense de Madrid, Spain*, and N.H. Andersen, *Department of Solid State Physics, Risø National Laboratory, Denmark*

Cation exchange may be used on a variety of metal oxides to form new phases where extensive parts of the framework are retained and only minor structural rearrangements take place. This kind of topotactic reactions provide an interesting "soft chemistry" route to obtain new spinel-like ferrites from α -NaFeO₂, which structure is a two-fold superstructure of the NaCl type. Nickel ferrite was obtained by ionic exchange using molten sodium nitrate as reaction medium. The reaction can be schematized as follows:



From chemical analysis the actual composition has been determined to be Ni_{1.3}Fe_{1.8}O₄. The cationic distribution and the magnetic structure have been studied by neutron diffraction using the multi-detector powder neutron diffractometer at the DR3 reactor at Risø National Laboratory. The structural parameters obtained from Rietveld analysis are given in Table I.

Table I: Structural parameters for Ni-Fe spinel-like material.

Atom	Site	x/a	y/b	z/c	Occupation	Biso (Å ²)
Fe1	8a	0.0	0.0	0.0	0.989(4)	0.31(2)
Fe2	16d	5/8	5/8	5/8	0.856(4)	0.36(4)
Ni1	16d	5/8	5/8	5/8	1.144(4)	0.36(4)
Ni2	16c	1/8	1/8	1/8	0.109(4)	0.32(2)
O	32c	u ^{a)}	u	u	4.00(2)	0.37(3)

(a) u=0.3804(1), Composition: Ni_{1.253(8)}Fe_{1.845(8)}O_{4.00(2)}
a=8.3353(3) Å, S.G:Fd3m, Rp=6.18%, Rwp=8.39%, Rexp=4.87%, R_B=4.69%, $\chi^2=2.97$

The crystal structure, which is neither a simple NaCl-type nor a simple spinel-type, has the following characteristics: The 16c positions, which are vacant in the ideal spinel, are partially occupied by nickel, and about 54 % of iron are located in tetrahedral sites, while the rest occupies octahedral positions. These values are in agreement with those obtained by Mössbauer spectroscopy (Fe^{tet} = 57 %, Fe^{oct} = 43 %).

Magnetization curves at room temperature are typical of ferrimagnetic ordering with saturation magnetization M₀ = 1.59 μ_B/f.u. To analyze these data it is assumed that the magnetic structure of the collinear ferrimagnetic spinels is maintained, and the magnetic moments of the extra ions in the 16c positions are antiparallel to those in 16d sites while parallel to those of ions in 8a sites. Based on these assumptions, μ_{NiII} = 2.2μ_B and μ_{FeIII} = 5.9μ_B, and the cationic distributions given in Table I, an estimated moment of 1.62 μ_B/f.u. is obtained, which is in good agreement with the bulk magnetization measurements of 1.59 μ_B/f.u. Refinement of the magnetic structure is in progress in order to confirm these hypotheses.

2.2.13 Effect of Al Doping on the Magnetism of $\text{YBa}_2\text{Cu}_3\text{O}_{6+x}$ Single Crystals

E. Brecht, W.W. Schmahl, H. Fuess, *FB Materialwissenschaft, TH Darmstadt, Germany*, H. Casalta, P. Schleger, B. Lebech, N.H. Andersen, *Department of Solid State Physics, Risø National Laboratory, Denmark*, and Th. Wolf, *ITP, KfK Karlsruhe, Germany*

In order to understand the role of Al on the magnetic properties of YBaCuO , magnetic neutron diffraction studies have been performed on reduced $\text{YBa}_2\text{Cu}_{3-x}\text{Al}_x\text{O}_{6+y}$ single crystals with different Al content x ($0.06 < x < 0.19$) and O content y ($0.18 < y < 0.36$). All crystals showed a transition from the paramagnetic to the AFI phase at $T_N \approx 400$ K. The corresponding cell is doubled in a and b directions and equal to the chemical cell along c, i.e. the moments on the Cu plane sites are antiferromagnetically long range and 3d ordered, while no moment is allowed on the Cu chain sites by symmetry. The moments on nearest neighbor Cu plane layers, which are antiferromagnetically coupled along the tetragonal c axis form an antiferromagnetic bilayer system. The average ordered moment is found to be $0.58(2) \mu_B$ and the spin-direction is lying within the ab plane. These results are similar to those observed in the undoped system.

At low temperatures a complete reordering into a second antiferromagnetic phase AFII occurs at a temperature T_2 . In this phase the cell is doubled in a and b as well as in c direction, with, in contrast to the AFI phase, ferromagnetic coupling of the bilayers along the c axis. The ordered moment of $0.55(2) \mu_B$ found on the Cu plane-sites is similar to that observed for the AFI phase, the spins lie in the ab plane, too. Although a moment on the Cu chain-sites is allowed by symmetry in this phase, no moment is found on these sites within the accuracy of our data, which is in agreement with recent NMR studies.

From our results we find a tendency that T_2 increases with increasing Al content x for the same O stoichiometry. The highest T_2 of 18 K is observed for a crystal with $x=0.19$ and $y=0.36$. Further, crystals, which were reduced under extreme conditions suggesting maximal Al cluster formation during the reduction process, show a decrease of T_2 . Therefore besides the Al content the distribution of Al on the Cu chain sites is also an important parameter effecting the AFII reordering.

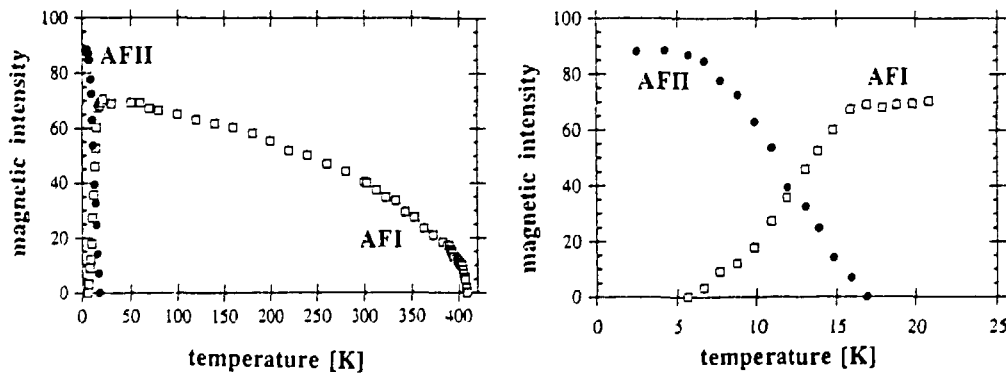


Fig. 1. (Left): Integrated intensity versus temperature of the $(\frac{1}{2}\frac{1}{2}2)$ and $(\frac{1}{2}\frac{1}{2}3)$ magnetic peaks associated with the AFI and AFII phase respectively for $\text{YBa}_2\text{Cu}_{2.81}\text{Al}_{0.19}\text{O}_{6.28}$. The integrated intensity of the $(\frac{1}{2}\frac{1}{2}2)$ magnetic peak shows a power law behavior $I \propto I_0(T_N - T)^{2\beta}$ with a critical exponent $\beta = 0.26(1)$.

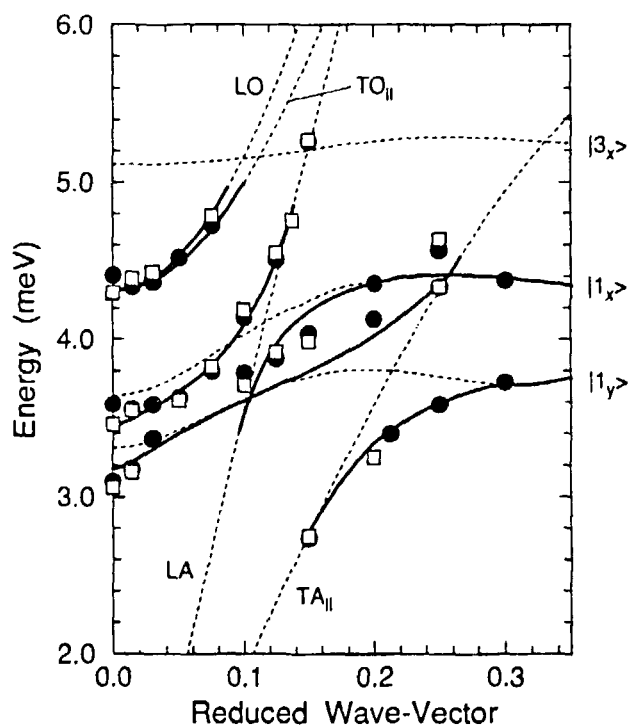
(Right): AFII ordering sets in at ≈ 17 K. In the temperature range between 6 K and 17 K the order parameter shows components of both phases indicating competing interactions. The AFI vanishes completely at $T < 6$ K, while the AFII order parameter saturates.

2.2.14 Crystal Fields and Conduction Electrons in Pr

S. Aa. Sørensen and K.N. Clausen, *Department of Solid State Physics, Risø National Laboratory, Denmark*, K.A. McEwen, *Department of Physics, Birkbeck College, London, UK*, A.R. Mackintosh and J. Jensen, *Niels Bohr Institute, Ørsted Laboratory, University of Copenhagen, Denmark*

The interaction between the crystal-field excitations, the phonons and the conduction electrons in Pr has been studied by inelastic neutron scattering. The low energy satellite to the crystal-field excitation, which is believed to be associated with propagating paramagnon modes of the conduction electron gas¹⁾, is quenched by a magnetic field which also introduces strong hybridisation with the phonons. The standard model of rare earth magnetism does not account for the satellite excitations, as they are quenched by increasing the field, but it gives an increasingly good prediction of the excitation spectrum, as illustrated in fig. 1. Furthermore, even though the energy-dependence of the magnetic scattering at small q and field is highly anomalous, the decrease in the total scattering with field is well described by the standard model, as is the q -dependence at different fields.

Fig. 1 The dispersion relations for excitations propagating in the b -direction at 4.2 K in a field of 45 kOe. The closed circles and open squares (0,0,4) and (0,0,2) respectively. The dashed and the solid line are the results of the standard model without and with magnetoelastic interactions.



¹⁾ K.N. Clausen, K.A. McEwen, J. Jensen and A.R. Mackintosh, *Phys. Rev. Lett.* **72**, 3104 (1994).

2.2.15 Energy-gap of Magnetic Fluctuations in UPd_2Al_3

T. Petersen, *Department of Solid State Physics, Risø National Laboratory, Denmark*, T. Mason *Department of Physics, University of Toronto, Canada*, G. Aeppli, A.P. Ramirez, E. Bucher, and R.N. Kleiman, *AT&T Bell Laboratories, USA*

The antiferromagnetic superconductor UPd_2Al_3 is one of the few existing systems where the magnetic fluctuations of heavy fermion materials can be studied and thus provides us with a unique opportunity to experimentally study the magnetic dynamics of this class of materials.

For momentum exchanges close to the antiferromagnetic ordering wave-vector $(00\frac{1}{2})$ a pronounced difference is seen between spin-waves directed along the c^* axis and those modulating the order in the hexagonal basal plane. The left panel of Fig 1 shows a series of high resolution scans taken for momentum transfers $\vec{q} = (hhl)$ in the region $-0.15 \leq h \leq 0.15$ and $0.4 \leq l \leq 0.6$ with an energy transfer of $\epsilon = 2.0\text{meV}$. A scan with fixed hk and varying l yields a well defined double peak, while the converse gives an unstructured and wider peak, corresponding to a larger dissipation of the spin-waves. A similar anisotropy is seen in the heavy fermion antiferromagnet URu_2Si_2 ¹⁾.

Examining the magnetic fluctuations at the antiferromagnetic ordering wave-vector $(00\frac{1}{2})$ as a function of the energy transfer we observe an intensity approximately proportional to the reciprocal of the energy transfer. If a spin-wave gap was present, as in almost all other known antiferromagnetic uranium compounds, the amplitude should drop to zero at low energies. We find that the reciprocal relationship holds down to at least 0.5meV suggesting that any gap would have a size much smaller than this.

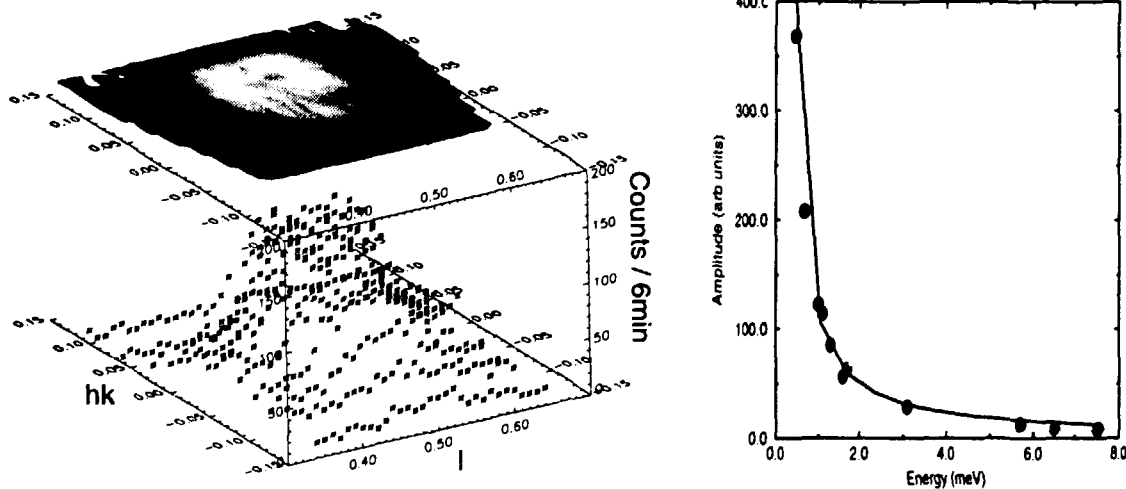


Fig. 1. Left: Constant energy scans at $\epsilon=2.0\text{meV}$ and $T=4.2\text{K}=0.30\times T_N$. Right: Amplitude of magnetic fluctuations as a function of energy exchange corrected for line-shape and resolution effects.

¹⁾ C. Broholm, H. Lin, P.T. Matthews, T. Mason, W.J.L. Buyers, M.F. Collins, A.A. Menovsky, J.A. Mydosh and J.K. Kjems, *Phys. Rev. B* **43**, 12809 (1991).

2.2.16 Quadrupolar Order in UPd₃

K.A. McEwen, *Department of Physics, Birkbeck College, University of London, UK*, U. Steigenberger, *ISIS Facility, Rutherford Appleton Laboratory, Didcot, UK*, K.N. Clausen, *Department of Solid State Physics, Riso National Laboratory, Denmark*, C. Kappler, and M.B. Walker, *Department of Physics, University of Toronto, Canada*

UPd₃ exhibits phase transitions at $T_1 \approx 7$ K and $T_2 \approx 5$ K. Polarised neutron diffraction measurements¹⁾ showed that a *structural* modulation with wavevector (1/2,0,0) takes place below T_1 . We have recently made a more detailed neutron diffraction study of this phase. From a group theory analysis of our results, we conclude that the ordered phase below T_1 is a triple- q antiferroquadrupolar structure involving Q_{zz} , Q_{xz} and $Q_{x^2-y^2}$ quadrupole moments of the uranium ions (See Fig. 1). The associated ionic displacements produce the structural modulation of the dhcp structure of UPd₃.

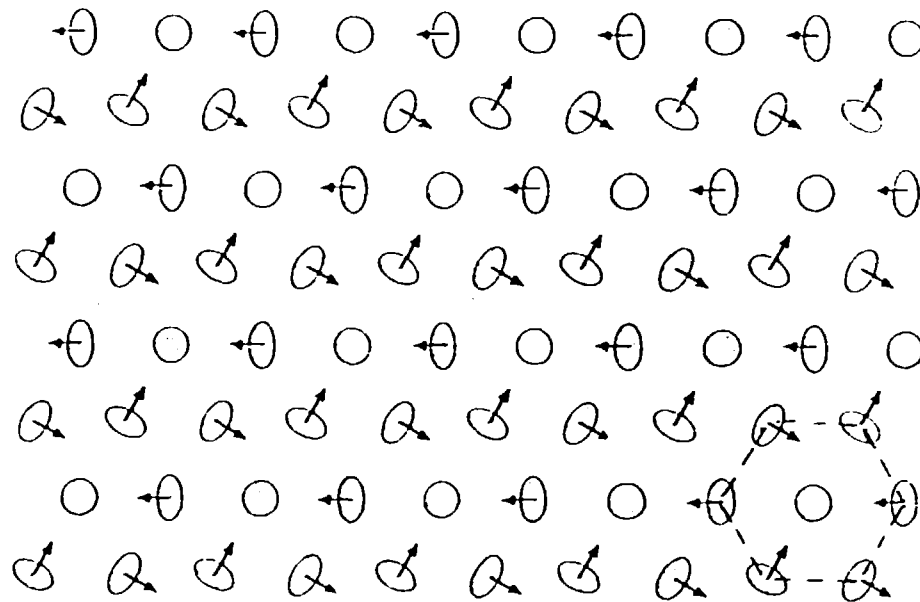


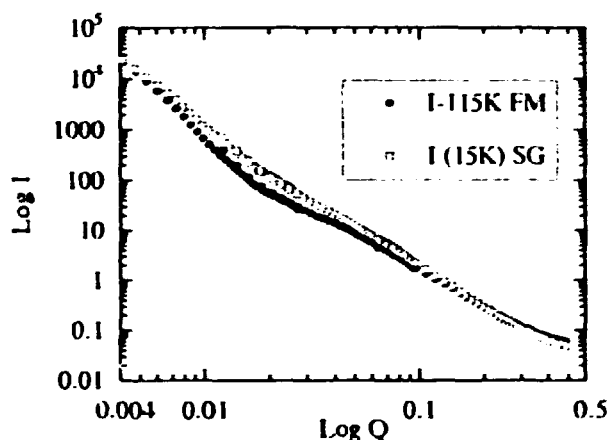
Fig. 1. Basal plane projection of the antiferroquadrupolar structure of the cubic sites below T_1 . The triple- q nature of the structure with a doubling of the lattice unit cell can be readily seen. There is a combination of quadrupole moments of the type $Q_{x^2-y^2}$, Q_{xz} and Q_{zz} . The uranium ions have a spheroidal charge distribution around the c -axis due to the Q_{zz} quadrupole moment. The figure shows the ellipsoidal charge densities associated with the $Q_{x^2-y^2}$ quadrupole moment. These are tilted either clockwise or anticlockwise around the arrows to give a Q_{xz} component. For the hexagonal sites only Q_{xz} and Q_{zz} moments are present.

¹⁾ U. Steigenberger, M.B. Walker *et al.*, *J. Magn. Magn. Mat.* **108**, 163 (1991).

2.2.17 Structural and Magnetic Small-Angle Neutron Scattering Study of $\text{Fe}_{90-x}\text{Zr}_{10+x}$ Amorphous Ribbons

L. Fernández Barquin, J.C. Gomez Sal, *Universidad de Cantabria, Santander, Spain, S.N. Kaul, University of Hyderabad, India, and J. Skov Pedersen, Department of Solid State Physics, Riso National Laboratory, Denmark*

The magnetic phase diagram in Fe-Zr (Fe-rich) amorphous alloys presents different magnetic states giving rise to controversial results in the recent years¹⁻³). To explain these behaviours, several explanations have been put forward, dealing some of them with the existence of spin clusters (Antiferromagnetically (AFM)¹) or Ferromagnetically (FM) coupled³) in a ferromagnetic matrix. It is straightforward that performing a complete SANS experiment with and without magnetic field would evidence directly the nature of clusters and their behaviour with temperature and field. For this purpose, we have performed SANS experiments without field between 15 and 300 K for a $\text{Fe}_{91}\text{Zr}_9$ sample, covering a lower Q range than previous measurements⁴) which can complete the previous ones (which are analysed together with the present ones). Our results show that there exist three humps in the $I(Q)$ curves at different Q regions, especially in the FM range. Plotting the results in $1/I(Q)$ vs. Q^2 (Lorentzian (L) shape of $I(Q)$) results in a deviation from any overall linear behaviour. In addition, from $1/Q$ vs. T plots it is difficult to state that there is not a divergence at T_c (and thus ruling out a ferromagnetic behaviour of these alloys⁵); a study sweeping carefully the temperature region around the Curie temperature would be necessary to be more conclusive. To account for the whole $I(Q)$ curve, it is also evident that the usual $L+L^2$ expression for ferromagnetic materials⁶) is not enough. Accordingly, we have tried preliminarily $L+L^2+L^3$ with good results. Plots of $I(T)$ versus T for different Q values show a continuous increase of the intensity when the alloy is cooled down below 100 K. At $T = 205$ K, a peak corresponding to the FM-PM transition is observed. So far, we cannot give further conclusions as in-field measurements are completely necessary to elucidate the behaviour of the clusters.



- ¹) N. Saito, H. Hiroyoshi, K. Fukamichi, and Y. Nakagawa, *J. Phys. F* **16**, 911 (1986).
- ²) D.H. Ryan, J.M.D. Coey, E. Batalla, Z. Altounian, and J.O. Ström-Olsen, *Phys. Rev. B* **35**, 8630 (1987).
- ³) S. N. Kaul, V. Siruguri, and G. Chandra, *Phys. Rev. B* **45**, 12343 (1992).
- ⁴) L. Fernández Barquin, J.C. Gomez Sal, and R. Heenan, *ISIS Exp. Rep.* A372 (1994).
- ⁵) J.J. Rhyne, R.W. Erwin, J.A. Fernandez-Barca, and G.E. Fish, *J. Appl. Phys.* **63**, 4080 (1988).
- ⁶) G. Acpli, S.M. Shapiro, R.J. Birgeneau, and H.S. Chen, *Phys. Rev. B* **28**, 5160 (1984).

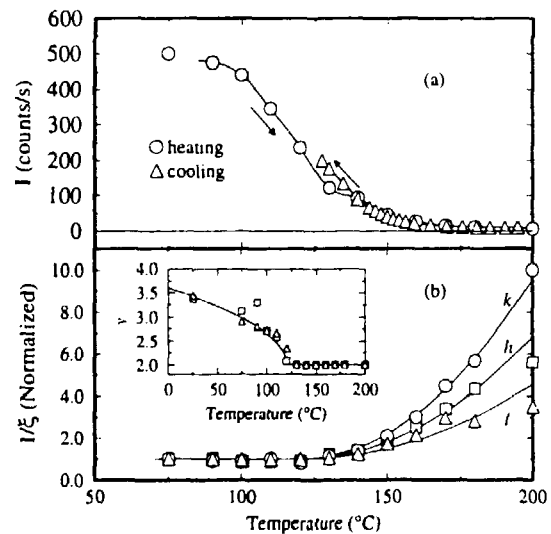
2.3 Superconducting Materials and Phenomena

2.3.1 Random-Field Structural Transition in $\text{YBa}_2\text{Cu}_3\text{O}_{6+x}$

P. Schleger, R.A. Hadfield, H. Casalta, N.H. Andersen, *Department of Solid State Physics, Risø National Laboratory, Denmark*, H.F. Poulsen, M. von Zimmermann, J.R. Schneider, *HASYLAB at DESY, Hamburg, Germany*, P. Dosanjh, Ruixing Liang, *Quantum Innovations, P.O. Box 78512, Vancouver, B.C. Canada*, and W.N. Hardy, *Department of Physics, The University of B.C., Vancouver, B.C., Canada*

Neutron and synchrotron x ray diffraction measurements on a high purity single crystal reveal that the absence of long range Ortho-II order in $\text{YBa}_2\text{Cu}_3\text{O}_{6+x}$ is most likely due to random-field effects. The Ortho-II superstructure peaks show three qualitative features consistent with random-field behavior: Firstly, instead of the development of a sharp Bragg peak at the transition $T_{\text{OII}}=125(5)$ °C (for $x=0.5$), the initial diffuse anisotropic Lorentzian (critical scattering) above T_{OII} transforms to a Lorentzian-squared form below T_{OII} (Fig. 1). Secondly, the equilibration time increases dramatically *at the onset* of ordering. And thirdly, the domain growth is logarithmic in time below T_{OII} . The neutron scattering measurements were conducted on TAS1, TAS6, and TAS7 at Risø. The x-ray scattering measurements were made on the newly developed, dedicated hard x-ray beam line BW5 at HASYLAB using 95 keV x-rays.

Fig. 1. Plot of the fitted Ortho-II superstructure peak intensity (a), inverse correlation length (b) and power law exponent y of the peak shape (inset) vs temperature T . The measured intensity S was fitted using a Lorentzian to a variable power: $S(q) = I/(1 + (\tilde{q})^2)^{y/2}$. Here I is the peak intensity, \tilde{q} is the deviation from the Ortho-II reciprocal lattice position, rescaled by the anisotropic correlations ξ , i.e. $\tilde{q} = 2\pi(\xi_a h, \xi_b k, \xi_c l)$. y is the power law exponent. Shown here are the fits to the x-ray scattering measurements. The neutron scattering data is qualitatively similar, but with somewhat worse counting statistics. More information is given in Ref. 1.



The origin for the random fields might be extrinsic, coming from cation substitutional defects or intrinsic, due to anisotropic strain fields caused by the ordering of the oxygen atoms themselves and the accompanying atomic displacements of the other atoms within the Ortho-II unit cell¹⁾. Indeed, the defect concentration estimated from chemical analysis is consistent with the typical Ortho-II correlation lengths (or volume) measured in well annealed samples. However, more work is required to clearly identify the source of the random fields.

¹⁾ P. Schleger, R.A. Hadfield, H. Casalta, N.H. Andersen, H.F. Poulsen, M. von Zimmermann, J.R. Schneider, P. Dosanjh, Ruixing Liang, and W.N. Hardy, (1994). *Phys. Rev. Lett.*, *accepted*.

2.3.2 Observation of Ortho-III Correlations by Neutron and Hard X-Ray Diffraction in an Untwinned $\text{YBa}_2\text{Cu}_3\text{O}_{6.77}$ Single Crystal

P. Schleger, H. Casalta, R. Hadfield, N.H. Andersen, *Department of Solid State Physics, Risø National Laboratory, Denmark*, H.F. Poulsen, M. von Zimmermann, J.R. Schneider, *HASYLAB at DESY, Germany*, R. Liang, P. Dosanjh, and W. Hardy *Physics Department, University of British Columbia, Canada*

Superstructure reflections of Ortho-III phase oxygen ordered domains have been measured in an untwinned single crystal of $\text{YBa}_2\text{Cu}_3\text{O}_{6.77}$ by neutron diffraction at Risø National Laboratory and hard x-ray (95 keV photons) diffraction at HASYLAB. A high purity single crystal, ($2.8 \times 3.5 \times 0.8 \text{ mm}^3$), was deoxidized at high temperatures and slowly cooled to room temperature while maintaining the oxygen stoichiometry. A uniaxial pressure device was inserted and used to obtain a virtually twin-free single crystal on cooling through the tetragonal-orthorhombic phase transition. The problem of resolving the two close lying peaks along the k direction, that appear in twinned crystals is hereby avoided.

The Ortho-III phase contains a sequence of two Cu-O chains and one chain with only Cu along the b axis which results in a tripling of the unit cell along the a axis and a modulation vector $(\frac{1}{3}00)$ as exemplified by the h scan through the $(\frac{2}{3}00)$ peak shown in Fig. 1. No superstructure peaks corresponding to Ortho-II phase was observed. The superstructure reflections are broadened along all three crystallographic directions due to the finite size of the Ortho-III domains. The peak shapes along the h and k directions could be properly described by a Lorentzian profile convoluted with a Gaussian resolution function. The corresponding correlation lengths, measured in lattice units at room temperature: $\xi_a = 5.0(1)$ and $\xi_b = 18.7(7)$, are comparable to characteristic values obtained for the Ortho-II phase. In the c direction strongly overlapping peaks were observed, indicating that the oxygen ordering is essentially two-dimensional. Upon heating, the superstructure intensity was found to decrease rapidly by temperature above 50 °C signaling a transition from Ortho-III to Ortho-I phase as shown in Fig. 2. A heating rate of approximately 2.5 °C was employed. Upon cooling to 50 °C at the same rate the original intensity was recovered. The low transition temperature explains why this phase is more difficult to observe than other superstructures in the material.

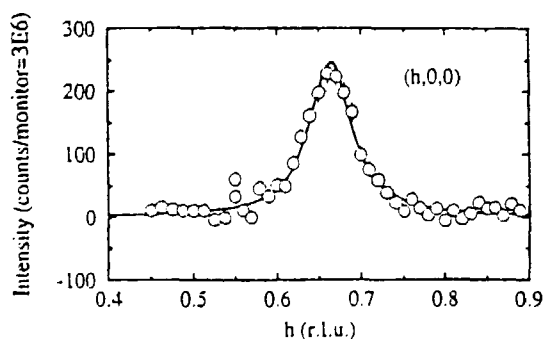


Fig. 1. Room temperature neutron diffraction measurement of the Ortho-III superstructure peak $(\frac{2}{3}00)$ in the h direction. The line is a fit using a Lorentzian-Gaussian convolution. The resolution is smaller than the size of the symbols.

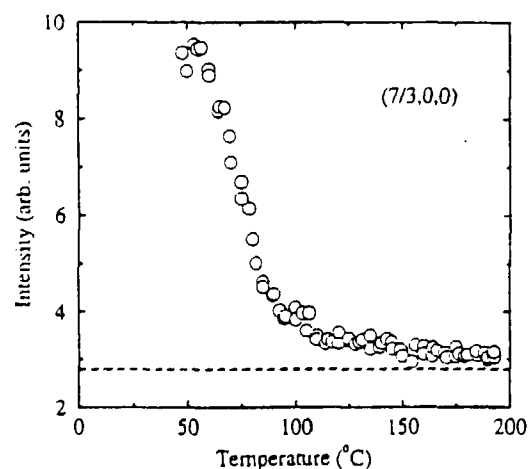


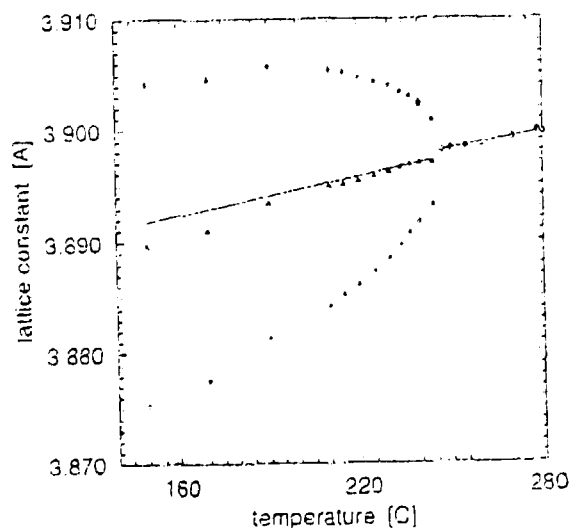
Fig. 2. Temperature dependence of the $(\frac{7}{3}00)$ superstructure peak measured on heating by hard x-ray diffraction. Dashed line is the background.

2.3.3 Structural Phase Transitions in $\text{YBa}_2\text{Cu}_3\text{O}_{6.37}$ Studied by Hard X-Ray Diffraction

H.F. Poulsen, M. von Zimmermann, J.R. Schneider, *HASYLAB at DESY, Germany*, P. Schleger, R. Hadfield, H. Casalta, N.H. Andersen, *Department of Solid State Physics, Risø National Laboratory, Denmark*, R. Liang, P. Dosanjh, and W. Hardy, *Physics Department, University of British Columbia, Canada*

The equilibrium and dynamic structural properties of an $\text{YBa}_2\text{Cu}_3\text{O}_{6+x}$ single crystal has been studied as function of temperature in the interval between 0 and 300 °C at the BW5 Wiggler beamline at HASYLAB (95 keV photons). The twinned $3 \times 3 \times 0.6 \text{ mm}^3$ crystal was initially annealed for six weeks in order to make the oxygen concentration homogeneous. The stoichiometry was determined to be $x=0.37(2)$ using the TAS2 4-circle neutron diffractometer at Risø National Laboratory. It was shown explicitly that the oxygen diffusion into/out of the crystal is negligible at the chosen temperatures. All measurements were therefore done in an inert gas environment. Two nearly reversible phase transitions were found: Ortho-II to Ortho-I (OII/OI), and Ortho-I to tetragonal (OI/T). The equilibrium behaviour of the former was found by measuring the intensity of the (2.5,0,0) Ortho-II superstructure peak, while the latter was characterized by measuring the lattice constants of the (200)/(020) pair of reflections (the orthorhombicity) using a set-up with a longitudinal resolution of $2 \times 10^{-4} \text{ \AA}^{-1}$. The determined phase transition temperatures are 80(10) °C and 246.5 °C for OII/OI and OI/T, respectively. In contrast to this, nearly all theoretical models (including the prevalent ASYNNI model) predicts a single OII/T phase transition with no Ortho-I phase in between at these temperatures. The detailed behaviour of the lattice constants near the OI/T transition is shown in Fig. 1. Evidence for a small first order transition is found (no detectable hysteresis). Using a conventional scaling ansatz the critical parameter β was found to be 0.36(1) on heating and 0.33(1) on cooling. Both values are in agreement with the expected value for a 3 dimensional Ising model, provided the coupling between strain and true order parameter is linear. Quench experiments from 300 °C showed near instantaneous creation of the Ortho-I phase (no phase separation) for temperatures well below 246.5 °C, while slow dynamics - reminiscent of tweed behaviour - was found close to the transition temperature.

Fig. 1. Lattice constants as function of temperature on heating. Full circles and open circles refer to the orthorhombic and tetragonal phase, respectively. Triangles represent the average of the two lattice parameters in the orthorhombic phase. Lines are guide to the eye only.



2.3.4 Influence of Al Doping on the Structural Properties of Al Doped $\text{YBa}_2\text{Cu}_3\text{O}_{6+x}$ Single Crystals

E. Brecht, W.W. Schmahl, H. Fuess, *FB Materialwissenschaft, TH Darmstadt, Germany*,
N.H. Andersen, *Department of Solid State Physics, Risø National Laboratory, Denmark*,
Th. Wolf, *ITP, Kernforschungszentrum Karlsruhe, Germany*

It is well known that doping of $\text{YBa}_2\text{Cu}_{3-x}\text{M}_x\text{O}_{6+y}$ with trivalent ions such as Fe^{3+} , Co^{3+} or Al^{3+} on the Cu(1) chain sites leads to a decrease of the orthorhombic long range order and causes a structural change from orthorhombic to a macroscopic tetragonal symmetry at a doping concentration x of about 0.09. However, these macroscopic tetragonal symmetry is related to small orthorhombic domains, which lead to a tweed-like contrast in TEM images.

In order to understand the role of Al on the structural properties in these compounds, we investigated single crystals with an Al content x of 0.19 by XRD, TEM and neutron diffraction. The as prepared crystals are tetragonal with a mean twin-domain size of about 5 nm. In x-ray single crystal studies we find an oxygen content $y < 1$ in the basal plane for these samples, which is in confirmation with theoretical calculations performed by Andersen *et al.*¹⁾ Neutron diffraction studies are in progress, in order to obtain the oxygen content more properly.

Reduction of these crystals at $T \approx 1073$ K and low oxygen partial pressure and reoxidation at $T \approx 623$ K lead to a change from tetragonal to orthorhombic symmetry. This structural change is related to the Al ions forming clusters during the reduction process. Since the reoxidation is performed at low temperatures, where the Al is not mobile, the orthorhombic order increases, which is related to the fact, that the defect-density decreases by the cluster formation.

The structural properties of crystals which were reduced under extreme conditions ($T_R = 1073$ K, $p(\text{O}_2) \leq 10^{-5}$) in order to get them as oxygen depleted as possible, were studied by neutron diffraction. The Al is found to enter only Cu(1) lattice sites. The oxygen content y in the basal plane is refined to 0.25. The oxygen cannot be removed completely from this basal plane, since the Al^{3+} is higher coordinated than the Cu^{1+} . Considering the Al content of $x=0.19$, each Al is therefore surrounded by about 5/4 oxygen neighbors in this plane. Under the assumption, that the Al ions are clustered, one O per Al in the basal plane would be expected for a tetrahedral coordination, whereas two Al are needed for an octahedral coordination. From our present data, an octahedral coordination can therefore be ruled out, whereas a tetrahedral coordination, which is very common in minerals, is more likely.

Since this situation is not yet fully clear, structural studies of the reoxidized, orthorhombic crystals may gain more information about the clustering of the Al ions and their coordination.

¹⁾ J.V. Andersen, N.H. Andersen, O.G. Mouritsen, and H.F. Poulsen, *Physica C* **214**, 143 (1993)

2.3.5 Oxidation Kinetics of $\text{YBa}_2\text{Cu}_3\text{O}_{6+x}$ at Relatively Low Temperature

Hae Seop Shim, *Korea Atomic Energy Research Institute, Taejon, Korea*, N.H. Andersen and B. Lebech, *Department of Solid State Physics, Risø National Laboratory, Denmark*

It is now well known that the superconducting and magnetic properties of $\text{YBa}_2\text{Cu}_3\text{O}_{6+x}$ depend on the oxygen stoichiometry ($0 < x < 1$). The superconducting phase, ($x > 0.3$), has an orthorhombic structure with the oxygen in the basal plane ordered as Cu-O chains along the b axis. The magnetic (non-superconducting) phase, ($x < 0.3$), has a tetragonal structure with disordered oxygen in the basal plane. Therefore, a detailed knowledge of the kinetics of the disorder-order process associated with oxidation will give useful information for the preparation of this high- T_c materials and for a better understanding of the phase properties. Specht *et al.*¹⁾ reported that the structural changes under the oxygen in-diffusion process at 385°C was completed within 2 hours. Als-Nielsen *et al.*²⁾ have studied the oxidation kinetics at 110°C , 165°C and 252°C . They observed the coexistence of orthorhombic and tetragonal phase and different transformation levels depending on temperature. These properties have been examined further in the present study. Oxidation studies have been performed on-line on the multi-detector neutron powder diffractometer at TAS3 on a powder sample mounted in a furnace and purged by pure oxygen. The starting material was reduced under a N_2 flow at 705°C . By Rietveld full profile analysis of the diffraction data an oxygen stoichiometry of $x = 0.29$ was found. Measurements of the oxidation kinetics were performed at constant temperatures, 105°C and 125°C . During oxidation, powder patterns were measured with time intervals of 2.7 hours using a neutron wavelength of $\lambda = 2.34 \text{ \AA}$. Hereby the tetragonal: $(200)_t$, and the orthorhombic $(200)_o$ and $(020)_o$ peaks could be resolved. Figure 1 shows the changes in the intensities of the $(200)_t$, and the sum $(200)_o + (020)_o$ with respect to time for the data measured at 105°C . Full profile Rietveld analysis of diffraction data obtained at the late state of the oxidation process showed that the tetragonal component had oxygen stoichiometry, $x = 0.29$, and the orthorhombic component, $x = 0.88$.

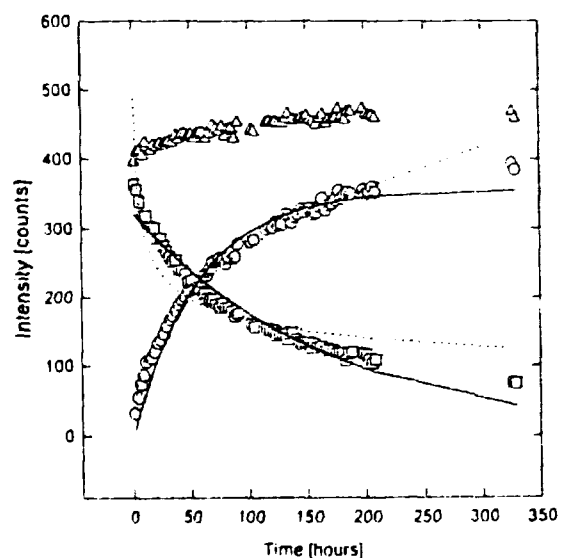


Fig. 1. Variation of the $(200)_t$, (\square), and the $(200)_o + (020)_o$, (\circ), diffraction intensities with time. The sum of the two intensities, (\triangle) should be essentially constant. The data cannot be fitted satisfactorily neither with an exponential (full line) nor an algebraic (dotted) expression.

¹⁾ E.D. Specht *et al.*, *Phys. Rev. B*, **37**, 7426 (1988).

²⁾ J. Als-Nielsen *et al.*, *IEEE Transactions on Magnetics*, **25**, 2254 (1989).

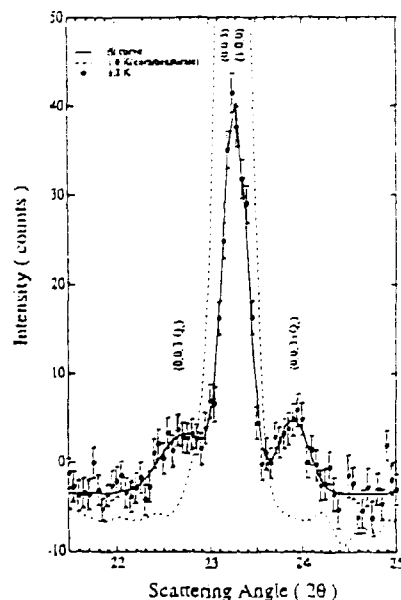
2.3.6 Investigations of the New $\text{RNi}_2\text{B}_2\text{C}$ ($\text{R} = \text{Rare Earth}$) Compounds

C.V. Tomy, L.J. Chang, D. McK. Paul, *Department of Physics, University of Warwick, UK*,
N.H. Andersen, *Department of Solid State Physics, Risø National Laboratory, Denmark*,
and M. Yethiraj, *Solid State Division, Oak Ridge National Laboratory, USA*

The newly discovered quaternary compounds $\text{RNi}_2\text{B}_2\text{C}$ are interesting materials due to their ability to support superconductivity at high temperatures, and the coexistence of this superconducting state with large ordered magnetic moments on the R site. Planar features are observed for the structure of these boron carbides which can be compared to the CuO_2 planes in the high- T_c cuprates. The structure of $\text{RNi}_2\text{B}_2\text{C}$ consists of $\text{Ni}_2\text{-B}_2$ planes separated by R-C planes. The $\text{RNi}_2\text{B}_2\text{C}$ phase can be stabilized for most of the R ions with large magnetic moments. Superconductivity is observed only for the magnetic ions with $\text{R} = \text{Tm}$, Er and Ho, whereas the other R magnetic-ion compounds show ordering of the magnetic moments with weak ferromagnetic nature. Two features clearly indicate the interplay between the tendency to superconducting and magnetic order. Firstly, T_c is reduced as the R ion moment is changed, roughly scaling as the *de Gennes* factor, with a T_c of 15.5 for Y1221, 10 for Er1221, 9 for Ho1221 and no superconductivity for Dy1221. Secondly, the upper critical field H_{c2} is considerably less in the materials containing magnetic ions than for the Y compound, and the H_{c2} curves show anomalies which correspond to the magnetic ordering.

A systematic neutron powder diffraction study has been carried out to establish the nature of the magnetic ordering in these compounds for $\text{R} = \text{Tm}$, Er, Ho and Dy. The most interesting features are observed in the case of $\text{HoNi}_2\text{B}_2\text{C}$. The magnetic ordering sets in at 8.5 K, just below the superconducting transition at 9.5 K, and the magnetic structure contains ferromagnetic planes with an antiferromagnetic modulation of wavelength 136 Å, ≈ 13 unit cells along the c axis. For $5.0 \text{ K} < T < 7.5 \text{ K}$, an additional modulation in the a direction is observed with a wavelength of ≈ 2.4 unit cells. At low temperatures ($T < 5 \text{ K}$), the magnetic order becomes commensurate with ferromagnetic $a - b$ planes antiferromagnetically coupled along the c axis. The exact reason for the additional modulation in the intermediate range is not clear, but it is in this temperature range that the anomalies in the magnetization as well as a near re-entrant behaviour in resistance measurements are observed. Preliminary analysis on the Er1221 compound with $T_c \approx 10 \text{ K}$ shows antiferromagnetic ordering of the Er moments at $\approx 8.5 \text{ K}$, with a modulation of the magnetic ordering along the a axis below T_N . Further analysis of these results, and the data for Dy1221 and Y-substituted Ho and Dy compounds, are in progress.

Fig. 1. Satellite peaks corresponding to a modulation of the magnetic order along the c direction measured at 6.2 K in $\text{HoNi}_2\text{B}_2\text{C}$. The stability range of this modulated phase is $5.0 \text{ K} < T < 8.5 \text{ K}$ as exemplified by the measurements at 1.6 K where the satellite peaks are absent.



2.3.7 Structural and Physical Modifications Induced by Chemical Oxidation of the High- T_c Superconductor $\text{La}_{2-x}\text{Ba}_x\text{CuO}_4$ ($x = 0.115, 0.125, 0.135$)

C. Rial, U. Amador, E. Morán, M.A. Alario-Franco, *Depto. Q. Inorgánica, Universidad Complutense de Madrid, Spain*, and N.H. Andersen, *Department of Solid State Physics, Risø National Laboratory, Denmark*

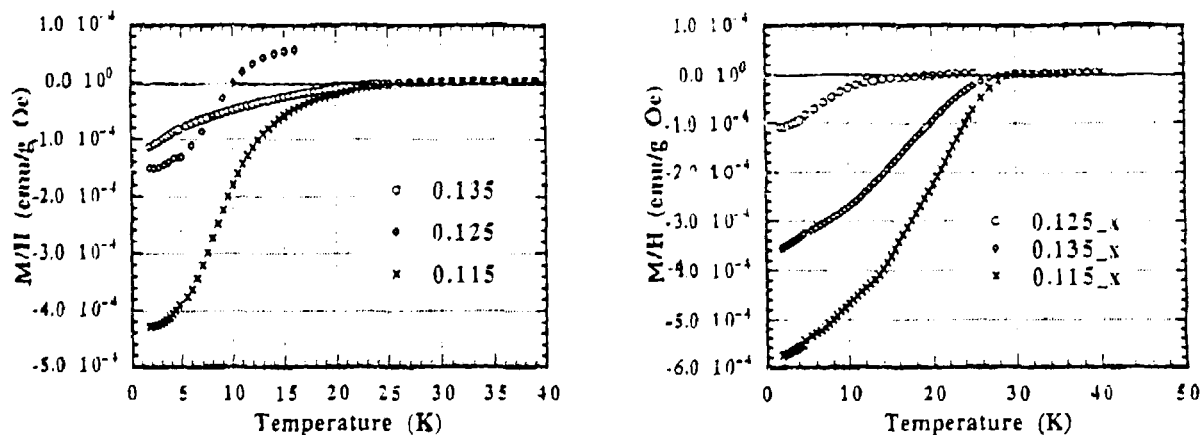
Room temperature chemical oxidation of the above compounds with a hypobromite aqueous solution have been performed. Neutron diffraction experiments using the multi-detector neutron powder diffractometer at the DR3 reactor at Risø National Laboratory, TGA analysis and magnetic susceptibility measurements versus temperature have been carried out. The following preliminary results of the structural and physical changes induced by the oxidation process have been obtained:

Thermogravimetric studies show the presence of extra oxygen in the oxidized samples. The amount of extra oxygen increases with increasing reaction time.

Neutron powder diffraction experiments on the oxidized samples at room temperature, 120 K and 10 K, also show the presence of interstitial oxygen. An important feature is that the oxidized samples do not undergo the structural transitions: $\text{HTT}(\text{F4}/\text{mmm})$ - $\text{LTO}(\text{Bmab})$ - $\text{LTT}(\text{P4}_2/\text{ncm})$ observed by several authors on fresh samples when lowering the temperature. Diffractograms recorded at different temperatures can all be refined with the tetragonal S.G. $\text{F4}/\text{mmm}$ taking into account the presence of orthorhombic anisotropic microstrains. Thus, the structural transitions to the LTO and the LTT phases (which imply tilt of the CuO_6 octahedra) are hindered by the presence of interstitial oxygen.

Susceptibility measurements (see Fig. 1) show that the superconducting transition temperature T_c increases in the oxidized materials, though the properties of the $x = 0.125$ sample show negligible improvement and anomalous behaviour.

Fig. 1. Left: Magnetic susceptibility of standard $\text{La}_{2-x}\text{Ba}_x\text{CuO}_4$. Right: and chemically oxidized $\text{La}_{2-x}\text{Ba}_x\text{CuO}_{4+y}$.



2.3.8 Structural Study of $\text{LnBaCuFeO}_{5+\delta}$, ($\text{Ln} = \text{Y}, \text{Pr}$)

M.J. Ruiz-Aragon, U. Amador, E. Morán, *Depto. Q. Inorgánica, Universidad Complutense de Madrid, Spain*, and N.H. Andersen, *Department of Solid State Physics, Risø National Laboratory, Denmark*

The structure of the above materials is closely related to that of the high- T_c superconductor $\text{YBa}_2\text{Cu}_3\text{O}_{6+x}$. It can be described as an oxygen-deficient two-fold perovskite superstructure with double layers of squared pyramids $[\text{BO}_5]$ sharing apical oxygen, where Ba^{2+} ions occupy the perovskite cuboctahedral A position and Y^{3+} is located in between the layers. However, there is some controversy about the B positions, and there is no definite model for the magnetic structure.

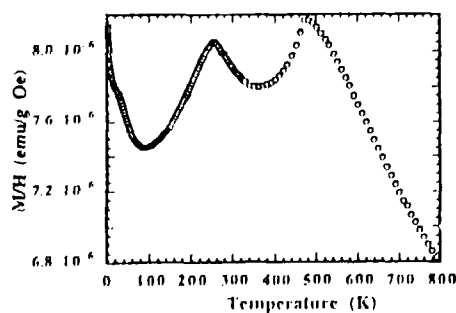
Materials were prepared by the "nitrate method". Neutron diffraction was performed at different temperatures on the multi-detector powder-diffractometer at the DR3 reactor at Risø National Laboratory. Refinements of the neutron diffraction data were first made with space group P4mmm, but the best results were obtained using P4/mmm. In this model iron and copper occupy one crystallographic position, being randomly distributed in the two equivalent $[\text{BO}_5]$ layers. Table I collects the structural parameters for PrBaCuFeO_y and YBaCuFeO_y at room temperature. It is worth noting that some extra oxygen ($\delta = 0.24(1)$) is found at $(\frac{1}{2}\frac{1}{2}\frac{1}{2})$ in the Pr-containing material, but not in the Y-material.

Table I. Structural parameters for $\text{PrBaCuFeO}_{5.24(1)}$ ("PBCF") and YBaCuFeO_5 ("YBCF") at 298K.
PrBaCuFeO_{5.24(1)}; S.G: P4/mmm, $a_N=3.9246(2)\text{Å}$, $c_N=7.7632(4)\text{Å}$, $V=119.6(1)\text{Å}^3$, $R_p=8.2\%$, $R_w=10.5\%$, $R_N=7.3\%$, $R_{\text{exp}}=4.4\%$, $\chi^2=5.8$
YBaCuFeO₅; S.G: P4/mmm, $a_N=3.8736(2)\text{Å}$, $c_N=7.6637(3)\text{Å}$, $V=115.0(1)\text{Å}^3$, $R_p=7.5\%$, $R_w=10.5\%$, $R_N=9.3\%$, $R_{\text{exp}}=4.7\%$, $\chi^2=10.6$.

ATOM		SITE	x/a	y/b	z/c		Occ.		$B_{\text{eq}}/\text{Å}^2$	
YBCF	PBCF				YBCF	PBCF	YBCF	PBCF	YBCF	PBCF
Ba		1a (4/mmm)	0	0	0	0	1		0.77(8)	0.66(8)
Y	Pr	1b (4/mmm)	0	0	1/2	1/2	1	1	0.20(3)	0.26(9)
Cu		2h (4mm)	1/2	1/2	0.2679(2)	0.2588(2)	1		0.33(3)	0.20(3)
Fe		2h (4mm)	1/2	1/2	0.2679(2)	0.2588(2)	1		0.33(3)	0.20(3)
O(1)		1c (4/mmm)	1/2	1/2	0	0	1		1.1(1)	0.96(9)
O(2)		4i (2mm)	1/2	0	0.3153(2)	0.2981(2)	4		0.57(2)	0.97(6)
O(3)		1d (4/mmm)	1/2	1/2		1/2	0.24(1)			0.96(9)

Interestingly enough, the $\text{PrBaCuFeO}_{5.24}$ sample shows no magnetic peaks at room temperature while YBaCuFeO_5 is antiferromagnetically ordered with a Néel temperature of about 490, a magnetic unit cell: $a_M = b_M = \sqrt{2}a_N$, $c_M = 2c_N$ and a propagation vector $(\frac{1}{2}\frac{1}{2}\frac{1}{2})$. A second magnetic phase transition at about 250 K has been found, as can be seen in Fig. 1, and at low temperature (≈ 22 K) an abnormal behaviour of the magnetic susceptibility has been found. The study of the magnetic structure at different temperatures of YBaCuFeO_5 is in progress.

Fig. 1. Magnetic susceptibility as a function of temperature. Two magnetic phase transitions are observed at 490 K and 250 K. At low temperature (22 K) an abnormal behaviour is evident.



2.3.9 Flux Lattice in the Superconducting Phases of UPt_3

U. Yaron, P. L. Gammel, D. J. Bishop and G. Aeppli, *AT&T Bell Laboratories, USA*, C. Broholm, *Johns Hopkins University, USA*, K. Mortensen *Risø National Laboratory, Denmark*, E. Bucher, *University of Konstanz* and N. Stücheli *ETH, Zürich, Switzerland*.

A strong case now exists that superconductivity in UPt_3 is not of the conventional s-wave variety. In particular, experimental evidence for at least three distinct superconducting phases is best accounted for by a two-component superconducting order-parameter transforming as a vector in the hexagonal basal plane. UPt_3 is a type II superconductor ($\kappa \approx 60 \gg 1/\sqrt{2}$), so there is reason to believe that phase transitions which occur at finite magnetic field are accompanied by some modification of the flux line lattice. Studying such changes is one of the most promising ways of extracting microscopic information about differences between the superconducting phases. In our first experiment, however, we found that there are no substantial modifications in the symmetry or periodicity of the flux lattice at the low temperature ($\mathbf{H} \parallel a^*$) field induced phase transition, and it became clear that the observation of any subtle changes which might have gone un-noticed would require improvements of the experimental set-up. One of the major problems in the previous experiment was SANS from the aluminum tail pieces of the dilution cryostat. By replacing aluminum in the beam path with sapphire it was possible to reduce this background contribution considerably. This improvement and the increased neutron flux available after the guide upgrade, allowed us to re-examine the phase transition with much greater sensitivity. We confirmed the conclusions of the previous experiment but discovered that, even though the overall symmetry of the flux line lattice does not change, the coherence length along the flux lines decreases from greater than $10\mu\text{m}$ to $1.7(5)\mu\text{m}$ as the superconductor enters the high-field phase. This is evident from the figure below, showing rocking scans through small angle diffraction peaks in the low and high field phases. The result indicates that the high-field superconducting state is more strongly affected by defect pinning. This may either be because the defect density changes, as it could if the field modifies the antiferromagnetic domain structure, or because the superconducting order parameter in the high-field phase is more strongly pinned to pre-existing defects. The result is important because it identifies a definite microscopic difference between superconductivity in two phases of UPt_3 .

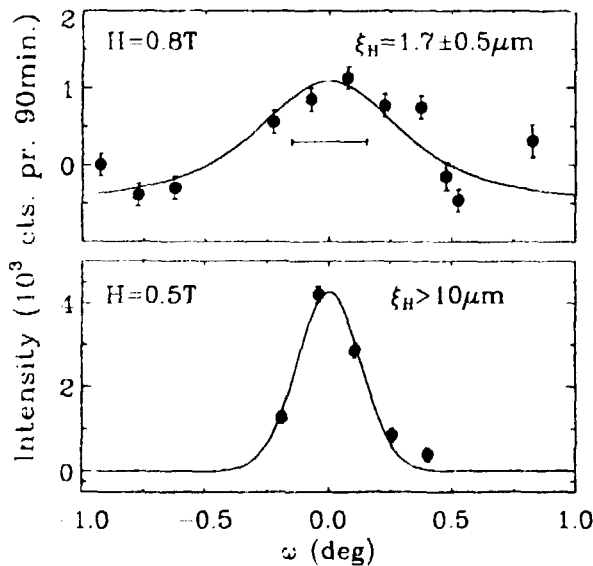


Fig. 1. Rocking scans of neutron diffraction from the flux lattice in two different superconducting phases of UPt_3 ($T=80\text{mK}$, $\mathbf{H} \parallel a^*$).

2.3.10 Small-Angle Neutron Scattering Studies of Pinned and Flowing Magnetic Flux Lattices in 2H-NbSe₂

U. Yaron, P. L. Gammel, D.A. Huse, R.N. Kleiman, C.S. Oglesby, B. Batlogg, D. J. Bishop, AT&T Bell Laboratories, USA, K. Mortensen, K.N. Clausen, Risø National Laboratory, Denmark, E. Bucher, University of Konstanz.

We report on detailed small angle neutron scattering studies of both pinned and flowing flux lattices (FLL) in 2H – NbSe₂. By measuring the FWHM of the rocking curves of the first order Bragg peaks we were able to determine the longitudinal correlation-length parallel to the flux lines, ξ_L . For field-cooled, pinned lattices, we were able to make the first quantitative direct test of the Larkin-Ovchinnikov collective pinning theory¹⁾. As shown in Fig. 1, we find excellent agreement between ξ_L and L_c^b , the collective pinning length of a vortex bundle predicted by this theory. Shown in Fig. 2 is the effect of applying a transport current, perpendicular to the flux lines, on the widths of the rocking curves. After cooling, the measurements were performed upon increasing the current from zero to twice the critical current, and then decreasing back to zero. Following a 1.5 kOe field-cooled process we find a lattice with FWHM of 0.21°, corresponding to $\xi_L \sim 5 \mu\text{m}$. As is evident from the figure, applying a transport current which is significantly smaller than the critical current, I_c , does not, to within our resolution, have an effect on ξ_L . For currents above $\sim 1.5I_c$ a significantly improved lattice is elastically flowing ($\xi_L \geq 25 \mu\text{m}$). The broadening of the rocking curves in the vicinity of I_c is the signature of a defected, incoherent fluid-like plastic flow, predicted by Koshev and Vinokur²⁾ to exist between the pinned and the elastically flowing states. The well ordered FLL observed at $I \geq 1.5I_c$ remains after the current is decreased back to zero. Thus a cycling of the applied current allows us to anneal away effect of pinning disorder³⁾.

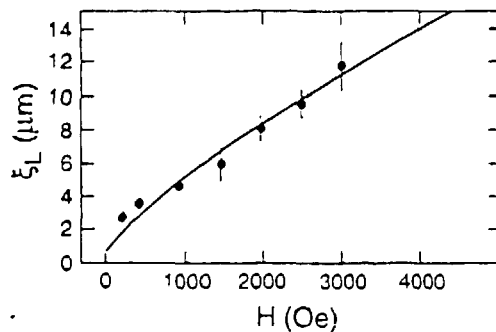


Fig. 1. The field dependence of ξ_L at 4.7 K (filled circles) with the prediction of the Larkin-Ovchinnikov Theory.

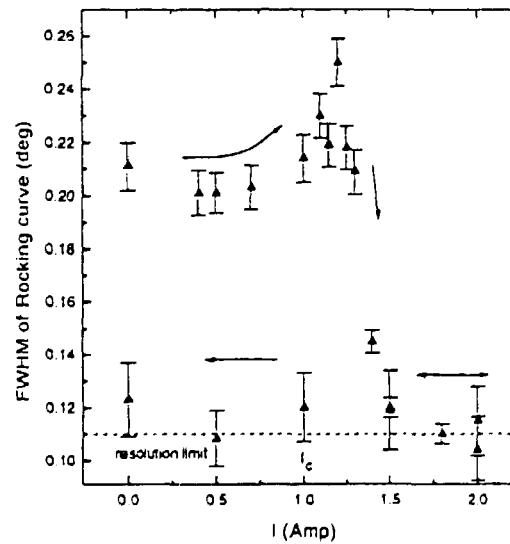


Fig. 2. FWHM of the rocking curves as a function of the applied current following a field-cooled process at 1.5 kOe.

¹⁾ A.I. Larkin and Yu. N. Ovchinnikov, J. Low. Temp. Phys. **34** 409 (1979).

²⁾ A.E. Koshelev and V.M. Vinokur (1994), Phys. Rev. Lett., *submitted*.

³⁾ U. Yaron *et al.*, Phys. Rev. Lett. **73**, 2748 (1994).

2.3.11 Flux-Lattice in BSCCO-2212 Studied by Small-Angle Neutron Scattering

E. M Forgan, R. Cubitt, M. T. Wylie, *University of Birmingham, Edgbaston, UK*, S. L. Lee, H. Keller, *University of Zürich, Zürich, Switzerland*, D. McK Paul, *University of Warwick, Coventry, UK*, H. A. Mook, M. Yethiraj, *Oak Ridge National Laboratory, Tennessee, USA*, P. H. Kes, T. W. Li, *Leiden University, The Netherlands*, A. A. Menevsky, Z. Tarnawski, *University of Amsterdam, The Netherlands* N. Koshizuka, J. Ricketts, *SRL-ISTEC, Koto-ku, Tokyo, Japan*, and K. Mortensen, *Risø National Laboratory, Roskilde, Denmark*

It appears that the flux lattice in the high- T_c copper oxides is much less stable than that in most low T_c materials¹⁾. As a result of the large Ginzburg-Landau parameter, $\kappa = \lambda/\xi$, (λ is magnetic penetration depth, ξ is the superconducting coherence length), the flux lattice can be sheared at short distances relative to the distance between two vortex lines. Moreover the materials are highly anisotropic. Therefore the flux lines in high T_c materials may easily suffer short-range static or dynamic disorder. Detailed information about flux structures within the bulk of superconductors can be obtained from small-angle neutron scattering. Measurements at relatively low magnetic fields and low temperatures reveal the anticipated Abrikosov triangular lattice in BSCCO-2212¹⁾. The scattering pattern is very sensitive to the sample orientation, as shown in Fig. 1²⁾. The scattered intensity rapidly disappears as the field is moved from the perpendicular to the in-plane configuration. By cooling the samples to low temperatures in increasing fields, the neutron diffraction signal disappears as expected for a decomposition into uncorrelated 2D array of flux pancakes. The diffraction signal from the low-field lattice also disappears on heating above the irreversibility line. More detailed investigations of the temperature dependence, as shown in Fig. 2, show a $I(T) \propto 1/\lambda^4(T)$ relationship, supporting d -wave type of superconductivity²⁾. Further indication of d -wave type is given by μ SR.

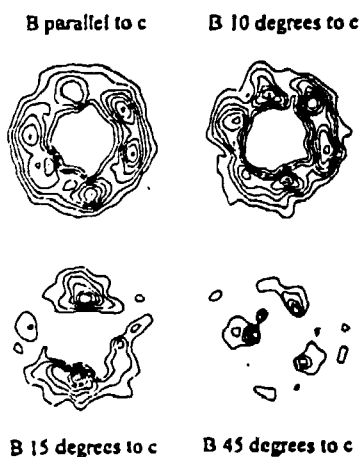


Fig. 1. SANS patterns of BSCCO at $T=4.2\text{K}$ and $B=40\text{ mT}$.

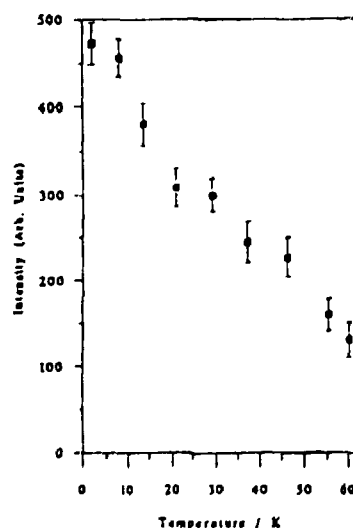


Fig. 2. Temperature dependence of the diffracted-neutron intensity from the flux lattice of BSCCO.

¹⁾ R. Cubitt *et al.*, (1993). *Nature* **365**, 407.

²⁾ E. M Forgan, *et al.*, (1994). *Proceedings from ISS-1994, accepted*.

2.4 Structures and Defects

2.4.1 Critical Scattering from Rb_2ZnCl_4

D.F. McMorrow, *Department of Solid State Physics, Risø National Laboratory, Denmark*, M. Zinkin, R.A. Cowley, *Oxford Physics, Clarendon Laboratory, UK*, and J. P. Hill, *Department of Physics, Brookhaven National Laboratory, USA*

Rb_2ZnCl_4 undergoes a second-order phase transition at T_c ($= 303$ K) into a one-dimensional incommensurate phase (IC). The phase transition belongs to the 3d XY universality class. The incommensurate phase consists of a lattice distortion, characterized by a modulation wave-vector q_s . In Rb_2ZnCl_4 $q_s = (1/3 - \delta)c^*$, where $\delta \approx 0.029$ just below T_c . Accompanying the primary satellite, higher order satellites are observed along c^* .

Within mean-field theory, the integrated intensity of the n 'th order harmonic should scale as $I_n \propto t^{2n\beta_1}$, where β_1 is the critical exponent of the order parameter of the first harmonic and t is the reduced temperature. In practice, this is expected to break down near T_c because of fluctuations. A multicritical scaling theory has been developed^{1,2)} for the behaviour of the hexatic order parameter at the smectic-A-hexatic-B phase transition and was found to successfully account for the temperature dependence of the order parameters in a hexatic liquid-crystal^{2,3)}. As the universality class of this phase transition is the same as that of the IC phase transition in Rb_2ZnCl_4 , the same scaling relationship should apply. Using X20C at the NSLS we have recently measured the order parameters of the first, second and third harmonics in Rb_2ZnCl_4 , where we found $\beta_1 = 0.343(50)$, $\beta_2 = 0.894(50)$ and $\beta_3 = 1.40(10)$. These results are in excellent agreement with the scaling theory which predicts that $I_n \propto t^{2\beta_1(n+0.3n(n-1))}$ with $\beta_1 = 0.345$, as summarised in Fig. 1.

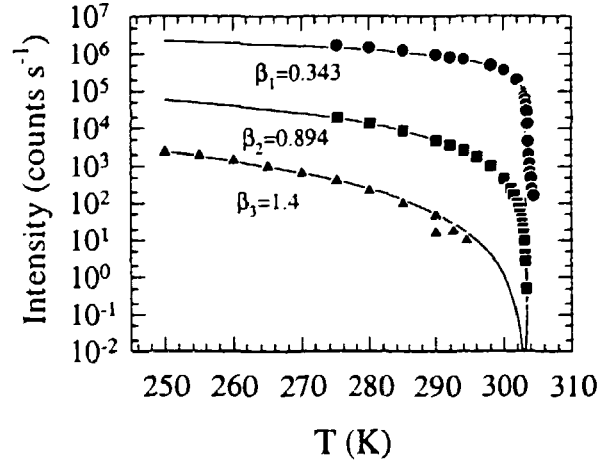


Fig. 1. The order parameter of the first, second and third harmonic in Rb_2ZnCl_4 .

We were also able to measure the critical scattering at the first-order satellite. Data analysis is ongoing and values for the correlation length and susceptibility exponents will be extracted along with the length scale of the fluctuations. We note that the critical scattering was found to be described by a two-component lineshape, as has been observed in a variety of other solid state transitions.

¹⁾ A. Aharony et. al., *Phys. Rev. Lett.* **57**, 1012 (1986).

²⁾ J.D. Brock et. al., *Phys. Rev. Lett.* **57**, 98 (1986).

³⁾ J.D. Brock et. al., *Z. Phys. B* **74**, 379 (1989).

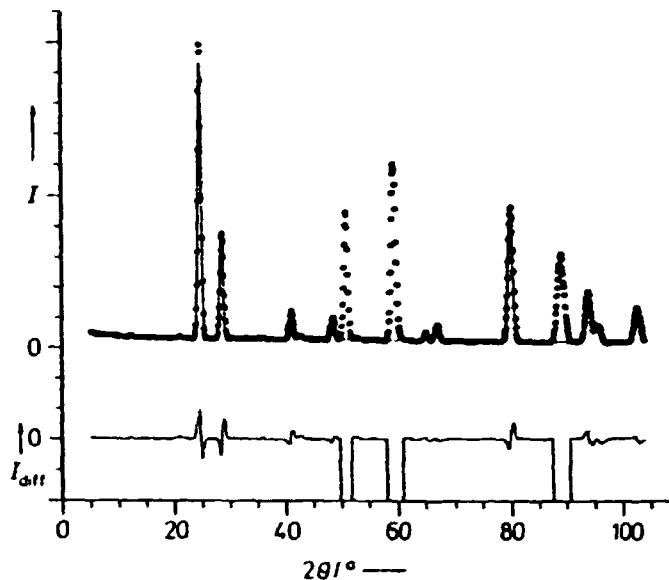
2.4.2 Neutron Diffraction on Ternary Alkali - Metal Platinum Deuterides

G. Auffermann, W. Bronger, P. Müller, *Institut für Anorganische Chemie der RWTH Aachen, Germany* and K. N. Clausen, *Department of Solid State Physics, Riso National Laboratory, Denmark*

Complex ternary alkali - metal platinum hydrides (deuterides) can be synthesized via the reaction of alkali metal hydrides (deuterides) with platinum sponge in a hydrogen (deuterium) atmosphere at temperatures between 600K and 900K.

Previous low pressure investigations (1-100 bar) revealed a series of new complex platinum hydrides (deuterides) with the composition A_2PtH_4 (A_2PtD_4) ($A = Na, K, Rb$ or Cs)¹⁾ and A_3PtH_5 (A_3PtD_5) ($A = Rb$ or Cs)²⁾. Recent experiments with an high - pressure autoclave led to the preparation of two new colourless hydrides (deuterides) with the composition Na_2PtH_6 (Na_2PtD_6)³⁾ and K_2PtH_6 (K_2PtD_6)³⁾ containing platinum in oxidation state +4. X-ray investigations on powdered samples revealed the atomic positions of the metal atoms. To determine the hydrogen positions neutron diffraction experiments on the deuterated compounds were carried out on TAS 1 (see fig. 1). These experiments led to the complete determination of the structures of these compounds^{3,4)}. Structural studies on K_2PtD_6 down to 15K revealed that no phase transition occurs.

Fig. 1. Neutron diffraction diagram of K_2PtD_6 ; in addition to the measured (o) and the calculated (-) profiles, the difference profile is shown. For the three ranges in which the Bragg reflections of K_2PtD_6 overlap with those of the aluminum tube, only the measured profile is given, since these three regions are excluded from the refinement. I = measured or calculated relative intensity; I_{diff} = difference between the measured and calculated relative intensities.



- 1) W. Bronger, G. Auffermann and P. Müller, *J. Less-Common Met.* **142**, 243 (1988).
- 2) W. Bronger, G. Auffermann and P. Müller, *Z. anorg. allg. Chem.* **566**, 31 (1988).
- 3) W. Bronger and G. Auffermann, (1994). *J. Alloys Comp.* *accepted*.
- 4) W. Bronger and G. Auffermann, *Angew. Chem. Int. Ed. Engl.* **33**, 1112 (1994).

2.4.3 Site Preferences for Deuterium in Zr_2NiD_x

B.C. Hauback, P. Runde, A. Maeland, *Department of Physics, Institutt for Energiteknikk, Kjeller, Norway*, H. Fjellvåg, *Department of Chemistry, University of Oslo, Norway*, and B. Lebech, *Department of Solid State Physics, Riso National Laboratory, Denmark*

Several members of the A_2B intermetallic compound family with the tetragonal $CuAl_2$ type crystal structure (space group $I4/mcm$) can absorb hydrogen to produce ternary metal hydride phases. Zr_2Ni is a member of this family, and studies of distribution of deuterium atoms over possible tetrahedral sites, and eventually preferred sites, are in progress for samples with different deuterium compositions. Furthermore, decomposition at higher deuterium contents to one or more different phases, or to an amorphous phase, so-called hydrogen-induced amorphization, is an important part of the investigation.

A powder sample with nominal composition $Zr_2NiD_{2.5}$ containing approximately 20% $Zr_2NiD_{0.35}$ was studied by neutron diffraction at room temperature. The Zr_2Ni alloy was prepared from high purity metals by arc melting in an argon atmosphere. The deuteride sample was prepared by reacting powdered Zr_2Ni with an appropriate amount of deuterium at low pressure (~ 1 atm) and at a temperature below $250^\circ C$.

Refinements of the structures were carried out using a multi-phase Rietveld program. The observed, calculated and difference patterns are shown in Fig. 1. For the $Zr_2NiD_{2.5}$ composition, the occupancy numbers were refined to 0.30(4), 2.04(10) and 0.17(9) for the D1 (8g, $4Zr$, $z = 0.77$), D2 ($16f$, $4Zr$, $x = 0.37$, $z = 0.88$) and D3 ($32m$, $3Zr/1Ni$, $x = 0.29$, $y = 0.88$, $z = 0.75$) sites, respectively. Most of the deuterium is therefore located on the D2 sites; the D4 ($16k$, $2Zr/2Ni$, $x = 0.10$, $y = 0.00$) sites are empty. These results are in agreement with Chikdene et al.¹⁾ The criterion which fixes the minimum distance between hydrogen (deuterium) atoms at about 2.1 \AA ²⁾, makes restrictions on simultaneous occupancy of the possible deuterium site positions. For the $Zr_2NiD_{0.35}$ composition, the deuterium is on the D2 sites only.

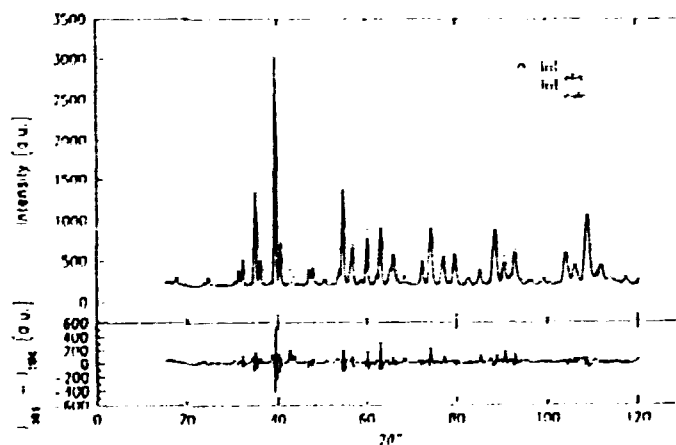


Fig. 1. Results of the Rietveld profile refinement.

¹⁾ A. Chikdene, A. Baudry, P. Boyer, S. Miraglia, D. Fruchart, and J.L. Soubeyrou, *Z. Phys. Chem. NF* **163**, 219 (1989).

²⁾ D.G. Westlake, *Mat. Res. Bull.* **18**, 1409 (1983).

2.4.4 Neutron Diffraction Investigation of the Atomic Defect Structure of Y-doped SrCeO₃

J. Rånø, *Materials Department, Risø National Laboratory, Denmark*, B. Lebech, *Department of Solid State Physics, Risø National Laboratory, Denmark*, and K. Nielsen, *Chemistry Department B, The Technical University of Denmark, Denmark*

The structures of the SrCeO₃ and its Y-doped equivalent Sr[Ce_{0.85}Y_{0.15}]O_{2.925}, a high temperature protonic conductors, have been examined by neutron powder diffraction at room temperature. Both compounds crystallize in a distorted perovskite-like structure and were refined in space group *Pnma* by full profile Rietveld methods¹⁾. Changes in neutron scattering densities, due to the substitution of Ce⁴⁺ by Y³⁺ are illustrated by difference scattering density maps around the atoms constructed from F_{obs} , phased by the F_{calc} , obtained from the Rietveld refinement. is computed as $\rho(\text{Sr}[\text{Ce}_{0.85}\text{Y}_{0.15}]\text{O}_{2.925}) - \rho(\text{SrCeO}_3)$ with the coordinates of the atoms in question translated to the origin (0 0 0). These maps provide a direct picture of the average of thermal vibrations and occupancies on atomic sites less biased by least squares methods than displacement parameters and occupancies obtained from refinement. It is shown that oxygen vacancies induced in order to maintain electro neutrality upon the substitution are confined to one out of two non-equivalent oxygen sites. This vacancy ordering selectively impedes oxygen vacancy migration, but not contributions to the total conductivity from protonic migration and electron holes²⁾. Our results are consistent with experimental observations on the transport properties of acceptor doped cerates^{3,4)}.

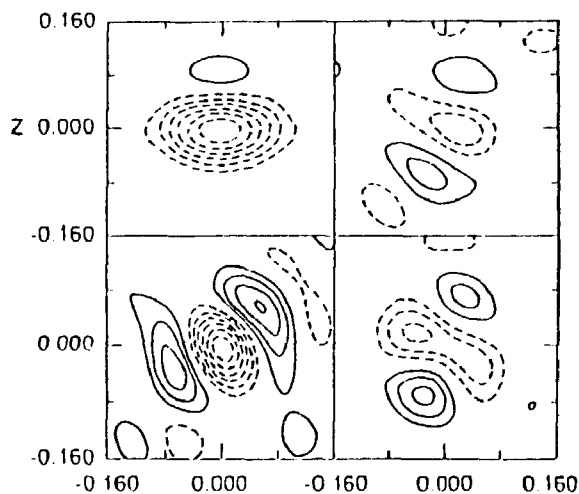


Fig. 1. (1 0 0) (top) and (0 1 0) (bottom) sections of the difference neutron scattering density around the O(1)-position (left) and the O(2)-position (right) both shifted to the origin (0 0 0). Contour intervals are $0.1 \cdot 10^{-12} \text{ cm}/\text{\AA}^3$ (full lines positive, dotted lines negative). It is remarkable that the contours around the O(2) position are low relative to those of the O(1) position indicating that oxygen vacancies are mainly confined to the O(1) position.

¹⁾ A.C.Larson and R.B.Von Dreele, GSAS, LANSCE MS-H805, Los Alamos National Laboratory, USA.

²⁾ J. Rånø, B. Lebech, and K. Nielsen (1995). *J. Mater. Chem.*, *submitted*.

³⁾ H. Iwahara, H. Uchida, and I. Yamasaki, *Int. J. Hydrogen Energy* **12**, 73 (1987).

⁴⁾ N. Bonanos, *Solid State Ionics* **53-56**, 967 (1992).

2.4.5 Neutron Powder Diffraction on the $K_2S_2O_7$ - $KHSO_4$ System

K. Nielsen, *Chemistry Department B, The Technical University of Denmark, Denmark*, J. Ranløv, *Materials Department, Risø National Laboratory, Denmark*, Hae Seop Shim, *Korea Atomic Energy Research Institute, Taejon, Korea*, and B. Lebech, *Department of Solid State Physics, Risø National Laboratory, Denmark*

Catalysts for production of sulphuric acid and for SO_2 removal from flue gases emitted e.g. from coal-fired power stations are based on vanadium oxides dissolved in pyro – sulphate hydrogen – sulphate melts. Knowledge of the chemical and physical as well as the structural properties of the $K_2S_2O_7$ – $KHSO_4$ system are therefore essential in order to throw light on the structure and stability of the catalytically active vanadium complexes. Both $KHSO_4$ and $K_2S_2O_7$ undergo solid state transitions and the crystal structures of the high temperature phases are unknown. Especially for the $K_2S_2O_7$, marked structural changes may be expected since the enthalpy of the phase transition is of the the same order of magnitude as the enthalpy of fusion (~ 21 kJ/mole).

High resolution neutron powder diffraction measurements have been carried out on the pure $K_2S_2O_7$ and $KHSO_4$ components, and on a mixture with a mole fraction of $KHSO_4$ of 0.25. Diffraction experiments have been carried out at several temperatures in the range from ambient temperature to $430^\circ C$. On the basis of these experiments we may establish the crystal structures of the unknown high temperature phases and determine the existence of possible intermediary compounds. Ultimately, we may extract some structural information on the melt of the two – components system.

2.4.6 Crystal Structure Refinement of RECoO₃ (RE = La, Pr and Tb)

Hae Seop Shim, *Korea Atomic Energy Research Institute, Taejon, Korea*, B. Lebech, *Department of Solid State Physics, Risø National Laboratory, Denmark*, and S. E Rasmussen, *The Chemical Institute, University of Aarhus, Aarhus, Denmark*

RECoO₃ (RE = Rare earth) compounds have orthorhombic or rhombohedral distortions of the cubic perovskite structure depending on the ratio, R_t between the radius of the rare earth and the metal ion. The structures of these compounds are interesting because of their high electrical conductivity, and several authors¹⁻⁴⁾ have studied crystal structure of LaCoO₃ using neutron diffraction, x-ray diffraction and transmission electron microscopy with somewhat conflicting results. PrCoO₃ was supposed to crystallize with a rhombohedral unit cell⁵⁾. However, in their recent work on RENiO₃, Lacorre et al.⁶⁾ proposed that a rhombohedral unit cell should be expected for LaCoO₃ and an orthorhombic unit cell for PrCoO₃. Their proposals were based on analogy to RENiO₃ and the expected distortion due to R_t for the two compounds.

Our neutron diffraction data from 10° to 115° in scattering angle were collected using the multi-detector powder diffractometer and incident neutrons of wavelength 1.039 Å for PrCoO₃ and LaCoO₃ and 1.449 Å and 2.268 Å for TbCoO₃. The collimations (neutron source to monochromator, monochromator to sample and sample to detector) were 60', 10' and 10'. The samples were contained in vanadium sample cans. The crystal structures were refined by combining the diffraction data with Rietveld type profile analyses. For the initial refinement of lattice parameters and peak profile parameters we used the programmes ALLHKL⁷⁾ or TREOR⁸⁾. These parameters were then used as input for the Rietveld full profile refinement using the programme FULLPROF⁹⁾. For the LaCoO₃ we used a hexagonal unit cell during the refinement, for PrCoO₃ and TbCoO₃ orthorhombic unit cells.

As proposed by Lacorre et al.⁶⁾, PrCoO₃ was found to crystallize in the orthorhombic *Pbnm* structure and LaCoO₃ in the rhombohedral *R-3c* structure. In the case of LaCoO₃, the lattice parameters have values similar to those of Menyuk et al.¹⁾ and Racciah et al.²⁾. TbCoO₃ has same structure as PrCoO₃, *Pbnm*, but the lattice parameter *a* is smaller than *b*, whereas *a* is larger than *b* in PrCoO₃. X-ray powder diffraction data were collected on the same samples at ambient temperature using Cu-K_α at the STOE powder diffractometer at the University of Aarhus. The analyses of these data are consistent with the results of the neutron diffraction data.

1) N. Menyuk, K. Dwight and P.M. Racciah, *J. Phys. Chem. Solids* **28**, 549 (1967).

2) P.M. Racciah and J.B. Goodenough, *Phys. Rev.* **155**, 932 (1967).

3) G.H. Jonker, *Philips Res. Rep.* **24**, 1 (1969).

4) J. Echigoya, S. Hiratsuka, and H. Suto, *Phys. Stat. Sol. (a)* **118**, 371 (1990).

5) R.W.G. Wyckoff, *Crystal Structures*, 2nd ed., Vol. 2, p.394, Interscience Publishers (1964).

6) P. Lacorre, J.B. Torrance, J. Pannetier, A.I. Nazzal, P.W. Wang, and T.C. Huang, *J. Solid State Chem.* **91**, 225 (1991).

7) G.S. Pawley, *J. Appl. Crystallogr.* **14**, 357 (1981).

8) P.E. Werner, L. Eriksson and M. Westdahl, *J. Appl. Crystallogr.* **18**, 367 (1985).

9) J. Rodriguez-Carvajal (1990). Abstracts of the Satellite Meeting on Powder Diffraction of the XVth Congress of the International Union of Crystallography (Toulouse, 1990) p. 127.

2.4.7 Small-Angle Neutron Scattering on Al-3 at.% Ag

A. Malik, B. Schönfeld, G. Kostorz, *Institute of Applied Physics, ETH Zürich, Switzerland*, and J. Skov Pedersen, *Department of Solid State Physics, Risø National Laboratory, Denmark*

The decomposition in Al-Ag strongly depends on the aging conditions. During the early stages of decomposition Guinier-Preston (GP) zones are formed. There are two kinds of GP zones, so called η zones which form at temperatures below about 443 K, and ϵ zones at higher temperatures. The aim of the present investigation was to determine the structure and composition of η zones by means of diffuse wide-angle and small-angle scattering and to compare these results with previous investigations on ϵ zones¹⁾. Small-angle scattering is a good supplement to diffuse wide-angle scattering, because close to the origin short-range order (SRO) intensity is nearly exclusively present, especially if the lattice misfit is small²⁾. The small-angle scattering was measured with the same single crystal of Al-3 at.% Ag as the diffuse wide-angle scattering. The sample was homogenized at 848 K for 2 h, quenched into iced water and aged at 413 K for 4 h. Neutrons with an average wavelength of 5.82 Å were used. The small-angle scattering showed an intensity distribution expected for a statistically isotropic system. The data were combined with the separated SRO intensity of the wide-angle scattering experiment, and a Fourier analysis was done to determine 400 Warren-Cowley SRO parameters. For α_{000} a value of 0.922 ± 0.041 was obtained, close to the theoretical value $\alpha_{000} = 1$. The Warren-Cowley SRO parameters were used for crystal modelling (see Fig. 1). The analysis of the GP zones from the model crystal gave an average size of about 11 Å and an average silver content of $(77 \pm 5) \%$. These results agree very well with the results obtained from the evaluation³⁾ of the small-angle scattering alone where a radius of gyration of (13.0 ± 1.2) Å and a silver content of 75 % are found. Further evaluation about the structure of the GP zones, especially whether there exists a silver-depleted core as previously proposed^{4,5)}, is in progress.

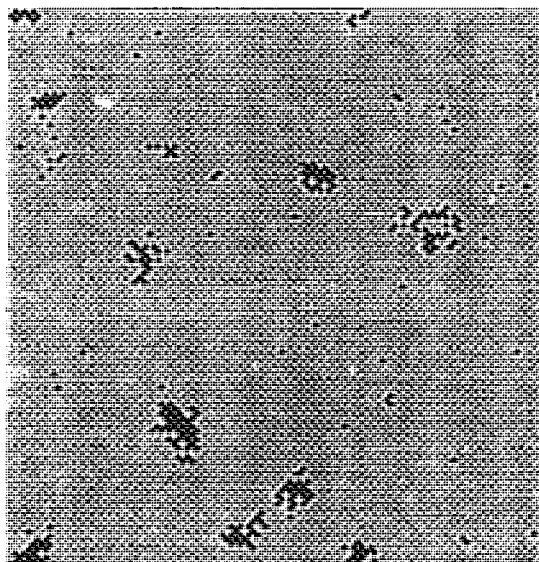


Fig. 1. One of the (001) planes of a modelled short-range ordered alloy.

- ¹⁾ B. Schönfeld, A. Göcmen, and G. Kostorz, *J. Phys. I* **2**, 1075 (1992).
- ²⁾ T. Ungár, P.A. Dubey, and G. Kostorz, *Acta Metall. Mater.* **38**, 2583 (1990).
- ³⁾ J.S. Pedersen, *Phys. Rev.* **B47**, 657 (1993).
- ⁴⁾ P.A. Dubey, Dissertation No. 9077, ETH Zürich (CH) (1990).
- ⁵⁾ P.A. Dubey, B. Schönfeld, and G. Kostorz, *Acta Metall.* **39**, 1161 (1991).

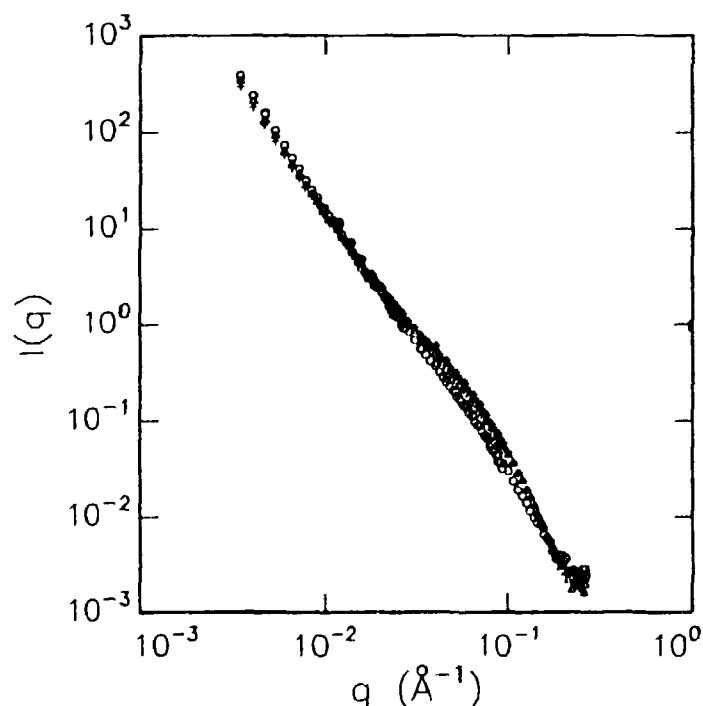
2.4.8 Precipitation in Supersaturated Solid Solution Thin Al(Ti) Films Studied by Small-Angle Neutron Scattering

S. Schmidt, H. Oettel, *Institute of Physical Metallurgy, Freiberg University of Mining and Technology, Germany*, and J. Skov Pedersen, *Department of Solid State Physics, Risø National Laboratory, Denmark*

Supersaturated solid solution thin Al-2,7 at% Ti films were prepared by magnetron sputtering on oxidized Si single crystal substrates. The films were deposited with a nanocrystalline columnar morphology and a mean size of about 60 nm. Cross-sectional transmission electron microscopy (XTEM) show the formation of Al₃Ti precipitates at the grain boundaries of the columnar grains after annealing.

Small-angle neutron scattering (SANS) has been employed to investigate the precipitation growth process after annealing treatments at 250°C and 300 °C. Fig. 1 show the SANS intensities after different aging times at 300°C. It was concluded that formation and growth of the shoulder is connected with the precipitate particle growth.

Special effort was made to separate the particle part from the experimental scattering data and to determine the distance distribution function $p(r)$ by the Indirect Fourier Transformation Method¹⁾ in order to estimate particle parameter. The particle distribution function was analytically calculated by introduction of a model that considers the special arrangement and size of the particles in the columnar film morphology. The development of the mean particle size after different aging treatments could be determined.



¹⁾ O. Glatter, *J. Appl. Cryst.* **10**, 415 (1977).

2.5 Surfaces and Interfaces

2.5.1 Growth of Ag on Ni(111) Studied by X-Ray Diffraction

R. Feidenhans'l, E. Landemark, M. Nielsen, D.-M. Smilgies, *Department of Solid State Physics, Risø National Laboratory, Denmark*, L. Pleth Nielsen, P. Sprunger, *Institute of Physics and Astronomy, University of Aarhus, Denmark*, L. Lottermoser, R. L. Johnson, *II. Institut für Experimentalphysik, Universität Hamburg, Germany*, and V. Etgens, *ESRF, Grenoble, France*

We have studied the heterogeneous growth of Ag on the Ni(111) surface by x-ray diffraction. The experiments were performed at the ID3 surface diffraction beamline at ESRF. The beamline is an undulator beamline and the experiments were performed at the fifth harmonic at an energy of 16 keV. In contrast to the behavior on the Ni(110) surface, the Ag atoms do not intermix with the Ni(111) surface, but form a flat Ag(111) overlayer in the monolayer regime. Due to the lattice misfit, the Ag layer is slightly rotated and recent Scanning Tunneling Microscopy (STM) investigation has shown very pronounced Moire patterns. The rotation angle changes as a function of preparation and Ag coverage and is typically in the range $1.4^\circ - 2^\circ$. The Ag in-plane lattice constant is observed to be in the range 4.09-4.15 Å, in contrast to the bulk value of 4.09 Å. We measured the Bragg rods for the Ag overlayer at different Ag coverages and followed the evolution from monolayer to 3D growth. Quite surprisingly, the Ag rods showed very pronounced peaks at momentum transfers in the direction normal to the surface at $l = -1.67, l = -0.67$ and $l = 1.33$. This corresponds to positions expected for the Ni bulk Bragg peaks. It means that the Ag overlayer makes a deep and substantial modulation in the underlying Ni(111) lattice. The modulation is seen also at higher coverages.

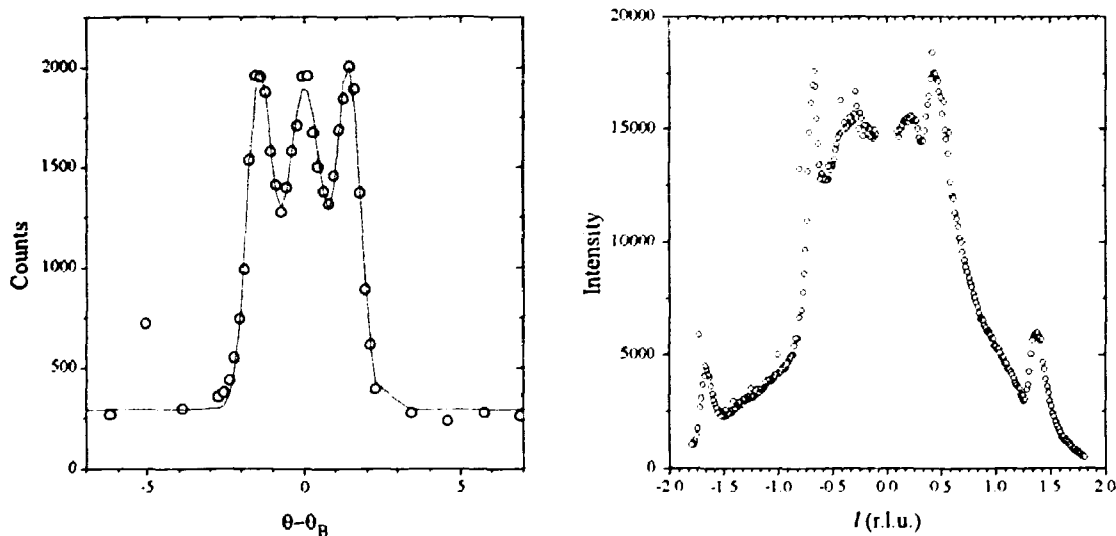


Fig. 1. On the left side is shown an ω -scan through the Ag overlayer peak before annealing of the Ag layer. The scan shows two rotated peaks and one non-rotated. After annealing the non-rotated disappears. On the right side a rod scan of the Ag reflection is shown. The sharp reflections at $l = -1.674, l = -0.67$ and $l = 1.33$ from the modulation of the Ni lattice are clearly seen. The peak at $l = 0.33$ disappears due to an interference effect with the Ag overlayer.

2.5.2 X-Ray Diffraction from Ag Clusters on Ni(110)

R. Feidenhans'l, E. Landemark, M. Nielsen, D.-M. Smilgies, *Department of Solid State Physics, Risø National Laboratory, Denmark*, L. Pleth Nielsen, P. Sprunger, *Institute of Physics and Astronomy, University of Aarhus, Denmark*, L. Lottermoser, R. L. Johnson, *II. Institut für Experimentalphysik, Universität Hamburg, Germany*, and V. Etgens, *ESRF, Grenoble, France*.

Scanning Tunneling Microscopy (STM) has recently shown a very unusual behavior when Au is evaporated onto a Ni(110) surface. Although Au and Ni are immiscible as bulk materials, Au atoms can substitute for Ni in the very first layer¹). The same effect has been observed for Ag, but STM measurements are more difficult due to the higher mobility of Ag. We have investigated the growth of Ag on Ni(110) by surface x-ray diffraction at the ID3 beamline at ESRF.

At low coverages Ag substitutes for Ni. At higher coverages up to one monolayer (ML) a dealloying occurs¹) and the Ag makes a (111) hexagonal overlayer on the Ni(110) surface. The overlayer is commensurate in one direction. The overlayer is completed at about 1 ML. At higher coverages 3-D cluster growth starts. Surprisingly, the hexagonal overlayer disappears and the Ag clusters grow epitaxially with the Ni lattice with Ag[001] \parallel Ni[001] and Ag[1 $\bar{1}$ 0] \parallel Ni[1 $\bar{1}$ 0]. Scans along the [1 $\bar{1}$ 0] directions through the Ag reflections show pronounced satellites. The satellites are displaced more and more away from the main peak as the momentum in the directions normal to the surface increases. The satellites can be interpreted as scattering from the facets of the Ag clusters and means that the clusters must be elongated along the [001] direction having (122) and (544) facets.

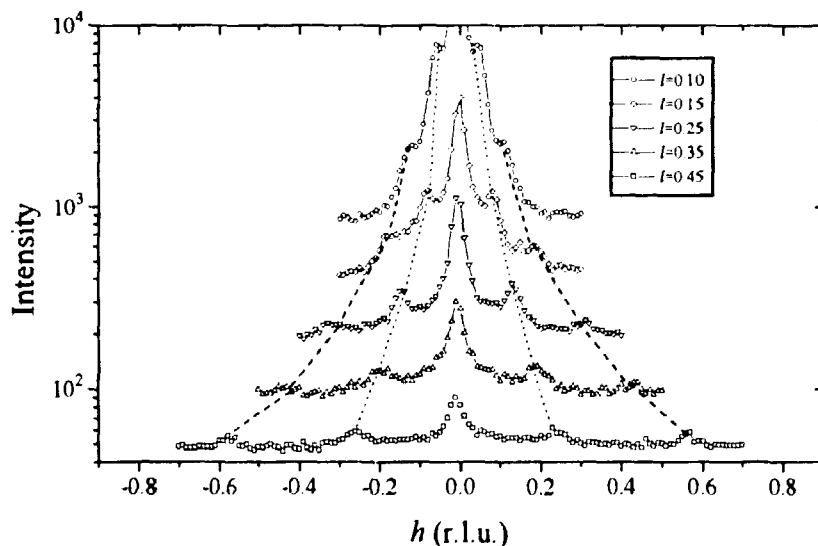


Fig. 1. Scans along the [1 $\bar{1}$ 0] directions at different momentum transfers l in the direction normal to the surface through the Ag reflection at (0,1.7, l). The satellites from the (122) facets are indicated with dotted lines, the satellites from the (544) facets are indicated with dashed lines.

¹) L. Pleth Nielsen *et al.*, Phys. Rev. Lett. **71**, 754 (1993)

2.5.3 Preliminary Investigations of the Close-packed Pb Structures on Ge(111) by Surface X-Ray Diffraction

L. Lottermoser, G. Falkenberg, L. Seehofer, R.L. Johnson, *II. Institute für Experimentalphysik, Universität Hamburg, D-22761 Hamburg*, V. Etgens, *ESRF, BP220, 38043 Grenoble-Cedex, France*, R. Feidenhans'l, E. Landemark, D. Smilgies, and M. Nielsen, *Department of Solid State Physics, Risø National Laboratory, Denmark*.

Pb monolayers adsorbed on Ge(111) surfaces constitute an ideal system for the study of 2-D phase transitions. Surface x-ray diffraction¹⁾ showed that the dense phase of Pb monolayers on Si(111) form an incommensurate structure, while the corresponding Pb on Ge(111) phase has a commensurate $\sqrt{3}\times\sqrt{3}R30^\circ$ structure, the β -phase²⁾. Recent STM measurements³⁾ revealed however, that also the Pb on Ge system goes incommensurate at densities slightly above that of the dense β -phase, and this phase transition has now been observed by x-ray diffraction. By monitoring fractional order diffraction peaks during Pb evaporation the phase transition is seen as a splitting of the single commensurate peaks into closely spaced, although not completely resolved groups, signalling the formation of long wave length density modulations. Figure 1 and fig. 2 show an STM picture and diffraction groups from a transverse scan near the reciprocal lattice point $(4/3,4/3)$, from the incommensurate striped Pb/Ge(111) phase. This has an uniaxial compressed structure with the small excess density residing in broad domain walls seen as bright stripes on the lower terrace in fig. 1, and creating the diffraction pattern of fig. 2.

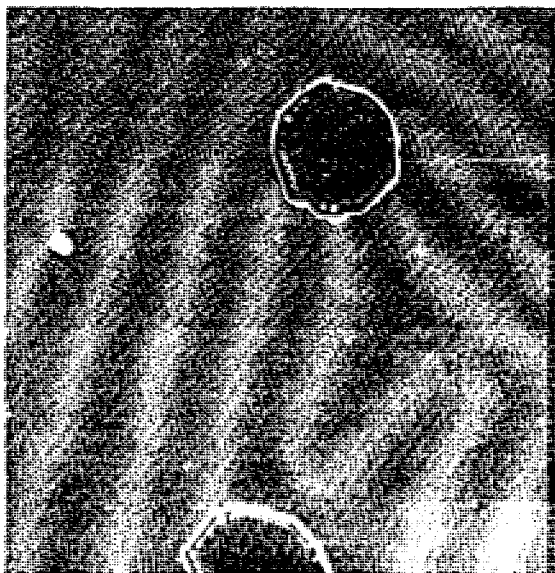


Fig. 1. STM topograph of the striped incommensurate phase of Pb on Ge(111). The scanned area is $800\times 800 \text{ \AA}^2$. The tunneling current was 1.5 nA and the sample bias 1.5 V.

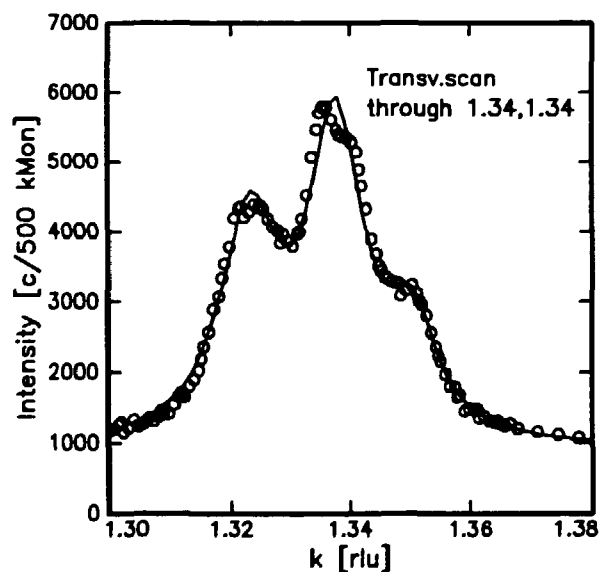


Fig. 2. Diffraction profile from the same incommensurate striped phase of Pb/Ge(111) as shown in fig. 1, measured in a scan near the commensurate truncation rod $(4/3,4/3,l)$, and $l=0.41$.

- ¹⁾ J.S. Pedersen, R. Feidenhans'l, M. Nielsen, F. Grey, and R.L. Johnson, *Surf.Sci.* **189/190**, 1047 (1987).
- ²⁾ R. Feidenhans'l, J.S. Pedersen, M. Nielsen, F. Grey, and R.L. Johnson, *Surf.Sci.* **178**, 927 (1986)
- ³⁾ L. Seehofer G. Falkenberg, D. Daboul, R.L. Johnson, *Surf.Sci.* **307-309**, 698 (1994).

2.5.4 Hutclusters on the Ge(100) Surface Studied by Surface X-Ray Diffraction

G. Falkenberg, L. Lottermoser, L. Seehofer, R.L. Johnson, *II. Institute für Experimentalphysik, Universität Hamburg, D-22761 Hamburg*, R. Feidenhans'l, E. Landemark, D. Smilgies, and M. Nielsen, *Department of Solid State Physics, Risø National Laboratory, Denmark*.

In epitaxial growth several systems develop intermediate regular structures in the transition between layer growth and three dimensional nucleated growth. In particular the STM technique has demonstrated surprisingly regular *small clusters* in the shape of huts appearing when Ge is grown on Si(100)¹⁾ or on Ge(100) surfaces under the influence of a small In-dosing. The huts are completely regular nano-crystals shaped like the roof of small houses all aligned crystallographically, and with roofs including the canted ends (gables) all having the same low index surface like (105) or (103). Under the right condition almost 100% coverage may occur and the huts form a superstructure with a limited range of order. Each hut is about 60 Å wide in their base plane and have very varying length. The creation of these clusters is caused by strain relaxation and by the dynamics of the growth limited by nucleation. We have studied hutclusters by x-ray diffraction in order to measure the strain in the clusters, and in their interphase with the substrate, and other properties. The most regular structures were found on Ge(100) with a small amount of In evaporated at 400 °C. The surface was first characterized by STM, and then studied by x-ray diffraction. Figure 1 and fig. 2 illustrate results. The absence, in the diffraction results, of the central rod, i.e the truncation rod from the hut-base-plane, show that these clusters have very little strain relative to bulk Ge.

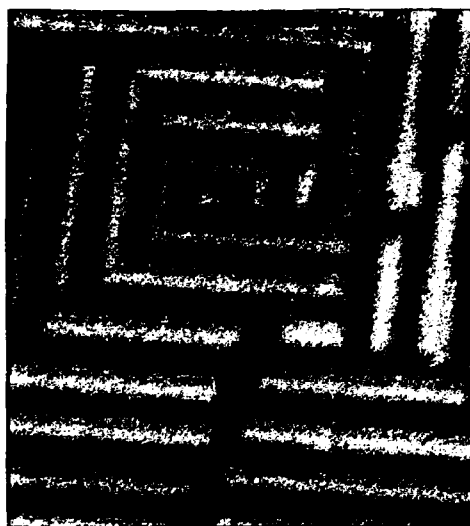


Fig. 1. STM topograph of the on Ge(100) surface with hutclusters. Area 550x600 Å². Tunneling current 1.7 nA and 1.3 V sample bias.

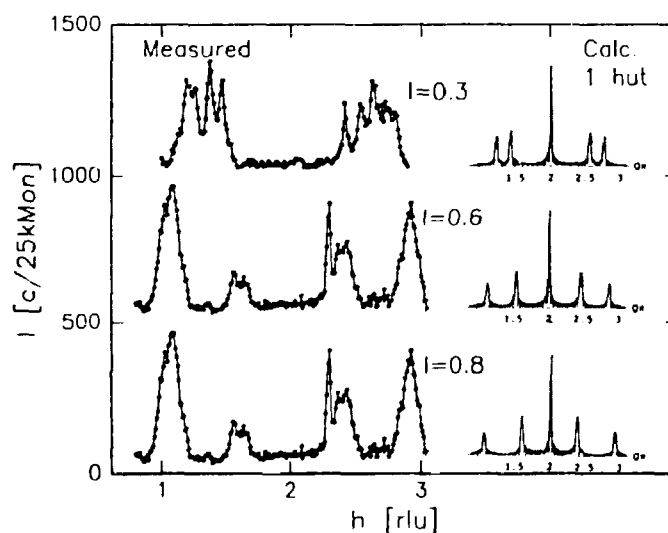


Fig. 2. Diffraction profiles scanning parallel with the surface at different height (l), above the surface. Insert show calculated profile from one hut including base plane rod.

¹⁾ Y.-W. Mo, D.E. Savage, B.S. Swartzentruber, and M.G. Lagaly, *Phys.Rev.Lett.* **65**, 1020 (1990)

2.5.5 X-Ray Diffraction from Incommensurate Surface Structures on In/Ge(111)

R. Feidenhans'l, E. Landemark, M. Nielsen, D.-M. Smiigies, *Department of Solid State Physics, Risø National Laboratory, Denmark*, J. Zegenhagen *Max-Planck-Institut für Festkörperforschung, Stuttgart, Germany*, L. Lottermoser, G. Falkenberg, L. Seehofer, and R.L. Johnson, *II. Institut für Experimentalphysik, Universität Hamburg, Germany*.

Several metals form discommensurate structures when adsorbed on Ge(111) or Si(111) with metal coverages less than a monolayer. Cu on Si(111) and Ga on both Si(111) and Ge(111) are examples such cases. On these surfaces domain-wall networks are formed. We have recently started to investigate In/Ge(111) by surface x-ray diffraction at beamline BW2 and by Scanning Tunneling Microscopy (STM). The In/Ge(111) system is somewhat different from the above mentioned cases, because it makes modulated 2×2 structures. We have studied two different surface preparations. One surface had an In coverage of about 0.25 ML, while the other was more dilute with 0.1 ML of In. Scans along the high symmetry directions in reciprocal space were performed in order to characterize the incommensurability. A more detailed data analysis is in progress.

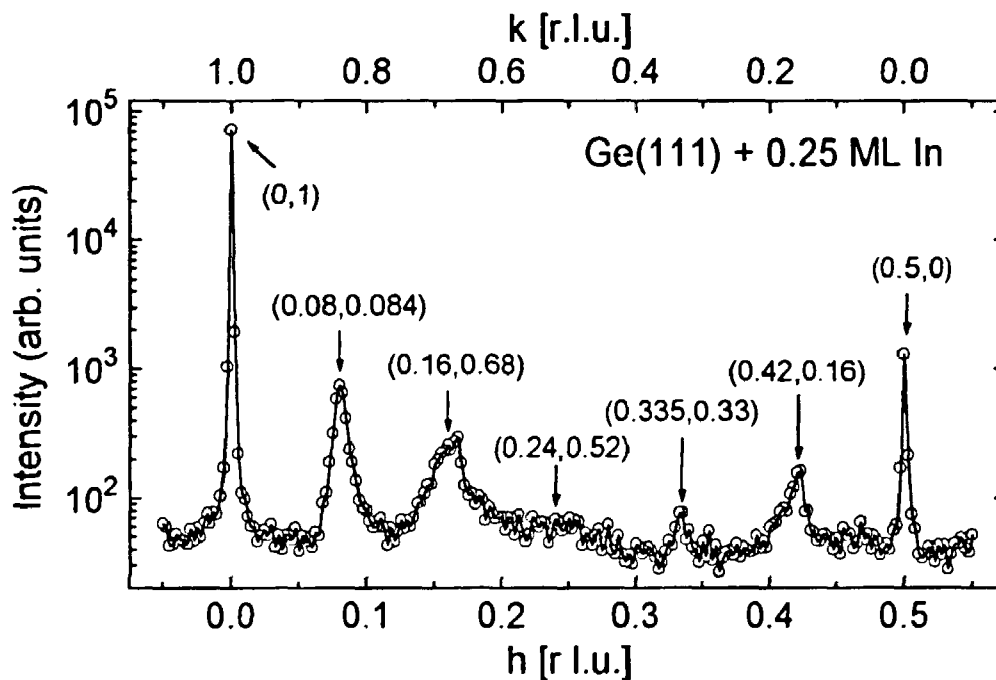


Fig. 1. Scan along the $[1\bar{2}]$ direction through the $(0,1)$ and $(0.5,0)$ reflections for a Ge(111) surface with an In coverage of 0.25 ML. Note the satellites are shifted in multiples of $(0.08,-0.16)$ away from the integer-order reflections.

2.5.6 Atomic Structure of the Ge(111) $\sqrt{3} \times \sqrt{3}$ -Ag Surface

E. Landemark, M. Nielsen, E. Findeisen and R. Feidenhans'l, *Department of Solid State Physics, Risø National Laboratory, Denmark*, M. Foss, *Institute of Physics and Astronomy, Aarhus University, Denmark*, T. Buslaps, L. Seehofer, R.L. Johnson, *II. Institut für Experimentalphysik, Universität Hamburg, Germany*, M. Göthelid and U.O. Karlsson, *Materials Physics, Royal Institute of Technology, Stockholm, Sweden*

Ag and Au both induce reconstructions with $\sqrt{3} \times \sqrt{3}$ periodicities when adsorbed on the (111) surfaces of Si and Ge¹⁾. Si(111) $\sqrt{3} \times \sqrt{3}$ -Ag is probably one of the most extensively studied surfaces in surface science. The structure that finally has emerged from all these investigations is the Honeycomb-Chained-Trimer (HCT) model, consisting 1 ML of substrate atoms arranged in trimers and 1 ML of metal atoms, with larger inter-atomic distances, forming chained trimers in a honeycomb arrangement. In the prevailing model for Au on Si, the Conjugated-Honeycomb-Chained-Trimer (CHCT) model, the role of substrate and adsorbate atoms are interchanged, so that the Au atoms form the smaller isolated trimers. The structure of Ge(111) ($\sqrt{3} \times \sqrt{3}$)-Ag has been controversial. An earlier, in plane, SXRD study²⁾ argued for the formation of Ag trimers (CHCT), while a recent LEED study found a HCT structure as for Ag on Si³⁾.

By recording the intensity of the Bragg rods over an extended range of perpendicular momentum transfers, at the BW2 beamline in Hasylab, we have been able to determine the structure of the Ge(111) $\sqrt{3} \times \sqrt{3}$ -Ag surface in detail. In Fig. 1 examples of such rodscans are shown together with the final structure obtained from the least-square fitting refinement. Our results show that Ge atoms form the trimer units and that the HCT model is valid. The bond length in the Ge trimers is 2.75 Å and the Ag-Ag distance is 3.67 Å. The Ag atoms are located 0.62 Å above the Ge trimers. Buckling is found in the third and fourth Ge layer (0.27 and 0.21 Å). We have also recorded a large data set for the Ge(111)4×4-Ag surface, but the analysis of these data is not yet finished.

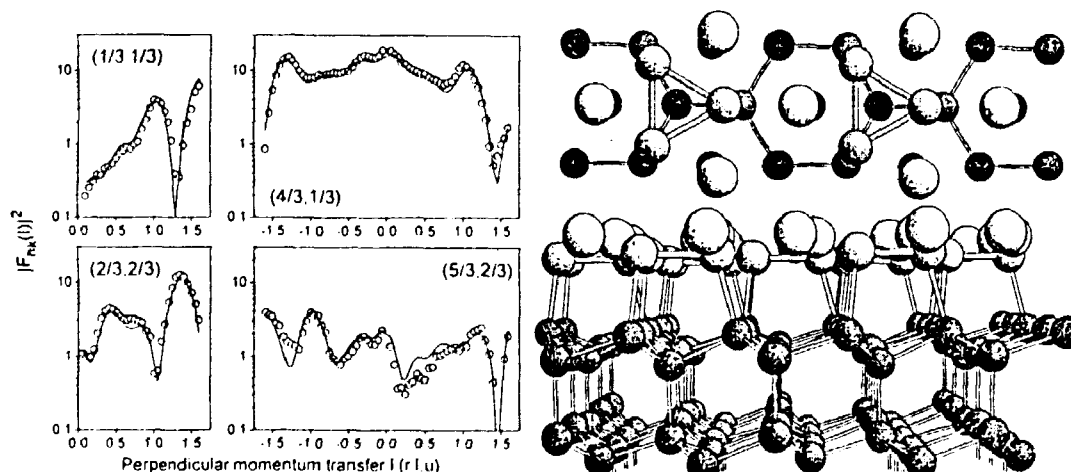


Fig. 1. Experimental and calculated X-ray diffraction rodscan data for the Ge(111) $\sqrt{3} \times \sqrt{3}$ -Ag surface. The obtained HCT structure is shown to the right.

¹⁾ For a recent review see: G. Le Lay *et al.*, *Surf. Sci.* **307-309**, 280 (1994).

²⁾ D. Dornisch *et al.*, *Surf. Sci.* **274**, 215 (1992).

³⁾ H. Huang, H. Over, S.Y. Tong, J. Quinn and F. Jona, *Phys. Rev. B* **49**, 13483 (1994).

2.5.7 Surface X-Ray Diffraction Studies of the Ag and Na Induced Si(111)3×1 Reconstructions

E. Landmark, M. Nielsen, D.-M. Smilgies and R. Feidenhans'l, *Department of Solid State Physics, Risø National Laboratory, Denmark*, L. Lottermoser, T. Buslaps, R. L. Johnson, *II. Institut für Experimentalphysik, Universität Hamburg, Germany*

There is currently a large interest for the metal induced 3×1 reconstructions of the Si(111) surface¹⁾. As observed by LEED and STM, Si(111)3×1 reconstructions with large similarities can be produced by deposition of Ag or alkali metals such as Li, Na or Ka. The deposition is preferably made at substrate temperatures in the desorption regime and the resulting metal coverage is now believed to be 1/3 ML. One interesting aspect is that the alkali induced 3×1 surfaces seems to be chemically passivated, which is remarkable since adsorption of alkali metals usually promotes the oxidation of Si surfaces. In addition to the 3×1 spots, some extra 6th order spots can be observed in the LEED pattern from the Ag induced reconstruction at RT. This doubling of the periodicity can also be observed in STM images at specific tunneling conditions²⁾.

We have studied the Si(111), 3×1-Ag and 3×1-Na, structures by surface x-ray diffraction at the BW2 wiggler beamline at Hasylab. We have collected both in-plane and out of plane data sets for these structures. Contour maps of the Patterson functions obtained from the fractional-order in-plane data are shown in Fig. 1. The three main irreducible interatomic vectors, that can be identified, are indicated in the figure together with the 3×1 unit cells. The differences in the two Patterson functions, i.e. the longer c vector for Na and the different elongations of peaks c and b, may indicate slightly different metal adsorption sites for Ag and Na. Displacements of Ag atoms away from symmetry sites may also explain the 6×1 periodicity. Modeling of the data by refinements of structural models is in progress.

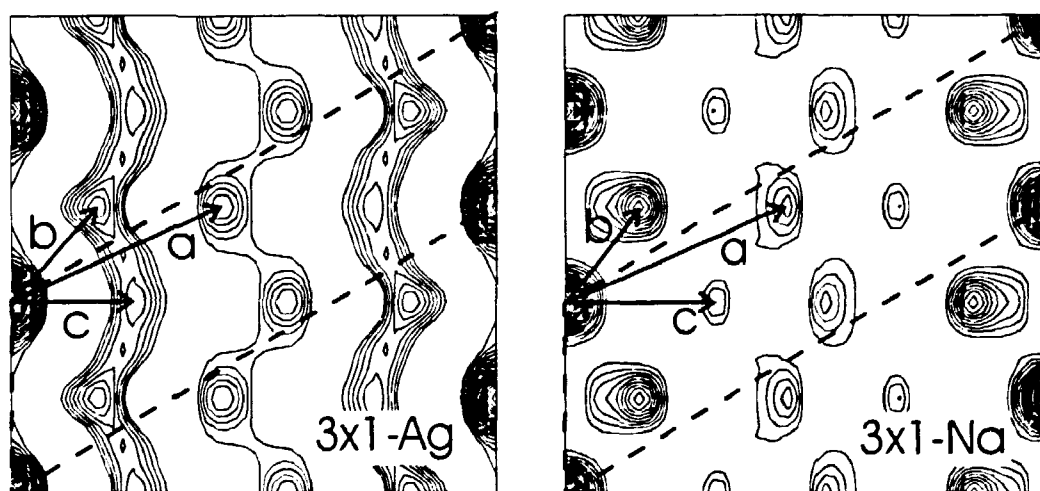


Fig. 1. Contour maps of experimental Patterson functions for Si(111)3×1-Ag and Si(111)3×1-Na.

¹⁾ H.H. Weitering, N.J. DiNardo, R. Pércs-Sandoz, J. Chen and E.J. Mele, *Phys. Rev. B* **49**, 16 837 (1994) and references therein.

²⁾ K.J. Wan, X.F. Lin, J. Nogami, *Phys. Rev. B* **47**, 13 700 (1993).

2.5.8 Relaxation Mechanism of Epitaxial Ge on Si(001) Studied by X-Ray Diffraction

A. H.H.F. Ettema, P.M.L.O. Scholte, A.J. Steinfort, F. Tuinstra, *Physical crystallography group, Dept. of Applied Physics, Delft. The Netherlands*, M. Nielsen, D.-M. Smilgies, E. Landemark, R. Feidenhans'l, *Department of Solid State Physics, Riso National Laboratory, Denmark*, G. Falkenberg, R.L. Johnson, *II. Institut für Experimentalphysik, Universität Hamburg, Germany*

The epitaxial growth of Ge(001) on Si(001) proceeds in the so-called Stranski-Krastanov mode. First a few monolayers of Ge grow in a layer-by-layer fashion. After a certain critical thickness has been grown (3-6 monolayers) three-dimensional islands form. From the GIXD study by Williams *et al.*¹⁾ it is known that at the same time the stress in the Ge-adlayer starts to relax. A more detailed examination with STM by Kohler *et al.*²⁾ of the 2D-growth of Ge on Si(001) showed that during this stage a pattern of missing dimers is formed that gives rise to the well known $2 \times n$ reconstruction. This missing dimers allows for some elastic relaxation. If the growths continues the missing dimers are (partially) filled and the surface starts to form 3D-clusters. Mo and Lagally *et al.*³⁾ found that during this transition from 2D to 3D growth small, anisotropically shaped clusters appear. These so-called hutclusters are metastable and appear only at growth temperatures below 530 C. They have a very large aspect ratio of approximately 1:8 and they are invariably oriented along the [100] and [010] directions. Also, their width shows a strikingly homogeneous distribution. If the growth continues, the hutclusters disappear and macroscopic clusters bounded by (113) facets appear. The role of the hutclusters in the relaxation process still is under debate. Williams *et al.* showed that the onset of relaxation coincides with the appearance of clusters. However it is not clear whether these clusters are the hutclusters or the macroscopic clusters. Also if the Ge adlayer relaxes by the formation of hutclusters, they should be relaxed. However from calculations it can be deduced that the high aspect ratio of the hutclusters is due to the stress in the clusters.

To clarify the role of the hutclusters in the relaxation process, we are striving to measure the relaxation of the hutclusters and the 2D Ge layer underneath separately. Since the hutclusters are bounded by (105) facets, the Crystal Truncation Rods (CTR) of the hutcluster will have a different orientation in reciprocal space than the CTR of the 2D Ge layer. By performing a 2D scan near a Bragg reflection, the exact orientation of the CTRs and the position of the Bragg reflections is determined. If the hutclusters and the 2D-Ge layers do not have the same degree of relaxation, the Bragg reflections of the hutcluster and the 2D Ge layer are shifted with respect to each other and with respect to the Bragg reflection of the Si substrate. From this shift both the in-plane and the out-of-plane relaxation of the hutcluster and of the 2D Ge layer can be determined independently. At the end of 1994 preliminary results are available only. The experiments will be continued in 1995. We were able to identify the rods due to the (105) facets of the hutclusters. Also it has been established that at least a part of the Ge is relaxed, leaving a residual strain of approximately 3%.

¹⁾ A.A. Williams *et al.*, Phys. Rev. **B43**, 5001 (1991).

²⁾ U. Kohler *et al.*, Ultramicroscopy **42-44**, 832 (1992).

³⁾ Y.-W. Mo *et al.*, Phys. Rev. Lett. **65**, 1020 (1990).

2.5.9 Coverage-Dependent Structures of Bismuth on Cu(110) Determined by Surface X-Ray Diffraction

L. Lottermoser, T. Buslaps, R. L. Johnson, *II. Institut für Experimentalphysik, Universität Hamburg, D-22761 Hamburg*, R. Feidenhansl, M. Nielsen, D.-M. Smilgies, and E. Landemark, *Department of Solid State Physics, Riso National Laboratory, Denmark*.

Surface x-ray diffraction has been used to analyse the adlayer structures of Bi on Cu(110) for submonolayer coverages *in-situ* at room temperature. The experiments were performed at the Wiggler beamline BW2 at HASYLAB in Hamburg. For bismuth coverages around 0.5 ML deposited on a clean Cu(110) surface an ordered $c(2 \times 2)$ quasi-hexagonal superstructure was observed. At coverages between 0.6-0.7 ML a more complicated incommensurate phases with main peaks at $(-1.295,0)$, $(0.598,0)$ and multiple peaks of $(-0.705,0)$. By increasing the Bi coverages slightly, the $(-0.705,0)$ peak shifts from $(-0.705,0)$ to $(-0.733,0)$. At higher coverages close to 0.75 ML a $p(4 \times 1)$ Bi-adlayer appears. More details of the phase diagram Bi on Cu(110) are discussed elsewhere¹⁾.

In addition to the determination of the Bi-phase diagram as a function of coverage the atomic arrangements of the Bi- $c(2 \times 2)$ and Bi- $p(4 \times 1)$ superstructures have been studied. We have collected both in-plane and out-of plane data sets of these structures. The $c(2 \times 2)$ and $p(4 \times 1)$ Bi-adlayer structures determined by a least-squares refinement are shown in Fig. 1. For the $c(2 \times 2)$ Bi-superstructure the theoretical coverage corresponds to 0.5 ML. The bismuth atoms are located in the energetically favorable fourfold-hollow sites of the Cu(110) surface. The long bismuth-bismuth nearest neighbour distance of 4.43 Å indicates a lateral repulsive interaction between the Bi atoms as discussed by Clendening and Campbell²⁾. The structural model of the $p(4 \times 1)$ Bi-adlayer has three Bi atoms per unit cell corresponding to a coverage of 0.75 ML. A more detailed description of the structural model is in preparation¹⁾.

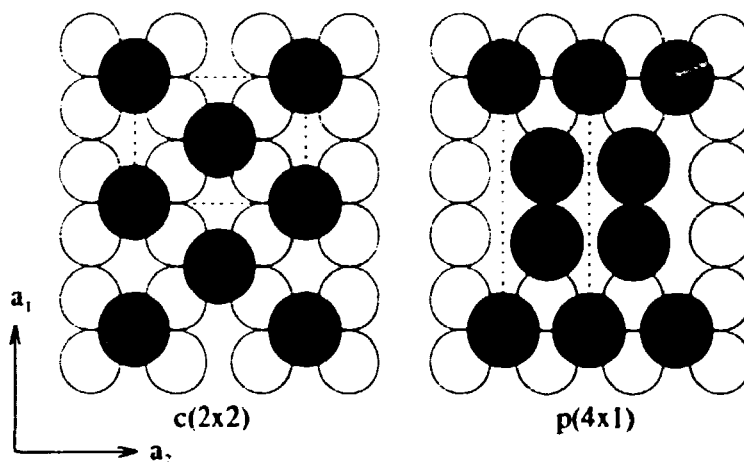


Fig. 1. Models for the Cu(110) $c(2 \times 2)$ -Bi and Cu(110) $p(4 \times 1)$ -Bi superstructures.

¹⁾ L. Lottermoser *et al.*, Surface Science (1995), *accepted*.

²⁾ W. D. Clendening and C. T. Campbell, J. Chem. Phys., **90**, 6656 (1989).

2.5.10 Sulphur Induced Reconstructions of the Ni(111) and Cu(111) Surfaces

M. Foss, *Institute of Physics and Astronomy, University of Aarhus, Denmark*, R. Feidenhans'l, E. Findeisen, M. Nielsen, *Department of Solid State Physics, Risø National Laboratory, Denmark*, T. Buslaps, R. L. Johnson, *II. Institut für Experimentalphysik, Universität Hamburg, Germany*, F. Besenbacher and I. Stensgaard, *Institute of Physics and Astronomy, University of Aarhus, Denmark*

We have studied the restructuring of Ni(111) and Cu(111) surfaces induced by sulphur adsorption by x-ray diffraction. We have identified the driving force behind the restructuring to be a tendency for sulphur to be four-fold coordinated although the surfaces have hexagonal symmetry. The surface structures have rather complex unit cell geometries. On Ni(111) a $5\sqrt{3} \times 2$ structure with a rectangular unit cell is formed, whereas on the Cu(111) surface a $\sqrt{7} \times \sqrt{7}R19.1^\circ$ or a $\begin{vmatrix} 4 & -1 \\ 1 & 4 \end{vmatrix}$ structure are formed, depending on sulphur coverage. The measurements were performed at the BW2 wiggler beamline at HASYLAB. In spite of the quite different unit cells, a crystallographic analysis show the basic unit in all three structures is a quadratic Me_4S cluster ($Me=Cu, Ni$), where S is four-fold coordinated in a local pseudo-(100) geometry. For the Ni(111) $5\sqrt{3} \times 2$ structure the intensities of the fractional in-plane data show that the structure is nearly having a glide-plane suggesting that the space group is $p2mg$. We derive a model consisting of four Ni_4S units rotated clockwise-anti clockwise in pairs of two. The structure is in good agreement with STM images. It includes 16 Ni atoms in the reconstructed layer and has a coverage of 0.4 ML of sulphur. For the $\begin{vmatrix} 4 & -1 \\ 1 & 4 \end{vmatrix}$ Cu(111) structure there are two Cu_4S units per unit cell.

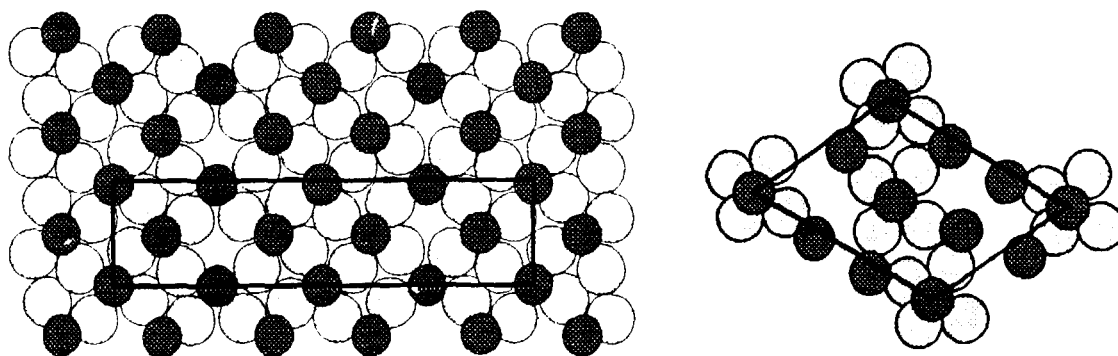


Fig. 1. Left: the Ni(111) $5\sqrt{3} \times 2$ -S structure. The shaded atoms are Sulphur. Right: the $\begin{vmatrix} 4 & -1 \\ 1 & 4 \end{vmatrix}$ Cu(111)-S structure.

2.5.11 The $c(8 \times 2)$ Reconstruction of the In-rich InSb(001) Surface

D.-M. Smilgies, E. Landemark, R. Feidenhans'l, M. Nielsen, *Department of Solid State Physics, Risø National Laboratory, Denmark*, L. Seehofer, G. Falkenberg, L. Lottermoser, R.L. Johnson, *II. Institut für Experimentalphysik, Universität Hamburg, Germany*, A.A. Davis, and R.G. Jones, *Department of Chemistry, University of Nottingham, UK*

We have studied the $c(8 \times 2)$ reconstruction of the InSb(001) surface with x-ray diffraction and scanning tunneling microscopy (STM). This surface structure is prepared by cycles of sputtering and annealing and the surface is believed to be In enriched ^{1,2}. Our STM pictures nicely show the $c(2 \times 8)$ periodicity; however, scans at positive bias (unoccupied states) and negative bias (occupied states) look quite different from each other making it impossible to deduce the structure from the STM graphs directly.

Subsequently we have taken an extensive structural data set, including in-plane scans as well as several rod scans, at the wiggler beamline BW2 in HASYLAB. 222 in-plane reflections were measured. In the Zinblende structure the (001) surface with In termination has only twofold symmetry. Thus there is only one rotational domain which was found to have two mirror planes. Most of the in-plane reflections were recorded in the irreducible quadrant; in addition several symmetrically equivalent reflections were checked. Figure 1 shows the Patterson function calculated from the fractional order reflections. The fundamental vector (40) (or (01), which is equivalent) is nearly as strong as (00). The other features in the Patterson function are comparatively weak. Their symmetry indicates that the structure is almost $p(4 \times 1)$ which implies that a (4×1) model should provide a good starting point for the structure determination.

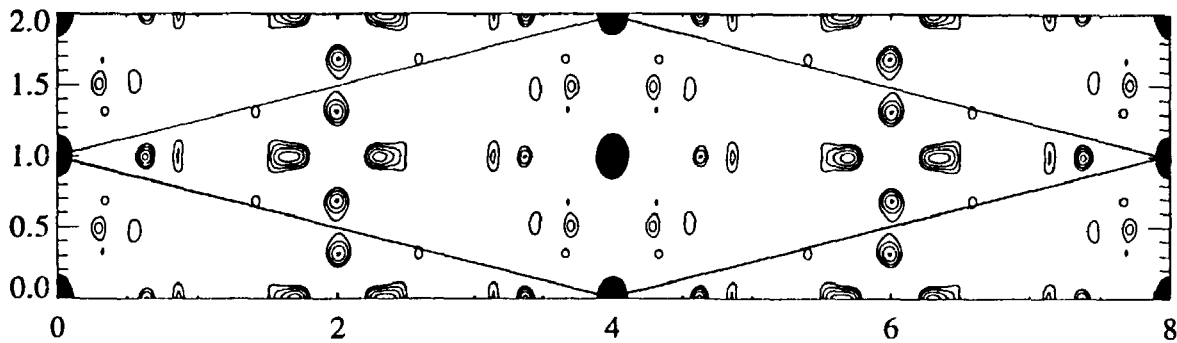


Fig. 1. In-plane Patterson function for the $c(8 \times 2)$ -InSb(001) surface. 154 symmetry-averaged fractional order reflections were used. The $c(8 \times 2)$ unit cell is indicated.

The crystal truncation rods, including the (00) rod, are quite structured, indicative of a deep reconstruction. The (00) rod has an interesting feature close to the (002) reflection, which should help to find the density distribution of the atoms near the surface. In view of the largeness of our data set, we believe it will be possible to solve this structure.

¹) T. John, T. Miller, and T.-C. Chiang, *Phys. Rev.* **B39**, 1730 (1989).

²) M.O. Schweitzer *et al.*, *Surf. Sci.* **280**, 63 (1993).

2.5.12 X-Ray Structure Analysis of the (1×2)-Phases of Bi/GaSb(110)

L. Lottermoser, T. van Gemmeren, R. L. Johnson, *II. Institut für Experimentalphysik, Universität Hamburg, D-22761 Hamburg*, R. Feiaenhans¹, M. Nielsen, D.-M. Smilgies, E. Landemark, *Department of Solid State Physics, Risø National Laboratory, Denmark*, C. Mariani and L. Gavioli, *Dipartimento di Fisica, Università di Modena, Italy*

Ordered nonreactive systems provide the best starting point for studying the structural and electronic properties of metal-semiconductors interfaces. Both bismuth and antimony adsorbed on (110) surfaces of many III-V compound semiconductors form well-ordered interfaces. Skeath *et al.*¹⁾ observed that a monolayer (ML) of Sb deposited on GaAs(110) at room temperature forms zigzag chains of Sb atoms bonded alternately to Ga and As atoms. Bi deposited on GaSb(110) at room temperature also shows an ordered (1×1) reconstruction consisting of Bi zigzag chains²⁾. The structure of the thermally more stable (1×2) reconstruction has not been determined previously.

Using surface x-ray diffraction at the Wiggler beamline BW2 at Hasylab in Hamburg, we have studied the atomic structure of the (1×2) reconstruction on GaSb(110). For the structural analysis we have collected a complete in-plane and out-of plane data set. All the fractional-order reflections can be indexed in terms of a (1×2) unit cell. The fractional-order structure intensities can be used to calculate directly the electron density auto-correlation function (Patterson function). A contour plot of the Patterson function gives a map of the interatomic vectors in the (1×2) surface unit cell as shown in Fig. 1. The data analysis has not yet yielded a definitive structural model. However, the data indicate that several sublayers are involved in the reconstruction, which makes the refinement of the structure more time-consuming.

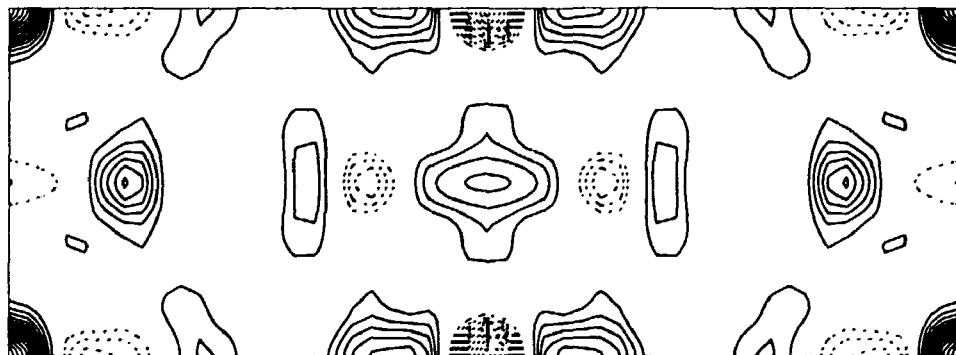


Fig. 1. Contour map of the Patterson function using the intensities of the fractional-order reflections. Positive contours are shown with solid lines and negative ones with dashed lines.

¹⁾ P. Skeath, L. Lindau, C.Y. Su, and W.E. Spicer, *J. Vac. Sci. Technol.* **19**, 556 (1989).

²⁾ T. van Gemmeren and R.L. Johnson, *Surf. Sci.*, *accepted*.

2.5.13 Metallic Thin Films and Superlattices

M.J. Christensen, J. Larsen, R. Feidenhans'l, *Department of Solid State Physics, Riso National Laboratory, Denmark*

In 1994 the work on metallic superlattices has included neutron diffraction on Cr/Mn superlattices, x-ray diffraction on Fe/V superlattices, and atomic force microscopy on MgO and Al₂O₃ substrates. These studies have now given us a good understanding of the structural properties of these systems, and we are considering to examine other systems like Cu/X multilayers where X is some metal. As a possible buffer layer for these multilayers, we have grown high quality Nb thin films on sapphire (11 $\bar{2}$ 0) substrates. The substrates have been annealed in air at 1600°C for 8 hours. This treatment improves the surface significantly. Figure 1 show a $\theta - 2\theta$ out of plane scan along sapphire (11 $\bar{2}$ 0). We see a narrow substrate peak, and a broader thin film peak. The Laue function with its side oscillations, correspond to 108 layers of a Nb(110) film. The fit is in reasonably agreement with the data. The shoulder to the left of the sapphire peak is due to the interface distance between Nb and sapphire, and has not been taken into account in the model. The coherence length of the film, obtained from the width of the central peak is equal to the film thickness. RHEED pictures of the surface showed very sharp streaks, also indicating the high quality of the film.

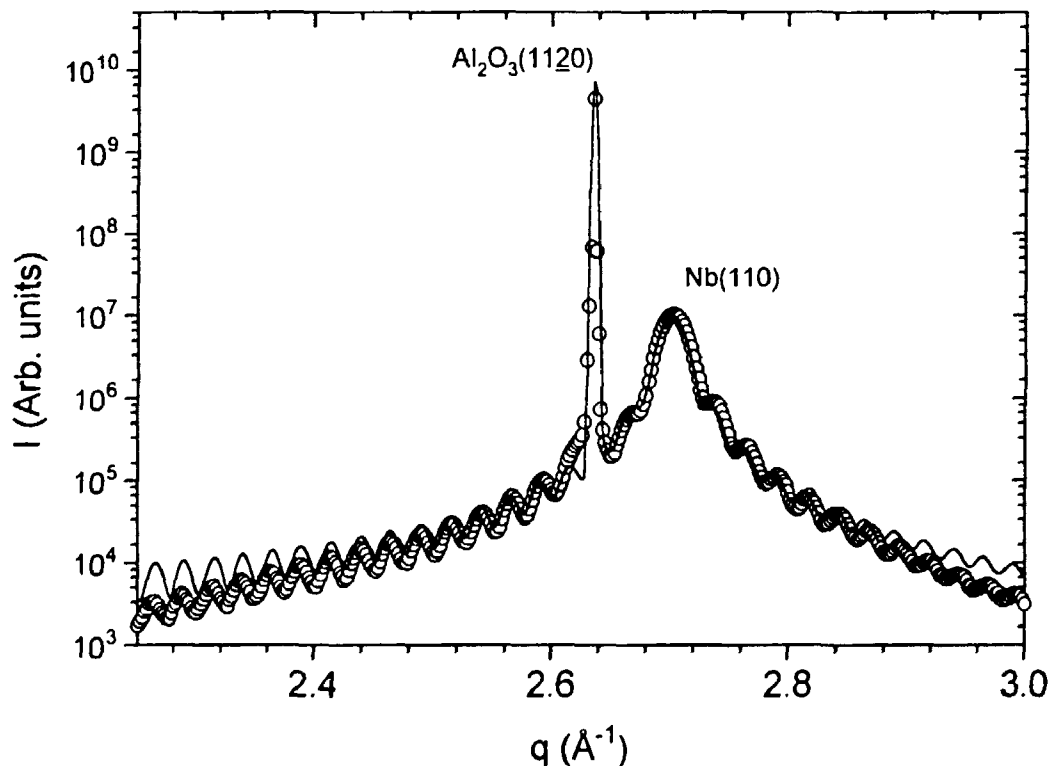


Fig. 1. Nb(110) thin film grown on Sapphire substrate which has been annealed in air at 1600°. The solid line indicates the fit.

2.5.14 Epitaxy of HTC Films on SrTiO₃ Substrates

D.-M. Smilgies, R. Feidenhans'l, M. Nielsen, *Department of Solid State Physics, Riso National Laboratory, Denmark*, Q. Jiang, J. Zegenhagen, and M. Cardona, *Max-Planck-Institut für Festkörperforschung, Stuttgart, Germany*

c-axis oriented films of SmBa₂Cu₃O₇ and GdBa₂Cu₃O₇ were grown on SrTiO₃ substrates by laser ablation. SmBa₂Cu₃O₇ and GdBa₂Cu₃O₇ exhibit a similar crystal structure and superconducting transition temperature as YBa₂Cu₃O₇. However, they have a smaller misfit with the substrate. Thick films of 800 Å and 1500 Å show the well-known twinning behavior due to the orthorhombic distortion. The twin boundaries are aligned along the [110] directions and the film diffraction spots show the typical fourfold splitting^{1,2)}.

Thin SmBa₂Cu₃O₇ films of 500 Å grow pseudomorphically, as can be seen from the single peak at the (2,0,0.310) position in Fig. 1. The reciprocal lattice units were chosen with respect to the SrTiO₃ lattice, which serves as a yardstick, in order to be able to detect subtle differences between the films' properties and the structure determined for the bulk material. Apart from the pseudomorphic maximum we observe four satellite peaks in the [110] directions. These satellites occur at constant *q*, as was verified at the (100) and (400) reflections and reveal a density modulation in the film with a very long wavelength of about 100 lattice constants. This behavior may be due to the formation of domain boundaries which help the pseudomorphic film to relieve some of its stress.

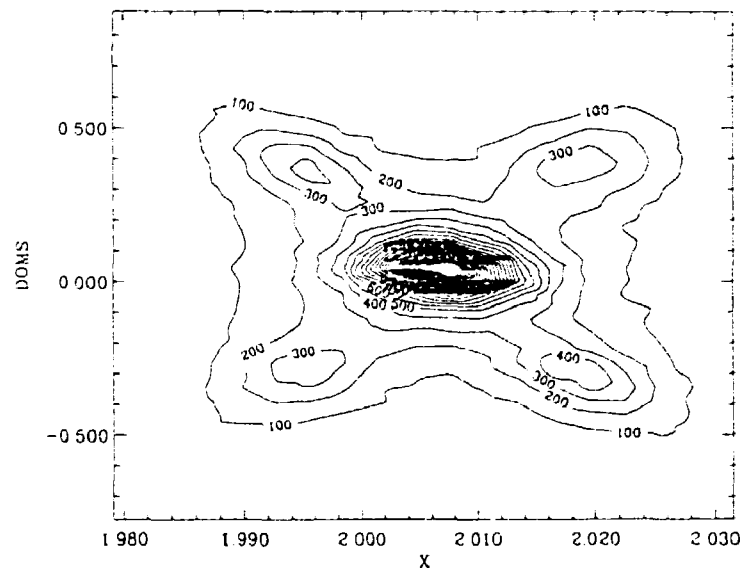


Fig. 1 (2,0,0.310) reflection of a thin SmBa₂Cu₃O₇ film grown on SrTiO₃. Thin films are pseudomorphic, but form domain walls to relieve stress, as can be seen from the four satellite peaks.

Satellites were also observed for a thinner sample (200 Å). Furthermore, second-order satellites were found around the (400) reflection. In future experiments we want to measure integrated intensities throughout reciprocal space in order to determine the nature of the density modulation and how the transition to twinning in the thicker films occurs.

¹⁾ Kromann *et al.*, J. Appl. Phys. **71**, 3419 (1992).

²⁾ Steinborn *et al.*, Physica C **220**, 219 (1994).

2.5.15 X-Ray Scattering from a SrTiO₃ Bicrystal Interface

A. Kazimirov, I. Denk, J. Maier, J. Zegenhagen, *Max-Planck-Institut für Festkörperforschung, Stuttgart, Germany*, D.-M. Smilgies, R. Feidenhans'l, *Department of Solid State Physics, Risø National Laboratory, Denmark*, and D. Abernathy, *European Synchrotron Radiation Facility, Grenoble, France*

SrTiO₃ crystals have important applications as gas-sensors, typically operated at high temperatures where the oxygen stoichiometry and thus the conductivity due to oxygen deficiency is a function of the oxygen partial pressure. Typically ceramic materials are used where the oxygen transport is strongly influenced by crystalline interfaces. As a prototype we studied the interface of a SrTiO₃ bicrystal at the TROIKA beamline at the ESRF. The two crystals with 18.4° miscut from the (001) direction along the [100] azimuth corresponding to a (103) surface normal, had been fused at elevated pressure and temperature. One of the crystals had been polished to a thickness of 10 μm and thus it could be penetrated by the 15.3 keV x-ray radiation (just below the Sr-K edge) we used to make the interface accessible. Transmission electron microscope pictures of similar samples suggest a well-ordered interface¹⁾.

We measured four different interface truncation rods, crossing the (103), (200), (400) and ($\bar{2}01$) reflections of the thick part of the bicrystal. All rods are normal to the (103) interface plane. The (103) reflection is common for both bicrystal parts. In Fig. 1a we show the result for the (400) rod. A fit to the data reveals a rather smooth interface with a root-mean-square roughness of ≈ 6 Å. The contribution of the surface of the bicrystal to the rod can be neglected, since atomic force microscopy shows a very rough surface. In Fig. 1b we present the results for the (103) rod. This rod does not smoothly decay, but a maximum can be distinguished at $\Delta q \approx -0.5$ which will allow us to deduce details about the interface structure, such as reconstruction or relaxation.

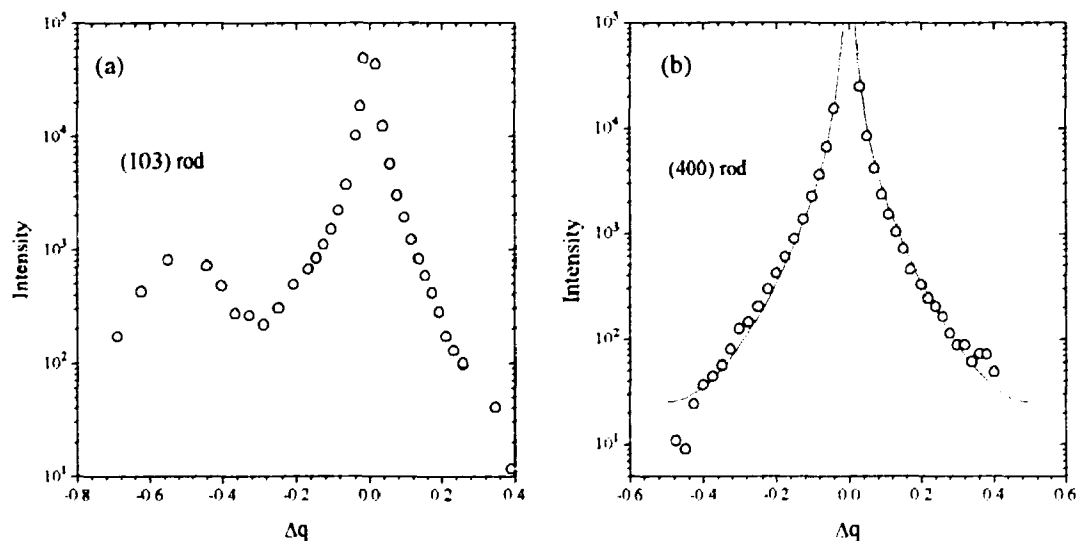


Fig. 1. Crystal truncation rods of a SrTiO₃ bicrystal interface. In panel a) the regular rod through (400) rod is shown. The rod through (103) in panel b) displays additional structure.

¹⁾ I. Denk *et al.*, unpublished.

2.5.16 In-situ X-Ray Characterization of the GaAs(001)-H₂SO₄(:Cu) Interface

G. Scherb, D. M. Kolb, *Abteilung Elektrochemie, Universität Ulm, Germany*, D.-M. Smilgies, R. Feidenhans'l, *Risø National Laboratory, Denmark*, A. Kazimirov, and J. Zegenhagen, *Max-Planck-Institut für Festkörperforschung, Stuttgart, Germany*

In contrast with metal electrodes, standard electrochemical methods do not provide much information about microscopic structural changes at semiconductor electrodes¹⁾. This is due to the limited carrier concentration and mobility in the semiconductors, leading to space charge regions and band bending. Therefore the actual electrochemical potential at the surface of the electrode is not known, but can, on the other hand, additionally be influenced by injection of carriers into the depletion layer, e.g. by photoabsorption. In a first step towards a better understanding of semiconductor electrode processes we investigated the GaAs(001)/H₂SO₄ interface and the adsorption of Cu from this acidic solution *in-situ* via X-ray diffraction at the HASYLAB BW2 beamline.

The energy of the x-ray beam (9.1 keV) was chosen 0.1 keV above the CuK absorption edge. Crystal truncation rods, measured at a glancing angle of incidence (1.0°) with various electrode potentials revealed a strong dependence of the surface roughness on the applied potential. Furthermore, carriers generated by the x-ray photo is in the depletion layer, strongly enhanced the roughening process. Thus the rods measured at equilibrium (currentless) conditions (-0.7 V vs. SCE) 15 and 30 minutes after filling of the cell with electrolyte clearly demonstrate the effect of x-ray-induced photocorrosion (Fig.1). Time-dependent measurements of the rod intensities showed that the roughening process can partially be reversed at negative electrode potentials.

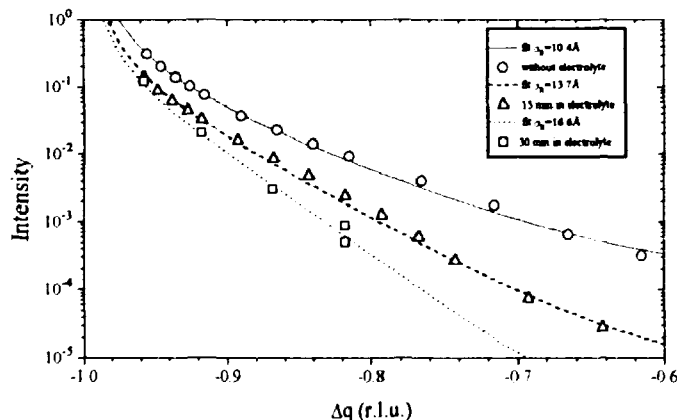


Fig. 1. (110) rod of a GaAs(001) surface in air and after 15 and 30 minutes in electrolytical environment. At currentless conditions the surface roughens considerably when exposed to the beam.

After copper deposition epitaxial Cu clusters were identified by radial scans, with <100> orientation along the <110> direction of the substrate (FWHM $\approx 5^\circ$). Measuring the Cu diffraction peak intensity across the sample revealed pronounced inhomogeneities: The metal coverage increased towards the edges of the sample. This is obviously due to the diffusion-controlled processes of the nucleation and deposition in the thin-film electrochemical cell.

¹⁾ H. Gerischer *et al.*, *Advances in Physics* **27**, 437 (1978).

2.5.17 X-Ray Diffraction Study of Polymer Films on Graphite and H-Si(111)

R. Feidenhans'l, *Department of Solid State Physics, Risø National Laboratory, Denmark*,
M. Sandberg and M. Sano, *Pi-Electron Materials Project - ERATO, Tsukuba, Japan*

Scanning Tunneling Microscopy (STM) investigations have recently shown that a single layer of a polymer can order epitaxially on a single crystal surface. In order to obtain more structural information about lattice constants, molecular order, etc. we have performed a preliminary x-ray diffraction experiment at beamline BW2 in HASYLAB.

We have investigated Poly(3,3-bis(chloromethyl)oxacyclobutane) on SuperGraphite (Graphite which is similar to, but with higher surface quality than Highly Oriented Pyrolytic Graphite HOPG) and on the hydrogen terminated H-Si(111) surface. The angle of incidence of the x-ray beam to the surfaces was set to the critical angle for total reflection in order to enhance the signal from the surface and reduce the background from the bulk. For H-Si(111) no reflections from an ordered polymer film could be detected. However, a number of unidentified powder peaks were observed. Measuring in the direction normal to the surface, the peaks had an characteristic onset, when the angle of exit was equal to the critical angle. This is strongly indicative for the signal arising from the surface. Furthermore, the Crystal Truncation Rods (CTR) from the H-Si(111) were extremely sharp, with a FWHM width of 6 mdeg in an ω -scan at the (10) in-plane CTR position. This means that the polymer film has prevented the surface to oxidize, which is an effect that normally happens on a time scale of a few hours on a clean H-Si(111) surface. An x-ray reflectivity scan of the surface showed a surface layer on the Si-surface with a thickness of about 15 Å. On the SuperGraphite, only a in-plane powder scan was performed, as shown in the figure. Again, the diffraction peaks cannot be related to to known reflections from the bulk polymer. More measurements are necessary.

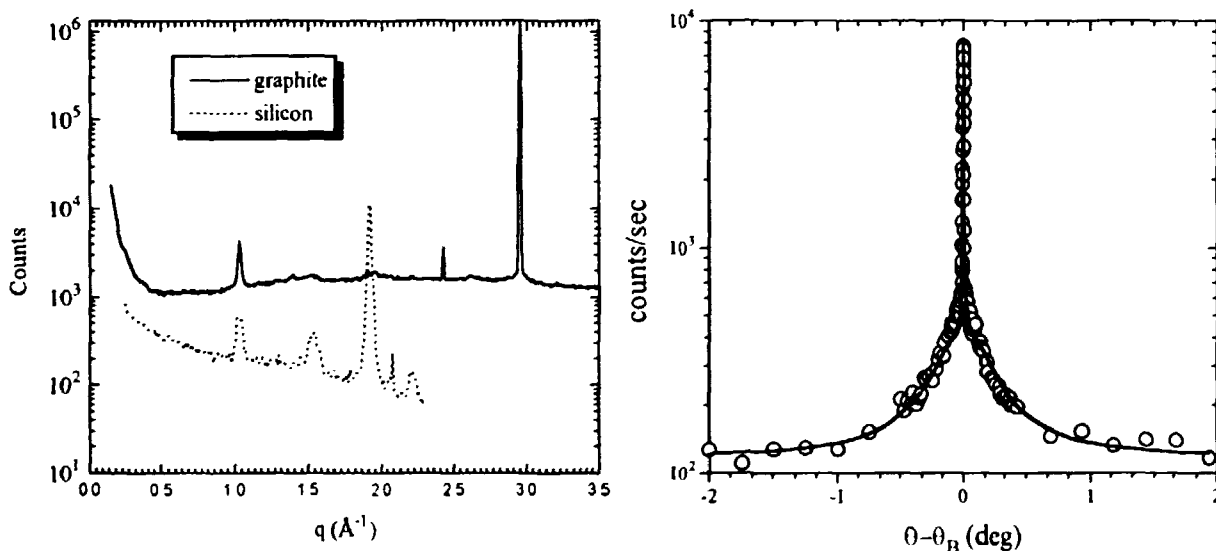


Fig. 1 On the left is the in-plane powder scan for the two samples shown. The peak at about 1.9Å^{-1} for the Si surface is a CTR signal, the peak at 2.95Å^{-1} is a powder Graphite peak. On the right an ω -scan of the (10) in-plane CTR for the H-Si(111) is shown.

2.5.18 Surfaces of an Organic Crystal: β -Alanine

D. Gidalevitz, L. Leiserowitz, *Weizmann Institute of Science, Israel*, D. M. Smilgies, and R. Feidenhans'l, *Department of Solid State Physics, Risø National Laboratory, Denmark*

The growth habits of crystals in solution are controlled to a large extent by the nature of the crystal-liquid interface, however, it is not easy to characterize. As a model system, we have studied the growth of organic crystals composed of zwitterionic molecules such as β -alanine ($^+\text{H}_3\text{N}-\text{C}_2\text{H}_4-\text{CO}_2^-$), in order to ensure strong molecular interactions. The morphologies of these crystals are strongly affected by ionic additives, such as CdBr_2 , when grown in aqueous solution. These changes were interpreted in terms of binding of the Cd^{++} or the Br^- ions to those crystal faces which expose the highest concentration of CO_2^- and NH_3^+ groups¹⁾.

β -alanine single crystals can be grown in solution to near perfection. The crystal structure is orthorhombic with 8 molecules per unit cell and spacegroup *Pbca*. The molecules form layers perpendicular to the *b*-axis which are strongly bonded. Neighboring layers are weakly bound by van-der-Waals interaction. Thus (010) is the cleavage plane of the crystal. We have performed x-ray scattering from a crystal cleaved in air at beamlines W1 and BW2, HASYLAB. The (0*k*0) rod could be measured between (020) and (040). Note the dip close to (0,2.3,0). In a simulation we could show that this feature is due to the structure factor of two molecules possessing a center of inversion; within the unit cell there are 4 such pairs.

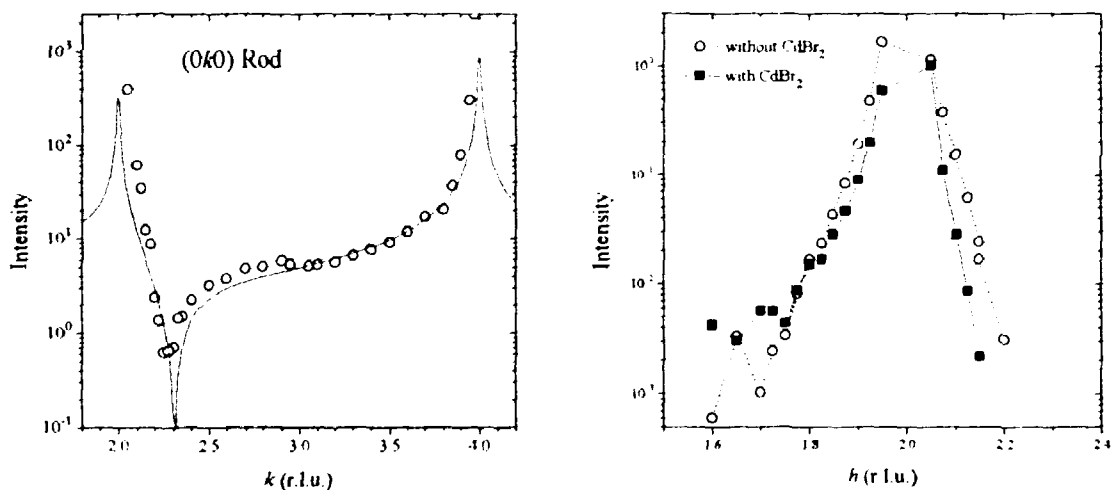


Fig. 1. Left: comparison of experimental data (symbols) and a structure factor calculation (solid line) for the (0*k*0) rod of β -alanine. Note the dip at $k = 2.3$. Right: The (202) CTR peak on the (100) surface with (filled squares) and without (open circles) CdBr_2

If CdBr_2 is added to the solution, in which the crystal grows, new faces of the single crystal are formed. They have been identified as (100) surfaces¹⁾. An incentive of our study is to determine the binding sites of the Cd^{++} and Br^- ions. First scans of a surface in contact with solution, with and without CdBr_2 , have been taken. However, up to now the prepared (100) surfaces are more rough than the (010) cleavage planes. A more detailed structural analysis is in progress.

¹⁾ D. Gidalevitz *et al.*, *J. Am. Chem. Soc.* **116**, 3271 (1994).

2.5.19 Molecular Structure within Self-Assembled Hexakis(hexylthio)-triphenylene: Monolayers

J.-C. Gabriel, K. Bechgaard, *Department of Solid State Physics, Riso National Laboratory, Denmark*, N.B. Larsen, M. Larsen, K. Schaumburg, *CISMI, Department of Chemistry, Science Park, University of Copenhagen, Fruebjergvej 3, DK-2100, Denmark*.

In recent years, liquid crystals, especially discotic liquid crystals, have been proposed as candidates for highly oriented thin film electronic conductors of one-dimensional molecular structures. We have studied the Hexakis(Hexylthio)-triphenylene (HHTT) (see Fig. 1), which is the only Hexakis(alkylthio)-triphenylenes that shows a discotic hexagonal ordered phase, D_{6h}. This ordering seems to be crucial for getting high conductivity¹⁾ within the columnar phase. The first step of our research was to investigate the assembling properties of these molecules at the liquid-graphite interface. This was achieved by Scanning Tunneling Microscopy (STM). It was also a rare example (if not the first) of an aromatic ring substituted with sulphur studied by STM. We observed two-dimensional patterns in an area as large as 100 × 100 nm². By using the graphite lattice as an internal reference, one could measure, with good precision, the parameters of its unit cell: $a = 22.2(2)\text{\AA}$, $b = 36.8(2)\text{\AA}$, $\gamma = 60.0(2)^\circ$. Figure 2 shows a high resolution scan of the monolayer, where the side-on triphenylene core shapes can clearly be recognized as the brightest zones. The size of these zones indicates that the core to be considered includes the six surrounding sulphur atoms. This can be seen in Fig. 2, where a packing model of this core is superimposed at the same scale. The molecules show two alternating different orientations that are opposite to each other and gives rise to a crystalline double row structure.

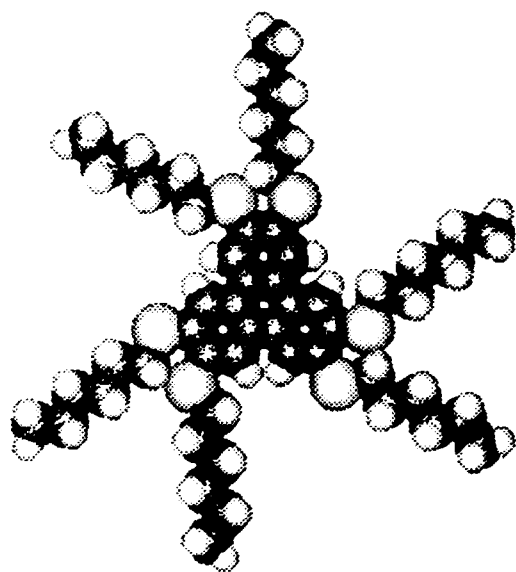


Fig. 1. Molecular structure of HHTT (yellow: S, blue: C and white: H)

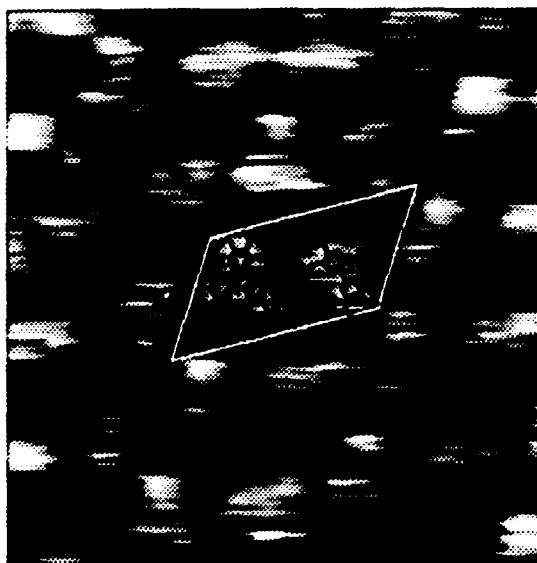


Fig. 2. HHTT monolayer at the interface with a solution and HOPG. Image size: 9.7 nm x 9.7 nm.

¹⁾ D. Adam *et al.*, *Nature* **371**, 141-143 (1994).

2.5.20 X-ray Diffraction Study of Cr/Mn Superlattices

J.G.Larsen, R.Feidenhans'l, M.J.Christensen, *Department of Solid State Physics, Riso National Laboratory, Denmark*, and J.Pohl, *Institute of Physics, University of Konstanz*

We have studied the growth of Cr/Mn superlattices on the MgO(001) and Ge(001) surfaces with a small Fe buffer layer 20 Å thick and with varying Mn thickness (5-20 Å), all grown at room temperature. In this way it is possible to stabilize the δ -Mn-phase, which is a high-temperature structure stable between 1150-1250°C. The structural relationship on Ge is : $\text{Ge}(001) \parallel \text{M}(001) \setminus \text{Ge}(100) \parallel \text{M}(100)$ and on MgO: $\text{MgO}(001) \parallel \text{M}(001) \setminus \text{MgO}(100) \parallel \text{M}(110)$ (M=Fe,Cr, δ -Mn).

X-ray diffraction measurements were performed at the rotating anode (Riso) using a graphite monochromator. Inplane measurements on 20 Å Fe (Cr₄₀Mn₂₀)_{33.5} films shows that Cr/ δ -Mn grow pseudomorphic on MgO, but form an incommensurate structure with Ge as substrate, as seen in figure 1a. From the rocking curves of these Bragg reflections it is found that the intralayer order is better for superlattices grown on MgO (1.082°) compared to Ge (1.473°). Hence as far as the inplane measurements concern, MgO is better suited for the epitaxial growth of Cr/ δ -Mn films, despite the fact that MgO(001) has a larger lattice mismatch with Fe and Cr than Ge(001). X-ray scans along the specular (00 l) direction is shown in figure 1b for the MgO sample. Also shown is a fit which is in good agreement with data. From the model and the inplane scans we have found that the Poisson's ratio for the metal layers is close to the bulk values independent of the substrates. The model also tells us that the interface should be much sharper for the MgO sample, as inplane measurements also indicates. Rocking curves of main peaks and the satellite peaks, indicate better layering along the modulation direction for samples grown on Ge. The coherence length in the plane of the films are on MgO samples about 25 % longer than on Ge samples, but the coherence length in the modulation direction is app. 65 % longer for Ge samples. This could mean that the pseudomorphic growth on MgO strains the superlattice substantially, such that it destroys the coherence along the modulation direction.

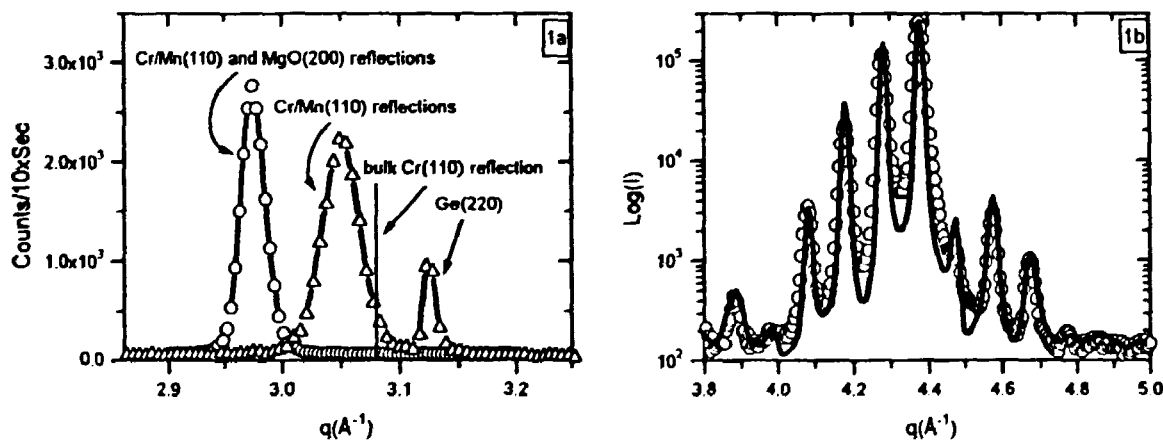


Fig. 1. 1a) Inplane scans illustrating the two different grow modes, pseudomorphic on MgO and the incommensurate structure on Ge. 1b) (00 l) scan on MgO sample along with a fit.

2.6 Langmuir Films

2.6.1 X-Ray 2D-Powder Diffraction Methods for Films at Liquid Surfaces

K. Kjær and W.G. Bouwman, *Department of Solid State Physics, Risø National Laboratory, Denmark*

Langmuir films (mono- or multilayers of - usually - amphiphilic molecules on the surface of liquids) have been studied by X-ray Grazing-Incidence Diffraction at the undulator beam line BW1 in HASYLAB at DESY, Hamburg. The samples are nearly always '2D powders', *i.e.*, rotating the sample container around a vertical axis has no effect on the scattering pattern observed. Thus, the experimental variables are the vertical incidence and exit angles $\alpha_i (\simeq 0)$, α_f , and the horizontal scattering angle $2\theta_{\text{hor}}$. Experimentally, 3-dimensional diffraction data (I vs. $(2\theta_{\text{hor}}, \alpha_f)$) are collected with the program TASCOM running in the BW1 μ VAX. A vertical linear PSD resolves α_f while $2\theta_{\text{hor}}$ is resolved by scanning a Soller collimator consisting of many vertical, parallel plates. Software has been written in the language IDL for visualising the data on-line during scans and for doing the first data analysis on-line. This runs on a Pentium PC which is linked to the BW1 μ VAX by the PCSA network protocol. New mirrors installed by HASYLAB in Nov. 1994 give an additional $\times 4$ gain in useful flux for liquid surface studies, chiefly because of improved horizontal focussing. Most systems form thin films that are horizontal over many mm^2 and many of them are 2D-'crystalline' powders. Hence, as function of horizontal scattering vector $q_{xy} \simeq (2\pi/\lambda)(1 + \cos^2 \alpha_f - 2 \cos \alpha_f \cos 2\theta_{\text{hor}})^{1/2} \sim (4\pi/\lambda) \sin(2\theta_{\text{hor}}/2)$, narrow peaks of constant q_{xy} (Bragg rods) are observed - their q_{xy} -width Δ_I limited by resolution and by lateral positional coherence length in the film. As function of the vertical component $q_z \simeq (2\pi/\lambda) \sin \alpha_f$, (*i.e.* along the Bragg rod) one observes broader maxima of q_z -width $\Delta_{II} \sim 2\pi/L$, L being the thickness of the film. Recently, however, we have found that some multilayer films (*e.g.*, C_{24} -alkane films, *cf.* Fig. 1 and a separate report in this volume) additionally exhibit a third type of broadening in the (q_{xy}, q_z) -plane: along lines of constant $q_{\text{tot}} = (q_{xy}^2 + q_z^2)^{1/2}$ (the *Scherrer rings*), indicating a *mosaic* distribution of 2D-crystallites. For small misorientation u , the broadening becomes $\tilde{\Delta}_{III} = \text{FWHM}u \cdot (G_z, -G_{xy})$. Thus, for $G_z \neq 0$, $\tilde{\Delta}_{III}$ can easily be separated from Δ_I and Δ_{II} , *cf.* Fig. 1a, but for $G_z \sim 0$, $\tilde{\Delta}_{III}$ resembles Δ_{II} . The cause of the mosaicity is under investigation.

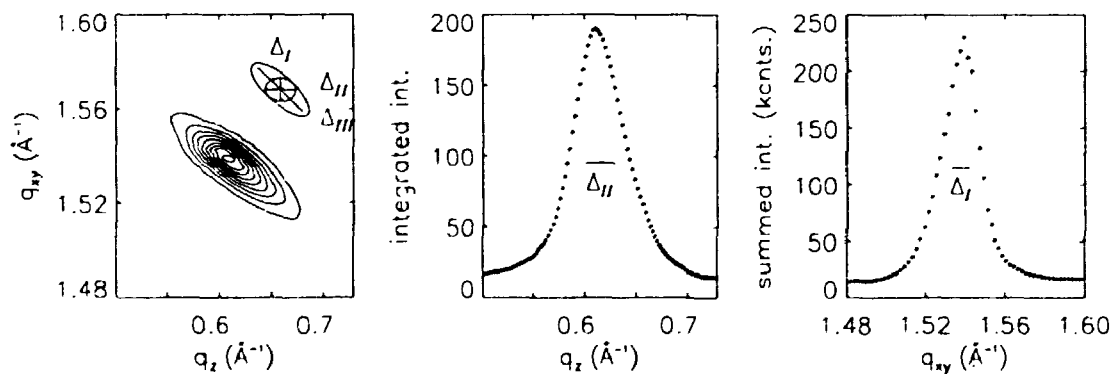


Fig. 1. Data for multilayers of $\text{C}_{24}\text{H}_{50}$. a) From analysis of the contour plot we find that $\text{FWHM}u = 1.6^\circ$, Δ_I is determined by the resolution, and Δ_{II} corresponds to a film thickness of 180\AA , corresponding to 6 layers. The projections b) and c) are broader than Δ_{II} , resp. Δ_I , due to the mosaicity contribution $\tilde{\Delta}_{III}$.

2.6.2 Tilted Monolayer Phases of Diol Derivatives Studied by Grazing Incidence X-Ray Diffraction

G. Brezesinski, E. Scalas, H. Möhwald, *Institut für Physikalische Chemie, Universität Mainz, Germany*, R. Rietz *Institut für Physicalische Chemie, Universität Halle, Germany*, W.G. Bouwman, and K. Kjær, *Department of Solid State Physics, Riso National Laboratory, Denmark*

Investigation of the influence of chirality on monolayer behaviour is of considerable interest because in Nature many processes are influenced by chiral molecules. Monolayers of a racemic mixture of the pure S- and R-enantiomers of 1-hexadecyl-glycerol have been investigated by grazing incidence X-ray diffraction (GID) using the liquid surface diffractometer on the undulator X-ray beam line BW1 at HASYLAB, DESY, Germany. For both the S-enantiomer and the (R,S) racemate, Fig. 1 shows contour plots of the corrected X-ray intensities as a function of the in-plane scattering vector component Q_{xy} and the out-of-plane scattering vector component Q_z at different surface pressures Π . At all pressures investigated the pure enantiomers exhibit three diffraction peaks although at higher lateral pressures two of them are barely resolved. These results indicate an oblique lattice. At lower surface pressures the molecules are tilted between the nearest- (NN) and the next-nearest-neighbour (NNN) directions. With increasing pressure the tilt direction changes slowly to NNN and above 28mN/m a constant tilt direction (very close to NNN) is observed for all pressures. The racemic mixture exhibits only two diffraction peaks, indicating a rectangular unit cell. Below 18mN/m the Bragg rod of the single peak has its maximum intensity at the horizon ($Q_z = 0 \text{ \AA}^{-1}$) whereas for the two-fold degenerate peak the maximum is at higher Q_z . Above 18mN/m both peaks have their maximum intensity at higher Q_z . The observed intensity distribution in Q_z can be explained by a tilt of the chains towards NN (below 18mN/m) and a tilt towards NNN (above 18mN/m).¹⁾

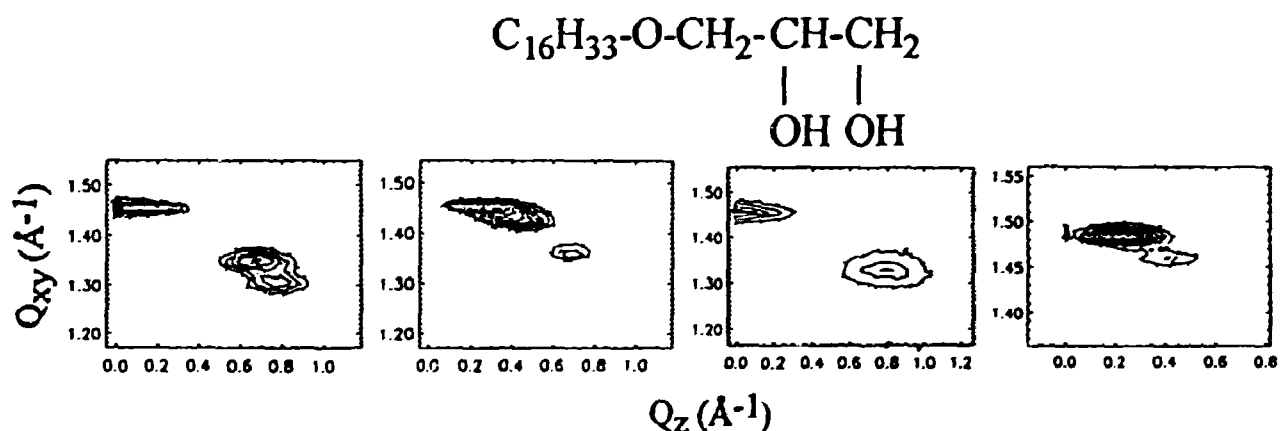


Fig. 1. Contour plots of the corrected X-ray intensities from monolayers versus in-plane and out-of-plane scattering vector components Q_{xy} and Q_z . From left to right, S-enantiomer at 12 and 24 mN/m, (R,S) racemate at 14 and 45 mN/m.

¹⁾ G. Brezesinski, R. Rietz, W.G. Bouwman, K. Kjær, and H. Möhwald (1994). *Il Nuovo Cimento*, *accepted*.

2.6.3 Structure of Monolayer Phases of a Simple n-alkane-1,2-diol

G. Brezesinski, K. de Meijere, B. Struth, E. Scalas, H. Möhwald, *Institut für Physikalische Chemie, Universität Mainz, Germany*. R. Rietz *Institut für Physicalische Chemie, Universität Halle, Germany*. F. Bringezu, *Institut für Pharmazeutische Chemie, Universität Halle, Germany*. W.G. Bouwman, and K. Kjær, *Department of Solid State Physics, Risø National Laboratory, Denmark*

One of the factors that influence the packing of monolayers is certainly the hydrophilic head-group. As compared to 1-hexadecyl-glycerol (see preceding abstract), nonadecane-1,2-diol (cf. Fig. 1) has a smaller headgroup because the ether oxygen (-O-) has been removed. This chemical modification yields a completely different phase behaviour. The isotherms indicate that nonadecane-1,2-diol forms only condensed films up to 40°C. At all pressures investigated the racemic (R,S) diol exhibits two diffraction peaks, indicating a rectangular unit cell. The different rectangular phases can be classified in terms of tilt direction and unit cell distortion direction: Starting from a hypothetical hexagonal lattice the NN distortion is obtained by stretching the lattice in the direction of nearest neighbours (NN); then for the degenerate peak, Q_{2xy} is smaller than for the non-degenerate peak Q_{1xy} , cf. Fig. 1. Conversely, if $Q_{2xy} > Q_{1xy}$ the distortion is in the next-nearest-neighbour (NXX) direction. At 20°C the molecules are tilted towards NN at all pressures. On increasing the lateral pressure the tilt angle changes continuously from 33° at 2 mN/m to 14° at 42 mN/m. Between 30 and 40mN/m a transition from NN- to NXX-distortion of the lattice takes place. At 5°C the same behaviour is observed at lower pressures: The transition from NN- to NXX-distortion occurs already between 15 and 20mN/m. Furthermore, between 25 and 30mN/m the tilt direction changes to NXX and the lattice distortion changes back to NN.

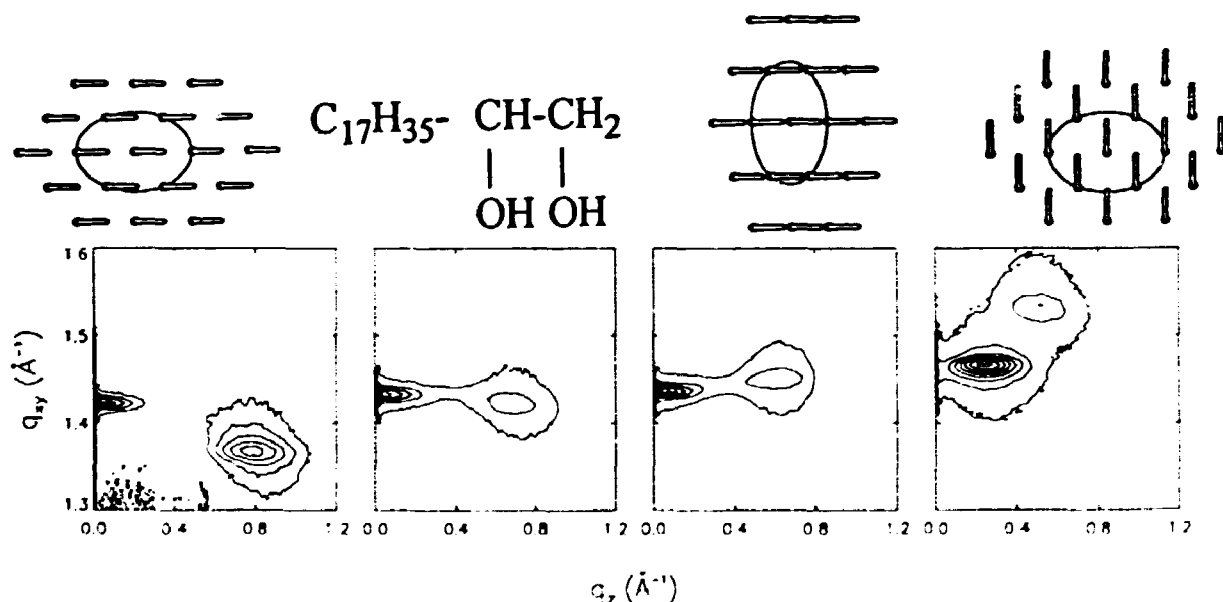


Fig. 1. Contour plots of the corrected x-ray intensities vs. (q_{xy}, q_z) , the horizontal and vertical components of the scattering vector, for nonadecane-1,2-diol monolayer phases at 5°C. From left to right 2, 15, 25, and 40 mN/m. The cartoons on the top represent top-views of the packing (left to right: NN tilt, NN distortion; structural formula: NN tilt, NXX distortion; NXX tilt, NN distortion).

2.6.4 Correlation between Domain Shapes and Monolayer Structures of Triple-chain Phospholipids on Water

A. Dietrich, G. Brezesinski, H. Möhwald, *Institut für Physikalische Chemie, Universität Mainz, Germany*, W.G. Bouwman, and K. Kjær, *Department of Solid State Physics, Risø National Laboratory, Denmark*

Phospholipids, as one of the dominant components of biological membranes, provide interesting model systems for studying the richness of monolayer phases. Two triple-chain phospholipid isomers were investigated at the air-water interface by means of fluorescence microscopy and Grazing-Incidence X-ray Diffraction (GID). Near the transition pressure Π_c one observes nucleation and growth of domains of condensed phase. For 1-(2C₁₄-16:0)-2H-PC (cf. Fig. 1) the domain initially grows as a circle. For 2-(2C₁₄-16:0)-2H-PC polygonal domains appear. Fig. 1 shows, for increasing surface pressure, the diffraction intensities as function of the in-plane component Q_{xy} of the scattering vector. The high pressure phase of these triple-chain lipids shows only one diffraction peak, indicating a hexagonal packing of the chains. Versus Q_z the maximum intensity occurs in the plane of the water surface ($Q_z = 0 \text{ \AA}^{-1}$) and hence a vertical chain orientation can be deduced. At lower pressures the occurrence of two peaks in the 2D powder pattern indicates a rectangular unit cell. The observed intensity distributions in Q_z can be explained by a tilt of the chains towards their next nearest neighbours. In the case of 1-(2C₁₄-16:0)-2H-PC the phase transition from rectangular to hexagonal packing occurs at a surface pressure between 13 mN/m and 20 mN/m. The tilt angle at 10 mN/m amounts to 7°, and at 13 mN/m to 4°. The low tilt angle just above the transition pressure Π_c indicates that this condensed phase is only slightly distorted from hexagonal packing. In the case of 2-(2C₁₄-16:0)-2H-PC the transition to the hexagonal phase occurs only between 30 mN/m and 40 mN/m. At the lowest pressure investigated (13 mN/m) a tilt angle t of 14° was found. These quantitative differences of the molecular structure may be connected to a change in the morphology of domains from circular to dendritic.

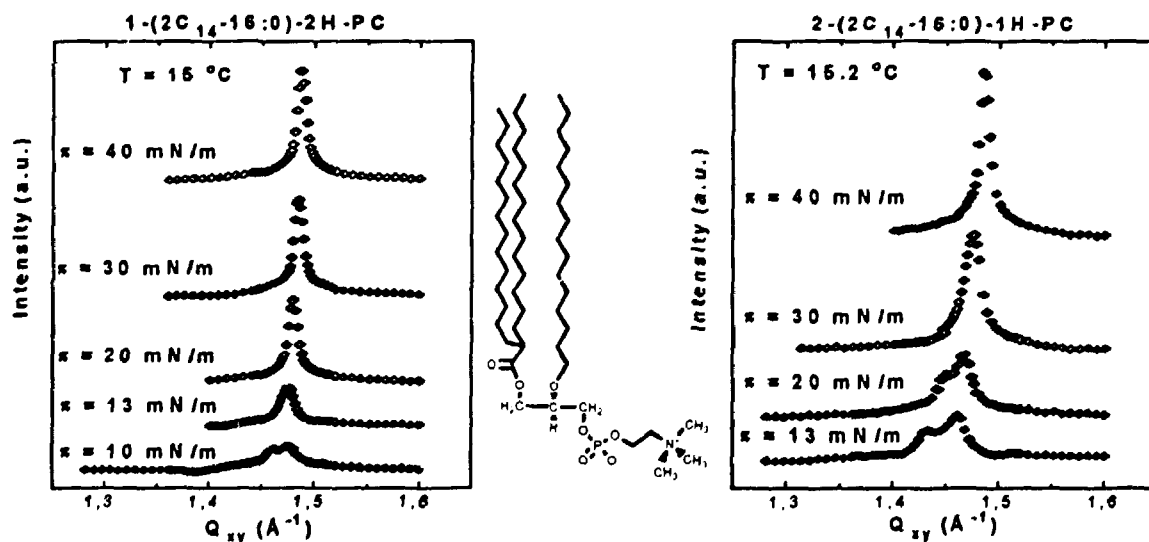


Fig. 1. Diffraction intensities (integrated over the whole Q_z -window of the PSD) versus in-plane component Q_{xy} of the scattering vector, for different surface pressures. Center: structural formula of 1-(2-tetradecyl-palmitoyl)-2-hexadecyl-phosphatidylcholine (1-(2C₁₄-16:0)-2H-PC). In 2-(2C₁₄-16:0)-2H-PC the branched and unbranched chains are interchanged.

2.6.5 Highly Compressed Phases of $C_{22}H_{45}OH$

R. Edgar, J. Majewski, M. Lahav, L. Leiserowitz, *Department of Materials and Interfaces, The Weizmann Institute of Science, Israel*, J. Als-Nielsen, W.G. Bouwman, and K. Kjær, *Department of Solid State Physics, Risø National Laboratory, Denmark*

On the surface of water, at sub-monolayer coverage, amphiphilic aliphatic alcohols $C_nH_{2n+1}OH$ form crystalline *monolayers*, the structure depending on chain length n .¹⁾ The tilt angle t (from vertical) of the molecular axes characteristically varies with n . For $n = 10$ we interpolate¹⁾ $t \sim 10^\circ$. By contrast, in 3D crystals the molecular chains are highly tilted from the normal to the layer plane by $\sim 35^\circ$. The question arose as to what would be the structure of a *multilayer*, *en route* to 3D crystal structure formation. $C_{22}H_{45}OH$ was spread on the water for 130% of monolayer coverage and compressed to 260% coverage at surface pressure 38mN/m. This corresponds to the so-called “collapsed monolayer state”. However, the GID Bragg rod intensity profiles by their q_z -widths and by detailed modelling nevertheless indicated a *monolayer* phase with unit cell $a = 5.0\text{\AA}$, $b = 7.4\text{\AA}$, $\gamma = 90^\circ$ and the molecular chains tilted by $t \sim 3^\circ$ along the $\vec{a}/a + \vec{b}/b$ direction. (α phase, Fig. 1a). The intensity distribution of the monolayer α phase is slightly skewed along lines of constant $q = (q_{xy}^2 + q_z^2)^{1/2}$ (the Scherrer ring, indicated by dashed lines in Fig. 1a), indicative of a slight deviation of the monolayer from horizontality, probably imposed by the high surface pressure. On spreading more material onto the x-ray footprint, diffraction was observed additionally from a dynamically growing β phase of *ca.* 5-6 layers thickness, according to the q_z -width of the Bragg rod (Fig. 1b). In the multilayer β phase ($a = 5.0\text{\AA}$, $b = 7.3\text{\AA}$, $\gamma = 90^\circ$) the molecular chains are tilted by about 5° in the \vec{b} direction. Thus, under the experimental conditions, the β multilayer phase has a tilt angle t much smaller than in the 3D crystal structure. There is, nevertheless, a tendency towards increased tilt from that of the compressed monolayer structure. In the future, what is required is to obtain multilayer alcohol crystallites in the uncompressed state.

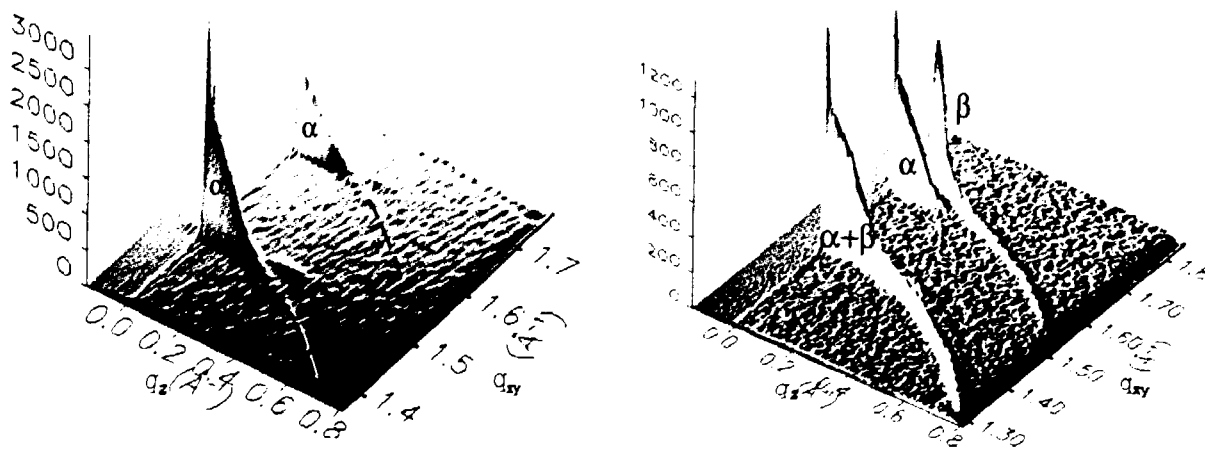


Fig. 1. a) 260% coverage (dashed lines: Scherrer ring $q \equiv \text{const.}$); b) coverage increased further.

¹⁾ J. Majewski, R. Popovitz-Biro, W.G. Bouwman, K. Kjær, J. Als-Nielsen, M. Lahav, and L. Leiserowitz. The structural properties of uncompressed crystalline monolayers of alcohols $C_nH_{2n+1}OH$ ($n = 13 - 31$) on water, *submitted*.

2.6.6 Influence of a Hydrophilic Spacer on the Structure of a Phospholipid Monolayer

B. Struth, E. Scalas, G. Brezesinski, H. Möhwald, *Institut für Physikalische Chemie, Universität Mainz, Germany*, F. Bringezu, *Institut für Pharmazeutische Chemie, Universität Halle, Germany*, W.G. Bouwman, and K. Kjær, *Department of Solid State Physics, Risø National Laboratory, Denmark*

Introducing hydrophilic spacers between the glycerol backbone and the phosphatidylcholine head-group can change intra- and intermolecular interactions and the size of the hydration shell around the head-group itself.¹⁾ As a spacer we used the oxy-ethylene group (-O-CH₂-CH₂-), a typical hydrophilic unit in non-ionic surfactants. The investigated compounds are ether lipids with $n = 0, 1, 2$ (see Fig. 1) which form stable monolayers on water. The introduction and elongation of the spacers lead to a fluidization of the monolayer. At all pressures investigated and for all the substances there are three diffraction peaks indicating an oblique structure whose lattice parameters change continuously with pressure. In Fig. 1 we show Grazing-Incidence Diffraction (GID) results for $n = 1$. The tilt angle decreases with increasing lateral pressure. At the highest pressure ($\Pi = 41\text{mN/m}$) for $n = 0$ the tilt angle is 21° , whereas for $n = 1$ and $n = 2$ the tilt angles are 18° and 13° , respectively. At this pressure the cross-sectional area of the chains amounts to $(20.2 \pm 0.2)\text{\AA}^2$, which is a typical value for rotator phases. The hydrophilic spacer reduces the area per molecule. A reason for this reduction could be the decoupling of the hydrophobic and hydrophilic moieties. This could lead to a change in the conformation of the head-groups or to their partial interdigitation. Comparing the chain cross-sectional areas and the tilt angle at the lowest pressure ($\Pi = 14\text{mN/m}$), we find that the introduction and elongation of spacers lead to an increase in cross-sectional area and simultaneously to a decrease of the tilt angle. One possible explanation of this fact could be a perturbation of the $n = 0$ head-group arrangement due to a larger hydration shell or to a modification of head-group interactions leading to a partial disordering of the chains.

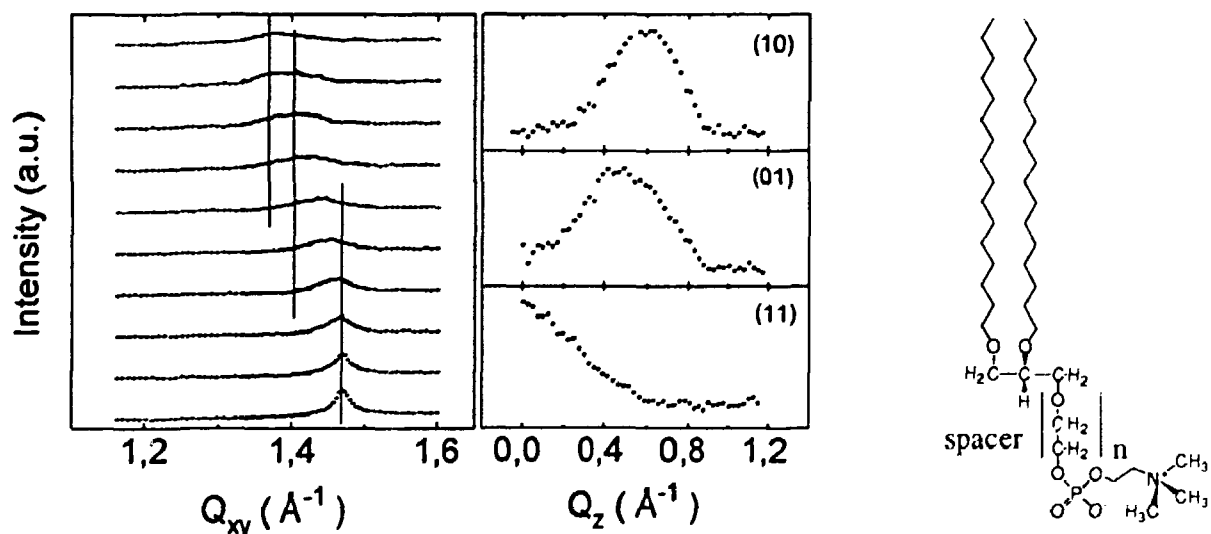


Fig. 1. (Left): GID data for $n = 1$. (Right): Schematic molecular structure.

¹⁾ B. Struth, E. Scalas, G. Brezesinski, H. Möhwald, F. Bringezu, W.G. Bouwman, and K. Kjær, (1994). *Il nuovo Cimento*, *accepted*.

2.6.7 Grazing-Incidence Synchrotron X-Ray Studies of Phase-Separated Mixtures of Amphiphilic Monolayers on the Surface of Water

J. Majewski, M. Lahav, L. Leiserowitz, *Department of Materials and Interfaces, The Weizmann Institute of Science, Israel*, W.G. Bouwman, J. Als-Nielsen, and K. Kjær, *Department of Solid State Physics, Risø National Laboratory, Denmark*

Previous studies have demonstrated that uncompressed monolayers of the alcohol $C_{31}H_{63}OH$ (C_{31}) can serve as very efficient nucleators for ice formation in supercooled water drops¹⁾, due, perhaps, to an epitaxial relation between their 2D crystal structure and the *ab* plane of hexagonal ice. In order to be able to control the size of the 2D crystallites of the C_{31} we designed an experiment in which $C_{31}H_{63}OH$ was mixed with $C_{10}F_{21}(CH_2)_2OH$ ($C_{12}F$). Such alcohol monolayer mixtures were expected to phase separate due to the different packing properties of the components. Our aim was (by varying the $C_{12}F/C_{31}$ ratio) to obtain 2-D islands of C_{31} of controllable size in a sea of $C_{12}F$ monolayer. By correlating the sizes with the temperature at which - on cooling - ice was nucleated in water drops covered by the mixed monolayers we aimed to obtain a measure of the minimum average size of C_{31} clusters which would nucleate ice crystals, and indirectly, the critical size of the ice nucleus under such conditions.

The two compounds are indeed phase separated. The fluorocarbon chains pack in a hexagonal unit cell ($a_H = 5.79\text{\AA}$) with molecules vertically aligned on the water surface. By contrast, the hydrocarbon alcohol molecules pack in a rectangular unit cell ($a = 4.95\text{\AA}$, $b = 7.6\text{\AA}$, $Z = 2$) arranged in a herring-bone structure in the plane group $p1g1$. The C_{31} molecules are tilted in the direction of the *b* axis by approximately $12^\circ \pm 1^\circ$, independent of the composition of the mixtures. Structural parameters were obtained by fitting models to the Bragg rod intensity profiles of both compounds. Remarkably, diffraction from C_{31} crystallites was observed for a little as 1% of C_{31} . The coherence lengths of the 2D C_{31} alcohol crystallites were anisotropic, extending approximately 300 to 500 \AA in the $\{1,1\}$ and 150 to 250 \AA in the $\{0,2\}$ crystallographic directions for C_{31} concentrations $\geq 5\%$. Only for C_{31} concentrations of 2.5% and 1% did the coherence length decrease. We have recently performed ice nucleation experiments with which to correlate the structural results obtained by Grazing-Incidence Diffraction. The results are presently being analysed.

¹⁾ M. Gavish, R. Popovitz-Biro, M. Lahav, L. Leiserowitz, *Science* **250**, 973 (1990).

2.6.8 Self-Aggregated 2D Crystal Structure of Mixed Monolayers of Triacontanoic Acid and Nonacosylamine. Evidence in Favour of an Ordered Arrangement of the Ionized Headgroups

D. Gidalevitz, I. Weissbuch, L. Leiserowitz, *Department of Materials and Interfaces, The Weizmann Institute of Science, Israel*, W.G. Bouwman, J. Als-Nielsen, and K. Kjær, *Department of Solid State Physics, Risø National Laboratory, Denmark*

Recently, we have reported¹⁾ the use of a mixed amphiphilic monolayer of octadecylamine ($C_{18}H_{37}NH_2$) and stearic acid ($C_{17}H_{35}CO_2H$) to mimic the crystal face of zwitterionic β -alanine ($^+H_3NCH_2CH_2CO_2^-$) which exposes CO_2^- and NH_3^+ groups. To find out if, in the mixed monolayer on pure water, the head groups are in the ionic CO_2^- and NH_3^+ states and arranged in an ordered manner (as in the face of β -alanine crystals) we have made use of a mixed monolayer of the longer chain compounds triacontanoic acid ($C_{29}H_{59}CO_2H$) and nonacosylamine ($C_{29}H_{59}NH_2$) in the uncompressed state. The GID pattern (Fig. 1) comprises nine peaks to yield a rectangular unit cell of dimensions $a = 4.97\text{\AA}$, $b = 7.42\text{\AA}$, area per molecule $A = 18.4\text{\AA}^2$. From the Bragg rods (not shown) we deduce that the molecules are approximately vertical. By comparison, in monolayers of $C_{29}H_{59}CO_2H$ on pure water the area per molecule $A = 20.6\text{\AA}^2$ and the molecular chains are tilted by an angle of 26° from the vertical.²⁾ Hence, a mixed phase with neighbouring carboxyl and amino groups – presumably ordered – has been formed. Now, without exception, in all 3D crystal structures of molecules of the type $HO_2C - X - NH_2$ or of the complex $X - CO_2H$ and $Y - NH_2$, the arrangement contains ions of the type CO_2^- and NH_3^+ , which are hydrogen bonded to each other. Thus it is very likely that at the aqueous solution interface such neighbouring groups are also in the ionized state.

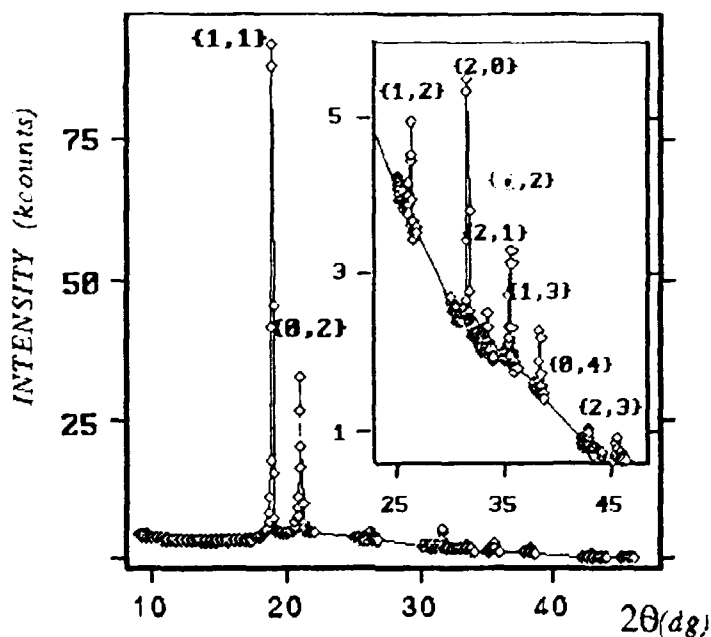


Fig. 1. Grazing-Incidence Diffraction pattern of $C_{29}H_{59}CO_2H / C_{29}H_{59}NH_2$ mixed monolayer at \sim zero surface pressure and at $5^\circ C$ over pure water. The $\{h, k\}$ indices of the reflections are indicated

¹⁾ D. Gidalevitz, I. Weissbuch, K. Kjær, J. Als-Nielsen, L. Leiserowitz, *J. Am. Chem. Soc.* **116**, 3271 (1994).

²⁾ F. Leveiller, D. Jacquemain, L. Leiserowitz, K. Kjær, J. Als-Nielsen, *J. Phys. Chem.* **96**, 10380 (1992).

2.6.9 Formation of a Copper Complex of Docosanoyl-(S)-Lysine, as Determined by GID at the Monolayer- Solution Interface

I. Weissbuch, M. Berfeld, M. Lahav, L. Leiserowitz, *Department of Materials and Interfaces, The Weizmann Institute of Science, Israel*, W.G. Bouwman, J. Als-Nielsen, and K. Kjær, *Department of Solid State Physics, Risø National Laboratory, Denmark*

According to (macroscopic) surface pressure vs. area isotherms, the binding of chiral solute molecules to the chiral head groups of Langmuir monolayers mediated by metal ion complexation should be very sensitive to the relative sense of chirality of the two species. Thus we undertook a study of the effect of water-soluble α -amino acids on the structure of the copper complexes of the α -amino acid *N*^c-docosanoyl-(S)-lysine, $\text{CH}_3\text{-(CH}_2\text{)}_{20}\text{-CO-NH-(CH}_2\text{)}_4\text{-CH(CO}_2^-)\text{-NH}_3^+$ monolayers. Grazing-Incidence diffraction (GID) data for the monolayer spread on water has shown the formation of two to four 2D-crystalline phases, depending on the temperature of spreading and that of the measurement (Fig. 1a). All the phases pack in cells of dimensions *ca.* $a \sim 5.6\text{\AA}$, $b \sim 7.9\text{\AA}$, $\gamma \sim 88^\circ$, $Z = 2$ and molecular area of 22.4\AA^2 with the molecules tilted by 22° (from the normal to the surface) along the *b* axis. This behavior may be related to the conformational and orientational freedom of the hydrocarbon chains, due to the large discrepancy between the packing of the chains that require a cross sectional area of $\sim 18.5\text{\AA}^2$ and that of the α -amino acid head groups that require $\sim 25\text{\AA}^2$. GID data for the same monolayer spread on a subphase containing 1 mM copper acetate (Cu^+ , CH_3CO_2^- , Fig.1b) shows the formation of a unique crystalline phase of structure different from that on pure water. The cell dimensions of this rectangular phase are $a = 5.7\text{\AA}$, $b = 8.4\text{\AA}$ and a molecular area of 23.8\AA^2 with a molecular tilt of about 29° . The increase of the molecular area as compared to that on water is consistent with the surface pressure-area isotherm measured on copper acetate which gives a larger limiting area per molecule. This behavior can be explained by the binding affinity of the copper ions to form a copper complex with both CO_2^- and NH_3^+ groups of the the α -amino acid monolayer. The formation of such a complex may "freeze" a specific molecular conformation resulting in only one crystalline phase. On addition of the soluble α -amino acid (R or S) serine ($\text{HO-CH}_2\text{-CH(CO}_2^-)\text{NH}_3^+$) into the subphase of the copper complex monolayer, no change was apparent in the GID data (not shown). The work continues.

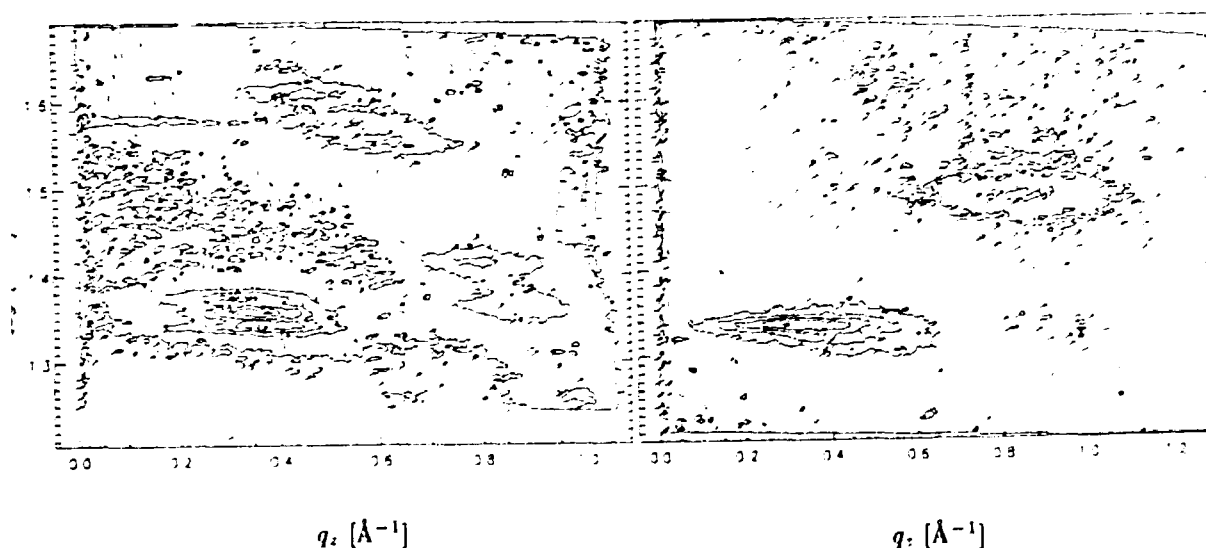


Fig. 1. a) S-monolayer on water

b) S-monolayer on 1 mM copper acetate

2.6.10 Dynamics of Chiral Microseparation in Amphiphilic Monolayers on the Surface of Water

I. Kuzmenko, E. Shavit-Gati, M. Lahav, L. Leiserowitz, *Department of Materials and Interfaces, The Weizmann Institute of Science, Israel*, W.G. Bouwman, J. Als-Nielsen, and K. Kjær, *Department of Solid State Physics, Risø National Laboratory, Denmark*

Chiral resolution of racemic mixtures, first discovered by Pasteur for three-dimensional crystals¹⁾, has now become an attractive subject for investigation of 2D systems due to the development of powerful methods of surface analysis, such as Grazing-Incidence Diffraction (GID), atomic force microscopy (AFM), Brewster angle microscopy, etc. As a possible candidate to form chiral crystal aggregates from a racemic mixture on a water surface α -hydroxydocosanoic acid ($C_{20}H_{41}CH(OH)COOH$), which possesses one chiral center, was chosen because the 3D crystal structure of its shorter-chain analogue $C_{12}H_{25}CH(OH)COOH$ consists of chiral layers related by centers of inversion²⁾. Therefore, it might undergo chiral segregation when crystallized in two dimensions. Toluene which has a high boiling point ($111^\circ C$) was chosen as a spreading solvent instead of the usual chloroform to provide the system additional time for possible chiral segregation. When crystallized from chloroform on the water surface at $5^\circ C$, the GID pattern indicates a rectangular cell with dimensions $a = 5.36, b = 8.82, \gamma = 90^\circ$ (Fig. 1A) with the molecular chains inclined along a . When crystallized from toluene under the same conditions diffraction looks similar ($a = 5.04, b = 9.07, \gamma = 90^\circ$) but the $\{1, \pm 1\}$ reflection is very expanded in q_z -direction and peaks at $q_z = 0$ (Fig. 1B). This could only be interpreted using a model of a twinned structure where two chiral domains are twinned about (01) and are scattering coherently. In each domain the molecules (all of the same chirality) are related by translational symmetry and are inclined in a general direction in the lattice. Chiral-resolved S - α -hydroxydocosanoic acid did not show any difference when spread from toluene in comparison to chloroform. In both cases the GID patterns yield an oblique cell which can be expressed in terms of an almost rectangular centered cell of dimensions: $a = 5.24, b = 9.02, \gamma = 92.5^\circ$ (Fig. 1C).

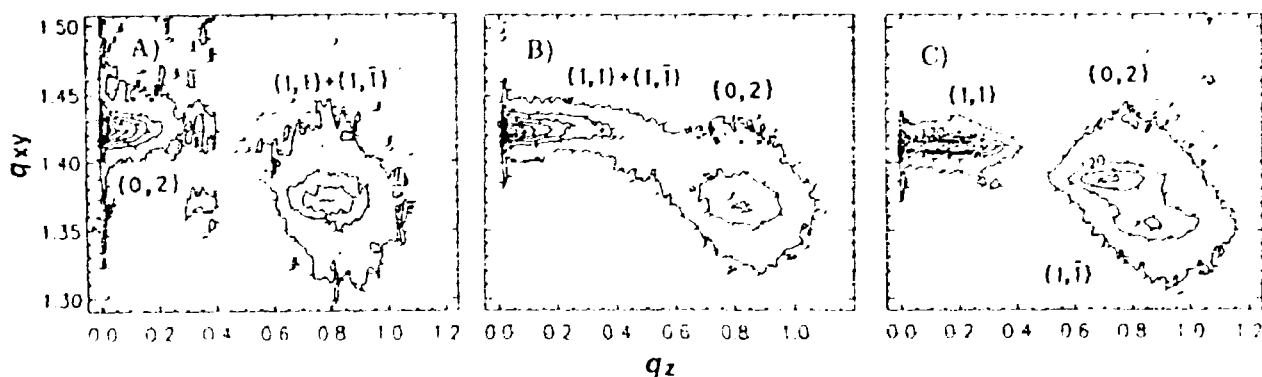


Fig. 1. (GID) patterns of monolayers on water spread at $5^\circ C$: A, (R,S)-hydroxydocosanoic acid spread from chloroform; B, (R,S)-hydroxydocosanoic acid spread from toluene; C, (S)-hydroxydocosanoic acid spread from toluene (spread from chloroform the same pattern is obtained).

¹⁾ L. Pasteur, *Ann. Phys.* **24**, 442 (1848).

²⁾ B. Dahl, B.M. Lunden, I. Pascher, *Act Cryst.* **B32**, 2059 (1976).

2.6.11 Influence of Handedness of Water-Soluble Additives on the Formation of Two-Dimensional Chiral and Racemic Amphiphilic Crystallites on Water Surfaces

I. Kuzmenko, E. Shavit-Gati, M. Lahav, L. Leiserowitz, *Department of Materials and Interfaces, The Weizmann Institute of Science, Israel*, and W.G. Bouwman, J. Als-Nielsen, K. Kjær, *Department of Solid State Physics, Risø National Laboratory, Denmark*

Chiral additives play an important role for all stages of crystal formation. They were successfully applied for separation of enantiomers which form conglomerates on crystallization¹⁾, for inducing growth of metastable crystalline polymorphs²⁾, and for oriented crystallization of glycine at the air-solution interface, in the presence of chiral resolved α -amino acids³⁾. Racemic (R,S) as well as chiral resolved *S*- α -hydroxydocosanoic acid ($C_{20}H_{41}CH(OH)COOH$), described in the preceding report, were deposited at 5° C with chloroform and toluene as spreading solvents on water solutions of chiral and racemic lactic acid ($CH_3CH(OH)COOH$), mandelic acid ($C_6H_5CH(OH)COOH$) and non-chiral glycolic acid ($CH_2(OH)COOH$) and explored by Grazing-Incidence Diffraction (GID). In the case of chiral *S*- α -hydroxydocosanoic acid, the presence of the α -hydroxyacids in the subphase induced noticeable shifts in the diffraction pattern for all three reflections (Fig. 1A) as compared to the pure water subphase (Fig. 1C in preceding report), but almost no difference was found when one chiral additive was replaced by another. In the case of (R,S)- α -hydroxydocosanoic acid with toluene as a spreading solvent, the diffraction pattern remained essentially unchanged when the chiral R or S-additives were used (Fig. 1B) in comparison to the pure water subphase (Fig. 1B in preceding report). Racemic mandelic acid and non-chiral glycolic acid solutions led to substantially different results. In the case of glycolic acid, the GID pattern (Fig. 1C) looks similar to the one found for the racemic monolayer crystallized from chloroform on pure water (Fig. 1A in previous report), which indicates similarity in the crystal packing arrangement with the molecular chains inclined along *a* by 35°. On racemic mandelic acid water solution, (R,S)- α -hydroxydocosanoic acid formed a centered rectangular cell ($a = 5.04, b = 9.17, \gamma = 90^\circ$) with the molecular chains inclined about 33° along the *b*-axis (Fig. 1D).

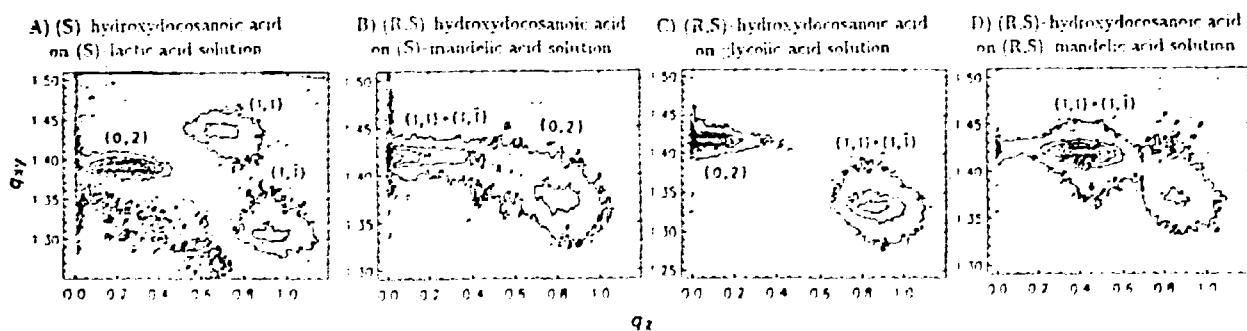


Fig. 1. (GID) patterns as described in the text.

- 1) Addadi, L., Weinstein, S., Gati, E., Weissbuch, I. and Lahav, M. (1982). *J. Am. Chem. Soc.* **104**, 4610.
- 2) Staab, E., Addadi, L., Leiserowitz, L. and Lahav, M. (1990). *Adv. Mat.* **2**, 40.
- 3) Weissbuch, I., Frolow, F., Addadi, L., Lahav, M. and Leiserowitz, L. (1990). *J. Am. Chem. Soc.* **112**, 7718.

2.6.12 Self-Assembled Crystalline Multilayers and Monolayers of *n*-Paraffins on Water Surfaces

S.P. Weinbach, I. Weissbuch, M. Lahav, L. Leiserowitz, *Department of Materials and Interfaces, The Weizmann Institute of Science, Israel*, W.G. Bouwman, J. Als-Nielsen, and K. Kjær, *Department of Solid State Physics, Riso National Laboratory, Denmark*

The *n*-paraffins C_nH_{2n+2} were found to spontaneously form crystalline multilayers or monolayers on water surfaces at 5° C. The alkane films were studied by pressure-area isotherms. Grazing-Incidence synchrotron X-ray Diffraction and reflectivity. The alkanes $n=36, 50$ form a crystalline monolayer with molecules aligned vertically in a herring-bone motif in plane group $pg1$. The alkanes $n=28, 29$ form a similar arrangement, but two to four layers thick in orthorhombic space groups $Pbc2_1$ and $Pbcm$, respectively. The alkanes $n=23, 24$ crystallise into films about 20 layers thick, in $Pbcm$ and (triclinic) $P\bar{1}$ space groups, respectively, as in their macroscopic crystals. With tailor made additives¹⁾ ($C_nH_{2n+1}OH$, $n = 27, 28$) in the films of $C_{23}H_{48}$ and $C_{24}H_{50}$, the number of layers is reduced to two. Such multilayers may be considered as intermediates in crystallisation, where a central question concerns the structure and threshold size for molecular clusters to adopt an arrangement akin to that of the macroscopic crystal¹⁾. The monitoring of such processes, comparable to the early stages of wax crystallisation, is of importance in the storage, transport and use of distillate petroleum fuels²⁾.

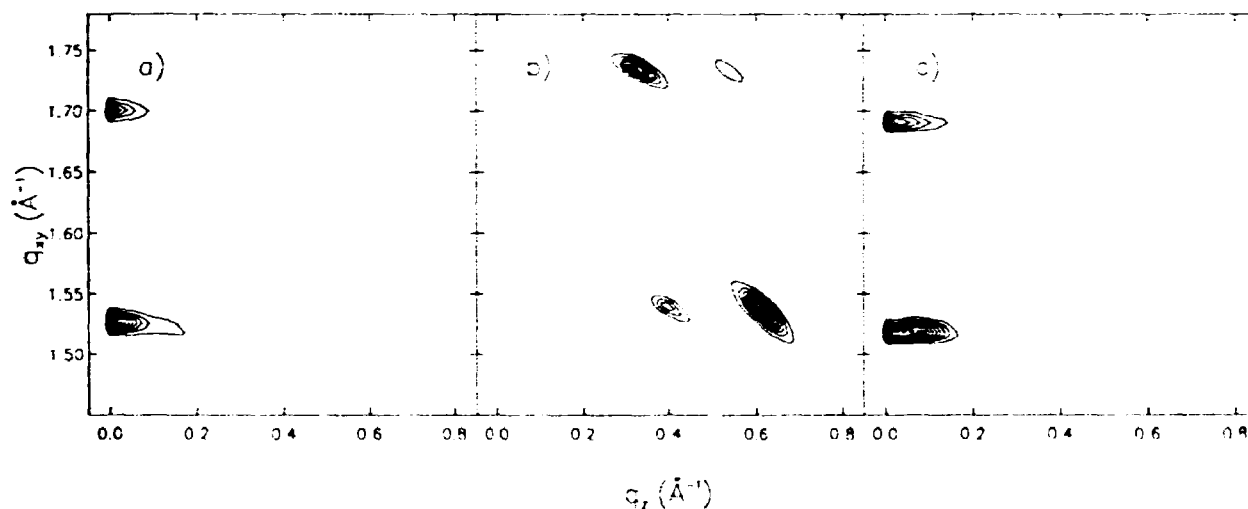


Fig. 1. Grazing Incidence Diffraction patterns for a) $C_{50}H_{102}$, b) $C_{24}H_{50}$, and c) $C_{24}H_{50}$ plus 10% $C_{28}H_{58}OH$.

¹⁾ S. Weinbach, K. Kjær, W.G. Bouwman, G. Grubel, J.F. Legrand, J. Als-Nielsen, M. Lahav, L. Leiserowitz, *Science* **264**, 1566 (1994).

²⁾ K. Lewtas, R.D. Tack, D.H.M. Beiny, J.W. Mullin, *Advances in Industrial Crystallization*; J. Garside Ed.; Butterworth-Heinemann: Oxford, 166-179 (1991).

2.6.13 *N*-Methyl Amides as Model Compounds for Understanding Monolayer and Multilayer Formation in Amphiphiles and Alkanes

S.P. Weinbach, M. Lahav, L. Leiserowitz, *Department of Materials and Interfaces, The Weizmann Institute of Science, Israel*, W.G. Bouwman, J. Als-Nielsen, and K. Kjær, *Department of Solid State Physics, Riso National Laboratory, Denmark*

Previously we have shown that the long chain amide arachidamide ($C_{19}H_{39}CONH_2$) on water forms a monolayer, while on formamide it forms a multiphase trilayer¹⁾ and that a related diamide ($C_{19}H_{39}CONHC_2H_4CONH_2$) forms a trilayer with essentially the same structure even on water²⁾. This year we have shown that (non-amphiphilic!) *n*-alkanes may also form multilayers on water (see preceding report). To understand the mechanism of formation of these multilayers and the conditions under which they form, we have performed analogous experiments on secondary amides, $C_{19}H_{39}CONHCH_3$ (1) and $CH_3HNCOC_{20}H_{40}CONHCH_3$ (2) which are intermediary between these amphiphilic and non-amphiphilic materials. Analysis of the Grazing-Incidence X-ray Diffraction (GID) patterns indicates that compound (1) forms a monolayer on water with orthorhombic-type herringbone packing of the molecules. Over formamide it initially forms primarily a monolayer with essentially the same packing mode as on water, but after four hours the film has grown to form a bilayer. If a tailor-made additive with a bulky group attached to the amide, $C_{19}H_{39}CONHCH_2C_5H_5$, is present in the spreading solution, then only a monolayer is formed on formamide. Compound (2) forms two monolayer phases on water (Fig. 1a), one with orthorhombic-type herringbone packing and the other with an oblique unit cell with the molecules μ -tilted along the $a + b$ axis, much like that found for the primary amides. After six hours (Fig. 1b) only the orthorhombic phase survives. On formamide (Fig. 1c) only the orthorhombic form, identical to the one found over water, is observed.

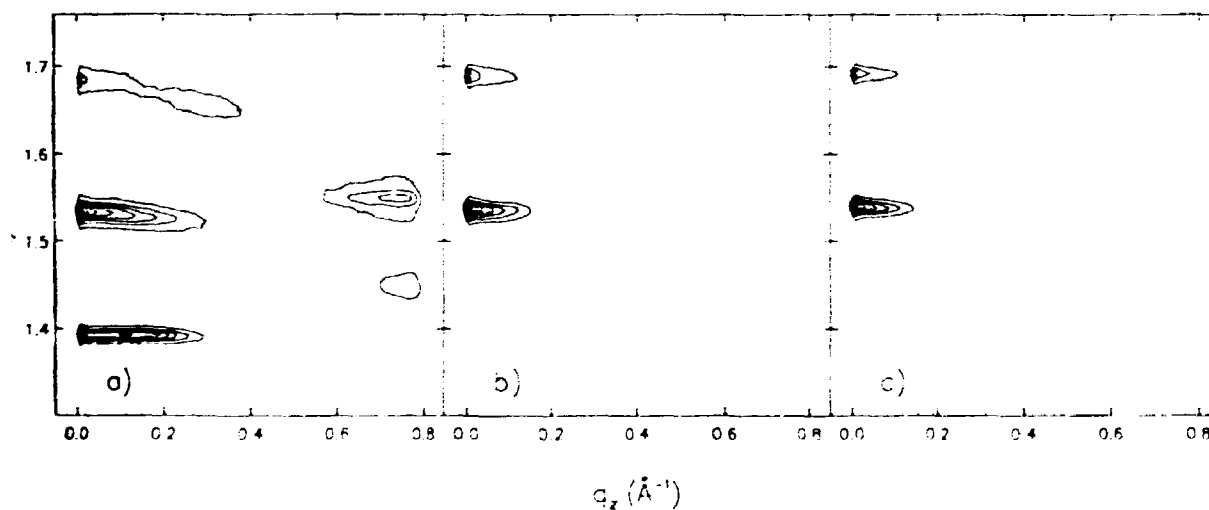


Fig. 1. GID patterns of compound (2) under conditions as described in the text.

¹⁾ S. Weinbach, K. Kjær, W.G. Bouwman, G. Grubel, J.F. Legrand, J. Als-Nielsen, M. Lahav, L. Leiserowitz, *Science* **264**, 1566 (1994).

²⁾ S. P. Weinbach, D. Jacquemain, F. Leveiller, K. Kjaer, J. Als-Nielsen, L. Leiserowitz, *J. Am. Chem. Soc.* **115**, 11110 (1993).

2.6.14 Two-Dimensional Crystalline Order at the Surface of Homogeneous Solutions

I. Weissbuch, M. Lahav, L. Leiserowitz *Department of Materials and Interfaces, The Weizmann Institute of Science, Israel*, W.G. Bouwman, J. Als-Nielsen, and K. Kjær, *Department of Solid State Physics, Riso National Laboratory, Denmark*

The surface excess of hydrophobic molecules in homogeneous aqueous solutions has been studied by surface tension measurements¹⁾, radiotracer counting and optical second harmonic generation techniques. Faceted domains at the surface of an aqueous solution of the surfactant $\text{CH}_3(\text{CH}_2)_{11}\text{-O-SO}_3^-\text{Na}^+$ (sodium dodecyl sulphate, or SDS for short), have been visualized by the addition of an insoluble fluorescent dye that was expelled during the domain growth process.¹⁾ None of these techniques have proved, however, the existence of a crystalline order at the surface of the homogeneous solution. Here we describe the first grazing incidence X-ray diffraction (GID) study showing the diffraction pattern from the surface of aqueous solutions of SDS below the critical micelle concentration $\text{cmc} \approx 0.26$ wt%. GID patterns for SDS solutions of concentration $c = 0.23, 0.18$ and 0.13 wt% at 5°C are shown in Fig. 1. The intensity of the Bragg peaks is seen to decrease with decreasing c . Unlike the case of insoluble surfactant, the number of surface molecules in the surface SDS film is not constant; its chemical potential is determined by c . For $c = 0.23$ wt% the broad Bragg peak and the extended Bragg rod are consistent with an essentially hexagonal cell ($a = 4.92\text{\AA}$) in which the chains are tilted by about 20° from the vertical (in a nearest-neighbour direction) and occupy an area per molecule of 21\AA^2 . This arrangement is somewhat similar to the chain packing in 3D crystals of SDS which has been described as an intermediate between the orthorhombic O_\perp and hexagonal chain-packing modes.²⁾ The data for lower concentration c are currently being analyzed.

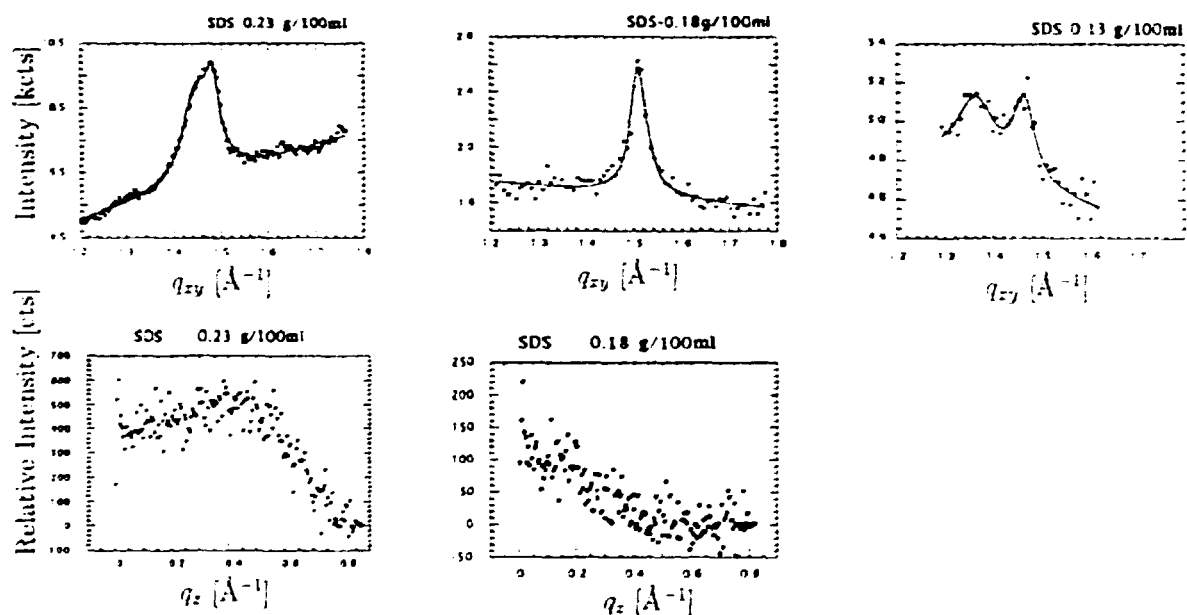


Fig. 1 Top: Intensity I vs. horizontal scattering vector q_{xy} . Bottom: I vs. vertical scattering vector q_z .

¹⁾ B. Berge, L. Faucher, K. Schwab, A. Libchaber, *Nature*, **350**, 322 (1991).

²⁾ S. Sundell, *Acta Chem. Scand. Ser. A*, **31**, 799 (1977).

2.7 Microemulsions, Surfactants and Biological Systems

2.7.1 Aggregation of Zinc-free Native Insulin and an Insulin Mutant Studied by Small-Angle Neutron Scattering

J. Skov Pedersen, *Department of Solid State Physics, Riso National Laboratory, Denmark*, S. Hansen, and R. Bauer, *Department of Mathematics and Physics, Royal Veterinary and Agricultural University, Denmark*

We have previously studied the aggregation behavior of native insulin in aqueous solutions as a function of pH, ionic strength, and protein concentration¹⁾. The data were analyzed by determining the distance distribution function $p(r)$, the z -averaged radius of gyration, R_g , and the weight-averaged molecular mass. Form factors of the oligomers were estimated from the known crystal structure²⁾, and the mass distributions were determined. These were found to be in very good agreement with the predictions of the equilibrium model by Kadima *et al.*³⁾. We have reanalysed these data by directly and simultaneously fitting the equilibrium model to all the SANS data sets. Only three parameters are optimized in the least-squares fit: the characteristic energies for, respectively, binding and charge repulsion, and a binding constant for Na^+ ions. This model gives very good agreement with the scattering data. We have extended the previous measurements on native insulin to higher protein concentrations (up to 20 mg/ml) and to lower ionic strength in order to emphasize the inter-particle interaction effects. These data will be analyzed using the structure factors calculated by integral-equation theory⁴⁾. We hope in this way to be able to obtain an independent determination of the protein/oligomer charge. We have also performed measurements on the insulin mutant (B9Ser→Asp) at different pH, ionic strength, and protein concentration. The distance distribution functions determined for the highly charged molecules at pH 11 and with a salt concentration of 10 mM NaCl clearly shows that the insulin mutant is present as monomer as opposed to native insulin which forms dimers under these conditions.

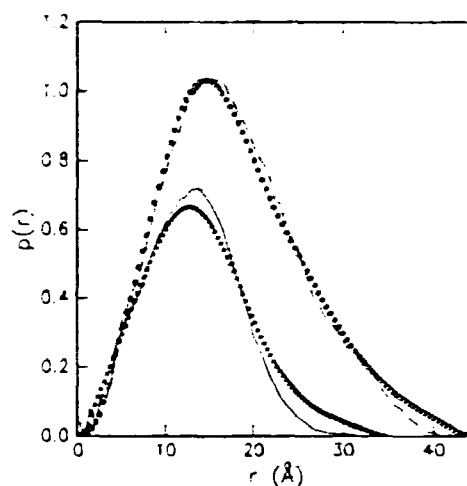


Fig. 1. $p(r)$ for the mutant (triangles) and for native insulin (circles). The curves are calculated from the crystal structure²⁾ for the monomer (full curve) and for the dimer (broken curve).

- 1) J. Skov Pedersen, S. Hansen, and R. Bauer, *Eur. Biophys. J.* **22**, 379 (1994), and *Eur. Biophys. J.* **23**, 227 (1994).
- 2) J. Badgar, M.R. Harris, C.D. Reynolds, A.C. Evens, E.J. Dodson, G.G. Dodson, and A.C.T. North, *Acta Cryst.* **B47**, 127 (1992).
- 3) W. Kadima, L. Ogedal, R. Bauer, N. Kaarsholm, K. Brodersen, J.F. Hansen, and P. Porting, *Biopolymers* **33**, 1643 (1993).
- 4) B. D'Aguzzo and R. Klein, *J. Chem. Soc. Faraday Trans.* **87**, 379 (1991).

2.7.2 Structure of Casein Micelles Studied by Small-Angle Neutron Scattering

S. Hansen, R. Bauer, *Department of Mathematics and Physics, Royal Veterinary and Agricultural University, Denmark*, S. Bredsted Lomholt, K. Bruun Quist, *Institute for Dairy Research, Royal Veterinary and Agricultural University Denmark*, J. Skov Pedersen, and K. Mortensen, *Department of Solid State Physics, Riso National Laboratory, Denmark*

The major part of the protein present in milk is in the form of casein micelles. We have studied the structure of casein micelles using small-angle neutron scattering (SANS). This was done for several pH values and after addition of rennet. From previous studies several models for casein micelles have been suggested. One model for the structure of casein is a sphere consisting of smaller spheres or submicelles. We found this model containing spherical submicelles to be consistent with our measured data.

Using SANS we were able to cover five orders of magnitude in intensity. The data corresponding to different settings of the SANS instrument were fitted simultaneously. This allows us for the first time to obtain information about the micellar as well as the submicellar structure simultaneously as we cover a size range of about 2 to 200 nm. To improve the model fit we included polydispersity in the model both for the spherical micelles and for the spherical submicelles. With this modification we obtained excellent agreement with the experimental data (see Figure). The addition of rennet did not give rise to any observable changes in the q range covered by SANS. For more detailed information about the size distribution of the micelles and the aggregation behaviour after the addition of rennet, light scattering which is able to probe larger sizes has been used.

The model fit gave an average micellar radius of about 100 nm and a submicellar radius of about 7 nm both with a polydispersity of about 40-50 %. The submicelles in the micelle were found to be closely packed, the volume fraction varying slightly with pH. These values are in good agreement with previous studies. Upon addition of rennet the submicellar structure remained unchanged within the experimental accuracy.

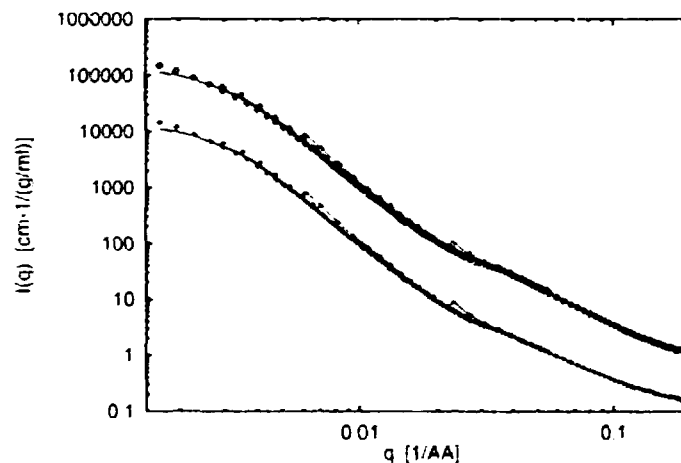


Fig. 1. Casein data at pH 6.65 (diamonds) and fit (full line). Casein data at pH 5.30 (+) and fit (full line) shifted vertically one decade for clarity.

2.7.3 Cross-Section Structure of Polymer-like Lecithin Reverse Micelles

P. Schurtenberger, G. Jerke, C. Cavaco, *Institut für Polymere, ETH Zürich, Switzerland*, and J. Skov Pedersen, *Department of Solid State Physics, Risø National Laboratory, Denmark*

We have studied the structural properties of polymer-like lecithin reverse micelles in deuterated cyclohexane and isooctane as a function of volume fraction, ϕ , and water to lecithin molar ratio, w_o . Detailed information on the local structure was obtained from "shell contrast" experiments, where H_2O in the core of the tubular microemulsion particles was exchanged with D_2O . The effect of this contrast variation is illustrated in Fig. 1A. The experiments were performed on absolute scale, and the data was analyzed using the indirect Fourier transformation (IFT) method¹⁾. The high- q part of the polymer-like scattering intensity reflects the local cylindrical symmetry of the micelles. IFT uses the assumption that the cross-sectional contribution to the total scattering can be decoupled from the rest. It has the advantage that it does not rely on the low- q part of the data used in normal model fitting approaches and that no specific model assumptions have to be made regarding the size distribution and overall structure of the micelles, and contributions from polydispersity and interaction effects are therefore minimized. The cross-section pair-distance distribution function $p(r)$, the cross-section scattering intensity $I_{sc}(0)$ which is directly related to the mass per length M_L , and the radius of gyration of the cylindrical cross section $R_{G,sc}$ were determined by IFT of $I(q)$ for $q < 0.04 \text{ \AA}^{-1}$. The $p(r)$ function can be deconvoluted into a radial cross-section scattering length density profile $\Delta\rho(r)$ using the square-root deconvolution procedure²⁾. Two examples of the thus determined model-independent cross-section profiles $\Delta\rho(r)$, which have been converted into absolute units (cm^{-2}), are shown in Fig. 1B. The results are in very good agreement with the proposed tubular model structure, and we obtain detailed information on the local structure of the water channel, the headgroup and the tail region of the surfactant in the tubular microemulsion particles.

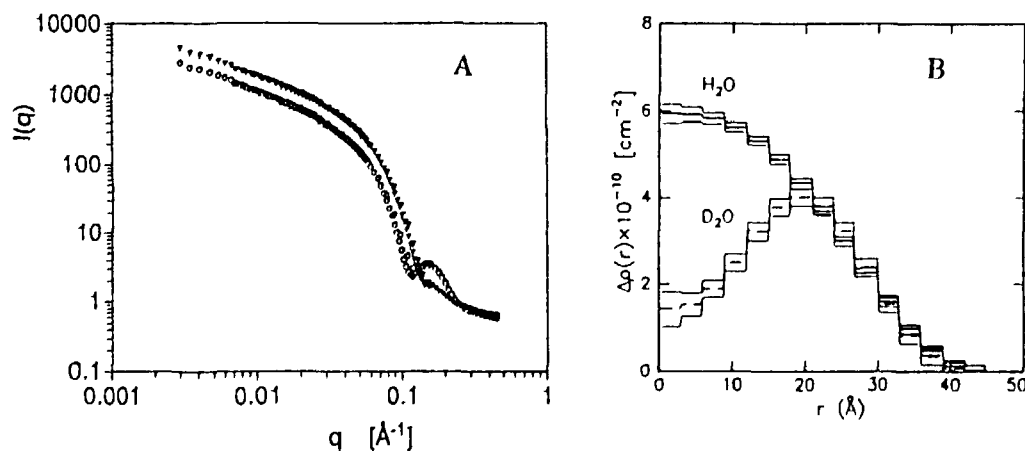


Fig. 1. (A) Normalized scattering intensity for lecithin reverse micelles in deuterated cyclohexane, $w_o = 10$ and $\phi = 2.16 \times 10^{-2}$, for H_2O (solid triangles) and D_2O (open circles). (B) The resulting radial cross-section scattering length density profile $\Delta\rho(r)$ for the two scattering curves shown in A.

¹⁾ O. Glatter, *J. Appl. Cryst.* **10**, 415 (1977).

²⁾ O. Glatter and B. Hainisch, *J. Appl. Cryst.* **17**, 435 (1984).

2.7.4 Formation of Polymer-like Mixed Micelles and Vesicles in Lecithin-Bile Salt Solutions

P. Schurtenberger, S.U. Egelhaaf, *Institut für Polymere, ETH Zürich, Switzerland*, and J. Skov Pedersen, *Department of Solid State Physics, Riso National Laboratory, Denmark*

We have recently re-analyzed the concentration dependence of the mixed micellar size and the previously postulated micelle-to-vesicle transition¹⁾ in bile salt-lecithin solutions using static and dynamic light scattering measurements²⁾. We showed that in the mixed micellar region of the phase diagram, the data are consistent with the presence of flexible cylindrical (wormlike) mixed micelles. At concentrations below the micellar phase limit, mixed lecithin bile salt vesicles form spontaneously. Close to the micellar phase limit we found (indirect) evidence for a coexistence of wormlike micelles and vesicles. We have performed small-angle neutron scattering measurements on two samples in the micellar and coexistence region of the phase diagram³⁾. Due to the much more extended q range of a SANS experiment, we can directly test the consistency of the data with the proposed structural models for the mixed micelles and vesicles. The experimental data from the SANS measurements with the two samples are summarized in Fig. 1. The data for the micellar sample are in quantitative agreement with a scattering function that was originally derived to describe 'wormlike' semiflexible polymers^{3,4)}, and the parameters describing flexibility (persistence length l_p) and local structure (mass per length M_L , linear density of lecithin molecules in the mixed micelles λ_L) obtained for the micellar sample are in very good agreement with those previously derived from static and dynamic light scattering²⁾. The SANS experiments also provide a direct support of the previously postulated coexistence of wormlike mixed micelles and vesicles (see figure 1B). When using SANS the existence of a micelle-vesicle coexistence can now be verified easily due to the very different q dependence of the scattering functions of spherical shells and wormlike cylinders at $q > 10^{-2} \text{ \AA}^{-1}$.

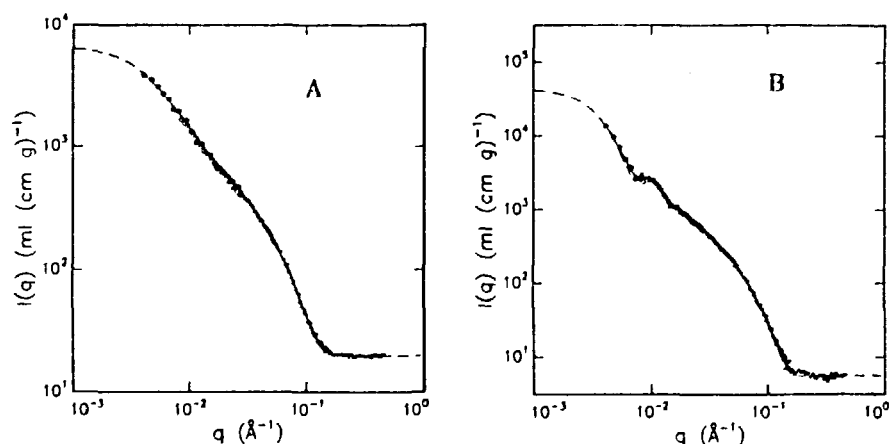


Fig. 1. Normalized scattering intensity for the mixed micellar sample (A), and the sample with coexisting micelles and vesicles (B).

¹⁾ P. Schurtenberger, N. Mazer, W. and Kanzig, *J. Phys. Chem.* **89**, 1042 (1985).

²⁾ S.U. Egelhaaf, and P. Schurtenberger, *J. Phys. Chem.* **98**, 8560 (1994).

³⁾ J.S. Pedersen, S.U. Egelhaaf, and P. Schurtenberger (1995). *J. Phys. Chem.*, *submitted*

⁴⁾ T. Yoshizaki and H. Yamakawa, *Macromolecules* **13**, 1518 (1980).

2.7.5 Structural Studies of a Micellar System with Cation Complexing Potential

L. Arleth, D. Posselt, *IMFUFU, Roskilde University Center, Denmark*, D. Gazeau, C. Larpent, T. Zemb, *Service de Chimie Moléculaire, CEN-Saclay, France*, K. Mortensen, and J. Skov Pedersen, *Department of Solid State Physics, Risø National Laboratory, Denmark*

Tetraaza-ACS is a surfactant with two hydrocarbon chains and a large polar head constituted by two glucose groups and one Tetraaza ring. The Tetraaza ring is capable of complex binding different cations in solution, *e.g.* Cu^{++} or Rh^{+++} . We have studied micelle formation in diluted aqueous solutions of Tetraaza-ACS with and without addition of salt. The system is characterized using UV and visible light absorption measurements, density and surface tension measurements. The surface tension measurements show that Tetraaza-ACS has a critical micellar concentration in water of 0.2 mM. The structural studies are performed using both SAXS (Service de Chimie Moléculaire, Saclay, France) and SANS (Risø National Laboratory) measurements. As SAXS and SANS emphasizes different parts of the micellar structure, the combination of the methods allows a good determination of the form factor. SANS is furthermore a good supplement to the SAXS measurements as it covers a larger q range, especially the information obtained at small q 's is important when the structure factor of the system is determined. From the combined measurements we conclude that Tetraaza-ACS without salt forms short cylindrical micelles (see figure). The length of the cylinders increases slightly with concentration. When cations (Cu^{++} or Rh^{+++}) are complexed by the Tetraaza-ACS molecule, the micelles become shorter and more spherical. The structure factor can in the case of Tetraaza-ACS without added electrolyte be modelled by that of a hard-sphere potential¹⁾, whereas, when cations are complexed to the Tetraaza-ACS molecules, the structure factor of the charged micelles should be modelled by that of a screened Coulomb potential²⁾. An example of a fit is shown in the figure. The theoretical $I(q)$ is fitted to the SANS and SAXS measurements simultaneously, applying the different contrasts for neutrons and x-rays. The micelles are modelled by the form factor of a short cylindrical micelle with a hydrocarbon core and a shell constituted by the hydrophilic part of the molecule and hydrating water molecules. The fit shown below is obtained with an aggregation number of 18 and a length of 68 Å of the cylindrical micelles. The number of water molecules per Tetraaza-ACS molecule in the micellar shell is, according to the fit, around 70. Such a high hydration number is rather unrealistic for glucoside groups, but certainly reflects a very open structure of the polar region.

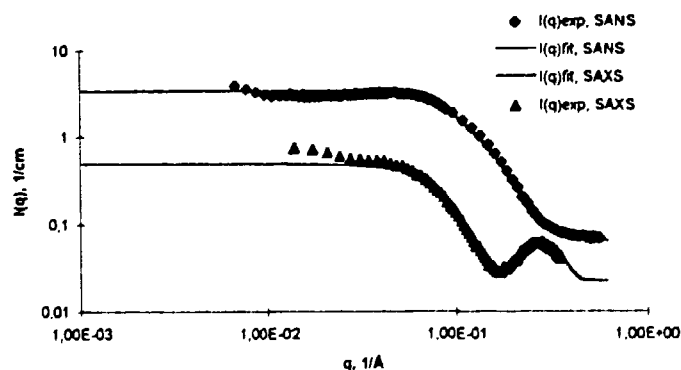


Fig. 1. Example of a data set and fit obtained for a 0.13 M solution of Tetraaza-ACS in water (H_2O for SAXS and D_2O for SANS).

¹⁾ N.W. Ashcroft and J. Lekner, *Phys. Rev.* **145**, 83 (1966).

²⁾ J.B. Hayter and J. Penfold, *Molecular Physics* **42**, 109 (1981).

2.7.6 Carbon Black Dispersion in Non-ionic Surfactant Water Solutions

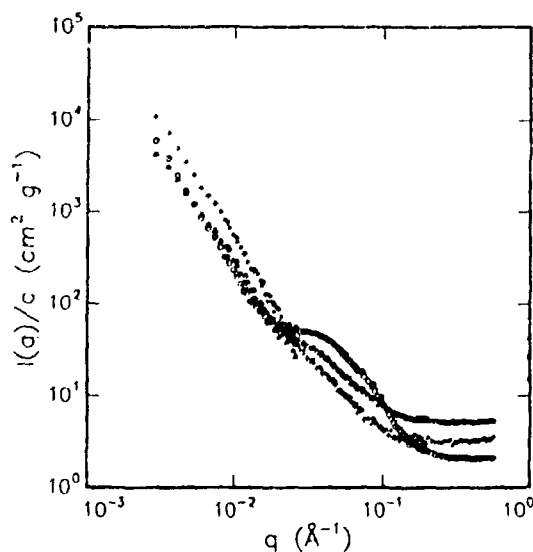
V.M. Garamus, *Frank Laboratory of Neutron Physics, Joint Institute for Nuclear Research, Dubna, Moscow Region, Russia*, and J. Skov Pedersen, *Department of Solid State Physics, Risø National Laboratory, Denmark*

It is well-known that the presence of a surfactant stabilizes colloidal dispersion of hydrophobic particles in water¹⁾. On the other hand, dispersed particles can shift macroscopic parameters of surfactant solutions such as critical micellar concentration (CMC). The aim of this project was to determine the structure of dispersed particles in non-ionic surfactant water solutions, and the influence of the dispersed particles on CMC.

Samples were prepared by ultrasonic dispersing grafitized carbon black²⁾ particles (CB) in non-ionic surfactant (Triton X-100) solutions³⁾. The aqueous solutions of CB particles without Triton X-100, with the concentration of Triton X-100 less than CMC and different surfactant/CB ratios with changing scattering length density of a solvent were measured at 25°C.

The neutron scattering data point to the existence of Triton X-100 micelles even in the region where the surfactant concentration is less than CMC. Contrast variation made it possible to decrease the scattering from the micelles. In the figure the neutron scattering cross sections at different contrast are given in double logarithmic scale. The slope of the curves at low and high q values point to the existence of at least two very different characteristic length scales for the structure of the CB particles.

We are currently trying to construct a structural model for the surfactant-coated carbon black particles. The aim is to take into account the known scattering density of the components and to fit to the three different D₂O concentrations simultaneously.



¹⁾ C. Tanford (1973). *The Hydrophobic Effect* (Wiley, New York).

²⁾ V.N. Moraru, F.D. Ovcharenko, L.I. Kobylinskaya, and T.V. Karmazina, *Russian Kolloidnij Journal* **46**, 1148 (1984).

³⁾ M. Corti and V. Degiorgio, *Optics Communications* **14**, 358 (1975).

2.7.7 The Cross-over from Meanfield to 3D-Ising Critical Behavior in a 3-Component Microemulsion

H. Seto, M. Nagao, E. Yokoi, S. Kumura, M. Imai, *Faculty of Integrated Arts and Science, Hiroshima University, Japan*, D. Schwahn, *Institut für Festkörperforschung, Forschungszentrum Jülich, Germany*, and K. Mortensen, *Department of Solid State Physics, Risø National Laboratory, Roskilde, Denmark*.

The susceptibility of three-component microemulsions and micellar systems have previously been studied near the critical point of phase-decomposition. It was argued that these systems belong to the 3D-Ising universality class of critical phenomena. The experimental findings showed, however, some deviations from the characteristic 3D Ising exponents. More recently, we have made structural studies on the complex fluid composed of water, n-decane and the surfactant AOT. The structure is a simple water-in-oil type of micellar system which is homogeneous at low temperatures, and decomposes into two phases at high temperatures. We found that if we take changes of the micellar sizes into account, the density fluctuation of the droplets are better described by simple mean-field characteristics ¹⁾. In an extended study with better temperature resolution we have found that the data obtained in this type of microemulsion basically lie within the cross-over regime from mean-field to the Ising range. This is seen in the figure, where the experimental data are shown together with a fit to the cross-over function given by Belyakov and Kiselev ²⁾. The experimental data were obtained using both the Risø-SANS and the SANS-U instrument at JAERI. Different samples near the critical composition were studied. They had all the water to surfactant ratio equal 5ml water/3g AOT. The volume fraction of water + AOT against the total volume, ϕ , were $\phi=0.096$, 0.098 , and 0.099 , respectively, which are all in the close vicinity of the expected critical composition.

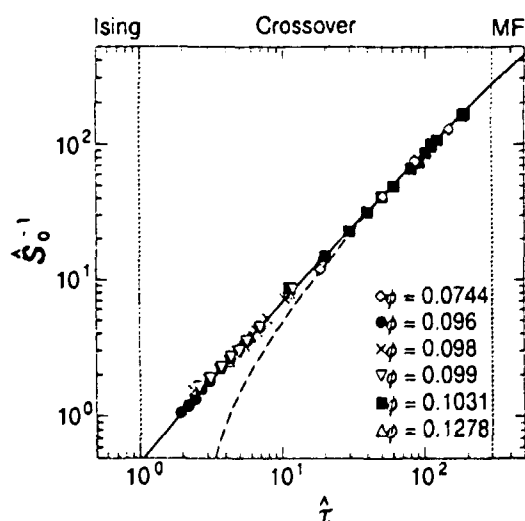


Fig. 1. The inverse of the reduced susceptibility $S(0)^{-1}$ for samples in the vicinity of the critical composition. The solid line is a fit to the cross-over function; the broken line is the mean-field function.

¹⁾ H. Seto, D. Schwahn, K. Mortensen, S. Komura, *J. Chem. Phys.* **99**, 3756 (1993).

²⁾ M.Y. Belyakov, S.B. Kiselev, *Physica A* **190** 75 (1992).

2.7.8 Micelles of Mixed Short-Chain Lecithin Molecules

J. Samseth, *Institute of Energy Technology, Kjeller, Norway*, T.L. Lin, *National Tsing-Hua University, Hsin-Chu, Taiwan*, and K. Mortensen, *Department of Solid State Physics, Risø National Laboratory, Roskilde, Denmark*.

The closely related synthetic short chain lecithin molecules, dihexanoyl-phosphatidylcholine (diC_6PC), and diheptanoyl-phosphatidylcholine (diC_7PC) form rather different aggregates when dispersed in aqueous solutions. Dihexanoyl-phosphatidylcholine, and diheptanoyl-phosphatidylcholine are double tailed zwitter ionic amphiphilic with respectively six and seven carbons in each of the fatty acyl linkage. Small angle neutron scattering studies have previously shown¹⁾ that diC_6PC lecithin molecules form globular micelles in aqueous solutions, whereas (diC_7PC) lecithin aggregates in the form of polydisperse rodlike micelles. In the present study, we have used small-angle neutron scattering experiments to investigate the structure of mixed micelles of diC_6PC and diC_7PC , with the aim to study the characteristics important for the aggregation form²⁾. It was found that the addition of small amount of diC_6PC to pure diC_7PC in general reduces the length of the mixed polydisperse rodlike micelles. Addition of small amounts of diC_7PC to a 10mM diC_6PC solutions, on the other hand, results in general in relative small rodlike mixed micelles with narrow size distribution, having a mean aggregation number of approximately 26 and a mean length of about 47Å.

It is concluded that the mixing of diC_6PC with diC_7PC significantly influence the number of surfactant molecules forming the end caps of the rodlike micelles such as to control the mean size of rodlike micelles.

¹⁾ T.L. Lin *et al.*, *J. Phys. Chem.* **94**, 7239 (1990), and references therein.

²⁾ preliminary work published in: T.L. Lin, J. Samseth, *Proceedings of 68th ACS Colloid and Surface Science Symposium 1994*.

2.7.9 Macrostructural Studies of Bile Salts by Small-Angle Neutron Scattering

F. Lopez, *University of Bordeaux I, France*. J. Samseth, *Institute of Energy Technology, Kjeller, Norway*, and K. Mortensen, *Department of Solid State Physics, Riso National Laboratory, Roskilde, Denmark*.

Scientists from the National Institute of Public Health have prepared a complex vaccine against serogroup B meningococcal disease from a B:15:1.7.16 meningococcal strain (44/76) using a bio-detergent Sodium Deoxycholate (NaDC). A crucial step in the production of the vaccine consists in determining the physico-chemical properties of sodium Deoxycholate in aqueous solutions. The aim of our work is then devoted to the study of the self aggregation patterns of pure NaDC and to the determination of their colligative properties. Small Angle Neutron Scattering (SANS) represent an efficient tool to perform structural studies on the DOC aggregates. Some important parameters will be, pH, temperature, detergent concentration as well as the influence of Magnesium Fluoride salts. When bile salts are dissolved in aqueous solvent, they form readily organized micellar structures. These micelles may form hard spheres, oblate or prolate ellipsoids, long rods, disks or may constitute complex associations of amphiphile molecules described by helical models or rods leading to gelatinous structures in some cases. Bile salts are steroid nucleus. This CIS A/B ring juncture makes their molecular structure in the shape of a truncated cone (wedge shape). If we confine our attention to the Sodium Deoxycholate NaDC compound, it would be of interest to study the interaction between solute and solvent molecules versus pH and NaDC concentration. Investigations were realized by SANS at constant concentration on 0.5%. They revealed a rod-like association which seems to be strongly dependent on the pH, as shown on the figure. The radius and length of such conformations compare reasonably well with the dimensions of helical models and rods previously observed by SAXS and ESR. A phase transition between solution and gel was observed and seems to take place at pH 7.5. Obviously, a pH decrease of NaDC solution when adding HCl tends to convert it into a gel even from quite dilute solution. Therefore, the growth of the aggregate occurs along the rod's axis and is favored by a decreasing pH. At the opposite, the decrease of the micellar size along the rod's axis is favored by an increase of the pH. As a matter of fact, small primary micelles are formed and associate at a critical micellar concentration (CMC) leading to the formation of larger aggregates and in some cases to gelation.

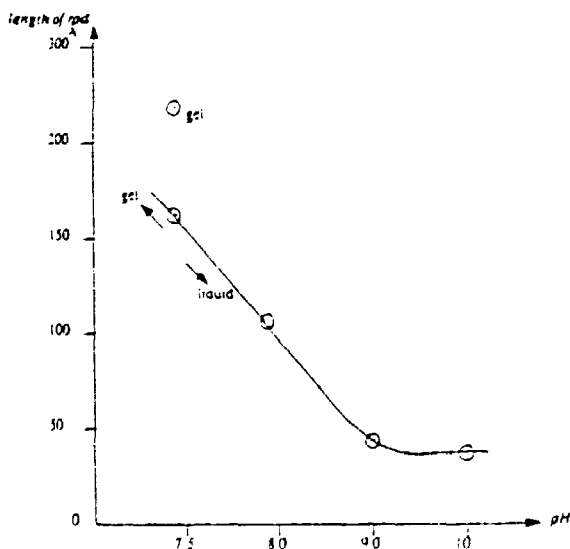


Fig. 1. Length of the micellar rod of DOC as a function of pH

2.7.10 Small-Angle Neutron Scattering Studies of DNA Complexes with RecA Protein

P. Wittung, B. Nordén, *Chalmers Institute of Technology, Göteborg, Sweden*, K. Mortensen, *Department of Solid State Physics, Riso National Laboratory, Denmark*, and M. Takahashi *Institute Curie, Orsay, France*.

RecA, recombination protein A, has a key role in the DNA repair of *E. coli*, including the promotion of general genetic recombination. Strand exchange between homologous DNAs, a crucial step in recombination, is also promoted by RecA *in vitro* and its interactions with DNA can be studied to get mechanistic insight into its biological function. RecA binds co-operatively to single as well as double stranded DNA to form rigid fibrous complexes in which RecA monomers are arranged in a helical manner around the DNA. To study the structure of RecA-DNA complexes in solution, optical linear dichroism spectroscopy (LD) has been used to determine the orientation of the DNA bases and various amino acid chromophores. The sample is aligned by shear flow in a concentric-cylinders flow apparatus and the differential absorption of orthogonal forms of linearly polarized light, the LD, is measured. LD can provide effective angles of the light-absorbing transition moment vectors relative to the orientation axis of the fibrous complex provided information is available about the degree of orientation of the overall fiber. From SANS "anisotropy" measured under identical flow conditions the second moment orientation function can be obtained by fitting the anisotropy calculated for flow model orientational distributions.

The structure of RecA complexes involving one or two DNA strands was studied using an etheno-adenine, dεA, homopolymer, as one of the strands, where the etheno chromophore enables the two DNA strands to be evaluated separately (normal DNA strand at 260 nm and etheno-adenine strand at 320 nm). Upon forming first a RecA-dεA complex, thereafter a RecA-dεA-dT complex, we found that the first DNA strand (dεA) did not alter its position in the second complex, showing an angle of appr. 65° between the nucleobases and the RecA fibre axis, while the bases of the second strand (dT) formed an angle of 78°. Another interesting feature is the ability of RecA to bind double-stranded DNA in which the heterocyclic cation ethidium is intercalated between the bases. The structure of this complex compares well with that of normal RecA-DNA, in presence of cofactor ATP γ S, as judged from LD and SANS giving an angle of the DNA bases of 82°.

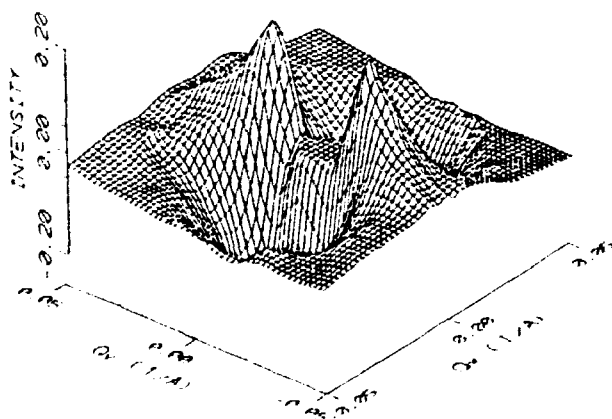


Fig. 1. Two-dimensional differential SANS-pattern of RecA-dεA complex with shear flow minus RecA-dεA at rest.

1) B. Nordén, C. Elvingson,, M. Kubista, B. Sjöberg, H. Ryberg, M. Ryberg, K. Mortensen, and M. Takahashi, *J. Mol. Biol.* **226**, 1175 (1992).

2.8 Polymers

2.8.1 On the N-scaling of the Ginzburg Number of Polymer Blends

D. Schwahn, S. Janssen, T. Schmackers, *Institut für Festkörperforschung, Forschungszentrum Jülich, Germany*, and K. Mortensen, *Department of Solid State Physics, Riso National Laboratory, Roskilde, Denmark*, G. Meier, *Max Planck Institute for Polymer Research, Mainz, Germany*.

The susceptibility related critical phenomena near a second-order phase transition has recently been described by a generalized cross-over function including the mean-field character far from the critical temperature T_c as well as the Ising behavior near T_c . This cross-over function was derived by Belyakov et al¹⁾ on the basis of renormalization theory. The validity of this crossover function has been demonstrated for polymer blends near the critical temperature for demixing^{2,3)}, by measuring the concentration fluctuations by scattering methods. By application of the crossover function to various polymers with different degree of polymerization, we have been able to extract detailed information on the N scaling of critical parameters as the bare correlation length ξ , the susceptibility, and the the Ginzburg number, G_i , which is a number giving the width of the 3d-Ising regime. N is the degree of polymerization. We found a quite unexpected dependence between the Ginzburg number and N : polymers with $N < 30$ give the same G_i -value as low molecular liquids and at N close to $N=30$ an increase of G_i of more than one order of magnitude is observed. Only blends with polymerization more than $N=30$ obey a 'polymer' type of scaling relation between N and G_i . The observed scaling relation $G_i \propto N^{-2}$ is even more steep than the $G_i \propto N^{-1}$ -relation proposed theoretically by de Gennes⁴⁾. Upon application of pressure, the Ginzburg-number decreases significantly, in opposition to expectations from the de Gennes evaluation of the cross-over⁴⁾. The reason for these findings can be explained by the large entropic contribution of the Flory-Huggins parameter related to the compressibility or free volume of the system in comparison with the combinatorial entropic term.

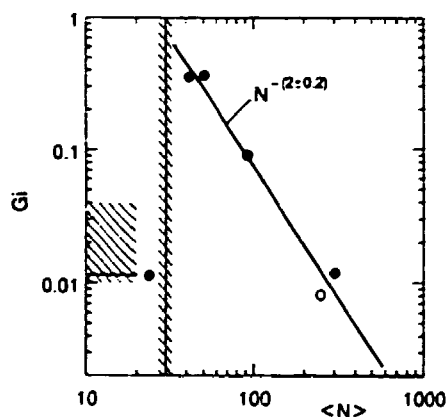


Fig. 1. Ginzburg Number G_i versus the mean degree of polymerization N .

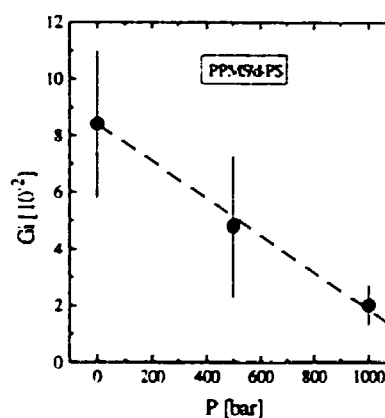


Fig. 2. Ginzburg Number G_i versus Pressure P , as measured on poly(phenylsiloxane)-poly(styrene).

¹⁾ M.Y. Belyakov, S.B. Kiselev, *Physica A* **190** 75 (1992).

²⁾ G. Meier, D. Schwahn, K. Mortensen, and S. Janssen, *Europhys. Lett.* **22** 577 (1993).

³⁾ D. Schwahn, G. Meier, K. Mortensen, and S. Janssen, *J. Phys. II* **4** 837 (1994).

⁴⁾ P.G. de Gennes, *J. Phys. France Lett.* **38** 441 (1977).

2.8.2 Spinodal Decomposition of Poly(styrene)-Poly(Cyclohexyl Acrylate-stat-Butyl Methacrylate) Blends

V. Abetz, *Gutenberg Universität, Mainz, Germany*, T. Hack, D. W. Schubert, M. Stamm, *Max-Planck Institute for Polymer Research, Mainz, Germany*, K. Mortensen, *Department of Solid State Physics, Riso National Laboratory, Denmark*, and W. Siol, *Röhm-GmbH, Darmstadt, Germany*

Most of the technologically important blends are multiphase systems, and their properties depends critically on the morphology. While some blends are heterogeneous all over the composition and available temperature range most blends decomposes. In a previous study¹⁾, it was shown that the polymer blend of poly(styrene), PS, and poly(cyclohexyl acrylate-stat-butyl methacrylate), P(CHA-stat-BMA) depending of composition shows both a lower critical solution temperature (LCST) and an upper critical solution temperature (UCST).

In this study²⁾, we have investigated the kinetics of spinodal decomposition (SD) of both compatible ($LCST > T_g$, T_g the glass temperature) and an incompatible ($LCST < T_g$) blends of PS and P(CHA-stat-BMA). The dynamics of SD was measured after temperature jumps from respectively the thermodynamic single phase and from the kinetically formed single phase state into the unstable part of the two phase region. The time evolution of the structure factor has been examined by both small angle neutron scattering, SANS, double crystal neutron diffraction, DCD, and light scattering techniques. These techniques give in combination access to a wide range of both momentum transfer and times. The activation energy of the diffusion process during spinodal decomposition was determined by scaling analysis of the later stages of SD.

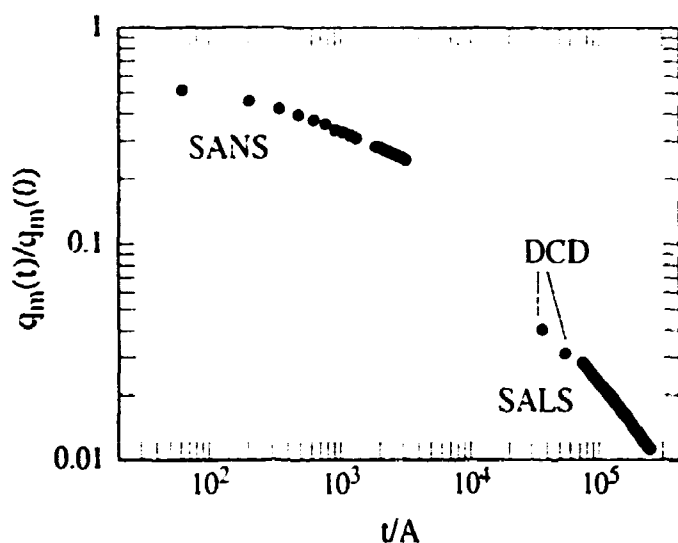


Fig. 1. Spinodal peak position as a function of time for PS-P(CHA-stat-BMA) blend

¹⁾ D.W. Schubert, V. Abetz, T. Hack, M. Stamm, and W. Siol, (1994). *Macromolecules*, submitted

²⁾ T. Hack, V. Abetz, D.W. Schubert, M. Stamm, K. Mortensen, and W. Siol, (1994). *Macromolecules*, submitted.

2.8.3 Epitaxial Growth and Shearing of the Body Centered Cubic Phase in Diblock Copolymer Melts

M.S. Schulz, F.S. Bates, *Chemical Engineering and Material Science, University of Minnesota, Minneapolis, MN, USA*, K. Almdal and K. Mortensen, *Department of Solid State Physics, Riso National Laboratory, Roskilde, Denmark*

Order-order phase transitions in condensed matter provide one of the most important mechanisms for manipulating and optimizing material properties. Growth of new phases frequently occur with preferred crystallographic orientations that are governed by symmetry and lattice spacing relationships between the original and the transformed states. Such epitaxial relationship has only recently been considered in soft materials which are characterized by disorder on short length scales (atomic distances)¹⁾.

In a small-angle neutron scattering study on the diblock copolymer poly(styrene)-poly(2-vinylpyridine), PS-PVP, we have identified an epitaxial relationship between the hexagonal cylinder phase and a bicontinued cubic phase with $Ia\bar{3}d$ space group²⁾. Fig. 1 shows the intensity contour plot of the hexagonal cylinder phase, as obtained on a shear aligned monodomain sample in the q_x - q_z and the q_y - q_z scattering planes, respectively (shear direction x , plane of shear x - z). Fig. 2 shows the scattering pattern after the sample has been heated up into the cubic phase. The phase transition has placed the threefold cubic [111] direction along the original sixfold hexagonal (i.e. cylinder) axis. More detailed investigations reveal the following epitaxial relationship: $(10) \leftrightarrow (0\bar{2}2)$ and $(11) \leftrightarrow (1\bar{2}1)$ ²⁾.

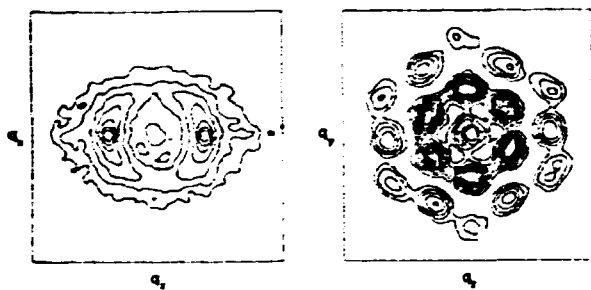


Fig. 1. SANS intensity contour plots taken at 140°C from the shear-aligned hexagonal cylinder phase of PS-PVP.

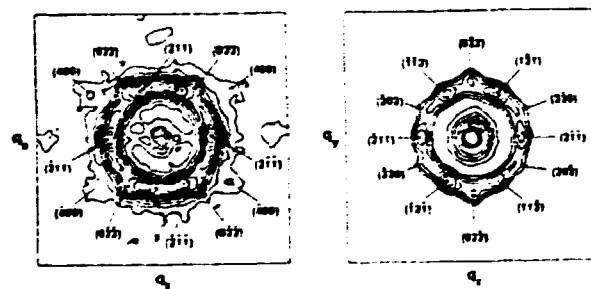


Fig. 2. Intensity contour plots after heating the sample to 140°C. The reflections have been indexed based on the $Ia\bar{3}d$ space group.

¹⁾ Y. Rancon and J. Charvolin, *J. Phys. Chem.* **92**, 2646 (1988).

²⁾ M.F. Schulz, F.S. Bates, K. Almdal, and K. Mortensen, *Phys. Rev. Lett.* **73**, 86 (1994).

2.8.4 Scattering Study on the Transamidation of Poly(Amide-4.6)

R. Scherrenberg, J. Moonen, *DSM-Research, Geleen, Belgium* and K. Mortensen *Department of Solid State Physics, Riso National Laboratory, Denmark*.

Interchange reactions in poly-condensates are of significant industrial importance since they minimize molar mass fluctuations and can lead to the formation of block copolymers in the case of two poly-condensates are trans-reacted. The latter aspect can lay an important role in the in-situ compatibilization of immiscible polymers in a blend. Unfortunately, the interchange process is very difficult to investigate. Recently, some successful studies on the kinetics of trans-esterification in polyesters have been reported using small-angle neutron scattering (SANS) technique¹⁾. In the order to further investigate the feasibility of SANS to study the kinetics of interchange reactions in general and trans-amidation in polyamides in particular, some preliminary experiments have been performed on a 50/50 blend of deuterated and hydrogenous polyamide-4.6, Stanyl. The results of this SANS study are very promising. An exponential relaxation time τ of approximately 1500 seconds is obtained at a processing temperature of 300°C. On the basis of this reaction time τ , the number of interchange reactions per chain as a function of the processing time at 300°C can be calculated. We find, for instance, that between 1 and 4 interchange reactions occur per chain in polyamide-4.6 during a typical processing time of 1 to 3 minutes at 300°C.

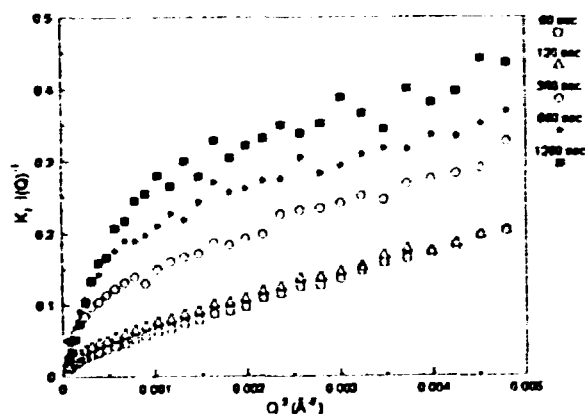


Fig. 1. Scattering function of Stanyl-D/Stanyl-H 50/50 blend as a function of time at 300°C.

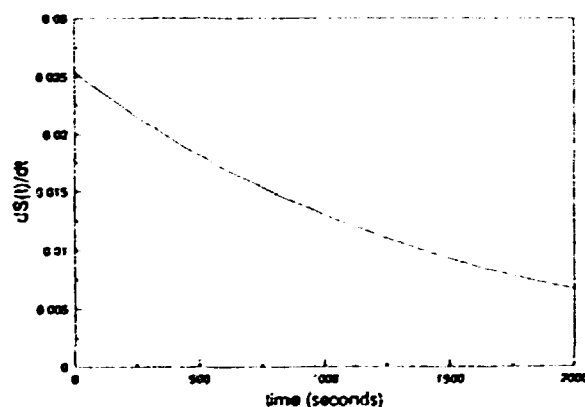


Fig. 2. The number of efficient chain scissions per second as a function of processing time (at 300°C), as obtained from the scattering data.

¹⁾ H. C. Benoit, E. W. Fischer, and H. G. Zachmann, *Polymer* **30**, 379 (1989).

2.8.5 Stretching Induced Correlations in Triblock Copolymer Gels of PS-PEP-PS

N. Mischenko, K. Reynders, H. Reynaers, *Department of Chemistry, Catholic University, Leuven, Belgium*, and K. Mortensen, *Department of Solid State Physics, Risø National Laboratory, Denmark*

Processing triblock copolymers of the poly(styrene)-poly(ethylene propylene)-poly(styrene), PS-PEP-PS, type with solvent selective for the middle rubber block results in highly elastic gels. It was previously shown by small-angle scattering that the insoluble polystyrene, PS, end-blocks associate into spherical domains, thereby providing junction points for a three-dimensional network of micelles¹⁾.

When exposed to uniaxial elongation various characteristic structural features develops, depending on both the mid-block length and flexibility, and on the copolymer concentration. The observed structures include both affine deformation of the network and improved angular specific correlation indicating formation of mesophases. In the absence of stretching, an azimuthally uniform broad correlation peak is observed, as shown in Fig.1. This reveal the liquid like ordering of the micellar PS-cores. At low elongation ratios (25%) this pattern changes to a uniform elliptically shaped correlation band. With higher elongation ratios, however, the structural respond is no longer an azimuthally isotrop ellipse. In stead we observe the development of diffraction spots. The best resolved spots are observed for such 12% PS-PEP-PS copolymer gel with relative high PS content (50 wt.% of the copolymer), as shown in the figure. Four spots are seen, arranged within the elliptical band at quadrants formed by the vertical and horizontal axes of the SANS pattern. In addition two diffuse arcs (or possible four other reflections) develops outside the ellipse within the equatorial direction, i.e. parallel to the stretching.

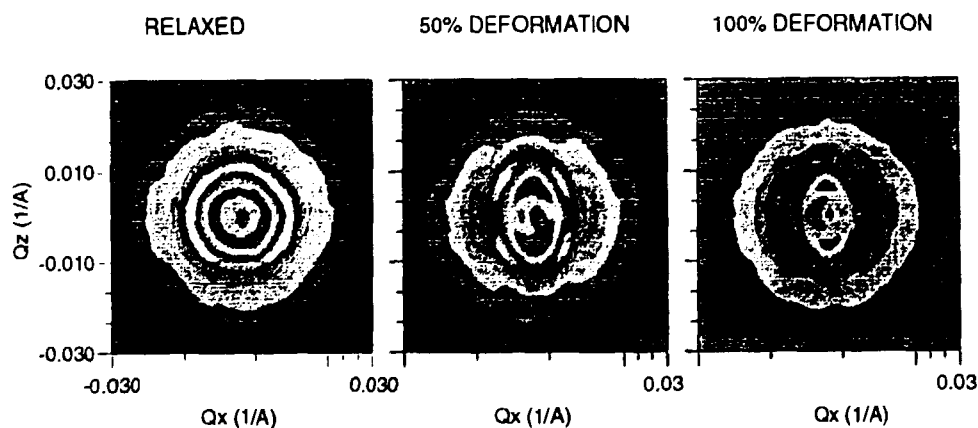


Fig. 1. SANS of 12% gel of PS-PE/P-PS with 50 % of PS in original relaxed state; 50% deformation; and 100% deformation.

¹⁾ N. Mischenko, K. Reynders, K. Mortensen, R. Scherrenberg, F. Fontaine, R. Graulus, and H. Reynaers, *Macromolecules* **27**, 2345 (1994).

2.8.6 Lamellar Meso-phase of PEO-PPO-PEO Melts and Water-swollen Mixtures

K. Mortensen, *Department of Solid State Physics, Risø National Laboratory, Denmark*, W. Brown, *Department of Physical Chemistry, University of Uppsala, Sweden*, and E. Jørgensen, *Roskilde University Center, Denmark*

The phase behavior of block copolymers has recently attracted great interest. Many studies have in particular been performed on amorphous di-block copolymers in which the mesophase formation is determined by the Flory-Huggins interaction parameter, fluctuations and conformational symmetry¹⁾. It appears, however, that mesophase formation also can be driven by other effects, as for example the tendency of one of the blocks to crystallize. This is shown in block copolymers composed of poly(ethylene oxide), PEO, and poly(propylene oxide), PPO²⁾. Studies of systems of crystalline blocks are rather rare, and not well understood. Such polymers have, however, great technological importance. A number of commercial block copolymers are based on poly(ethylene oxide) which crystallizes at a low temperature depending on the molecular weight as well as the structure of the surrounding blocks.

Structural studies performed by small-angle neutron scattering have shown that triblock copolymers of both the type PEO-PPO-PEO and PPO-PEO-PPO form lamellar mesophases at low temperatures. The order-to-disorder transition is closely related to the melting transition of the PEO subunit. When water is incorporated into the copolymer melt, a single phase is formed at high temperatures. At low temperatures, on the other hand, the system decomposes into two phases, of which the one have properties similar to the high temperature phase while the other is lamellar like the pure copolymer, but swollen up to 10%.

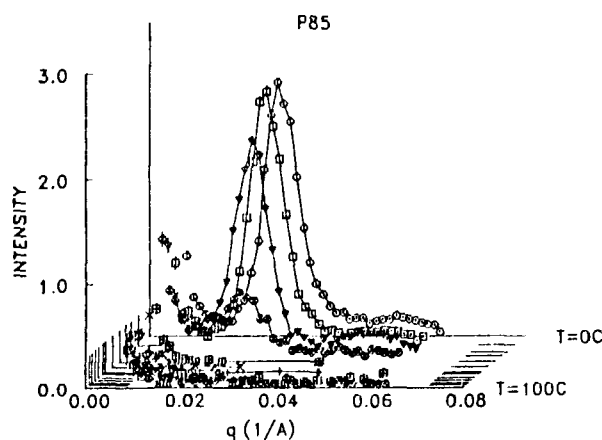


Fig. 1. Neutron scattering function of P85-melt as obtained at temperatures between $T=7^{\circ}\text{C}$ and $T=80^{\circ}\text{C}$.

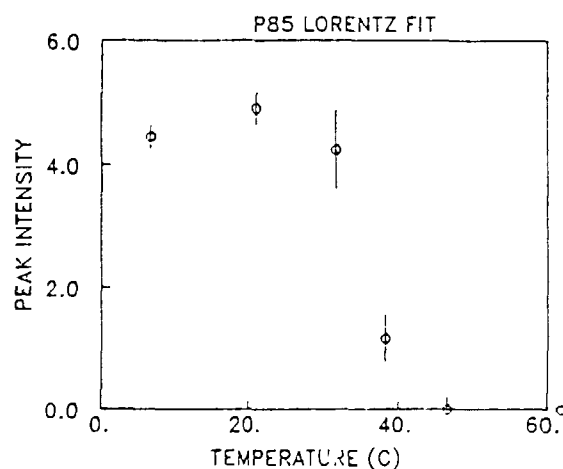


Fig. 2 Peak intensity I_0 as a function of temperature, as obtained by Lorentz-fit to the experimental data.

¹⁾ F.S. Bates, M.F. Schultz, A.K. Khandpur, S. Förster, J.H. Rosedale, K. Almdal, and K. Mortensen, (1994). *Trans. Faraday Soc.*, *submitted*.

²⁾ K. Mortensen, W. Brown, E. Jørgensen (1995) *Macromolecules*, *submitted*.

2.8.7 Interaction of PEO-PPO-PEO Block Copolymers with Ionic Surfactants

E. Hecht, M. Gradzielski, H. Hoffmann, *Physical Chemistry, University of Bayreuth, Germany*, and K. Mortensen *Department of Solid State Physics, Risø National Laboratory, Denmark*.

Block copolymers of the type PEO-PPO-PEO (with PEO poly(ethylene oxide) and PPO poly(propylene oxide)) form micelles in aqueous solutions that have a hydrophobic core of PO and a strongly hydrated shell of EO-blocks¹⁾. The critical micellization temperature CMT of the poloxamers is strongly influenced by cosolutes like surfactants. The interaction of F127 (EO₉₇PO₆₉EO₉₇) with the anionic surfactant SDS was investigated by small-angle neutron scattering (SANS), static light scattering and differential scanning calorimetry (DSC)²⁾. It was found that addition of SDS can suppress the micellation of F127 completely, as seen from analysis of scattering curves like the example shown in Fig. 1 (3% F127). A simple model can describe this suppression of polymer micelles by ionic surfactants. The surfactants binds cooperatively on the block copolymer molecules and the hydrophobic block is thereby made hydrophilic. At saturation conditions 4-5 SDS molecules bind to one F127 molecule. The bound amount of SDS increases somewhat with increasing polymer concentration. At higher concentration (≥ 20 wt.%), pure F127 forms a cubic mesophase with increasing temperature³⁾. Addition of SDS to a fixed F127 concentration decreases the cubic region, until the mesophase completely disappears. The "melting" of the mesophase is a result of the suppression of the poloxamer micelles. With increasing surfactant concentration the hard sphere volume fraction ϕ of micelles decreases below 0.53, the critical value for hard sphere crystallization. Fig. 2 shows the regime of cubic mesophase, for 20%, 25% and 30% F127.

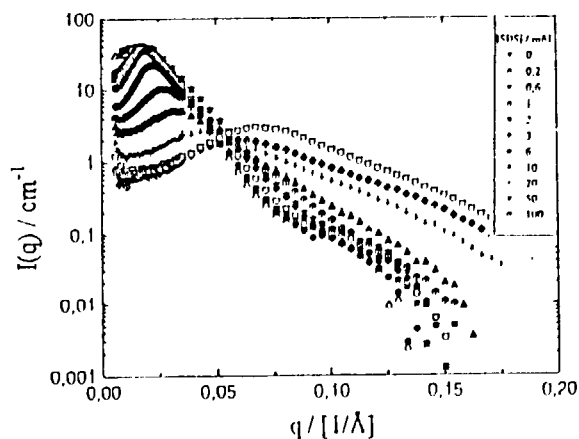


Fig. 1. Scattering function of 3% F127 + SDS in D₂O at various SDS concentration, obtained at T=27°C.

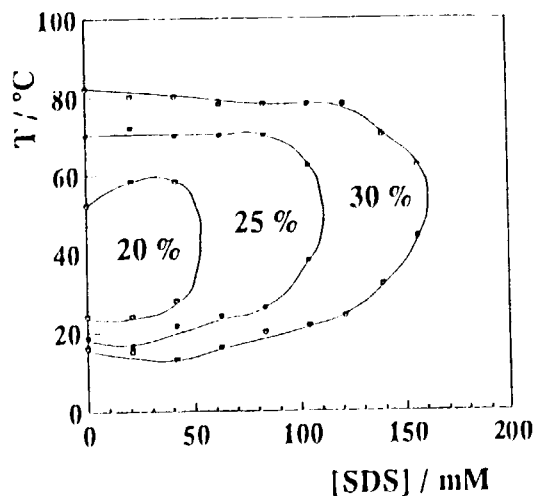


Fig. 2. Cubic regime of the phase diagrams for F127/SDS/D₂O at fixed F127 concentration (20%, 25% and 30%).

¹⁾ K. Mortensen, J.S. Pedersen, *Macromolecules* **26** 805 (1993).

²⁾ E. Hecht, K. Mortensen, M. Gradzielski, and H. Hoffmann (1994) *J. Phys. Chem.*, *submitted*.

³⁾ K. Mortensen, *Polymer Preprint* **35** 626 (1994).

2.8.8 Phase Behavior of Triblock Copolymers Melt and Aqueous Solutions of Poly(Propylene Oxide)-Poly(Ethylene Oxide)-Poly(Propylene Oxide)

K. Mortensen, *Department of Solid State Physics, Riso National Laboratory, Denmark*
W. Brown, *Department of Physical Chemistry, University of Uppsala, Sweden*, and E. Jørgensen, *Roskilde University Center, Denmark*.

Polymeric surfactants have recently attracted great interest, both as a result of their commercial utility, and because of their novel physical behavior. Especially, many studies have been performed on aqueous solutions of the block copolymer PEO-PPO-PEO, where PEO is poly(ethylene oxide) and PPO is poly(propylene oxide). It is now well established that these block copolymers associate into micellar aggregates of spherical, rod-like or possibly layered forms, depending on molecular design and temperature, and that these micellar aggregates constitute the basis for a variety of crystalline mesophases¹⁾. The proven utility of the PEO-PPO-PEO surfactant macromolecules has led to further research to find structural modifications that would offer even broader selections of surfactant properties. Reversal of the hydrophobic and hydrophilic blocks (Pluronic-R) is among such new candidates. We have studied such copolymer $PO_{15}EO_{156}PO_{15}$, abbreviated 25R8. The studies include small-angle neutron scattering, static and dynamic light scattering, and rheology²⁾. Complex aggregation behavior is observed as illustrated in the phase diagram shown in the figure. At low temperatures and low concentrations the PPO-PEO-PPO copolymers are dissolved as independent macromolecules. In a wide temperature range of dilute concentrations, the scattering patterns indicate formation of large domains of networks of copolymer strands, interconnected randomly through the hydrophobic poly(propylene oxide) end-blocks. At higher concentrations an interconnected network of micelles is formed, in which micellar cores of hydrophobic PPO are interconnected by PEO strands. For concentrations above 50 wt.% this network constitutes the whole sample, resulting in a transparent homogeneous phase. Close to 60% copolymer concentration, the micellar network forms a low temperature solid-like mesophase. At higher polymer concentrations and low-temperatures an elastic two-phase system is formed of coexisting swollen lamellar and micellar network.

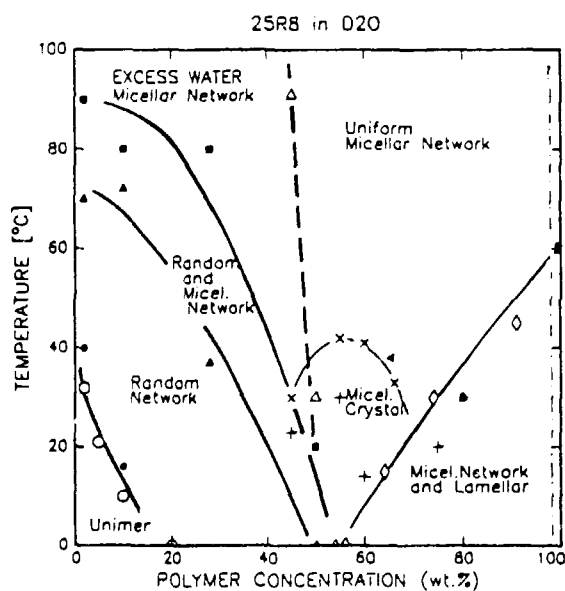


Fig. 1. Phase diagram of the Pluronic-R system 25R8. Closed symbols refer to neutron scattering results, open symbols to light scattering, and crosses to rheological data.

¹⁾ K. Mortensen, *Europhys. Letters* **19** 599 (1992).

²⁾ K. Mortensen, W. Brown, E. Jørgensen, *Macromolecules* **27** 5654 (1994).

2.8.9 Epitaxial Growth and Shearing of the Body Centered Cubic Phase in Diblock Copolymer Melts

K. Almdal, K. Mortensen, *Department of Solid State Physics, Risø National Laboratory, Denmark*, K.A. Koppi, M. Tirrell, and F.S. Bates, *Department of Chemical Engineering and Materials Science, University of Minnesota, USA*

A poly(ethylenepropylene)-poly(ethylethylene) (PEP-PEE) diblock copolymer melt, containing 25% by volume PEP, was investigated using small-angle neutron scattering (SANS) and rheological measurements¹⁾. The SANS measurements were performed with the aid of an *in situ* shearing device operated directly in the neutron beam. The sample has three equilibrium phases in the experimental temperature window: two ordered phases at low temperatures and a disordered phase at high temperatures. The low temperature phases are hexagonally packed (HEX) cylinders and body centered cubic (BCC) spheres, respectively. Application of a large amplitude dynamic shear deformation to the HEX phase leads to well-aligned cylinders, with the cylinders parallel to the *x*-axis in Fig. 1. Upon heating through the HEX-to-BCC transition, the BCC phase grows epitaxially, with the [111] direction coincident with the original cylinder axis, leading to a well-defined twinned microstructure. SANS measurements performed while the BCC specimens were dynamically sheared showed different creeping and deformation mechanisms. The twinned state appears at low and high shear rates, while two dimensional disordering is observed at intermediate shear rate. A schematic representation of the mechanism for these processes are shown in Fig. 1.

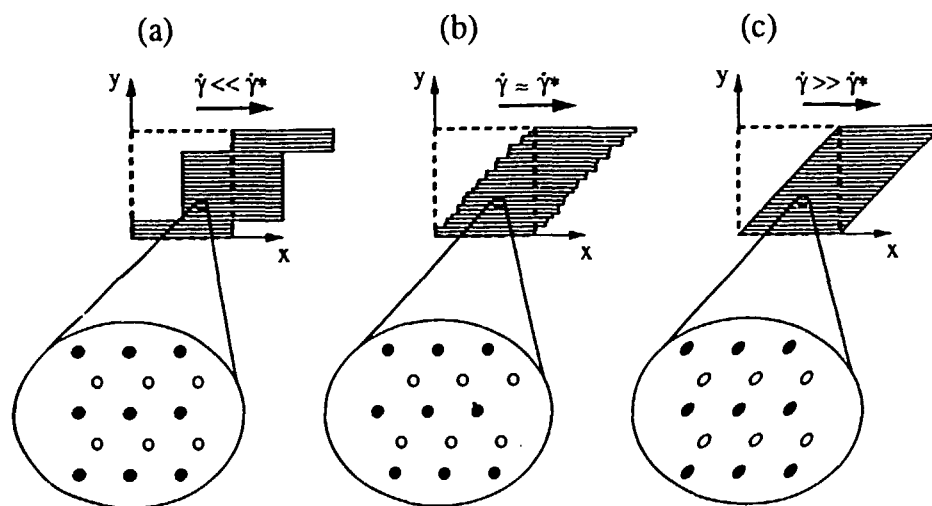


Fig. 1. Schematic illustration of the three deformation mechanisms for BCC spheres: (a) slow shearing and associated creeping deformation; (b) intermediate shear rate with the generation of numerous defects leading to a loss of translational order; (c) fast shear rate with affine elastic deformation. The layers shown represent {110} planes of the BCC system. $\dot{\gamma}^*$ represents the inverse relaxation time of the defects. The *x*-axes and the *y*-axes are the directions of the shear and shear gradient, respectively.

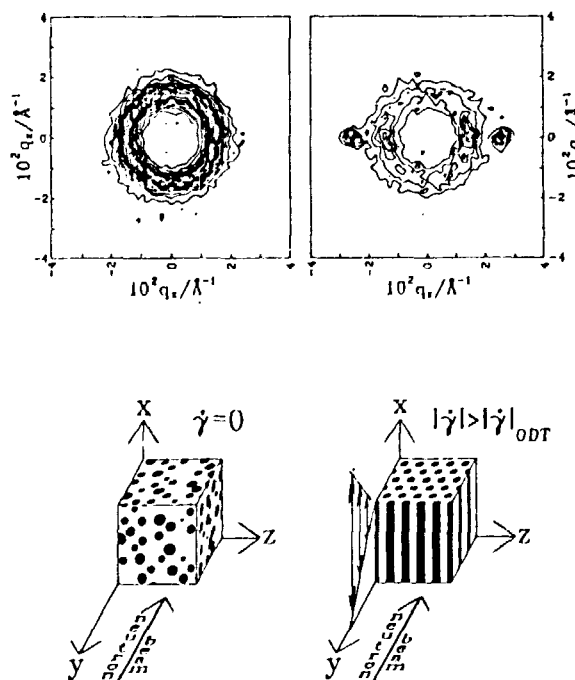
¹⁾ K.A. Koppi, M. Tirrell, F.S. Bates, K. Almdal, and K. Mortensen, *J. Rheol.*, **38**, 999 (1994).

2.8.10 Influence of Shear on the Hexagonal-to-Disorder Transition in a Diblock Copolymer Melt

K. Almdal, K. Mortensen, *Department of Solid State Physics, Risø National Laboratory, Denmark*, F. S. Bates, K.A. Koppi, and M. Tirrell, *Department of Chemical Engineering and Materials Science, University of Minnesota, USA*

The influence of shear on the hexagonal-to-disorder phase transition has been investigated in a poly(ethylenepropylene)-poly(ethylethylene) (PEP-PEE) diblock copolymer melt¹⁾. This sample (referred to as PEP-PEE-7) contains 77% by volume PEP and the PEE block is 75% deuterium labelled to provide contrast for neutron scattering. In the absence of shear a transition from a hexagonally packed rod ordered structure to a disordered state with composition fluctuations occurs at $155 \pm 1^\circ\text{C}$. We have utilized a shearing device that can be operated *in situ* while conducting small-angle neutron scattering (SANS) measurements. The response of the sample at 157°C serves to illustrate the influence of shear. In the absence of shear the material exist in a fluctuating disordered state as evidenced by an azimuthally symmetric scattering pattern that contains a well-defined ring of intensity at $|\mathbf{q}| = q^*$ (where $|\mathbf{q}| = 4\pi\lambda^{-1} \sin(\theta/2)$). Upon tuning the shear on with $\dot{\gamma} = 6\text{s}^{-1}$ the material rapidly transforms into an oriented hexagonal cylinder phase. SANS data and a sketch of these effects are given in Fig. 1. Aside from the steady-state results it was observed that upon abruptly stopping the shear a transient state with body centred cubic (BCC) symmetry exists. The interpretation of this phenomenon is that the rods break up into spherical domains (or possibly undulating rods) which initially are placed on a BCC-lattice. The shear quench experiment offers a possibility of forcing the block copolymer melt into a non-equilibrium state and follow the path taken towards equilibrium.

Fig. 1 Contour plots of SANS-data from sample PEP-PEE-7 at 157°C . The contour lines are drawn at equidistant levels of intensity on a linear scale. On the left data is given with no shear applied to the sample. The sketch illustrates a snapshot of the disordered state with spherical like composition fluctuations. On the right data is given after application of reciprocating shear ($\dot{\gamma} = 6\text{s}^{-1}$, strain amplitude approximately 300%). The sketch illustrates the formed hexagonally packed rod structure as evidenced by the scattering pattern.



¹⁾ F. S. Bates, K.A. Koppi, M. Tirrell, K. Almdal, and K. Mortensen, *Macromolecules*, **27**, 5934 (1994).

2.8.11 Investigation of the Surface Induced Ordering of P85 on Quartz

M. C. Gerstenberg, J. Skov Pedersen, K. Mortensen, *Department of Solid State Physics, Risø National Laboratory, Denmark*, and G. Smith, *Los Alamos Neutron Scattering Center H-805, Los Alamos National Laboratory, New Mexico, USA*

The structural properties of $\text{EO}_{25}\text{PO}_{40}\text{EO}_{25}$ (P85) have previously been investigated with Small Angle Neutron Scattering (SANS)¹⁾. The amphiphilic nature of P85 above app. 15°C in aqueous solution gives rise to a large diversity of phases *e.g.* micelles in a body-centered cubic structure, hexagonal rods and lamellar phases. Furthermore, poly-crystalline P85 in the BCC phase has been shown to align instantaneously when exposed to shear forming a single crystal²⁾. In order to further investigate the local ordering of P85 near a surface a static and a shear flow³⁾ reflection cell were used. The thermostated cells are based on the transparency of quartz to neutrons. One face of a quartz single crystal delimits a Teflon enclosure, thus enabling neutrons to traverse through the quartz and reflect off the solid-liquid interface. Initially, a series of static reflectivity studies of P85 in aqueous solution with varying concentration have been performed. It was evident, that further investigations of the off-specular scattering were necessary, hence the cell was mounted on SANS using the 2D-detector. The data showed a specular peak superposed on a bulk related signal. Further analysis will indicate to what extent the bulk signal can be subtracted to arrive at the surface signal. The SANS measurements of 30 w% P85 showed clear indication of alignment when exposed to pre-measurement shear. The spectra were different from the expected bulk behaviour (see fig. 1.). In addition, the reflectivity scans of the non-sheared 30 w% P85 showed evidence of an approximately 230 Å layered structure perpendicular to the quartz surface in a BCC bulk phase. Suggestively, it could indicate the lamellar phase seen in high concentrated P85 solutions. Both the SANS and the reflectivity studies are thus an indication of possible surface ordering.

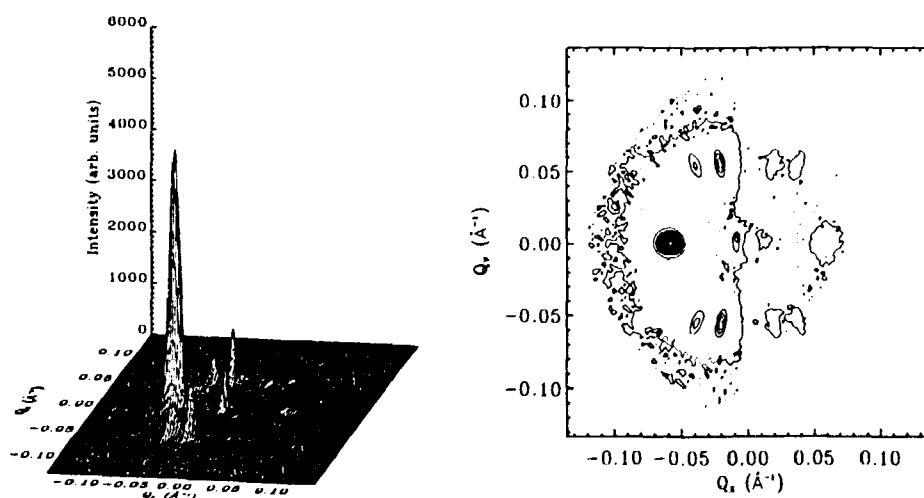


Fig. 1. Two representations of a SANS image for 30 w% P85 after application of shear. The specular peak are situated at $(Q_x, Q_y) = (-0.01, 0)$. The remaining peaks are bulk related. Positive and negative Q_x corresponds to reflected and transmitted intensity, respectively.

- 1) K. Mortensen and J. S. Pedersen, *Macromolecules*, **26**, 805-812 (1993).
- 2) K. Mortensen, *Europhys. Lett.*, **19** (7), 599-604 (1992).
- 3) S. Baker et al., *Rev. Sci. Instrum.*, **65** (2), 412-416 (1994).

2.8.12 Butterfly Effect in Randomly Cross-Linked PDMS Gels. Classical Deformation at Large Scales

A.N. Falcão, *Physics Department, INETI/ICEN, Portugal*, J. Skov Pedersen, and K. Mortensen, *Department of Solid State Physics, Risø National Laboratory, Denmark*

The macroscopic deformation of a uniaxially stretched polymer gel varies continuously from a maximum extension (along the direction parallel to the stress), to a maximum compression (along the direction perpendicular to the stress). Information on the microscopic effect of the deformation can be obtained by means of scattering techniques. Typically, scattering patterns obtained from stretched gels display characteristic “butterfly”-like shapes in the low scattering vector (q) region. These are *not expected from classical deformation models* that picture the gel as a regular network of Gaussian strands that deform affinely with the macroscopic deformation. We have compared the scattering of swollen gels in the isotropic state and uniaxially stretched. The samples used were polydimethylsiloxane (PDMS) networks produced by electron irradiation. When stretched, they were measured after the mechanical relaxation was completed. For the stretched samples, the patterns recorded at the detector were divided into angular sectors, 10° each. The data were analyzed by means of a model that uses two characteristic lengths: ξ_S - distance below which single chain behaviour is observed; ξ_L - distance above which large scale fluctuations of polymer concentration are no longer observed. This model has been shown¹⁾ to describe well the scattering of isotropically swollen gels. Upon stretching ξ_L becomes anisotropic, varying continuously from a maximum value observed in the direction parallel to the stress, to a minimum value along the perpendicular direction. Taking into account the extra swelling that occurs when the samples are stretched, we found that the angular dependence of ξ_L is very close to the one predicted by a classical affine deformation model.

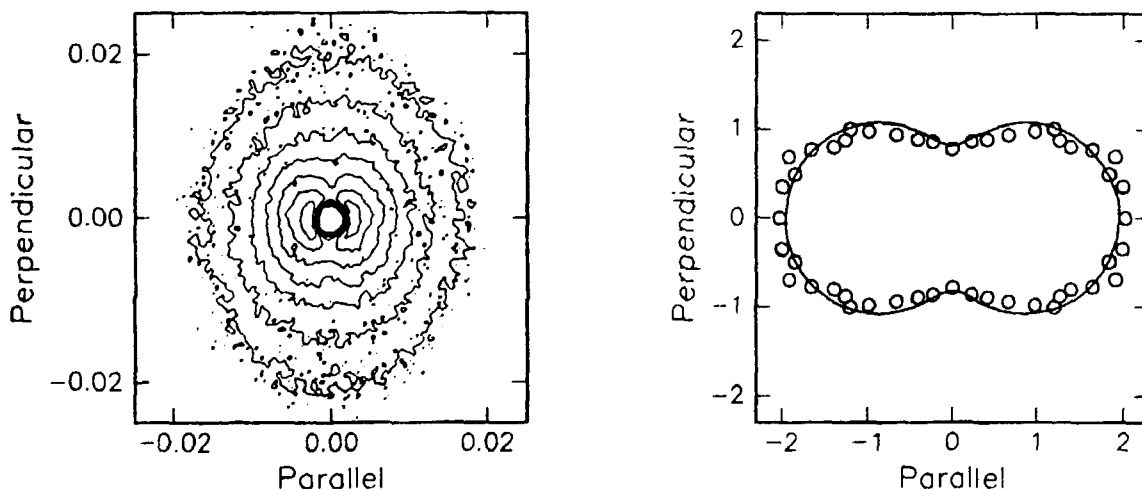


Fig. 1. a) Isointensity contours obtained from a swollen network stretched to $\lambda = 1.9$. In the low q region, the characteristic butterfly pattern is observed. At a certain value q^* the isointensity contours are approximately circular. For $q > q^*$ the contours show a classical elliptical shape elongated in the direction perpendicular to the stress. b) Open circles: observed ratio ξ_L/ξ_{L0} between the large scale characteristic lengths the stretched and the corresponding non-stretched sample; full line: expected from a classical deformation model.

¹⁾ A.N. Falcão, J.S. Pedersen, and K. Mortensen, *Macromolecules* **26**, 5350 (1993).

2.9 Molecular Science

2.9.1 Self-Assembling Molecular Wires

M. Jørgensen and K. Bechgaard, *Department of Solid State Physics, Risø National Laboratory, Denmark*, T. Bjørnholm, P. Sommer-Larsen, L. G. Hansen and K. Schaumburg, *Centre for Interdisciplinary Studies of Molecular Interactions, University of Copenhagen, Denmark*

A gel-forming compound: 4,4'-bis[[N,N'-bis[2-hydroxy-1,1-bis(hydroxymethyl)ethyl]-7,7-diamidoheptyl]thio]-5,5'-dimethyltetrathiafulvalene (**1**) or bis-arborol-tetrathiafulvalene, has been prepared with the aim of manufacturing a self-assembling "molecular" wire¹⁾.

"Molecular" scale electronic and optical components are of current interest as materials chemistry goals, complementary to conventional semiconductor miniaturization. In order to connect the nano scale active components the equivalent of a wire is needed. Here we describe an attempt to manufacture a prototype "molecular" wire by utilizing self-assembly principles. The molecular requirements of self-assembling structures have been studied extensively during the last decade. Of special interest to us was the work of Newkome et al.²⁾ who prepared the so-called bis-arborols that readily form gels in water consisting of string like structures. Bis-arborols are bidirectional molecules with a lipophilic central chain (or trunk) terminated by highly branched polyalkohol groups (the branches and roots). We have attempted to give the structure electronic conductivity by replacing part of the lipophilic chain with a tetrathiafulvalene unit. The tetrathiafulvalene family of compounds are well known to give highly conductive salts, were the partly oxidized heteroaromatic systems form stacks with high electron mobility along the stacking axis.

Synthesis of the target compound **1** was achieved in five steps through build-up of the central tetrathiafulvalene core and attachment of polyalcohol arborol groups. When dissolved in water-ethanol (3:1) **1** indeed formed a gel. Phase contrast optical microscopy revealed string like assemblies with a length of the order of microns. Transmission electron microscopy (TEM) and atomic force microscopy (AFM) was used to further characterize the finer details in the gel structure. String or band like structures were clearly visible with diameters in the order of 100 nm. This is much larger than one would expect from the molecular dimensions of ca. 3.5 nm and suggests that the observed structures consist of aggregates, perhaps build-up from molecular strings. UV spectroscopic characterization of the gel in solution or dried on quartz, shows that on doping with iodine an absorption band occurs at 874 nm. This is diagnostic for the formation of dimers and higher oligomers of partially oxidized tetrathiafulvalene units in a stack structure, which is prerequisite for electrical conductance.

¹⁾ M. Jørgensen, K. Bechgaard, T. Bjørnholm, P. Sommer-Larsen, L.G. Hansen and K. Schaumburg, *J. Org. Chem.* **59**, 5877 (1994).

²⁾ G.R. Newkome et al., *Angew. Chem., Int. Ed. Engl.*, **31**, 917 (1994).

2.9.2 Synthesis of New Non-linear Organic Materials

M. Jørgensen and K. Bechgaard, *Department of Solid State Physics, Risø National Laboratory, Denmark*, T. Geisler, *Department of Physics, University of Aalborg, Denmark*

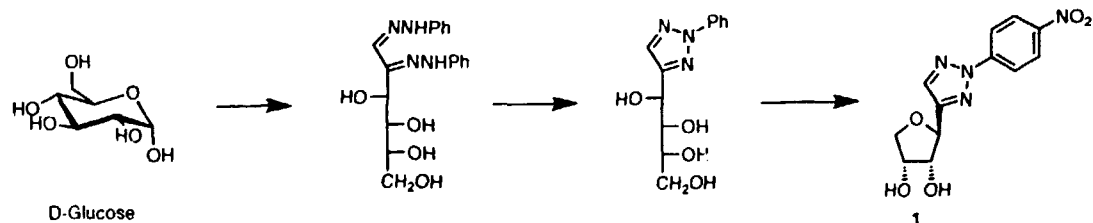
Non-linear optical organic polymers are conventionally made by cooling through the glass transition temperature (T_g) while applying a strong electrical field. This so-called poling procedure serves to orient the chromophores and to add up their individual contributions to the polarization tensor. This uniformly polarized state however tends to relax back to the random orientation state with zero resulting non-linear optical moment.

To surcumvent this deficiency, we have prepared monomeric chromophores with a build-in mirror asymmetry. Crystals and polymers of these materials have thus no centrosymmetry and therefore have a resulting non-linear optical moment. Unlike for conventional polymers no poling process is nescesary.

One of the most readily available compounds with mirror asymmetry is D-glucose. Through the reactions outlined below (Fig. 1) it was transformed into 2-((4-nitrophenyl)-1,2,3-triazol-4-yl)-3,4-dihydroxy-oxole **1**. The nitrophenyl-triazole unit is a novel non-linear element, while the substituted oxole ring has mirror asymmetry. The two hydroxy groups serve as handles for polymerisation.

Preliminary measurements show high second order non-linear generation of the crystalline monomer.

Fig. 1.



2.9.3 Novel Peptide Nucleic Acids

M. Egholm, O. Buchardt *Research Center for Medical Biotechnology, The H.C. Orsted Institute, University of Copenhagen, Denmark*, P.E. Nielsen, *Department of Biochemistry B, The Panum Institute, University of Copenhagen, Denmark*, and R.H. Berg, *Department of Solid State Physics, Risø National Laboratory, Denmark*

Peptide nucleic acids (PNA) are oligonucleotide analogs in which the sugar-phosphate backbone is replaced by a backbone consisting of *N*-(2-aminoethyl)glycine units to which the nucleobases are attached through methylene carbonyl linkers. We have previously demonstrated the very high binding affinity between such PNA oligomers and single- and double-stranded DNA as well as the sequence specificity of hybridization¹⁻³). Thus, PNAs are potential candidates for gene-targeted drugs and for tools in molecular biology and diagnostics. In previous studies on the structure activity relationship of PNA we have shown the importance of having the correct interbase distance. For example, when extending the original *N*-(2-aminoethyl)glycine backbone on the linker to the base by one methylene group, the binding affinity was lowered while the sequence specificity was preserved. In order to examine further to which extent the backbone can be modified without destroying the PNA-DNA binding properties, we have synthesized a PNA decamer in which one of the amide bonds between two units is reversed. In this PNA, the interbase distance is the same as in the original PNA oligomer and it was shown that the binding affinity for DNA of this new PNA oligomer is retained⁴). Furthermore, the preparation of mixed- sequence PNA oligomers containing the four natural nucleobases has been reported⁵).

¹)P.E. Nielsen, M. Egholm, R.H. Berg, and O. Buchardt, *Science* **254**, 1497 (1991).

²)M. Egholm, O. Buchardt, P.E. Nielsen, and R.H. Berg, *J. Am. Chem. Soc.* **114**, 1895 (1992).

³)M. Egholm, P.E. Nielsen, O. Buchardt, and R.H. Berg, *J. Am. Chem. Soc.* **114**, 9677 (1992).

⁴)P.-H. Lagriffoul, M. Egholm, P.E. Nielsen, R.H. Berg, and O. Buchardt, *BioMed. Chem. Lett.* **4**, 1081 (1994).

⁵)K.L. Dueholm, M. Egholm, C. Behrens, L. Christensen, H.F. Hansen, T. Vulpius, K.H. Petersen, R.H. Berg, P.E. Nielsen, and O. Buchardt, *J. Org. Chem.* **59**, 5767 (1994).

2.9.4 New Solid Supports and Linkers for Peptide Synthesis

L. Winther, W. Batsberg Pedersen, R.H. Berg, *Department of Solid State Physics, Riso National Laboratory, Denmark*, C. Schafer-Nielsen, *Department of Clinical Chemistry, Glostrup Hospital, Denmark*

PEPS *film* supports provide state-of-the-art peptide synthesis¹⁾. In addition, they offer exceptional ease of handling, permitting the simultaneous production of multiple peptides in a parallel fashion²⁾. We report now on the construction of PEPS *tubes* as new flow resins for peptide synthesis³⁾. To construct a PEPS tube, polystyrene is grafted onto the inner surface of a polyethylene tube and functionalized with, *e.g.* aminomethyl groups. The tube geometry simplifies the set-up for automatic solid-peptide synthesis since the flexibility and strength of the polyethylene tubes are maintained. Peptide synthesis only takes place on the inner surface of the tube. In this way the polyethylene tube becomes the reaction vessel of the synthesis. The problems associated with filters and free support are therefore eliminated. In addition, the resin is mechanically stable and gives a constant counter pressure during the synthesis. The resin is stable at elevated temperatures, allowing use of a wide variety of methods of functionalization.

Benzhydrylamine-based linkers are the most widely used for solid-phase synthesis of peptide amides employing the Boc-benzyl protection scheme. A critical step is the final cleavage of the peptide amide from the solid support. This step is often carried out by use of strong acids such as anhydrous HF. The conventional strong acid method, which operates through the S_N1 mechanism, produces very active carbocations that often lead to serious alkylation and acylation of sensitive residues in the peptide chain. As an improvement, we have now developed sulfoxide derivatized benzhydrylamine linkers that are cleaved by the sulfide-assisted acidolytic S_N2 deprotection method, which removes the precursors of harmful carbocations to form inert sulfonium salts.

¹⁾ R.H. Berg, K. Almdal, W. Batsberg Pedersen, A. Holm, J.P. Tam, and R.B. Merrifield, *J. Am. Chem. Soc.* **111**, 8024 (1989), and U.S. Patent 5,258,454 (1993).

²⁾ R.H. Berg, K. Almdal, W. Batsberg Pedersen, A. Holm, J.P. Tam, and R.B. Merrifield (1991). In: *Peptides 1990*, E. Giralt and D. Andreu, eds. (Escom, Leiden), pp. 149-190.

³⁾ L. Winther, C. Schafer-Nielsen, W. Batsberg Pedersen, and R.H. Berg (1994). In: *Abstracts of 23rd European Peptide Symposium, Braga, Portugal*.

2.9.5 Side-Chain Liquid Crystalline Polyesters for Optical Information Storage

S. Hvilsted, *Department of Solid State Physics, Risø National Laboratory, Denmark*, P.S. Ramanujam, *Optics and Fluid Dynamics Department, Risø National Laboratory, Denmark*, H.W. Siesler, *Department of Physical Chemistry, University of Essen, Germany*, P. Magagnini, *Chemical Engineering Department, University of Pisa, Italy*, and F. Andruzzi, *CNR, Chemical Engineering Department, University of Pisa, Italy*

The project with the acronym LICRYPOIS is a collaborative focussed fundamental research project performed by the above international consortium and supported financially in part by the European Economic Community in the framework of the Brite/Euram programme. The management of the project is in the department. LICRYPOIS has a well established three year workprogramme extending for almost two years.

The objective of LICRYPOIS is to perform basic research in the development of new side-chain liquid crystalline (SCLC) polyester materials suitable for optical information storage and processing. Specifically, the research is directed towards the development of an erasable and rewritable holographic memory having diffraction efficiencies greater than 30% and providing very high recording densities on the order of 1 Gbit/cm².

A range of new SCLC polyesters with the photoactive cyanoazobenzene chromophore has been prepared. Structural parameters such as main-chain spacing between side-chains, the length of the flexible spacer linking the photoactive group to the main-chain, and the substituent on azobenzene have been varied. These new materials have been thoroughly investigated and characterized by a range of different analytical techniques in order to understand and correlate the material response to laser light irradiation at different wavelengths.

A spin coating technique to prepare uniform thin films suitable for optical information storage applications has been developed. Recording of holograms and assessment of images have been successfully performed. Computer generated holograms and text have been directly recorded on films of these new SCLC polyester materials. In this manner it is possible *e.g.* to produce a system of Fresnel microlenses where each lens is about 0.5 mm. Furthermore, text with letter size of 50 μm can be directly written into the film. The information can be completely erased by heating the film to about 80°C for a few minutes, and the films can be reused for information storage.

The materials and components developed under this project can be used in state-of-the-art apparatus performing analog optical processing such as vision systems and in digital devices, *e.g.* optical digital memories.

2.9.6 New Azobenzene Based Polyesters for Optical Storage

M. Pedersen, S. Hvilsted, *Department of Solid State Physics, Riso National Laboratory, Denmark*, P.S. Ramanujam, *Optics and Fluid Dynamics Department, Riso National Laboratory, Denmark*, and J. Kops, *Department of Chemical Engineering, The Technical University of Denmark, Denmark*

A key design parameter and building block for side-chain liquid crystalline polyesters for optical storage is the azobenzene containing 1,3-propanediols. In the photoactive azobenzene chromophore of these precursor diols, the para substituent on the azophenyl moiety has been extensively varied and studied. In the diol series with the substituents: H, OCH₃, CN, and NO₂, the maximum light absorption position in the UV-visible range seems to reflect the electron acceptor character of the particular substituent on the azobenzene chromophore. The substituent also has a significant influence on the mesomorphic behaviour and transition temperatures of the diols as determined by polarizing optical microscopy and differential scanning calorimetry. While the unsubstituted diol is a simple crystalline compound, the methoxy diol shows a nematic and the cyano diol shows both nematic and smectic A liquid crystalline phases but both diols exhibit monotropic behaviour. The nitro diol also has a smectic A phase but demonstrates enantiotropic behaviour.

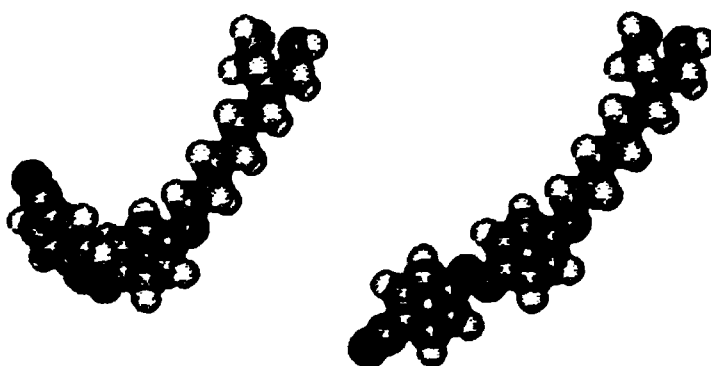


Fig. 1 *cis* and *trans* isomers of the 2-[6-(4-(4-cyanophenylazo)phenoxy)hexyl]-1,3-propanediol.

Theoretical dipole moments of the different azobenzene chromophores in the mesogenic diols have been calculated with the modelling programme *HyperChemTM* in both the *cis* and *trans* isomers (example in Fig. 1). The largest dipole moments were found for the nitro substituted diol which also showed a large difference between the values of the *cis* and *trans* conformation. Minor differences and smaller values of the *trans* isomer dipole moments, respectively, were calculated in the cyano, methoxy and unsubstituted azobenzene diol, mentioned in order of decreasing dipole moments. Measurements of laser induced optical anisotropy on polyesters based on these diols show that the nitro and methoxy polyesters are almost insensitive, whereas optical anisotropy can easily be generated both in the cyano (as already well documented) and the unsubstituted derivative. In other words, dipole moments alone do not play a key role when performing optical storage in these materials. In order to get a better understanding of the influence of the substituent *e.g.* if steric hindrance plays a role, other diols with a CH₃, CF₃, and F substituent, respectively, have been synthesized and spectroscopically characterized. Investigations of phase transitions and polyester preparations are in progress.

2.9.7 The Influence of Spacer Length and Substituents on the Orientational Behaviour of Novel Azobenzene Side-Chain Polyesters

I. Zebger, C. Hendann, H.W. Siesler, *Department of Physical Chemistry, University of Essen, Germany*, F. Andruzzi, *CNR, Chemical Engineering Department, University of Pisa, Italy*, P.S. Ramanujam, *Optics and Fluid Dynamics Department, Risø National Laboratory, Denmark*, S. Hvilsted, C. Kulinna, and M. Pedersen, *Department of Solid State Physics, Risø National Laboratory, Denmark*

The physics of optical storage is being examined in detail in an ongoing project on liquid crystalline azobenzene side-chain polyesters. The polyesters exhibit permanent local changes in refractive index due to laser induced *trans-cis* isomerization. We have made a detailed investigation on the implications of optical storage caused by a change in the length of the flexible methylene spacer linking the azobenzene chromophore to the polyester main-chain¹). Time-dependent measurements of optically induced anisotropy in cyanoazobenzene polyesters with 6, 8, and 10 methylene groups in the spacer show that the transmission through the films depends on the argon laser intensity employed. Furthermore, the polyesters with shorter flexible spacers respond more readily to low irradiation intensities.

Laser induced anisotropy and holographic storage have been investigated in substituted (nitro, cyano, methoxy and unsubstituted) azobenzene polyesters²). These investigations have been carried out at 413 and 488 nm. The highest efficiency obtained at 413 nm is about $2\text{-}3 \cdot 10^{-3}$ for the cyano and unsubstituted azobenzene polyesters. Much higher efficiencies are obtained at 488 nm, however, with higher incident intensities. A maximum of 13% has been achieved for the cyano polyester at this wavelength. The poor efficiency at 413 nm is attributed to two reasons. Firstly, the absorption in the polyester films at 413 nm is generally three times as much as at 488 nm; this leads to the formation of absorption gratings whose efficiencies are much less than those of pure phase gratings. Secondly, since the absorption is larger, the light is probably getting absorbed within the first few nanometers of the film, rather than penetrating the entire depth. Thus much of the azobenzene chromophores are probably not utilized. The nitro and methoxy substituted polyesters seem to give much smaller diffraction efficiencies. These findings are in agreement with polarization FTIR measurements. This is remarkable as one might expect that azobenzene chromophores with higher dipole moments might provide higher mobility when interacting with light.

Maybe the most interesting physical aspects of the optical storage in these polyesters is that the storage is permanent in the polyesters with 12 methylene groups in the main-chain even though the glass transition temperature is around 20°C. Through an investigation of the UV-Vis spectra, it has been shown that the lifetimes of the *cis* states in these polyesters are only of the order of 6 hours. A HeNe laser beam has been shown to induce back-transition to the *trans* states within the lifetimes of the *cis* states, resulting in a biphotonic process.

¹) P.S. Ramanujam, F. Andruzzi, and S. Hvilsted, *Optical Review* **1**, 3 (1994).

²) I. Zebger, C. Kulinna, H.W. Siesler, F. Andruzzi, M. Pedersen, P.S. Ramanujam, and S. Hvilsted, (1994). *Macromol. Symp.*, *submitted*.

2.10 Instrument Development

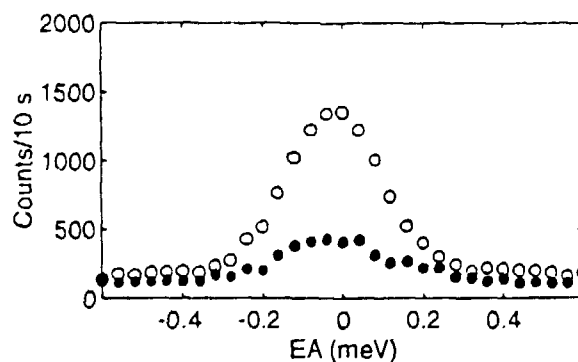
2.10.1 First Test of the RITA Analyser System

D.F. McMorrow, K.N. Clausen, *Department of Solid State Physics, Risø National Laboratory, Denmark*, G. Aeppli *AT & T Bell Laboratories, USA*, C. Broholm *JHU, USA*, and T. Mason, *Department of Physics, University of Toronto, Canada*

One of the key design criteria of the RITA spectrometer will be to maximise the useful neutron flux, while minimising the background from fast and thermal neutrons, in such a way that the configuration of the instrument can be changed easily. In particular, it is envisaged that the analyser system will combine the use of an array of analyser crystals with a large two-dimensional detector, thus allowing one of several different modes of operation. For example, the analyser array may be tuned to give point-to-point focussing from the sample to the detector, or it may be set so that different final energies are selected enabling a trajectory in (\mathbf{Q}, ω) space to be mapped out for one setting of the spectrometer.

A prototype analyser system fulfilling the above requirements has been constructed and tested recently on TAS7. The basic construction consists of a tank that may be evacuated to eliminate air scatter and which has single-crystal sapphire windows allowing it to be operated in a small-angle mode. A cladding of polythene, 200 mm thick, provides the shielding against fast neutrons, while the inside is coated with Boral to remove any stray thermal neutrons. For this test the analyser consisted of eleven independently tunable blades of PG, and the detector was a one-dimensional micro-strip PSD with one hundred and twenty eight channels. The main aim of the test was firstly to establish whether or not the shielding was adequate, and more importantly to begin to investigate different focussing geometries. A comprehensive test of the performance of the shielding was performed by placing a plastic, incoherent scatterer at the sample position and then recording the intensity of the detector for various configurations of the internal Boral shields. The results of these tests indicate that the overall background seen at the detector may be reduced to the fast neutron background with only very modest Boral shielding, and that the overall rejection ratio is 2×10^{-6} or better.

Fig. 1. Energy scans for focussed (open circles) and unfocussed (closed circles) setting of the analyser array. The sample was a plexi glass rod, 12 mm in diameter.



In this test we also tested a point-to-point focussing geometry. A variety of incoherent scatterers were used as the sample. Inelastic scans were performed by varying E_f with $E_i = 4.5$ meV enabling a PG filter to be used in the incident beam. The results are summarised in Fig. 1. The main conclusion is that four-fold gains are achievable with point-to-point focussing even for sizeable sample.

2.10.2 Characterization of an Image-Plate Detector used for Small-Angle X-Ray Scattering

A.M. Hussain, K. Mortensen, J. Skov Pedersen, and M. Vigild, *Department of Solid State Physics, Risø National Laboratory, Denmark*

A *Molecular Dynamics* image-plate (IP) detector system is currently being characterized for future application in SAXS measurements. Self exposure and linearity of the IP has been measured. Experiments on self decay, resolution, uniformity, smearing and sensitivity will be performed. Software has been developed that converts the image plates TIFF format so that it can be used within existing SANS software.

The IP is a flat aluminium plate ($20 \times 25 \text{ cm}^2$) coated with fine photostimulable phosphor crystals, BaFBr:Eu^{2+} , combined in an organic binder. By X-ray excitation, a part of the Eu^{2+} ions are ionized to Eu^{3+} and electrons which are excited to the conduction band are trapped at F^+ -centers. By visible light irradiation from a He-Ne laser within a *Molecular Dynamics Phosphorimager*, the trapped electrons at F-centers are again liberated to the conduction band and return to Eu^{3+} ions converting them to excited Eu^{2+} ions. As the excited Eu^{2+} ions return to the ground state, the released energy is emitted as blue light, with intensity proportional to the absorbed radiation dose. The emitted light is then detected by the scanner within the phosphorimager. This mechanism leaves the IP with a dynamic range of about five orders of magnitude.

The linearity of the IP was measured using following procedure. The plates were exposed with different X-ray sources for a time Δt varying between 20 and 600 s. Figure 1 shows the linear relation between the arbitrary Molecular Dynamics counts and the exposure dose from a Cu source. The conversion factor (between arbitrary MD counts and exposure dose) is found as the slope of the linear fit.

The measurements of the self exposure shows (see Fig. 2) that the self exposure consists of a part originating from natural radioactivity (cosmic radiation, surrounding materials and the materials of which the plates are composed) and a constant part presumably caused by the noise level of the IP scanner system.

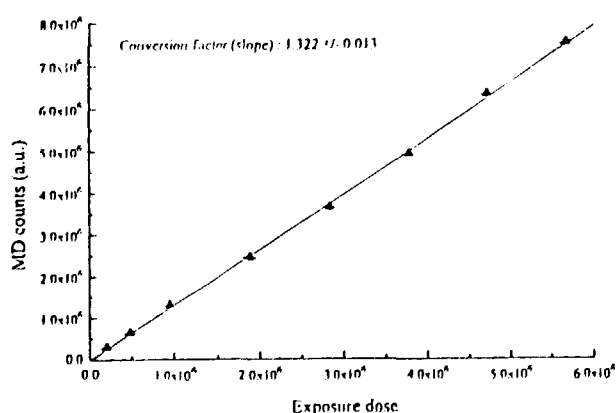


Fig. 1. Linearity measurement of the image plate using a Cu source. The solid line is the linear fit.

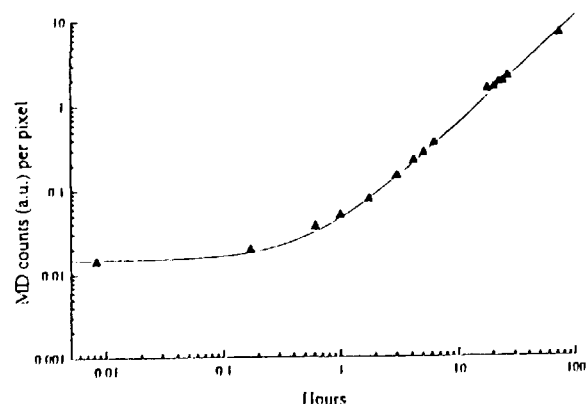
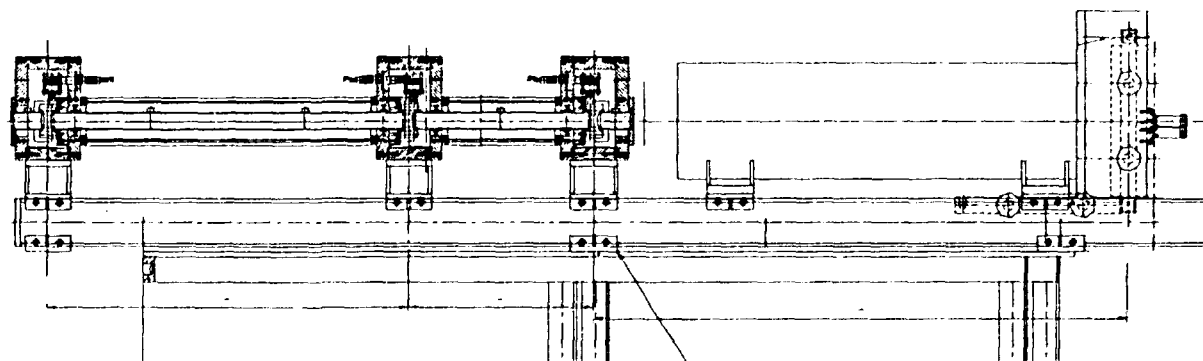


Fig. 2. Self exposure of the image plate. The solid line is a fit to a power law plus a constant.

2.10.3 A Pin-Hole Small-Angle X-Ray Scattering Instrument

O. Rasmussen, T. Kjær, A.M. Hussain, M.E. Vigild, K. Mortensen, and J. Skov Pedersen,
Department of Solid State Physics, Risø National Laboratory, Denmark

A small-angle X-ray scattering instrument is currently being designed, built, and installed. The X-ray source is the 12 kW *Rigaku* rotating anode in the Department, which was put back in operation again in the beginning of December 1994 after a longer repair. The instrument employs a double graphite monochromator, and three sets of slits. The double monochromator allows the use of both Cu $K\alpha$ and Mo $K\alpha$ radiation by rotation of the monochromator box and translation the crystals. Only smaller adjustments of the slits are required. Special care has been taken to select graphite crystals of good quality with high reflectivities (better than 50%). The slits are commercially available slits from *Huber*, which have been motorized at Risø and built into boxes, allowing an integrated evacuated flight path from the monochromator to the sample position. The two first slits define the collimation of the beam and the third slit is a guard slit, which is used for removing parasitic scattering from the second slit and thus reducing the background. The two collimating slits, of size $0.70 \times 0.70 \text{ mm}^2$ and $0.45 \times 0.45 \text{ mm}^2$, respectively are separated by 760 mm. The guard slit is placed 380 mm after the second slit. The instrument uses an image-plate detector system from *Molecular Dynamics*. During the summer the monochromator, the optical bench, and the collimation system were installed. These components have been aligned and a preliminary arrangement for the flight tube after the sample, a beamstop, and a holder for the image plate have been set up. The first measurements on a silica aerogel and block copolymers are currently being performed. The instrument covers a range of scattering vectors down to 0.01 \AA^{-1} . The first estimates of the flux at sample position give a value of about 10^6 photons per second, in good agreement with the expected value. The drawings for the final detector flight tube, including motorized beamstop translations and a cassette system for the image plate, will be ready in the beginning of January 1995. The installation should be completed in the early spring. In the final state the instrument will cover scattering vectors up to 0.65 \AA^{-1} .



2.10.4 Performance Test of the BW2 Beamline

R. Feidenhans'l, E. Landemark, D.-M. Smilgies, M. Nielsen, *Department of Solid State Physics, Risø National Laboratory, Denmark*, L. Lottermoser, G. Falkenberg, L. Seehofer, and R. L. Johnson, *II. Institut für Experimentalphysik, Universität Hamburg, Germany*, H. Schulte-Schrepping, R. Treusch and W. Drube, *HASYLAB, DESY, Hamburg, Germany*

It has been a few years ago that the commissioning of the bypass at the DORIS III storage ring was completed. Furthermore, DORIS III recently became a dedicated synchrotron radiation source with very good and stable beam conditions. We therefore felt that was appropriate to perform a benchmark experiment to demonstrate the capabilities of the new ring. X-ray diffraction from single crystal surfaces can provide such a test, because only a sufficient intense and high quality beam can give acceptable counting rates. The experiment was performed at the wiggler beamline BW2¹⁾. We choose the dimerized Ge(100)2x1 surface to be the test candidate. The surface structure is well known and consists of Ge-dimers and additional subsurface relaxation. Furthermore, the surface has been studied in many laboratories, so counting rates obtained at different sources can be compared and the recipe for surface preparation, i.e. how to obtain a high quality surface, is well-known.

As shown in the figure, we obtained 100000 counts/sec in the (3/2,0) peak at a DORIS current of 100 mA. The measurement was performed at a wavelength of $\lambda = 1.5\text{\AA}$ and was done with an angle of incidence equal to the critical angle enhancing the signal by a factor of two. The incoming beam was 1 mm wide parallel to the surface and the signal was detected with a scintillation counter 910 mm away from the sample with a 2×10 mm slit in front of the detector. Correcting the signal for deadtime, we obtained 120000 counts/sec. The FWHM of the peak in an ω -scan rocking around the surface normal was 0.08° . This width can be decreased to 0.04° by narrowing the resolution in the direction normal to the surface. This width is then limited by the domain size on the surface. The count rate is comparable to values obtained at a third generation synchrotron radiation source and shows the high flux of the BW2 beamline.

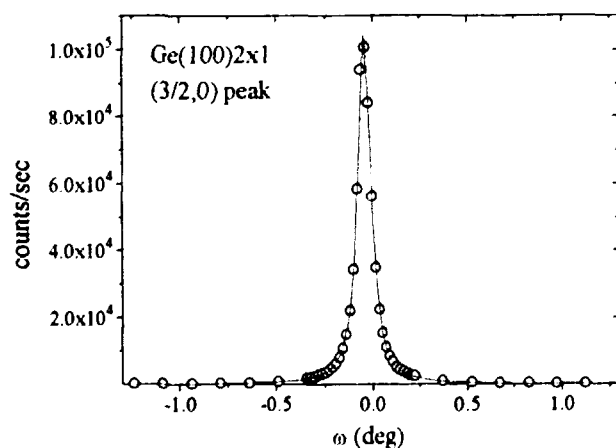


Fig. 1. An ω -scan of the (3/2,0) peak from the Ge(100)2x1 structure. The peak width is 0.08° .

¹⁾ W. Drube *et. al.*, *Rev. Sci. Instr.*, *submitted*.

2.10.5 AFM of Insulating Surfaces

J.G.Larsen, S.Quist Nielsen, M.Christensen and R.Feidenhans'l, *Department of Solid State Physics, Riso National laboratory, Denmark*

The substrate is of great importance in any successful attempt to grow high quality thin films and superlattices by molecular beam epitaxy (MBE). Characterization and control of the substrate surface roughness is therefore crucial.

We have used Atomic Force Microscopy (AFM) as a probe for surface roughness of insulating surfaces and other thin film surfaces. The system is a commercial Rasterscope model 4000 from DME that operates in air and utilizes an optical deflection detection system. It is equipped with a 50 μm scanhead producing good images in the range 250-50000 nm. The scanning is performed using a piezoelectric tube scanner, which drives the triangular cantilever having a spring constant of app. 0.1 N/m (contact mode) across the sample surface. The cantilever tip interacts with the surface through it's small pyramidal Si_3N_4 tip by van der Waals, electrostatic, or chemical attractive forces and coulomb repulsive forces. In search of methods for preparing smoother surfaces we have tried annealing Al_2O_3 substrates in air at 1600°C for 24 hours as shown in figures 1a and 1b. In figure 1a we have an untreated sapphire crystal showing a very rough surface and in figure 1b is shown the annealed sapphire surface displaying atomically smooth terraces. The terraces are approximately 300 nm wide and several thousand nm long, separated by 7 nm high steps kinked along alternative lattice directions. Also seen is a few smaller steps approximately 0.4-0.7 nm high.

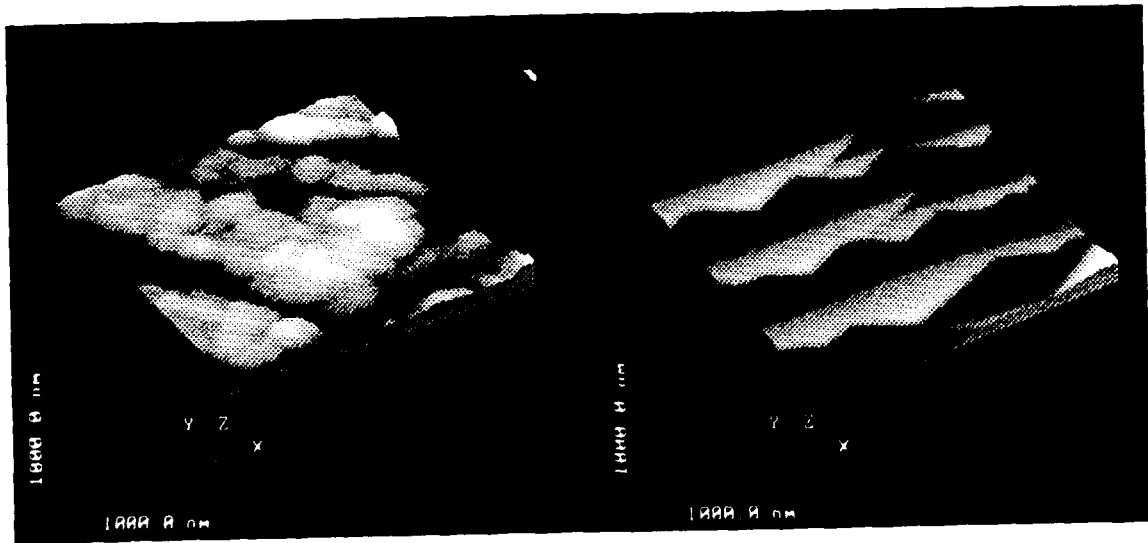
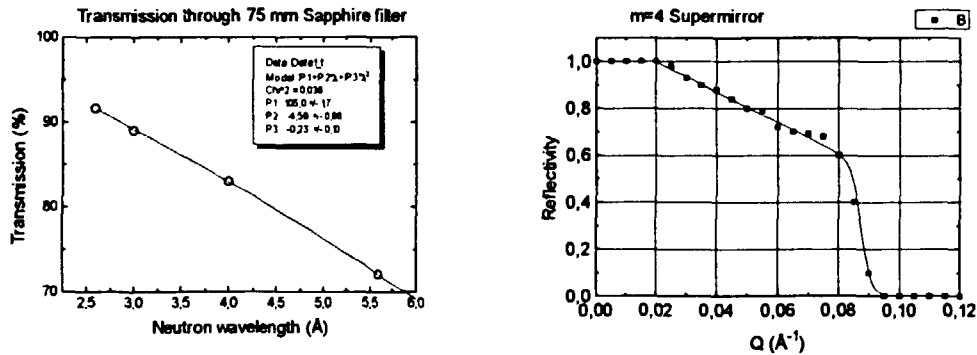


Fig. 1. Showing the effect of annealing for 24 hours at 1600°C. 1a) polished sapphire crystal. 1b) polished sapphire crystal annealed to 1600°C for 24 hours.

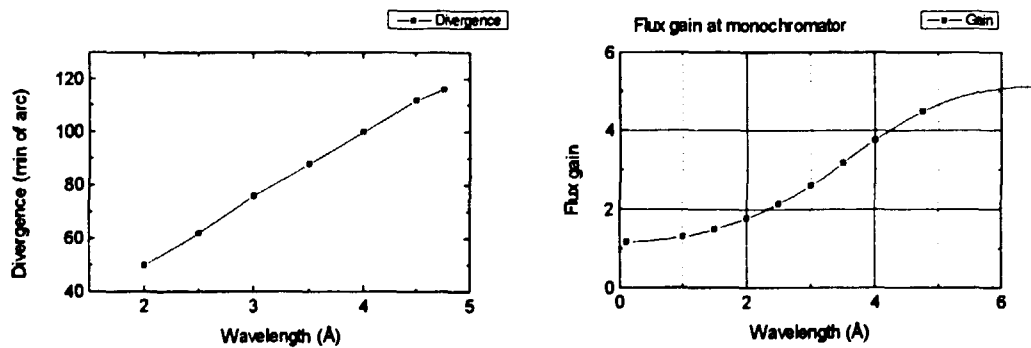
2.10.6 Calculation of the Performance of the New RITA Cold-plug

K.N. Clausen, *Department of Solid State Physics, Risø National Laboratory, Denmark*

The new cold plug for the Rita spectrometer has been designed and is now being fabricated at the Risø workshop. The plug consists of the cold source chamber followed by a sapphire filter a super mirror (SM) neutron guide, a velocity selector pre-monochromator and higher order filter and another piece of SM guide before the beam emerges at the monochromator position. The gain of this setup relative to the old system has been calculated using ray-tracing methods.



The length of the sapphire filter is 75 mm and the measured transmission is shown above. The supermirror has a reflectivity of approximately 1.0 until the critical angle for Ni is reached ($m=1$). Above this Q the reflectivity is due to Bragg scattering from the SM. Reflectivity extends out to 4 times the critical Q for Ni. ($m = 4$ SM guide from P. Böni, PSI, Switzerland)



The calculated horizontal and vertical divergence of the beam is approximately given by $m \cdot \lambda \cdot 6$ min of arc/Å, λ is the neutron wavelength. The calculated gain in flux at the monochromator was based on a transmission through the velocity selector filter equal to the transmission through a Be or PG filter which should otherwise be used. At 4 Å the gain in flux is expected to be of the order of 3-4 times. At the same time the background is expected to be reduced due to the removal of fast neutrons by the sapphire filter and neutrons outside a 10% window around the wanted wavelength by the velocity selector plus improved shielding around the filters.

2.11 LIP - CEC Large Installation Programme at Risø

K.N. Clausen, *Department of Solid State Physics, Risø National Laboratory, Denmark*, A.R. Mackintosh, *Niels Bohr Institute, Ørsted Laboratory, University of Copenhagen, Denmark*

The CEC Large Installation Programme was initiated in order to make large national facilities available to users from the whole EU, to promote European collaboration and to make more facilities available to the less favoured regions in the EU. The cold neutron facilities at DR3 has been included in this programme since early 1992. This year, the contract under the second framework programme expired, and a new 2 year contract under the third framework programme was started.

Proposals for experiments are refereed by a group of four international experts. A.R. Mackintosh acts as a Risø independent user representative in the management of the programme, and participates in beam allocation meetings, which are held 4 times every year. The LIP programme covers marginal expenses in connection with neutron scattering experiments at Risø. These expenses are (1) travel and subsistence for the users, (2) salaries to staff employed to run the user programme, (3) consumables and other running costs in connection with the experiments, (4) purchase of auxiliary equipment requested by the users and (5) a contribution to the continued modernisation and upgrade of the facilities.

A new Orange cryostat, a Displex cryostat and workstations for TAS7 and TAS8 has been installed during 1994. In connection with the upgrade of the control computers to UNIX stations on these two instruments a new C-version of TASCUM - the instrument control language - has been installed.

During 1994 a total of 526 instrument days (75 beam weeks) were used by 99 scientists from 7 different European countries. In total 59 experiments were performed, and 131 visits were supported by the programme.

The experiments carried out at Risø with support from the Commission of the European Communities Large Installation Programme during 1994 are listed below in chronological order. The column marked proposer is the first proposer on the application.

Proposer	Title of experiment
S.M. Hayden	Magnetic excitations in overdoped $\text{La}_{2-x}\text{Sr}_x\text{CuO}_4$
J.A.K. Howard	Single crystal neutron diffraction study of a thermal dyotropomer
W.H. de Jeu	Neutron reflectivity of lamellar triblock copolymer films
R. Strauss	Neutron diffraction on single crystals of $[(\text{CD}_3)_3\text{Sn}]_2\text{XO}_4 \cdot 2\text{D}_2\text{O}$, X=S, Se
C. Cavaco	Flexibility and local structure of polymerlike reverse micelles
R.A. Cowley	Phase diagram of magnetic multilayers

Proposer	Title of experiment
D. Schwahn	The pressure and temperature dependence of the Flory-Huggins parameter
G.H. Lander	Search for magnetic excitation at low energy in UFe_2
E. Brecht	Change of the crystal structure of heat and stress treated, Al doped $YBa_2Cu_{3-x}Al_xO_{7-y}$, $x=0.18$, single crystals
B.D. Rainford	Spin waves in CePdSb, a ferromagnetic Kondo-lattice compound
H.-G. Brokmeier	Texture development in titanium alloys in the temperature range from 800 to 1050 °C
R.A. Cowley	Magnetic structure of Ho/Er superlattices and alloys
M.E. Fitzpatrick	Interaction between stresses in Al/SiC metal matrix composite systems
M. Stamm	Conformation and morphology of blockcopolymers near the micropase separation temperature
E. Brecht	Magnetic structure of oxygen deficient Al doped $YBa_2Cu_{3-x}Al_xO_{7-y}$ single crystals ($x=0.19$)
R.L. McGreevy	Magnetic structure of magnetic polarons in $Nd_{0.5}Pb_{0.5}MnO_3$
A.T. Boothroyd	Magnetic excitations in $PrBa_2Cu_3O_{6+x}$
M.S. Lehmann	Test of image-plate multidetector
M. Lösche	Structure of reassembled monomolecular bacterial S-protein layers at air/water interfaces
H. Oettel	Investigation of precipitate formation in thin metallic films
J. Pohl	Structure and magnetism of Cr/ δ -Mn and Fe/ δ -Mn superlattices
C. Gomez-Sal	Structural and magnetic SANS study of the $Fe_{90-x}Zr_{10+x}$ amorphous ribbons
B.D. Rainford	Dynamical response of $CeRu_2Si_{2-x}Ge_x$ alloys
M. Lösche	The adsorption of molecular polyelectrolyte layers to amphiphilic interface layers
E. Brecht	Magnetic structure of oxygen deficient Al doped $YBa_2Cu_{3-x}Al_xO_{7-y}$ single crystals ($x=0.19$)
R.A. Cowley	Magnetic structure and fluctuations of frustrated antiferromagnetic $CsNiFeF_6$
F.J. Bermejo	Collective dynamics in molecular glass-formers
R. Cubitt	Flux lattice structures in high temperature superconductors
G. Balakrishnan	Investigations on the new (RE) Ni_2B_2C superconductors below T_c
E.M. Forgan	Investigation of the "nearly Kondo" system $CeAl_2$
D. Schwahn	The pressure and temperature dependence of the Flory-Huggins parameter
R.A. Cowley	Phase diagram of magnetic multilayers
M. Lösche	Inorganic salt concentration dependence of the structure of polymer films grown by deposition of polyelectrolytes
G.H. Lander	Search for magnetic excitation at low energy in UFe_2

Proposer	Title of experiment
A.T. Boothroyd	The magnetic structures in $\text{PrBa}_2\text{Cu}_3\text{O}_{6+x}$
U. Steigenberger	Magnetic excitations of UPd_3 in a field
W.G. Stirling	Phonon temperature-dependence in superfluid ^4He at $p = 20$ bar
M. Alario-Franco	Structural study of room temperature chemically oxidized $\text{La}_{2-x}\text{Ba}_x\text{CuO}_{4+y}$ ($x=0.115, 0.125, 0.135$)
D. Gazeau	Self organization of aza-crown-ether surfactants
F.J. Bermejo	Collective dynamics in molecular glass-formers
H.M.A. Winand	Creep deformation in particulate metal matrix composites
H. Reynaers	SANS on triblockcopolymer gels
G. Balakrishnan	Investigations on the new $(\text{RE})\text{Ni}_2\text{B}_2\text{C}$ superconductors below T_c
E. Brecht	Study of the antiferromagnetic (AFI/AFII) / superconducting phase stability in Al doped $\text{YBa}_2\text{Cu}_{3-x}\text{Al}_x\text{O}_{7-y}$ single crystals
P. Müller	Spin structure determination of Na_6MnS_4 and determination of D-positions in new ternary deuterides
R.M. Crevecoeur	Transition of $S(k,\omega)$ for ^4He to hydrodynamics
H.W. de Wijn	Ordering of frustrated two dimensional magnetic systems
U. Steigenberger	Magnetic excitations of UPd_3 in a field
J. António Paixão	Structure refinement and investigation of the magnetic structure of HoFe_4Al_8
K.A. McEwen	Magnetic Excitations in Single Crystal $\text{U}_{0.45}\text{Y}_{0.55}\text{Pd}_3$
J.B. Booth	Structure of Incommensurate B20 Alloys
M. Margarida R.R. da Costa	Antiferromagnetism in the Cr-Ga system
M.T. Weller	Nickel distribution in doped 247 superconductors
M.T. Weller	The structure of sodium copper (II) oxide, Na_2CuO_2
R.A. Cowley	Magnetic structure of rare earth multilayers
M. Loewenhaupt	Magnons in the different phases of NdCu_2
P. Klimanek	Interrelation between grain size and texture development during isothermal grain growth in copper and brass
E. Brecht	Study of the antiferromagnetic (AFI/AFII) / superconducting phase stability in Al doped $\text{YBa}_2\text{Cu}_{3-x}\text{Al}_x\text{O}_{7-y}$ single crystals
F. López	SANS-studies of deoxy cholate micelles, LPS and LPS NaDOC complex

3 Publications, Educational and Organizational Activities, Colloquia

3.1 Publications

in international journals and books

Aeppli, G., Littlewood, P., Cheong, S.W., Mook, H.A., Mason, T.E., Clausen, K.N., Hayden, S.M., Taylor, A.D., Perring, T.G., Fisk, Z., Neutron scattering and magnetic dynamics in insulators, metals and superconductors. In: Perspectives in many-particle physics. Broglia, R.A. (ed.), (North-Holland, Amsterdam, 1994) (International School of Physics Enrico Fermi, Course 121), 205-230.

Almdal, K., Dyre, J., Hvidt, S., Kramer, O., What is a 'gel'. Makromol. Chem. Macromol. Symp. (1993) **76**, 49-51.

Als-Nielsen, J., Diffraction, refraction and absorption of x-rays and neutrons: A comparative exposition. In: Proceedings of the HERCULES course, Neutron and synchrotron radiation for condensed matter studies. Vol. 1. Theory, instruments and methods. Baruchel, J., Hodeau, J.-L., Lehmann, M.S., Regnard, J.-R., Schlenker, C. (eds.), (Springer-Verlag, Berlin, 1994), 3-33.

Als-Nielsen, J., Freund, A.K., Grübel, G., Linderholm, J., Nielsen, M., Sanchez del Rio, M., Sellschop, J.P.F., Multiple station beamline at an undulator x-ray source. Nuc. Instr. Meth. Phys. Res. B (1994) **94** 306-318.

Als-Nielsen, J., Jacquemain, D., Kjær, K., Lahav, M., Leveiller, F., Leiserowitz, L., Principles and applications of grazing incidence x-ray and neutron scattering from ordered monolayers at the air-water interface. Phys. Rep. (1994) **246**, 252-313.

Als-Nielsen, J., Freund, A.K., Wulff, M., Hanfland, M., Häusermann, D., Performance of diamond as x-ray monochromator under very high heat flux in a synchrotron beam. Nuc. Instr. Meth. Phys. Res. B (1994) **94**, 348-350.

Andersen, N.H., Füg, T., Lindgård, P.-A., Mannstaedt, S., Mouritsen, O.G., Berlin, J., Structure factor calculation and metal-ion doping effects of $\text{YBa}_2\text{Cu}_3\text{O}_{6+x}$. Physica C (1994) **235-240**, 2423-2424.

Andruzzi, F., Hvilsted, S., Paci, M., Synthesis and characterization of comb-shaped polyesters based on 2-octadecyl-1,3-propanediol and phthalic acids. Polymer (1994) **35**, 4449-4455.

Bartels, V.T., Abetz, V., Mortensen, K., Stamm, M., Microphase separation of a symmetric poly(styrene-B-paramethylstyrene) diblock copolymer. Polym. Prep. (1994) **35**, 645-646.

Bartels, V.T., Abetz, V., Mortensen, K., Stamm, M., Microphase separation of a symmetric poly(styrene-B-paramethylstyrene) diblock copolymer. Europhys. Lett. (1994) **27**, 371-376.

Bates, F.S., Koppi, K.A., Tirrell, M., Almdal, K., Mortensen, K., Influence of shear on the hexagonal-to-disorder transition in a diblock copolymer melt. Macromolecules (1994) **27**, 5934-5936.

Bechgaard, K., Jacobsen, C.S., Mortensen, K., Pedersen, H.J., Thorup, N., The properties of five highly conducting salts: $(\text{TMTSF})_2\text{X}$, $\text{X}^- = \text{PF}_6, \text{AsF}_6, \text{SbF}_6, \text{BF}_4, \text{NO}_3$, derived

- from Tetramethyl-tetraselenafulvalene (TMTSF). *Solid State Commun.* (1993) **88**, 963-969.
- Belrhali, H., Yaremchuk, A., Tkalco, M., Larsen, K., Berthet-Colominas, C., Leberman, R., Beijer, B., Sproat, B., Als-Nielsen, J., Grübel, G., Legrand, J.-F., Lehmann, M., Cusack, S.* Crystal structures at 2.5 Ångstrom resolution of seryl-tRNA synthetase complexed with two analogs of seryl adenylate. *Science* (1994) **263**, 1432-1436.
- Berge, B., Konovalov, O., Lajzerowicz, J., Renault, A., Rieu, J.P., Vallade, M., Als-Nielsen, J., Grübel, G., Legrand, J.F.* Melting of short 1-alcohol monolayers on water: Thermodynamics and x-ray scattering studies. *Phys. Rev. Lett.* (1994) **73**, 1652-1655.
- Biljakovic, K., Nad, F., Lasjaunias, J.C., Monceau, P., Bechgaard, K.* The dynamics around the glass transition in the spin density wave ground state of TMTSF₂PF₆. *J. Phys. Cond. Matter* (1994) **6**, L135-L142.
- Brecht, E., Schmahl, W.W., Miehe, G., Fuess, H., Andersen, N.H., Wolf, T.* Reduction and reoxidation experiments on YBa₂Cu_{3-x}Al_xO_{6+δ} single crystals. *Physica C* (1994) **235-240**, 471-472.
- Brecht, E., Casalta, H., Schleger, P., Andersen, N.H., Schmahl, W.W., Fuess, H., Wolf, T.* Antiferromagnetic ordering in Al doped YBa₂Cu_{3-x}Al_xO_{6+y} single crystals. *Physica C* (1994) **235-240**, 871-872.
- Buyers, W.L.J., Tun, Z., Petersen, T., Mason, T.E., Lussier, J.-G., Gaulin, B.D., Menovsky, A.A.* Spin wave collapse and incommensurate fluctuations in URu₂Si₂. *Physica B* (1994) **199 & 200**, p. 95.
- Böhm, C., Leveiller, F., Jacquemain, D., Möhwald, H., Kjær, K., Als-Nielsen, J., Weissbuch, I., Leiserowitz, L.* Packing characteristics of crystalline monolayers of fatty acid salts, at the air-solution interface, studied by grazing incidence x-ray diffraction. *Langmuir* (1994) **10**, 830-836.
- Casalta, H., Schleger, P., Brecht, E., Montfroyij, W., Andersen, N.H., Lebeck, B., Schmahl, W.W., Fuess, H., Liang, R., Hardy, W.N., Wolf, T.* Absence of a second antiferromagnetic transition in pure YBa₂Cu₃O_{6+x}. *Phys. Rev. B* (1994) **50**, 9688-9691.
- Casalta, H., Schleger, P., Brecht, E., Montfroyij, W.T., Andersen, N.H., Lebeck, B., Schmahl, W.W., Fuess, H., Liang, R., Hardy, W.N., and Wolf, T.* No antiferromagnetic reordering at low temperature in pure YBa₂Cu₃O_{6+x}. *Physica C* (1994) **235-240**, 1623-1624.
- Clausen, K.N., McEwen, K.A., Jensen, J., Mackintosh, A.R.* New mode of magnetic excitation in praseodymium. *Phys. Rev. Lett.* (1994) **72**, 3104-3107.
- Dueholm, K.L., Egholm, M., Behrens, C., Christensen, L. Hansen, H.F., Vulpius, T., Petersen, K.H., Berg R.H., Nielsen, P.E., Buchardt, O.* Synthesis of peptide nucleic acid monomers containing the four natural nucleobases: thymine, cytosine, adenine, and guanine and their oligomerization. *J. Org. Chem.* (1994) **59**, 5767-5773.
- Egholm, M., Nielsen, P.E., Buchardt, O., Berg, R.H.* Design, properties and potential of peptide nucleic acids (PNAs). In: *Innovations and Perspectives in Solid-Phase Synthesis*. R. Erton (ed.), (Mayflower Worldwide Ltd., Birmingham) (1994) 145-148.
- Enderle, M., Kakurai, K., Clausen, K.N., Inami, T., Tanaka, H., Steiner, M.* Integer vs. Half-integer-spin antiferromagnetic chains, an experimental test of the Haldane conjecture: Excitations in the S=5/2 system CsMnI₃ vs. excitations in the S=1 CsNiCl₃. *Europhys. Lett.* (1994) **25**, 717-722.

- Falcão, A.N., Pedersen, J.S., Mortensen, K.*, Optimum intensity in small-angle neutron scattering. An experimental comparison between symmetric and asymmetric geometries. *J. Appl. Cryst.* (1994) **27**, 330-337.
- Fig, T., Gorman, B.M., Rikvold, P.A., Novotny, M.A.*, Numerical transfer-matrix study of a model with competing metastable states. *Phys. Rev. E* (1994) **50**, 1930-1947.
- Findeisen, E., Feidenhans'l, R., Vigild, M.E., Clausen, K.N., Hansen, J.B., Bentzen, M.D., Goff, J.P.*, Hydrogen concentration and mass density of density of diamond-like carbon films obtained by x-ray and neutron reflectivity. *J. Appl. Phys.* (1994) **76**, p. 4636-4642.
- Findeisen, E., Feidenhans'l, R., Vigild, M.E., Nielsen, M., Clausen, K.N., Foss, M.*, Distribution function, density and hydrogen content of amorphous, diamondlike, carbon films obtained by x-ray and neutron scattering. *Mat. Res. Soc. Symp. Proc.* (1994) **349**, 495-496.
- Foss, M., Feidenhans'l, R., Nielsen, M., Findeisen, E., Johnson, R.L., Buslaps, T., Steensgaard, I., Besenbacher, F.*, Sulfur chemisorption on Ni(111): The clock structure of the $(5\sqrt{3} \times 2)S$ phase. *Phys. Rev. B.* (1994) **50**, 8950-8953.
- Frederiksen, P., Bjørnholm, T., Madsen, H.G., Bechgaard, K.*, Electroluminescence of organic thin films based on blends of polystyrene and fluorescent dyes. *J. Mat. Chem.* (1994) **4**, 675-678.
- Førland, G.M., Samseth, J., Høiland, H., Mortensen, K.*, The effect of medium chain length alcohols on the micellar properties of sodium dodecyl sulfate in sodium chloride solutions. *J. Colloid Interface Sci.* (1994) **164**, p. 163-167.
- Gammel, P.L., Huse, D.A., Kleiman, R.N., Batlogg, B., Oglesby, C.S., Bucher, E., Bishop, D.J., Mason, T.E., Mortensen, K.*, Small angle neutron scattering study of the magnetic flux-line lattice in single crystal $2H-NbSe_2$. *Phys. Rev. Lett.* (1994) **72**, 278-281.
- Garnæs, J., Larsen, N.B., Bjørnholm, T., Jørgensen, M., Kjær, K., Als-Nielsen, J., Jørgensen, J.F., Zasadzinski, J.A.*, Langmuir-Blodgett films of a functionalized molecule with cross-sectional mismatch between head and tail. *Science* (1994) **264**, 1301-1304.
- Gensterblum, G., Hevesi, K., Han, B.-Y., Pireaux, J.-J., Thiry, P.A., Caudano, R., Lucas, A.A., Bernaerts, D., Amelinckx, S., Van Tendeloo, G., Bendele, G., Buslaps, T., Johnson, R.L., Foss, M., Feidenhans'l, R., LeLay, G.*, Growth mode and electronic structure of the epitaxial $C_{60}(111)/GeS(001)$ interface. *Phys. Rev. B* (1994) **50**, 11981-11995.
- Gibaud, A., McMorrow, D.F., Cowley, R.A.*, Sinusoidal modulation of a thin film of Nb on sapphire. *Physica B* (1994) **198**, 63-65.
- Gidalevitz, D., Weissbuch, I., Kjær, K., Als-Nielsen, J., Leiserowitz, L.*, Design of two-dimensional crystals as models for probing the structure of the solid-liquid interface. *J. Am. Chem. Soc.* (1994) **116**, 3271-3278.
- Grübel, G., Als-Nielsen, J., Freund, A.K.*, The TROIKA beamline at ESRF. *J. de Phys.* (1994) **4**, C9-27.
- Habekost, S., Norby, P., Jørgensen, J.E., Lebech, B.*, Neutron and x-ray powder diffraction studies of lanthanum manganite, a nonstoichiometric perovskite. *Acta Chem. Scand.* (1994) **48**, 377-381.
- Hadfield, R.A., Schlegel, P., Casalta, H., Andersen, N.H., Poulsen, H.F., von Zimmermann, M., Schneider, J.R., Hutchings, M.T., Keen, D.A., Liang, R., Dosanjh, P.*

- Hardy, W.V.*, Simultaneous neutron and x-ray refinement of Ortho-II superstructure in $\text{YBa}_2\text{Cu}_3\text{O}_{6.5}$. *Physica C* (1994) **235-240**, 1267-1268.
- Hamley, J.W., Pedersen, J.S.*, Analysis of neutron and x-ray reflectivity data. I. Theory. *J. Appl. Cryst.* (1994) **27**, 29-35.
- Harris, P., Lebeck, B., Bernhard, J., Higashi, I., Shishido, T., Fukuda, T., Takei, H.*, Crystal and magnetic structure of ErRh_3B_2 studied by neutron diffraction. *Japan J. Appl. Phys.* (1994) **10**, 146-147.
- Harris, P., Lebeck, B., Achiwa, N.*, Crystalline and magnetic ordering in the monoclinic phase of the layered perovskite PAMC. *J. Phys. Condens. Matter* (1994) **6**, 3899-3907.
- Harris, P., Larsen, F.K., Lebeck, B., Achiwa, N.*, Crystal structure of the commensurately modulated ζ phase of PAMC. *Acta Cryst.* (1994) **B50**, 676-684.
- Hjorth, M., Thorup, N., Frederiksen, P., Bechgaard, K.*, Crystal structure of a complex of peri-xanthenoxanthene (PXX) with tetracyanoquinodimethane (TCNQ). *Acta Chem. Scand.* (1994) **48**, 139-143.
- Holzer, B., Strobl, G., Stühn, B., Andersen, N.H.*, Local motion in the β -transition range of partially crystalline polyethylene studied by neutron scattering. *Colloid & Polymer Sci.* (1994) **272**, 1396-1402.
- Honger, T., Mortensen, K., Hjort Ipsen, J., Lemmich, J., Bauer, R., Mouritsen, O.G.*, Anomalous swelling of multilamellar lipid bilayers in the transition region by renormalization of curvature elasticity. *Phys. Rev. Lett.* (1994) **72**, 3911-3914.
- Janssen, S., Schwahn, D., Mortensen, K., Springer, T.*, Pressure dependence of the Flory-Huggins interaction parameter in binary polymer blends investigated by SANS. *J. Phys. IV France* (1993) **3** (no.C8), 17-20.
- Jehan, D.A., McMorrow, D.F., Simpson, J.A., Cowley, R.A., Swaddling, P.P., Clausen, K.V.*, Collapsing cycloidal structures in the magnetic phase diagram of erbium. *Phys. Rev. B* (1994) **50**, 3085-3091.
- Jorgensen, J.-E., Andersen, N.H.*, Crystal structure and charge localization in $\text{Pb}_2\text{Sr}_2\text{Tb}_{1-x}\text{Ca}_x\text{Cu}_3\text{O}_8$ for $x = 0$ and 0.5. *Physica C* (1994) **235-240**, 877-878.
- Jorgensen, M., Bechgaard, K., Bjørnholm, T., Sommer-Larsen, P., Gram Hansen, L., Schaumburg, K.*, Synthesis and structural characterization of a bis-arborol-tetrathiafulvalene gel: Toward a self-assembling molecular wire. *J. Org. Chem.* (1994) **59**, 5877-5882.
- Kjær, K.*, Some simple ideas on x-ray reflection and grazing-incidence diffraction from thin surfactant films. *Physica B* (1994) **198**, 100-109.
- Kjær, K., Als-Nielsen, J., Lahav, M., Leiserowitz, L.*, Two-dimensional crystallography of amphiphilic molecules at the air-water interface. In: *Proceedings of the HERCULES course, Neutron and synchrotron radiation for condensed matter studies. Vol. 3. Applications to soft condensed matter and biology.* Baruchel, J., Hodeau, J.-L., Lehmann, M.S., Regnard, J.-R., Schlenker, C. (eds.), (Springer-Verlag, Berlin, 1994), 47-68.
- Koppi, K.A., Tirrell, M., Bates, F.S., Almdal, K., Mortensen, K.*, Epitaxial growth and shearing of the body centered cubic phase in diblock copolymer melts. *J. Rheol.* (1994) **38**, 999-1027.
- Kulinna, C., Zebger, I., Hvilsted, S., Ramanujam, P.S., Siesler, H.W.*, Characterization of the segmental mobility of liquid-crystalline side-chain polyesters by Fourier-Transform infrared spectroscopy. *Macromol. Symp.* (1994) **83**, 169-181.

- Kulys, J., Buch Rasmussen, T., Bechgaard, K., Razunas, V., Kazlauskaitė, J., Marcinkevičienė, J., Christensen, J.B., Hansen, H.E.*, Study of the new electron transfer mediators in glucose oxidase catalysis. *J. Mol. Cat.* (1994) **91**, 407-420.
- Lagriffoul, P.H., Egholm, M., Nielsen, P.E., Berg, R.H., Buchardt, O.*, The synthesis, co-oligomerization and hybridization of a thymine-thymine heterodimer containing PNA. *BioMed Chem. Lett.* (1994) **4**, 1081-1082.
- Lasjaunias, J.C., Biljakovic, K., Nad, F., Monceau, P., Bechgaard, K.*, Glass transition in the spin-density wave phase of $(\text{TMTSF})_2\text{PF}_6$. *Phys. Rev. Lett.* (1994) **72**, 1283-1286.
- Lay, G. Le, Aristov, V.Y., Seehofer, L., Buslaps, T., Johnson, R.L., Gothelid, M., Hammar, M., Karlsson, U.O., Flodström, S.A., Feidenhans'l, R., Nielsen, M., Find-eisen, E., Uhrberg, R.I.G.*, STM and synchrotron radiation studies of prototypical metal/semiconductor systems. *Surf. Sci.* (1994) **307/309**, 280-294.
- Lebech, B., Wolny, J., Moon, R.M.*, Magnetic phase transitions in double hexagonal close packed neodymium metal – commensurate in two dimensions. *J. Phys. Condens. Matter* (1994) **6**, 5201-5222.
- Lefmann, K., Buras, B., Pedersen, E.J., Shabanovna, E.S., Thorsen, P.A., Rasmussen, F.B., Sellschop, J.F.P.*, NMR spectra of pure ^{13}C diamond. *Phys. Rev. B* (1994) **50**, 15623-15627.
- Lefmann, K., Hedegård, P.*, Neutron-scattering cross section of the $S=1/2$ Heisenberg triangular antiferromagnet. *Phys. Rev. B* (1994) **50**, 1074-1083.
- Legrand, J.F., Renault, A., Konovalov, O., Chevigny, E., Als-Nielsen, J., Grubel, G., Berge, B.*, X-ray grazing incidence studies of the 2D crystallization of monolayers of 1-alcohols at the air water interface. *Thin Solid Films* (1994) **248**, 95-99.
- Leveiller, F., Böhn, C., Jacquemain, D., Möhwald, Leiserowitz, L., Kjær, K., Als-Nielsen, J.*, Two-dimensional crystal structure of cadmium arachidate studied by synchrotron x-ray diffraction and reflectivity. *Langmuir* (1994) **10**, 819-829.
- Lindgård, P.-A., Hendriksen, P.V.*, Estimation of electronic and structural influence on the thermal magnetic properties of clusters. *Phys. Rev. B* (1994) **49**, 12291-12294.
- Lindgård, P.-A., Hendriksen, P.V.*, Thermal magnetic properties of clusters. In: *New Trends in Magnetism, Magnetic Materials, and Their Applications*, J.L. Morán-López and J.M. Sanchez (eds.). Plenum Press, New York (1994), 37-46.
- Lindgård, P.-A., Vives, E.*, Elastically driven phase transitions studied by a continuous Monte Carlo method. In: *Statics and dynamics of alloy phase transformations*. Turchi, P.E.A., Gonis, A. (eds.), (Plenum Press, New York, 1994) (NATO Advanced Science Institutes Series B: Physics, 319), 683-686.
- Lindgård, P.-A.*, Computer simulation of the structure factor. In: *Springer Proceedings in Physics. Computer simulation studies in condensed matter physics VII*. Landau, D.P., Mon, K.K., Schüttler, H.-B. (eds.), Springer-Verlag, Heidelberg (1994) **78**, 69-82.
- Longmore, A., Nutley, M.P., Boothroyd, A.T., Andersen, N.H., Casalta, H., Schleger, P., Chen Changkang, Hu Youngle, Christensen, A.N.*, Magnetic order in $\text{PrBa}_2\text{Cu}_3\text{O}_{6+x}$. *Physica C* (1994) **235-240**, 1581-1582.
- Lösche, M., Erdelen, C., Rump, E., Ringsdorf, H., Kjær, K., Vaknin, D.*, On the lipid head group hydration of floating surface monolayers bound to self-assembled molecular protein layers. *Thin Solid Films* (1994) **242**, 112-117.
- Majewski, J., Popovitz-Biro, R., Kjær, K., Als-Nielsen, J., Lahav, M., Leiserowitz, L.*, Toward a determination of the critical size of ice nuclei. A demonstration by graz-

- ing incidence x-ray diffraction of epitaxial growth of ice under the $C_{31}H_{63}OH$ alcohol monolayer. *J. Phys. Chem.* (1994) **98**, 4087-4093.
- Mannstaedt, S., Fiig, T., Andersen, N.H., Lindgård, P.-A., Mouritsen, O.G.*, Monte Carlo simulation of a two-species diffusive lattice gas in optimized C^* on the connection machine. Metal-ion doping effects in the high-temperature superconductor $YBa_2Cu_{3-y}M_yO_{6+x}$ ($M=Co,Fe,Al$). *Comput. Mater. Sci.* (1994) **3**, 9-20.
- Mischenko, N., Reynders, K., Mortensen, K., Scherrenberg, R., Fontaine, F., Graulus, R., Reynaers, H.*, Structural studies of thermoplastic triblock copolymer gels. *Macromolecules* (1994) **27**, 2345-2347.
- Mortensen, K.*, PEO-PPO-PEO triblock copolymer in aqueous solution. Micelle formation and crystallization. *J. Phys. IV France* (1993) **3** (no.C8), 157-160.
- Mortensen, K.*, Small-angle scattering on soft materials. *Nukleonika* (1994) **39**, 169-184.
- Mortensen, K.*, Block copolymer in aqueous solution. Dependence on shear temperature and pressure. *Polym. Prep.* (1994) **35**, 626-627.
- Mortensen, K., Brown, W., Jørgensen, E.*, Phase behavior of poly(propylene oxide)-poly(ethylene oxide)-poly(propylene oxide) triblock copolymer melt and aqueous solutions. *Macromolecules* (1994) **27**, 5654-5666.
- Odin, J., Lasjaunias, J.C., Biljakovic, K., Monceau, P., Bechgaard, K.*, Low temperature specific heat of the spin-density-wave compound $(TMTSF)_2PF_6$. *Sol. State Comm.* (1994) **91**, 523-527.
- Pedersen, J.S.*, Resolution effects and analysis of small-angle neutron scattering data. *J. Phys. IV France* (1993) **3** (no.C8), 491-498.
- Pedersen, J.S.*, Determination of size distributions from small-angle scattering data for systems with effective hard-sphere interactions. *J. Appl. Cryst.* (1994) **27**, 595-608.
- Pedersen, J.S., Hansen, S., Bauer, R.*, The aggregation behavior of zinc-free insulin studied by small-angle neutron scattering. *Eur. Biophys. J.* (1994) **22**, 379-389, cf. (erratum) *ibid.* (1994) **23**, 227-229.
- Pedersen, J.S., Hamley, I.W.*, Analysis of neutron and x-ray reflectivity data. II. Constrained least-squares methods. *J. Appl. Cryst.* (1994) **27**, 36-49.
- Pedersen, J.S., Hamley, I.W.*, Analysis of neutron and x-ray reflectivity data by constrained least-squares methods. *Physica B* (1994) **198**, 16-23.
- Pengra, D.B., Thoft, N.B., Wulff, M., Feidenhans'l, R., Bohr, J.*, Resonance-enhanced magnetic x-ray diffraction from a rare-earth alloy. *J. Phys. Condens. Matter* (1994) **6**, 2409-2422.
- Petersen, T., Mason, T.E., Aeppli, G., Ramirez, A.P., Bucher, E., Kleiman, R.N.*, Magnetic fluctuations and the superconducting transition in the heavy Fermion material UPd_2Al_3 . *Physica B* (1994) **199 & 200**, 151-153.
- Popovitz-Biro, R., Majewski, J., Wang, J.L., Kjær, K., Als-Nielsen, J., Lahav, M., Leiserowitz, L.*, Langmuir films of amphiphilic alcohols and surfaces of polar crystals as templates for ice nucleation. In: *Computational approaches in supramolecular chemistry*. Wipff, G. (ed.), (Kluwer Academic Publishers, Dordrecht, 1994) (NATO Advanced Science Institutes Series C: Mathematical and Physical Sciences, 426), 411-418.
- Posselt, D., Egeberg, E.D., Pedersen, J.S., Mortensen, K.*, Small-angle scattering studies of freeze-dried silica gels. *J. Phys. IV France* (1993) **3** (no.C8), 353-356.

- Ramanujam, P.S., Andruzzi, F., Hvilsted, S.*, Optical storage in side-chain liquid crystalline polyesters. *Opt. Rev.* (1994) **1**, 3-5.
- Rial, C., Amador, U., Morán, E., Alario-Franco, M.A., Andersen, N.H.*, Evidence of interstitial oxygen in room temperature oxidized $\text{La}_{2-x}\text{Sr}_x\text{CuO}_{4+y}$ ($0 < x < 0.1$). *Physica C* (1994) **234**, 237-248.
- Rial, C., Amador, U., Morán, E., Andersen, N.H., Alario-Franco, M.A.*, Structural and physical aspects of room temperature oxidized $\text{La}_{2-x}\text{Sr}_x\text{CuO}_{4+y}$ ($0 < x < 0.15$). *Physica C* (1994) **235-240**, 561-562.
- Ruiz-Aragón, M.J., Amador, U., Morán, E., Andersen, N.H.*, Neutron diffraction study of $(\text{La}_{1-x}\text{Ca}_x)\text{BaCuFeO}_{5+\delta}$, ($\text{Ln} = \text{Y, Pr}$). *Physica C* (1994) **235-240**, 1609-1610.
- Samseth, J., Spontak, R.J., Smith, S.D., Ashraf, A., Mortensen, K.*, Microphase-separated tapered triblock copolymers. *J. Phys. IV France* (1993) **3** (no.C8), 59-62.
- Schins, A.G., Nielsen, M., Arts, A.F.M., DeWijn, H.W.*, Neutron-scattering study of the two-dimensional frustrated antiferromagnet $\text{Rb}_2\text{Cu}_{0.12}\text{Co}_{0.88}\text{F}_4$. *Phys. Rev. B.* (1994) **49**, 8911-8919.
- Schleger, P., Hadfield, R.A., Casalta, H., Andersen, N.H., Poulsen, H.F., von Zimmermann, M., Schneider, J.R., Liang, R., Dosanjh, P., Hardy, W.N.*, The line shape of the Ortho-II superstructure reflections in $\text{YBa}_2\text{Cu}_3\text{O}_{6.5}$. *Physica C* (1994) **235-240**, 1269-1270.
- Schulz, M.F., Bates, F.S., Almdal, K., Mortensen, K.*, Epitaxial relationships for hexagonal-to-cubic phase transition in a block copolymer mixture. *Phys. Rev. Lett.* (1994) **73**, 86-89.
- Schwahn, D., Meier, G., Mortensen, K., Janssen, S.*, On the N-scaling of the Ginzburg number and the critical amplitudes in various compatible polymer blends. *J. Phys. II France* (1994) **4**, 837-848.
- Schwahn, D., Mortensen, K., Janssen, S.*, Critical scattering in a polymer blend above and below the critical point of demixing: Critical exponents and amplitude ratios. *Phys. Rev. Lett.* (1994) **73**, 1452-1455.
- Seto, H., Yokoi, E., Komura, S., Schwahn, D., Mortensen, K., Suzuki, J., Ohnuma, M., Ito, Y.*, Small angle neutron scattering study on a phase separation in a 3-component microemulsion system. *J. Phys. IV France* (1993) **3** (no.C8), 161-164.
- Seto, H., Schwahn, D., Mortensen, K., Yokoi, E., Komura, S., Suzuki, J., Funahashi, S., Ito, Y.*, Small angle neutron scattering study of a phase separation in a 3-component microemulsion system. In: *Neutrons as Microscopic Probe*, Takahashi, H. (ed.), JAERI-Conf-2 (1993) 547-554.
- Simpson, J.A., McMorro, D.F., Jehan, D.A., Cowley, R.A., Ward, R.C.C., Wells, M.R., Clausen, K.N.*, Competing anisotropies in holmium-erbium superlattices. *Phys. Rev. Lett.* (1994) **73**, 1162-1166.
- Sjöberg, B., Mortensen, K.*, Interparticle interactions and structure in nonideal solutions of human serum albumin studied by small angle neutron scattering and Monte Carlo simulations. *Biophys. Chemistry* (1994) **52**, 131-138.
- Svergun, D.I., Koch, M.H.J., Pedersen, J.S., Serdyuk, I.N.*, Structural model of the 50 S subunit of *Escherichia coli* ribosomes from solution scattering. *J. Mol. Biol.* (1994) **240**, 78-86.
- Svergun, D.I., Pedersen, J.S.*, Propagating errors in small-angle scattering data treatment. *J. Appl. Cryst.* (1994) **27**, 241-248.

- Swaddling, P.P., McMorro, D.F., Cowley, R.A., Ward, R.C.C., Wells M.R., Determination of the interfacial roughness exponent in rare-earth superlattices. *Phys. Rev. Lett.* (1994) **73**, 2232-2235.
- Tennant, D.A., McMorro, D.F., Nagun, S.E., Cowley, R.A., Fák, B., Spin waves in the spin-flop phase of RbMnF_3 . *J. Phys. Condens. Matter* (1994) **6**, 10341-10355.
- Walker, M.B., Kappler, C., McEwen, K.A., Steigenberger, U., Clausen, K.N., Triple-Q quadrupolar order in UPd_3 . *J. Phys. Condens. Matter* (1994) **6**, 7365-7371.
- Wang, J.L., Leveiller, F., Jacquemain, D., Kjær, K., Als-Nielsen, J., Lahav, M., Leiserowitz, L., Two-dimensional structures of crystalline self-aggregates of amphiphilic alcohols at the air-water interface as studied by grazing-incidence synchrotron x-ray diffraction and lattice energy calculation. *J. Am. Chem. Soc.* (1994) **116**, 1192-1204.
- Wang, J.Y., Vaknin, D., Uphaus, R.A., Kjær, K., Lösche, M., Fullerene films and fullerene-dodecylamine adduct monolayers at air-water interfaces studied by neutron and x-ray reflection. *Thin Solid Films* (1994) **242**, 40-44.
- Weinbach, S.P., Kjær, K., Bouwman, W.G., Grübel, G., Legrand, J.-F., Als-Nielsen, J., Lahav, M., Leiserowitz, L., Control of structure and growth of polymorphic crystalline thin films of amphiphilic molecules on liquid surfaces. *Science* (1994) **264**, 1566-1570, cf. (erratum) *ibid.* (1994) **266**, 1791-1792.
- Winkelmann, M., Graf, H.A., Andersen, N.H., Magnetic structure of MgCu_2O_3 and doping-induced spin reorientation in $\text{Mg}_{1-x/2}\text{Li}_x\text{Cu}_{2-x/2}\text{O}_3$. *Phys. Rev. B* (1994) **49**, 310-317.
- Winther, L., Almdal, K., Batsberg Pedersen, W., Kops, J., Berg, R.H., Hydrophilic film supports. In: *Peptides: Chemistry, Structure and Biology*. R.S. Hodges and J.A. Smith, (eds.), Escom Science Publishers B.V., Leiden, (NL) (1994), 872-873.
- Winther, L., Almdal, K., Batsberg Pedersen, W., Kops, J., Berg, R.H., Hydrophilic film supports for use in peptide synthesis and bioassays. In: *Innovations and Perspectives in Solid-Phase Synthesis*. R. Epton (ed.), (Mayflower Worldwide Ltd., Birmingham, 1994), 705-706.
- Yaron, U., Gammel, P.L., Huse, D.A., Kleiman, R.N., Oglesby, C.S., Bucher, E., Batlogg, B., Bishop, D.J., Mortensen, K., Clausen, K.N., Bylle, C.A., de la Cruz, F., Neutron diffraction studies of flowing and pinned magnetic flux lattice in 2H-NbSe_2 . *Phys. Rev. Lett.* (1994) **73**, 2748-2751.
- Österberg, R., Boive, T., Wang, W., Mortensen, K., Saito, A., Sinohara, H., Ikai, A., Small-angle scattering study of α_1 inhibitor III from rat blood plasma. *Biochim. Biophys. Acta* (1994) **1207**, 152-158.
- Österberg, R., Mortensen, K., The growth of fractal humic acids: cluster correlation and gel formation. *Radiat. Environ. Biophys.* (1994) **33**, 269-276.
- Österberg, R., Mortensen, K., Fractal geometry of humic acids. Temperature-dependent restructuring studied by small-angle neutron scattering. In: *Humic substances in the global environment and implications on human health*. Senesi, N., Miano, T.M. (eds.), (Elsevier, Amsterdam, 1994), 127-132.
- Österberg, R., Szajdak, L., Mortensen, K., Temperature-dependent restructuring of fractal humic acids: A proton-dependent process. *Environ. Int.* (1994) **20**, 77-80.

3.2 Other Publications

articles for a broader readership, theses and reports

- Andersen, N.H.*, Relations between structural and superconducting properties of bulk and thin film high- T_c materials. Risø-R-754(EN) (1994), 51 p.
- Andersen, N.H.*, På sporet af iltens rolle i $YBa_2Cu_3O_{6+x}$ superledere. Kvant (1994) **5** (no.2), 6-10.
- Andersen, N.H., Mortensen, K.*, Nyt gennembrud for superledning er måske lige om hjørnet. Risønyt (1994) (no.1), 6-7.
- Füg, T.*, Ordering phenomena and non-equilibrium properties of lattice gas models. Risø-R-734(EN) (1994) 214 p. (thesis).
- Findeisen, E.*, X-ray and neutron scattering from amorphous diamondlike carbon and hydrocarbon films. Risø-R-748(EN) (1994) 100 p. (thesis).
- Grübel, G., Als-Nielsen, J., Abernathy, D., Vignaud, G., Brauer, S., Stephenson, G.B., Mochrie, S.G.J., Sutton, M., Robinson, I.K., Fleming, R., Pindak, R., Dierker, S., Legrand, J.F.*, Scattering with coherent x-rays. ESRF Newslett. (1994) **20**, 14-15.
- Harris, P.*, Neutron and x-ray diffraction from modulated structures. Risø-R-747(EN) (1994) 102 p. (thesis).
- Oddershede, L., Jacobsen, R.H., Lefmann, K., Thoft, N.B.*, FOTON – et optisk spil. Kvant (1994) **4**, 9-18.
- Pedersen, J.S., Almdal, K., Feidenhans'l, R., Clausen, K.N., Bechgaard, K.* (eds.), Annual progress report of the Department of Solid State Physics 1 January - 31 December 1993. Risø-R-725(EN) (1994), 164 p.

3.3 Conferences

presentations at conferences and workshops

- Almdal, K.*, Finite chain length: The origin of complexity in block copolymer phase behaviour. MODECS, Frederiksdal (DK) (October).
- Almdal, K., Mortensen, K., Bates, F.S., Koppi, K.A., Tirrell, M.*, The hexagonal-to-disorder phase transition in a diblock copolymer melt under the influence of shear. Nordic Polymer Days 1994, Copenhagen (DK) (May).
- Almdal, K., Mortensen, K., Koppi, K.A., Tirrell, M., Bates, F.S.*, The body centred cubic phase in diblock copolymer melts. Response to shear and epitaxial growth from the hexagonally packed rod phase. Nordic Polymer Days 1994, Copenhagen (DK) (May).
- Almdal, K., Mortensen, K., Bates, F.S., Koppi, K.A., Tirrell, M.*, The hexagonal-to-disorder phase transition in a diblock copolymer melt under the influence of shear. European Polymer Federation Symposium on Polymeric Materials, Basel (CH) (October).
- Almdal, K., Mortensen, K., Bates, F.S., Koppi, K.A., Tirrell, M.*, Shear induced suppression of fluctuations near the order-to-disorder phase transition in an asymmetric diblock copolymer melt. The Royal Society of Chemistry. Faraday Division. Discussion no. 98: Polymers at Surfaces and Interfaces, Bristol (GB) (September).
- Almdal, K., Mortensen, K., Bates, F.S., Koppi, K.A., Tirrell, M.*, Order-to-disorder phase

- transition in an asymmetric diblock copolymer melt under the influence of shear. The Polymer Physics Gordon Research Conference, Newport, RI (US) (August).
- Als-Nielsen, J.*, Complementarity between x-ray and neutron reflectivity. Workshop on Thin Films and Interfaces, Institute M. et P. Curie, Paris (FR) (March).
- Als-Nielsen, J.*, Structure of Langmuir layers studied by synchrotron x-rays and neutron reflectivity. American Chemical Society, Spring Meeting March 1994, San Diego CA (US) (March).
- Als-Nielsen, J.*, Surface structure analysis by synchrotron x-ray diffraction. Workshop on New Opportunities Offered by a Swiss Synchrotron Light Source, Giessbach (CH) (October).
- Andersen, N.H.*, Studies of oxygen ordering and superconductivity in oxygen deficient and metal ion doped $\text{YBa}_2\text{Cu}_3\text{O}_{6+x}$. Nordic Symposium on Superconductivity, Varberg (SE) (May).
- Andersen, N.H.*, Studies of oxygen ordering and magnetic structure of $\text{YBa}_2\text{Cu}_3\text{O}_{6+x}$ type high T_c superconductors. NORDITA Conference on Physics in 2+1 Dimensions, Copenhagen (DK) (June).
- Andersen, N.H., Füg, T., Lindgård, P.-A., Andersen, J.V., Bohr, H., Mannstaedt, S., Mouritsen, O.G., Poulsen, H.F.*, Studies of oxygen ordering in oxygen deficient and metal ion doped $\text{YBa}_2\text{Cu}_{3-y}\text{M}_y\text{O}_{6+x}$ ($M = \text{Al, Fe, Co}$) high T_c superconductors. In: Fifteenth European Crystallographic Meeting (ECM-15), Dresden (DE) (August).
- Bartels, V.T., Abetz, V., Mortensen, K., Stamm, M.*, Microphase separation of a symmetric poly(styrene-b-paramethylstyrene) diblock copolymer. Der Deutschen Physikalischen Gesellschaft E.V.: Polymerphysik, Halle (DE) (March).
- Bartels, V.T., Abetz, V., Mortensen, K., Stamm, M.*, Microphase separation of a symmetric poly(styrene-b-paramethylstyrene) diblock copolymer. 1994 National Meeting of the American Chemical Society. Division of Polymer Chemistry. Block Copolymer Dynamics, San Diego, CA (US) (March).
- Bates, F.S., Koppi, K., Tirrell, M., Almdal, K., Mortensen, K.*, Role of fluctuations in the hexagonal-to-disorder transition. 1994 March meeting of the American Physical Society, Pittsburgh, PA (US) (March).
- Bates, F.S., Schulz, M.F., Khandpur, A.K., Förster, S., Rosedale, J.H., Almdal, K., Mortensen, K.*, Fluctuations, conformational asymmetry and block copolymer phase behaviour. The Royal Society of Chemistry. Faraday Division. Discussion no. 98: Polymers at Surfaces and Interfaces, Bristol (GB) (September).
- Bechgaard, K.*, Organic conductors. NATO Advanced Research Workshop, Hindsgaul, Fyn (DK) (May).
- Bechgaard, K.*, Molecular materials. Magnetic properties of low dimensional solids. International Conference on Inorganic Chemistry, EICS V, Davos (CH) (June).
- Bohr, J.*, Resonant-enhanced magnetic x-ray diffraction from a rare-earth alloy. Workshop on Photon and Neutron Studies of Magnetic Materials, Marathon (GR) (April).
- Bouwman, W.G.*, Pitfalls in low resolution reflectometry. Workshop on X-ray and Neutron Reflectivity on Thin Films and Interfaces. Institute M. et P. Curie, Paris (FR) (March).
- Brecht, E., Casalta, H., Schleger, P., Andersen, N.H., Schmahl, W.W., Fuess, H., Wolf, T.*, Antiferromagnetic ordering in Al doped $\text{YBa}_2\text{Cu}_{3-x}\text{Al}_x\text{O}_{6+y}$ single crystals. Fifteenth European Crystallographic Meeting (ECM-15), Dresden (DE) (August).

- Brecht, E., Schmahl, W.W., Mieke, G., Fuess, H., Andersen, N.H., Wolf, T.*, Reversible change of microstructure of $\text{YBa}_2\text{Cu}_{3-x}\text{Al}_x\text{O}_{6+y}$ single crystals due to heat treatment in different atmospheres. Fifteenth European Crystallographic Meeting (ECM-15), Dresden (DE) (August).
- Brecht, E., Schmahl, W.W., Mieke, G., Fuess, H., Casalta, H., Andersen, N.H., Wolf, T.*, Clustering and magnetic ordering in doped $\text{YBa}_2\text{Cu}_{3-x}\text{M}_x\text{O}_{6+y}$. 3rd Workshop on: The Influence of the Local Structure on the Superconducting Properties for Samples in the Y-Ba-Cu-O and Related Systems, Orvieto (IT) (January).
- Brecht, E., Schmahl, W.W., Mieke, G., Fuess, H., Andersen, N.H., Wolf, T.*, Reversible change of microstructure of $\text{YBa}_2\text{Cu}_{3-x}\text{Al}_x\text{O}_{6+y}$ single crystals due to heat treatment in different atmospheres. 4th International Conference on Materials and Mechanisms of Superconductivity, High-Temperature Superconductors (M²S-HTSC IV), Grenoble (FR) (July).
- Brecht, E., Casalta, H., Schleger, P., Andersen, N.H., Schmahl, W.W., Fuess, H., Wolf, T.*, Antiferromagnetic ordering in Al doped $\text{YBa}_2\text{Cu}_{3-x}\text{Al}_x\text{O}_{6+y}$ single crystals. 4th International Conference on Materials and Mechanisms of Superconductivity, High-Temperature Superconductors (M²S-HTSC IV), Grenoble (FR) (July).
- Brecht, E., Schmahl, W.W., Fuess, H., Casalta, H., Schleger, P., Lebech, B., Andersen, N.H., Schmenn, S., Luetgemeier, H., Wolf, T.*, Influence of Al on the antiferromagnetic properties of reduced $\text{REBa}_2\text{Al}_x\text{Cu}_{6+y}$ single crystals. 4th Workshop on: The Influence of Local Structure on the Superconducting Properties for Samples in the Y-Ba-Cu-O and Related Systems, Seeheim-Jugenheim (DE) (October).
- Brecht, E., Schmahl, W.W., Fuess, H., Casalta, H., Schleger, P., Lebech, B., Andersen, N.H., Schmenn, S., Luetgemeier, H., Wolf, T.*, Antiferromagnetic ordering in $\text{REBa}_2\text{Cu}_{3-x}\text{Al}_x\text{O}_{6+y}$ single crystals. Karlsruher Supraleitertreffen, Karlsruhe (DE) (October).
- Casalta, H., Schleger, P., Montfroiij, W., Andersen, N.H., Lebech, B., Brecht, E., Schmahl, W.W., Fuess, H., Liang, R., Hardy, W.N., Wolf, T.*, Absence of the second magnetic transition T_{N2} in $\text{YBa}_2\text{Cu}_3\text{O}_{6+x}$. 4th International Conference on Materials and Mechanisms of Superconductivity, High-Temperature Superconductors (M²S-HTSC IV), Grenoble (FR) (July).
- Casalta, H., Schleger, P., Brecht, E., Montfroiij, W., Andersen, N.H., Lebech, B., Schmahl, W.W., Liang, R., Hardy, W.N., Wolf, T.*, Absence of the second magnetic transition, T_{N2} , in $\text{YBa}_2\text{Cu}_3\text{O}_{6+x}$. International Conference on Magnetism. Warsaw (PL) (August).
- Casalta, H., Schleger, P., Andersen, N.H., Montfroiij, W.T., Brecht, E., Schmahl, W.W., Wolf, T., Liang, R., Dosanjh, P., Hardy, W.N.*, Magnetic structure of pure and doped $\text{YBa}_2\text{Cu}_{3-y}\text{Al}_y\text{O}_{6+x}$. 3rd Workshop on: The Influence of the Local Structure on the Superconducting Properties for Samples in the Y-Ba-Cu-O and Related Systems. Orvieto (IT) (January).
- Casalta, H., Schleger, P., Montfroiij, W.T., Lebech, B., Andersen, N.H., Brecht, E., Schmahl, W.W., Liang, R., Hardy, W.N., Wolf, T.*, Absence of the second magnetic transition [T_{N2}] in $\text{YBa}_2\text{Cu}_3\text{O}_{6+x}$. 4th International Conference on Materials and Mechanisms of Superconductivity, High-Temperature Superconductors (M²S-HTSC IV), Grenoble (FR) (July).
- Christensen, L., Buchardt, O., Egholm, M., Nielsen, P.E., Berg, R.H.*, Film-supported PNA synthesis. 23rd European Peptide Symposium. Braga (PT) (September).

- Christensen, M.J., Feidenhans'l, R., Nielsen, M.,* Fe/V superlattices: X-ray and neutron scattering investigations. 4th European Vacuum Conference, Uppsala (SE) (June).
- Clausen, K.N., McEwen, K.A., Jensen, J., Mackintosh, A.R.,* A new mode of magnetic excitation in praseodymium. Workshop on Photon and Neutron Studies of Magnetic Materials, Marathon (GR) (April).
- Clausen, K.N., Mortensen, K., Yaron, U., Gammel, P.L., Huse, D.A., Kleiman, R.N., Olgesby, C.S., Bucher, E., Batlog, B., Bishop, D.J., Bolle, C.A., Cruz, F. de la,* Neutron diffraction studies of flowing and pinned magnetic flux lattices in 2H-NbSe₂. Workshop on Magnetic Structures and Phase Transitions, Krakow (PL) (August).
- Clausen, K.N., Sørensen, S.Aa., McEwen, K.A., Jensen, J., Mackintosh, A.R.,* Crystal fields and conduction electrons in praseodymium. International Conference on Magnetism, Warsaw (PL) (August).
- Egelhaaf, S.U., Pedersen, J.S., Schurtenberger, P.,* Shape transformation in biological mixed surfactant systems: from cylinders to vesicles. VIII International Colloid and Interface Society Conference, Montpellier (FR) (September).
- Enderle, M., Kakurai, K., Clausen, K.N., Steiner, M., Inami, T., Tanaka, H.,* Excitations of CsMnI₃ (S=5/2) in the magnetic field in comparison to CsNiCl₃ (S=1): A test of the Haldane conjecture. International Conference on Neutron Scattering, Sendai (JP) (October).
- Feidenhans'l, R., Smilgies, D.M., Gidalevitz, D., Leiserowitz, L.,* First surface x-ray diffraction investigation of an organic crystal in solution. Danish Physical Society Spring Meeting, Odense (DK) (June).
- Feidenhans'l, R., Smilgies, D.M., Gidalevitz, D., Leiserowitz, L.,* First surface x-ray diffraction investigation of an organic crystal in solution. The 26th Annual Danish Meeting of Crystallographers, Gammel Avernæs (DK) (June).
- Függ, T., Lindgård, P.-A.,* Disorder, order and phase separation studied by the structure factor. Workshop on Non-Equilibrium Ordering Dynamics, Danish Technical University, Lyngby (DK) (September).
- Függ, T., Andersen, N.H., Lindgård, P.-A., Schleger, P., Uimin, G., Mannstaedt, S., Mouritsen, O.G., Berlin, J.,* Recent model studies of oxygen ordering in YBaCuO superconductors. Workshop on: The Influence of the Local Structure on the Superconducting Properties of Samples in the Y-Ba-Cu-O and Related System, Seeheim-Jugenheim (DE) (October).
- Függ, T., Lindgård, P.-A., Andersen, N.H., Berlin, J.,* Improved mean-field theory and structure factor calculation of YBa₂Cu₃O_{6+x}. Danish Physical Society, Spring Meeting, Odense (DK) (May).
- Függ, T., Mannstaedt, S., Andersen, N.H., Berlin, J., Lindgård, P.-A., Mouritsen, O.G.,* Metal-ion doping effects and structure factor calculation of YBa₂Cu₃O_{6+x}. 4th International Conference on Materials and Mechanisms of Superconductivity, High-Temperature Superconductors (M²S-HTSC IV), Grenoble (FR) (July).
- Forgan, E.M., Cubitt, R., Wylie, M.T., Lee, S.L., Paul, D.M., Mook, H.A., Yethiraj, M., Mortensen, K.,* Observation of magnetic flux lines in high-temperature superconductors by neutron diffraction. Danish Physical Society Spring Meeting, Odense (DK) (June).
- Forgan, E.M., Shaikh, S.J., Watson, D., Rainford, B.D., Lebech, B.,* Magnetic ordering and critical scattering from CeAl₂. Workshop on Magnetic Structures and Phase Transitions, Krakow (PL) (August).

- Forgan, E.M., Cubitt, R., Wylie, M.T., Lee, S.L., Keller, H., Paul, D.M., Yethiraj, M., Mook, H.A., Kes, P.H., Li, T.W., Menovsky, A.A., Tarnawski, Z., Koshizuka, N., Ricketts, J., Mortensen, K.*, Observation of the flux-line lattice by neutron diffraction and Muon-spin rotation. Katakayushu (JP) (November).
- Foss, M., Feidenhans'l, R., Nielsen, M., Findeisen, E., Johnson, R.L., Buslaps, T., Besenbacher, F., Stensgaard, I.*, Determination of the $N_i(111)(5\sqrt{3} \times 2)$ -S structure by x-ray diffraction. European Crystallographic Meeting, Dresden (DE) (August).
- Foss, M., Feidenhans'l, R., Nielsen, M., Findeisen, E., Johnson, R.L., Buslaps, T., Besenbacher, F., Stensgaard, I.*, X-ray diffraction investigation of sulfur induced restructuring of metal surfaces. European Conference on Surface Science (ECOSS-14), Leipzig (DE) (September).
- Foss, M., Feidenhans'l, R., Nielsen, M., Findeisen, E., Johnson, R.L., Buslaps, T., Besenbacher, F., Stensgaard, I.*, X-ray diffraction investigation of sulfur induced restructuring of metal surfaces. Danish Physical Society Spring Meeting, Odense (DK) (June).
- Foss, M., Feidenhans'l, R., Nielsen, M., Findeisen, E., Johnson, R.L., Buslaps, T., Besenbacher, F., Stensgaard, I.*, X-ray diffraction investigation of sulfur induced restructuring of metal surfaces. The 26th Annual Danish Meeting of Crystallographers, Gammel Avernæs, (DK) (June).
- Gammel, P.L., Yaron, U., Huse, D.A., Kleiman, R.N., Batlogg, B., Oglesby, C.S., Bucher, E., Bishop, D.J., Mason, T.E., Mortensen, K.*, Small angle neutron scattering from the flux-line lattice in $2H-NbSe_2$. 6. Joint MMM-Intermag Conference, Albuquerque, NM (US) (June).
- Geisler, T., Bjørnholm, T., Petersen, J.C., Madsen, H.G., Bechgaard, K.*, Third-harmonic generation in alkoxy substituted oligo-p-phenylene doped polymer thin films. Danish Physical Society, Spring Meeting, Odense (DK) (June).
- Gerstenberg, M.C., Pedersen, J.S., Christensen, M.J., Larsen, J.G.*, The magnetism of an epitaxially grown Fe layer. Danish Physical Society, Spring Meeting, Odense (DK) (June).
- Gerstenberg, M.C., Pedersen, J.S., Christensen, M.J., Larsen, J.G.*, The magnetism of an epitaxially grown Fe layer. European Summer School on Nanoscale Materials Physics, Helsingør (DK) (August).
- Gorman, B.M., Fiig, T., Rikvold, P.A., Novotny, M.A.*, Finite-range scaling analysis of nucleation in model systems with long-range interactions. American Physical Society, Pittsburg PA (US) (March).
- Hadfield, R.A., Schleger, P., Casalta, H., Andersen, N.H., Poulsen, H.F., von Zimmermann, M., Schneider, J.R., Liang, R., Dosanjh, P., Hardy, W.N.*, Simultaneous neutron and x-ray refinement of Ortho-II superstructure in $YBa_2Cu_3O_{6.5}$. 4th International Conference on Materials and Mechanisms of Superconductivity, High-Temperature Superconductors (M²S-HTSC IV), Grenoble (FR) (July).
- Harris, P., Lebech, B., Shim, H.S., Mortensen, K., Pedersen, J.S.*, Small angle neutron studies of the magnetic phase diagram of MnSi. International Conference on Neutron Scattering, Sendai (JP) (October).
- Hvilsted, S.*, A novel side-chain liquid crystalline polyester architecture for erasable optical storage. Nordic Polymer Days 1994, Copenhagen (DK) (May).
- Hvilsted, S.*, A novel and versatile side-chain liquid crystalline polyester architecture for erasable optical storage. Light and molecules. MODECS F&U Forum, Risø (DK) (May).

- Hvilsted, S., Pedersen, M., Ramanujam, P.S., Andruzzi, F.*, Erasable optical storage in azobenzene side-chain polyesters. 5. European Polymer Federation Symposium on Polymeric Materials, Basel (CH) (October).
- Hønger, T., Mortensen, K., Hjort Ipsen, J., Lemmich, J., Bauer, R., Mouritsen, O.G.*, Anomalous swelling of lipid bilayers. 38. Annual Meeting of the Biophysical Society, New Orleans, LA (US) (March).
- Janssen, S., Schwahn, D., Springer, T., Mortensen, K., Hasegawa, H., Dudowicz, J., Freed, K.F.*, Investigation of the pressure dependence and the Gibbs potential for polymer blends by means of SANS. International Conference on Neutron Scattering, Sendai (JP) (October).
- Jørgensen, J.-E., Andersen, N.H.*, Crystal structure and charge localization in $\text{Pb}_2\text{Sr}_2\text{Tb}_{1-x}\text{Ca}_x\text{Cu}_3\text{O}_8$ for $x = 0.00$ and 0.5 . 4th International Conference on Materials and Mechanisms of Superconductivity, High-Temperature Superconductors (M²S-HTSC IV), Grenoble (FR) (July).
- Kawano, S., Sørensen, S.Aa., Achiwa, N., Lebech, B.*, High pressure neutron diffraction studies of magnetic structures of erbium single crystal. International Conference on Magnetism, Warsaw (PL) (August).
- Kjær, K.*, Performance of BW1 - 2-dimensional structure of monolayers on water. HASY-LAB Nutzertreffen und Statusseminar. Forschung mit Synchrotronstrahlung, Hamburg (DE) (January).
- Kulinna, C., Zebger, I., Siesler, H.W., Hvilsted, S., Ramanujam, P.S.*, Characterisation of the orientational behaviour of liquid-crystalline side-chain polymers for reversible optical data storage by Fourier-Transform-IR-Spectroscopy. 9. International Conference on Fourier Transform Spectroscopy, Bellingham, WA (US) (1993).
- Landemark, E., Nielsen, M., Findeisen, E., Feidenhans'l, R., Foss, M., Buslaps, T., Seehofer, L., Johnson, R.L.*, Atomic structure of $\text{Ge}(111)\sqrt{3}\times\sqrt{3}\text{-Ag}$ determined by surface x-ray diffraction. MAX LAB User Meeting, Lund (SE) (September).
- Langridge, S., Stirling, W.G., Lander, G.H., Lebech, B., Vogt, O.*, Neutron scattering study of the magnetic phases of $\text{USb}_{0.8}\text{Te}_{0.2}$. International Conference on Neutron Scattering, Sendai (JP) (October).
- Larsen, J.G. Pohl, J., Christensen, M., Feidenhans'l, R.*, X-ray and neutron scattering investigations of Cr/Mn and Fe/V superlattices. Danish Physical Society Spring Meeting, Odense (DK) (June).
- Laurer, J.H., Spontak, R.J., Smith, S.D., Ashraf, A., Samseth, J., Mortensen, K.*, Morphological studies of weakly-segregated diblock copolymer/homopolymer and copolymer/copolymer blends. 1994 March meeting of the American Physical Society, Pittsburgh PA (US) (March).
- Lebech, B., Shim, H.S.*, Commensurate-commensurate magnetic phase transitions in CeSb. Workshop on Magnetic Structures and Phase Transitions, Krakow (PL) (August).
- Lebech, B., Wolny, J.*, Commensurate-incommensurate magnetic phase transitions in dhcp Nd metal. Workshop on Photon and Neutron Studies of Magnetic Materials, Marathon (GR) (April).
- Lebech, B., Harris, P., Pedersen, J.S., Mortensen, K., Gregory, C.I., Bernhoeft, N.R., Jermy, M.*, Magnetic phase diagram of MnSi. International Conference on Magnetism, Warsaw (PL) (August).
- Lebech, B.*, Modulated magnetic ordering and magnetic phase transitions. Third Interna-

- tional School of Theoretical Physics – Symmetry and Structural Properties of Condensed Matter, Poznan (PL) (September).
- Lebeck, B.*, Magnetic structures and correlations in Dzyaloshiinski spirals studied by small-angle neutron crystallography. Condensed Matter and Materials Physics Conference - 1994, Warwick (UK) (December).
- Lefmann, K., Rischel, C.*, Exact Diagonalization of the $S = 1/2$ Heisenberg chain. Danish Physical Society, Spring Meeting, Odense (DK) (June).
- Lefmann, K., Clausen, K.N., Rasmussen, F.B., Nummila, K.K., Tuoriniemi, J.T., Metz, A., Siemensmeyer, K., Steiner, M.*, Nuclear ordering in silver. Danish Physical Society, Spring Meeting, Odense (DK) (June).
- Lefmann, K., Broholm, C., Davidovic, D., Dender, D., Reich, D., Aeppli, G., Erwin, R.*, Neutron scattering study of a 1-dimensional antiferromagnet. Danish Physical Society, Spring Meeting, Odense (DK) (June).
- Lindgård, P.-A.*, Computer simulation of the structure factor. 7th Annual Workshop: Recent Developments in Computer Simulation Studies in Condensed Matter Physics. Athens, GA (US) (February).
- Lindgård, P.-A., Bohr, H.*, Towards a structural classification of protein foldings: A simplified approach. Danish Physical Society, Spring Meeting, Odense (DK) (June).
- Lindgård, P.-A.*, What determines the martensitic transformation temperature. ESO-MAT'94, Barcelona (ES) (September).
- Lindgård, P.-A., Bohr, H.*, How many fold classes are to be found. Symposium on Distance-based Approaches to Protein Structure Determination II, Copenhagen (DK) (November).
- Lindgård, P.-A.*, Aspects of dynamical research in Denmark. EUDYN'94, Berlin (DE) (December).
- Lindgård, P.-A., Hendriksen, P.V.*, Magnetic properties of clusters. Workshop on Magnetic Structures and Phase Transitions, Krakow (PL) (August).
- Loewenhaupt, M., Reif, T., Gratz, E., Rotter, M., Arons, R.R., Lebeck, B.*, The magnetic phases of NdCu_2 . Workshop on Magnetic Structures and Phase Transitions, Krakow (PL) (August).
- Longmore, A., Nutley, M.P., Boothroyd, A.T., Andersen, N.H., Casalta, H., Schleger, P., Chen Changkang, H.Y., Christensen, A.N.*, Magnetic order in $\text{PrBa}_2\text{Cu}_3\text{O}_{6+x}$. 4th International Conference on Materials and Mechanisms of Superconductivity, High-Temperature Superconductors (M²S-HTSC IV), Grenoble (FR) (July).
- Mason, T.E., Aeppli, G., Hayden, S.M., Ramirez, A.P., Mock, H.A.*, Magnetic fluctuations in superconducting $\text{La}_{2-x}\text{Sr}_x\text{CuO}_4$. In: Fourth Nordic Symposium on Superconductivity. Varberg (SE) (May).
- Mason, T.E., Aeppli, G., Petersen, T., Tun, Z., Bucher, E.*, Magnetic correlations in heavy fermion metals and semiconductors. International Conference on Neutron Scattering, Sendai (JP) (October).
- McEwen, K.A., Steigenberger, U., Clausen, K.N., Kappler, C., Walker, M.B.*, Quadrupolar and magnetic structures of UPd_3 . International conference on Neutron Scattering, Sendai (JP) (October).
- McMorrow, D.F.*, Competing anisotropies in rare-earth superlattices. International Conference on Magnetism, Warsaw (PL) (August).

- McMorrow, D.F.*, The structure and magnetic properties of rare-earth superlattices. Photon and Neutron Scattering Studies of Magnetism, Marathon (GR) (April).
- Mortensen, K.*, Block copolymer surfactants. Random and micellar networks and mesophases. Nordic Polymer Days 1994, Copenhagen (DK) (May).
- Mortensen, K.*, Phase behavior of di- and tri-block copolymer surfactants forming micellar crystals and micellar networks. Symposium on Frontiers of Neutron Scattering Research in Polymer Science, Kyoto (JP) (October).
- Mortensen, K.*, Block copolymers in aqueous solutions - dependence on shear, temperature and pressure. 1994 National meeting of the American Chemical Society. Division of Polymer Chemistry. Block Copolymer Dynamics, San Diego, CA (US) (March).
- Mortensen, K.*, Block copolymer surfactants. Random and micellar networks, and mesophases. The Royal Society of Chemistry. Faraday Division. Discussion no. 98: Polymers at Surfaces and Interfaces, Bristol (GB) (September).
- Mortensen, K.*, Crystalline mesophases in pluronics and pluronics-R melts and aqueous solutions. Plurionics Workshop. Roskilde University Center, Roskilde (DK) (September).
- Mortensen, K., Almdal, K., Bates, F., Koppi, K., Tirrell, M.*, Shear induced mean-field behavior near the order-to-disorder transition in a diblock-copolymer melt. Danish Physical Society Spring Meeting, Odense (DK) (June).
- Mortensen, K., Almdal, K., Bates, F., Koppi, K.*, Structural studies on block copolymers melts and solutions, dependence on shear field. International Conference on Neutron Scattering, Sendai (JP) (October).
- Mortensen, K., Schwahn, D., Janssen, S.*, Mean-field to 3d-Ising crossover in polymer blends. Critical exponents and discussion of the Ginzburg criterium. Workshop on Non-Equilibrium Ordering Dynamics. Danish Technical University, Lyngby (DK) (September).
- Nielsen, M., Als-Nielsen, J., Freund, A.K., Grübel, G., Linderholm, J., Sanchez Del Rio, M., Sellshop, J.P.F.*, Multiple station beamline at an undulator x-ray source. Danish Physical Society, Spring Meeting, Odense (DK) (June).
- Oddershede, L., Lefmann, K., Thoft, N.B., Jacobsen, R.H.*, Photon, a physics game. Danish Physical Society, Spring Meeting, Odense (DK) (June).
- Papadakis, C., Posselt, D., Almdal, K.*, Phase behaviour of symmetric diblock copolymers. 1. International Conference on Scaling Concepts and Complex Fluids, Catanzaro (IT) (July).
- Paul, D.M., Forgan, E.M., Cubitt, R., Lee, S.L., Wylie, M., Mook, H.A., Yethiraj, M., Mortensen, K.*, Neutron scattering from the flux-line lattice. International Conference on Neutron Scattering, Sendai (JP) (October).
- Pedersen, J.S., Hansen, S., Bauer, R.*, The aggregation behaviour of zinc-free insulin studied by small-angle neutron scattering. 1. International Conference on Scaling Concepts and Complex Fluids, Catanzaro (IT) (July).
- Pedersen, J.S.*, Analysis of x-ray and neutron reflectivity data by constrained least-squares methods. Workshop on X-ray and Neutron Reflectivity on Thin Films and Interfaces. Institut M. et P. Curie, Paris (FR) (March).
- Pedersen, J.S., Hansen, S., Bauer, R.*, The aggregation behaviour of zinc-free insulin studied by small-angle neutron scattering. 8. European Colloid and Interface Society Conference, Montpellier (FR) (September).

- Pedersen, J.S.*, Small-angle scattering studies of macromolecular aggregates such as clathrin-coated vesicles and insulin. Minisymposium on New Structural Probes in Chemistry. Niels Bohr Institute, Copenhagen (DK) (October).
- Pedersen, M., Hvilsted, S., Andruzzi, F., Ramanujam, P.S.*, New side-chain liquid crystalline polyesters for optical storage. Nordic Polymer Days 1994. Copenhagen (DK) (May).
- Petersen, T.*, Magnetic fluctuations in the heavy Fermion superconductor UPd₂Al₃. The 1994 Meeting of the American Physical Society, Pittsburg PA (US) (March).
- Ramanujam, P.S., Andruzzi, F., Hvilsted, S.*, Influence of the length of flexible spacers on the optical storage properties of side-chain liquid crystalline polyesters. Topical Meeting of the International Commission for Optics, Kyoto (JP) (April).
- Rasmussen, F.B., Lefmann, K., Buras, B., Pedersen, E.J., Shabonovna, E.S., Thorsen, P.A., Sellschop, J.F.P.*, NMR studies of a new material: ¹³C diamond. Danish Physical Society, Spring Meeting, Odense (DK) (June).
- Rial, C., Amador, U., Morán, E., Andersen, N.H., Alario-Franco, M.A.*, Structural and physical aspects of room temperature oxidized La_{2-x}Sr_xCuO_{4+y} (0 ≤ x ≤ 0.2). 4th International Conference on Materials and Mechanisms of Superconductivity, High-Temperature Superconductors (M²S-HTSC IV), Grenoble (FR) (July).
- Ruiz-Aragón, M.J., Amador, U., Morán, E., Andersen, N.H.*, Neutron diffraction study of (La_{1-x}Ca_x)BaCuFeO_{5+δ}. (Ln = Y, Pr; 0 ≤ x ≤ 0.2). 4th International Conference on Materials and Mechanisms of Superconductivity, High-Temperature Superconductors (M²S-HTSC IV), Grenoble (FR) (July).
- Schleger, P.*, Combined structural investigation of intermediate range Ortho-II ordering in YBa₂Cu₃O_{6.5}. 3rd Workshop of the Working Group on the Influence of the Local Structure on the Macroscopic Superconducting Properties for Samples in the Y-Ba-Cu-O and Related Systems, Orvieto (IT) (January).
- Schleger, P., Hadfield, R.A., Casalta, H., Poulsen, H.F., von Zimmermann, M., Andersen, N.H., Schneider, J.R., Liang, R., Dosanjh, P., Hardy, W.N.*, Experimental investigations of oxygen ordering and atomic displacements in the Ortho-II phase of YBa₂Cu₃O_{6.5} by neutron and synchrotron x-ray diffraction. 4th Nordic Symposium on Superconductivity, Varberg (SE) (May).
- Schleger, P., Hadfield, R.A., Casalta, H., Andersen, N.H., Poulsen, H.F., von Zimmermann, M., Schneider, J.R., Liang, R., Dosanjh, P., Hardy, W.N.*, The line shape of the Ortho-II superstructure reflection in YBa₂Cu₃O_{6.5}. 4th International Conference on Materials and Mechanisms of Superconductivity, High-Temperature Superconductors (M²S-HTSC IV), Grenoble (FR) (July).
- Schleger, P.*, Random-field structural transition in YBa₂Cu₃O_{6.5}. 4th Workshop of the Working Group on the Influence of the Local Structure on the Macroscopic Superconducting Properties for Samples in the Y-Ba-Cu-O and Related Systems. Seeheim-Jugenheim, (DE) (October).
- Schulz, M.F., Förster, S., Bates, F.S., Almdal, K., Mortensen, K.*, Epitaxial growth of cubic phases in diblock copolymers. American Physical Society, Pittsburg, PA (US) (March).

- Schwahn, D., Janssen, S., Willner, L., Springer, T., Meier, G., Mortensen, K., Hasegawa, H., Imai, M., Takeno, H., Jinnai, H., Hashimoto, T.*, Critical crossover phenomena in compatible polymer blends studied with SANS. International Conference on Neutron Scattering, Sendai (JP) (October).
- Shim, H.S., Lebech, B., Rasmussen, S.E.*, Crystal structure refinement of RECoO₃ (RE = La, Pr and Tb) using high resolution neutron powder diffraction and x-ray powder diffraction. 26. Meeting of Danish Crystallographers, Gl. Avernæs, Fyn (DK) (June).
- Simpson, A., Cowley, R.A., Ward, R.C.C., Wells, M.R., McMorrow, D.F.*, The magnetic structure of IO/PR superlattices. Condensed Matter and Material Physics Conference, Warwick (GB) (December).
- Smilgies, D.-M., Wu, H., Hinch, B.J., Erans-Lutterodt, K., Tang, M.-T.*, In-situ study of the etching of silicon surfaces. Danish Physical Society, Spring Meeting, Odense (DK) (June).
- Smilgies, D.-M., Wu, H., Hinch, B.J., Erans-Lutterodt, K., Tang, M.-T.*, In-situ study of the etching of silicon surfaces. 14th European Conference on Surface Science, Leipzig (DE) (September).
- Steiner, M., Metz, A., Nummila, K., Tuoriniemi, J., Lefman, K., Clausen, K.V.*, Nuclear magnetic order in Ag at Picokelvin temperature. International Conference on Neutron Scattering, Sendai (JP) (October).
- Sørensen, S.A., Lebech, B.*, Magnetic structures in erbium under high pressure. Workshop on Photon and Neutron Studies of Magnetic Materials, Marathon (GR) (April).
- Thoft, N.B., Bohr, J., Buras, B., Johnson, E., Johansen, A., Andersen, N.H., Sarholt-Kristensen, L.*, Melting and solidification of bismuth inclusions in aluminium. Danish Physical Society Spring Meeting, Odense (DK) (June).
- Tomy, C.V., Balakrishnan, G., Chang, L.J., Paul, D.M., Andersen, N.H.*, Neutron diffraction in RENi₂B₂C (RE = Rare Earth) above and below T_c. International Conference on Neutron Scattering, Sendai (JP) (October).
- Winther, L., Almdal, K., Batsberg Pedersen, W., Kops, J., Berg, R.H.*, Hydrophilic film supports for peptide synthesis. Nordic Polymer Days 1994, Copenhagen (DK) (May).
- Winther, L., Schafer-Nielsen, C., Batsberg Pedersen, W., Berg, R.H.*, PEPS tubes - a simplification of flow resins. 23rd European Peptide Symposium, (1994), Braga (PT) (September).
- Wolny, J., Lebech, B.*, Temperature dependencies of magnetic modulation vectors in Nd and Nd-rich Nd-Pr alloys. Workshop on Magnetic Structures and Phase Transitions, Krakow (PL) (August).
- Wolny, J., Lebech, B.*, Magnetic modulation vectors in Nd-rich Nd-Pr alloys. International Conference on Magnetism, Warsaw (PL) (August).
- Yethiraj, M., Mook, H.A., Forgan, E.M., Cubitt, R., Wylie, M., Lee, S.L., Paul, D.M., Kes, P.H., Li, T.W., Menovsky, A.A., Tarnawski, Z., Mortensen, K.*, Temperature dependence of the flux-line lattice in a single crystal of Bi_{2.15}Sr_{1.95}CaCu₂O_{8+x}. American Physical Society, Pittsburgh, PA (US) (March).
- Yethiraj, M., Mook, H.A., Forgan, E.M., Cubitt, R., Wylie, M., Lee, S.Y., Paul, D.M., Kesand, P.H., Li, T.W., Menovskyand, A.A., Tarnawski, Z., Mortensen, K.*, Small-angle neutron scattering study of the flux line lattice in a single crystal of Bi_{2.15}Sr_{1.95}CaCu₂O_{8+x}. 6. Joint MMM-Intermag Conference, Albuquerque, NM (US) (June).

- Zebger, I., Siesler, H.W., Andruzzi, F., Pedersen, M., Ramanujam, P.S., Hvilsted, S.*, The influence of substituents on the orientational behaviour of novel azobenzene side-chain polyesters. 11. European Symposium on Polymer Spectroscopy, Valladolid (ES) (July).
- Zinkin, M.P., McMorrow, D.F., Hill, J.P.*, A synchrotron x-ray scattering study of the normal-incommensurate structural phase transition in Rb_2ZnCl_4 . Condensed Matter and Material Physics Conference, Warwick (GB) (December).

3.4 Lectures

- Almdal, K.*, Shear field-structure couplings and general phase behaviour in diblock copolymers melt. Department of Chemical Engineering. Polytechnic University, New York, NY (US) (August).
- Almdal, K.*, Epitaxial growth of the body centred cubic phase in diblock copolymer melts. IVC Seminar, Materials Department, Risø National Laboratory (DK) (December).
- Almdal, K., Mortensen, K., Bates, F.S., Koppi, K.A., Tirrell, M.*, The hexagonal-to-disorder phase transition in a diblock copolymer melt under the influence of shear. Rheology Group Seminar, Risø National Laboratory (DK) (March).
- Als-Nielsen, J.*, Examples of undulator beam research at ESRF. Photon Factory, KEK, (JP) (March).
- Als-Nielsen, J.*, Examples of undulator beam research at ESRF. Japan Society for the Promotion of Science (JP) (March).
- Als-Nielsen, J.*, Examples of undulator beam research at ESRF. RIKEN Laboratory, Tokyo, (JP) (March).
- Als-Nielsen, J.*, The possible simplicity of undulator beam research. Advanced Photon Source User Meeting, Argonne National Laboratory (US) (May).
- Als-Nielsen, J.*, The possible simplicity of undulator beam research. ESRF, Grenoble (FR) (June).
- Als-Nielsen, J.*, Diffraction and absorption of x-rays and neutrons: A comparative exposition. Introductory Lectures HERCULES, Grenoble (FR) (February).
- Als-Nielsen, J.*, Melting of a monomolecular film – an x-ray undulator study. Physikalisches Kolloquium, DESY, Hamburg (DE) (November).
- Als-Nielsen, J.*, Liquid surfaces studied by synchrotron x-rays – A nostalgic review. Harvard Symposium (US) (November).
- Andersen, N.H.*, Superledning ved høje temperaturer (Superconductivity at High Temperatures). High School Summer Course on Physics, Sorø (DK) (June).
- Bechgaard, K.*, Research project in the Department of Solid State Physics at Risø National Laboratory, Dept. of Chemistry, University of Copenhagen (DK) (November).
- Berg, R.H.*, Seminar for Løvens Kemiske Fabrik, Risø National Laboratory (DK) (June).
- Berg, R.H.*, Kunstigt DNA. Section of Plant Biology, Risø National Laboratory (DK) (December).
- Clausen, K.N.*, Neutron optics and planned upgrades of neutron facilities at Risø. Meeting at KURRI, Kyoto University Research Reactor on Development of International Neutron Scattering Facilities, Kyoto (JP) (October).

- Clausen, K.N.*, Quadrupolar and magnetic ordering of UPd₃, Hahn-Meitner Institut, Berlin (DE) (November).
- Feidenhans'l, R.*, Restructuring of metal surfaces induced by sulphur adsorption. Ruhr-University, Bochum (DE) (June).
- Johannsen, I.*, Surface characterisation and modification of polymers. The Danish Society for Polymer Technology, Copenhagen (DK) (November).
- Lebech, B.*, Neutron scattering activities at Risø National Laboratory. Korea Atomic Energy Research Institute, Taejon (KR) (October).
- Lebech, B.*, Magnetic ordering in MnSi and FeGe by small angle neutron scattering. Korea Atomic Energy Research Institute, Taejon (KR) (October).
- Lebech, B.*, Modulated magnetic structures. Korea Atomic Energy Research Institute, Seoul (KR) (October).
- Lebech, B.*, Small-angle neutron scattering of the magnetic ordering in the Cubic Isomorphs MnSi and FeGe. University of Kobe, Kobe (JP) (October).
- Lejmann, K.*, The S = 1/2 Heisenberg triangular antiferromagnet. Hahn-Meitner-Institute, Berlin (DE) (April).
- Lindgård, P.-A.*, Lecture course of 4 × 2 hours in "Theory of Statistical Physics". Barcelona University (ES) (February).
- Lindgård, P.-A.*, Theory and simulations of structures in 2 dimensions: Vacancy stabilized structures and elastic interactions. Florida State University, FL (US) (February).
- McMorrow, D.F.*, Recent advances in rare-earth magnetism. Danish Technical University, Lyngby (DK) (April).
- McMorrow, D.F.*, Magnetic nanolattices. Summer School on Nanoscale Materials Physics, Copenhagen (DK) (August).
- Pedersen, J.S.*, Analyse af småvinkelsprednings-data: Anvendelse af numeriske metoder baseret på mindste-kvadraters principper. Roskilde Universitetscenter, Roskilde (DK) (March).
- Pedersen, J.S.*, The tree-dimensional resolution function of a SANS instrument and analysis of the magnetic scattering from MnSi. Institute of Applied Physics, ETH Zürich (CH) (August).
- Pedersen, J.S.*, Ligevægtsaggregeringsopførsel af insulin. Niels Bohr Institute, Copenhagen (DK) (October).
- Schleger, P.*, The character of the Ortho-II phase in YBa₂Cu₃O_{6.5}. The University of British Columbia, Vancouver CA (US) (May).
- Smilgies, D.-M.*, Epitaxy of high-temperature superconductor films on SrTiO₃ substrates. Max-Planck-Institut für Festkörperforschung, Stuttgart (DE) (November).

3.5 Organization of Meetings and Courses

LIP Users' Meeting

6-7 May, Risø National Laboratory, Denmark

The second annual users' meeting of the LIP programme was attended by 62 scientists from the EU member states. The programme consisted of 7 plenary lectures listed below and a poster session with 25 contributions.

Organization

McMorrow, D.F., Clausen, K.N., Risø National Laboratory, Denmark Mackintosh, A.R., Niels Bohr Institute, Denmark

Programme

Hayden, S.M., *H.H. Wills Physics Laboratory, University of Bristol, England.*
Neutron Scattering and the Superconducting State of $\text{La}_{2-x}\text{Sr}_x\text{CuO}_4$.

Bermejo, F.J., *Instituto de Estructura de la Materia, CSIC, Spain.*
Correlated Atomic Motion in Glasses: Selenium.

Schurtenberger, P., *Polymer Institut, ETH-Zürich, Switzerland.*
Equilibrium Polymers - A small Angle Scattering Study.

Engler, O., *Institut für Metallkunde und Metallphysik, RWTH Aachen, Germany.*
Measurements of Crystallographic Texture by X-ray and Neutron Diffraction.

Reynaers, H., *K.U. Leuven, Department of Chemistry, Belgium.*
Gel Formation of Biological and Synthetic Macromolecules.

Steigenberger, U., *ISIS Facility, Rutherford Appleton Laboratory, England.*
Phase Transitions and Magnetic Excitations in UPd_3 .

Lösche, M., *Fakultät für Physik und Geowissenschaften, Universität Leipzig, Germany.*
Structural Organization of Protein Monolayers Bound to Functionalized Interfaces.

Nordic Polymer Days

30 May – 1 June, H.C. Ørsted Institute, Copenhagen, Denmark.

The 31st Nordic Polymer Days covered a broad range of polymer chemistry and physics. Special sessions were devoted to biomedical polymers, polymer composites and blends, rheology and processing, and recycling of polymer materials. A large part of the 156 participants were doctoral students or young scientists presenting the majority of the 76 oral and poster contributions. In addition, 6 plenary lectures (listed below) with relation to the above topics were presented. Furthermore an exhibition of analytical equipment was presented.

Organization

Lyngaae-Jørgensen, J., Technical University of Denmark, Denmark

Bune, C., A/S N.P. Utzon, Denmark

Hansen, C.M., Force Institutes, Denmark

Hvilsted, S., Risø National Laboratory, Denmark

Kramer, O., H.C. Ørsted Intitute, Denmark

Thomsen, L.D., Radiometer Medical A/S, Denmark

Wagner, I., Danish Engineering Society, Denmark

Plenary Lectures

Ugelstad, J., *Technical University of Norway, Trondheim, Norway*, Application of Monodisperse Polymer Particles for Special Separation Processes.

Hansen, C.M., *Force Institutes, Denmark*, Diffusion in Polymers.

Klason, C., *Chalmers University of Technology, Gothenburg, Sweden*, Use of Microporous Metal in Polymer Processing.

Chapoy, L.L., *Wesley-Jessen Corporation, Des Plaines, Il, USA*, Contact Lenses: Polymer Technology Aspects.

Buchnall, C.B., *Cranfield University, Bedford, U.K.*, Rubber Particle Cavitation and Its Consequences in Roughened Plastics.

Stein, R.S., *University of Massachusetts, Amherst, Ma, USA*, The Polymer Solid Waste Problem.

Ph.D. Course in Statistical Physics and Soft Matter

May – December, Risø National Laboratory, Danish Technical University, Lyngby and Niels Bohr Institute, Copenhagen, Denmark.

Organization

Lindgård, P.-A., Risø National Laboratory, Denmark and Mouritsen, O.G., Technical University of Denmark, Denmark.

Twelve full-day courses were arranged running from May to December with lectures given by a number of lecturers: G. Besold, J. Dyre, H.C. Fogedby, J.H. Ipsen, P.-A. Lindgård, G.C.A. Mooij, O.G. Mouritsen, S. Toxværd and M. Zuckermann. The location was at Risø, DTU and Copenhagen University. P.-A. Lindgård taught the first two topics of the following:

Mean-field Theory of Continuous Transitions.

Mean-field Theory of Discontinuous Transitions.

Scaling Theory and the Renormalization Group.

Interfaces, Roughening, and Wetting.

Surfactants, Emulsions, and Microemulsions.

Statistical Physics of Polymers.

Random Surfaces and Fluctuating Manifolds.

Monte Carlo Stimulation Techniques Applied to Soft Matter.

Molecular Dynamics Methods Applied to Soft Matter.

Lipid Monolayers and Bilayers.

Biological Membranes as Soft Matter.

Stochastic Processes and the Langevin equation.

The course was attended by Ph.D. students, post.docs. and others. Eleven Ph.D. students completed the course with a qualifying talk on a given subject.

3.6 Membership of Committees and Boards

Als-Nielsen, J.,

Member of the Proposal Evaluation Board for Advanced Photon Source (APS), Argonne National Laboratory, USA.

Member of the Panel of Synchrotron Radiation to the Israel Academy of Sciences and Humanities (from July).

Member of the Panel of Protein Crystallography at ESRF - a TROIKA Beamline (from November).

Member of the Danish National Committee for Crystallography.

Andersen, N.H.,

Consultant for the Swedish Superconductivity Consortium.

Bechgaard, K.,

Chairman of the Danish National Committee for Chemistry.

Member of the Advisory Board of Journal of Materials Chemistry.

Member of the EEC COST D-4 Committee.

Member of the Academy Council of the Danish Academy of Technical Sciences.

Member of the NATO Special Programme Panel on Supramolecular Chemistry.

Berg, R.H.,

Member of the Editorial Advisory Board, Journal of Peptide Science.

Councillor of the European Peptide Society.

Clausen, K.N.,

Member of the Board of Risø National Laboratory.

Feidenhans'l, R.,

Member of the Danish National Committee for Crystallography.

Lebech, B.,

Member of the Danish National Committee for Crystallography.

Member of the European Neutron Scattering Association.

Member of the Board of the Neutron Diffraction Commission under the International Crystallographic Union.

Correspondent for Neutron News.

Lindgård, P.-A.,

Vicechairman of the Magnetism Section of International Union of Pure and Applied Physics (IUPAP).

Chairman of the Condensed Matter Committee at NORDITA.

Mortensen, K.,

Member of the Board of Solid State Division of the Danish Physical Society.

Nielsen, M.,

Member of Forschungsbeirat Synchrotronstrahlung HASYLAB, DESY, Hamburg

Member of Synkrotronstrålingsudvalget under SNF.

Pedersen, J.S.,

Co-editor of Journal of Applied Crystallography (from July).

3.7 Colloquia

in addition a weekly 'tea briefing' on current subjects is organized

- Bourdelle, K.K., *Niels Bohr Institute for Astronomy, Physics and Geophysics, Denmark*. Evolution of Precipitates in Lead Implanted Aluminum. A Backscattering and Channeling Study (January).
- Ho, K.M., *Ames Laboratory, USA*. Tight Binding Molecular Dynamics Simulation of Carbon Systems (January).
- Hovmöller, S., *Structural Chemistry, Stockholm University, Sweden*. Electron Crystallography - Structure Determination of Unknown Crystals by Electron Microscopy and Electron Diffraction (January).
- Oeffner, R., *H.C. Orsted Institute, Denmark*. Simulated Annealing of Clusters of Atoms (January).
- Xiaodong, Z., *Structural Chemistry, Stockholm University, Sweden*. Electron Crystallography - Structure Determination of Unknown Crystals by Electron Microscopy and Electron Diffraction (January).
- Böhringer, M., *Institut de Physique Expérimentale, Université de Lausanne, Switzerland*. Unidirectional and Isotropic Stress Relief in the System Ge(111)/In Studied by STM (March).
- Müller, U., *Max-Planck-Institut für Polymerforschung, Germany*. Linear and Cyclic Anthrylene Systems as Models for Electron Transfer and High Spin Formation (March).
- Xian, D., *Synchrotron Radiation Committee, China*. Beijing Synchrotron Radiation Facility and Activities (March).
- Joensen, K., *Harvard-Smithsonian Center for Astrophysics, Cambridge, USA*. X-ray Supermirrors: Novel Broad-band Grazing-incidence Multilayer for X-ray Optics (June).
- Robinson, K.M., *Institut für Energieverfahrenstechnik, Jülich, Germany*. In Situ X-ray Surface Diffraction Studies of the Under Potential Deposition of Pb and Cu Monolayers on Au(100) Single Crystals (June).
- Vinther, R., *Niels Bohr Institute, Department of Geophysics, Denmark*. Tabu Search - A Heuristic Optimization Procedure (June).
- Gorman, B.M., *Supercomputer Computations Research Institute, Department of Physics, Florida State University, USA*. Finite-Range Scalling Analysis of Nucleation in Model Systems with Long-Range Interactions (July).
- Guenther, C., *Supercomputer Computations Research Institute, Department of Physics, Florida State University, USA*. Application of a Constrained-transfer-matrix Method to Metastability in the d=2 Ising Ferromagnet (August).
- Talmon, Y., *Israel Institute of Technology, Department of Chemical Engineering, Israel*. Microstructure of Complex Fluids studied by Cryo-TEM (August).
- Lüken, E., *European Synchrotron Radiation Facility, France*. Nanometer Thin-film Multilayers for X-ray and Neutron Optics: Applications, Characterization and Growth Control (September).
- Sommer-Larsen, P., *The Engineering Academy of Denmark, Department of Chemistry, Denmark*. Light Induced Structural Changes and Electron Transfer in Bianthrone Compounds (September).
- Luther, A., *Nordita, Denmark*. Interacting Electrons on a Square Fermi Surface (October).
- Vorm, O., *Odense University, Denmark*. Matrix Assisted Laser Desorption Ionisation-Time of Flight Mass Spectroscopy. Technique and Applications (October).
- Metzger, H., *Ludwig-Maximilians-Universität München, Sektion Physik, Germany*. Diffuse X-ray Scattering from Roughness Correlations of Interfaces (November).

4 Participants in the Work in the Department

4.1 Staff

Almdal, Kristoffer
Als-Nielsen, Jens (Stationed at ESRF, Genoble, France until August 31)
Andersen, Niels Hessel
Bechgaard, Klaus (Head of the Department)
Berg, Rolf Henrik
Buras, Bronislaw (Part time consultant until November 22)
Bohr, Jakob (Until April 30)
Clausen, Kurt N. (Head of Research Programme)
Eskildsen, Morten Ring (Temporary from November 1)
Feidenhans'l, Robert (Head of Research Programme)
Fiig, Thomas (Temporary from April 1)
Hvilsted, Søren
Johannsen, Ib (From March 1, Head of Research Programme)
Jørgensen, Mikkel (From February 1)
Kjær, Kristian
Lebech, Bente
Lebech, Jens
Lindgård, Per-Anker
McMorrow, Des
Mortensen, Kell
Nielsen, Mourits
Pedersen, Jan Skov
Pedersen, Walther Batsberg
Petersen, Klaus (Temporary from May 5)

Ph.D. Students and Students

Christensen, Morten Jagd
Falcão, Antonio (Until February 1)
Fiig, Thomas (Until March 31)
Findeisen, Eberhard (Until September 30)
Gerstenberg, Michael C.
Harris, Pernille (Until August 1)
Hussain, Ahsen (From October 1)
Hviid, Lene (From April 14)
Krog, Thomas (From February 17)
Larsen, John Greibe (From February 14)
Lefmann, Kim
Madsen, Jesper (From July 5)
Pedersen, Marianne
Petersen, Thomas
Sørensen, Steen Aagaard
Thoft, Nina Bjørn (Until December 1)

Vigild, Martin
Wang, Christian (From February 14)
Winther, Lars

Technical Staff

Bang, Steen
Berentsen, Allan Nørtoft
Breiting, Bjarne
Hansen, John Erik (Temporary from October 23)
Hedeboe, Vivi
Hubert, Lene
Jensen, Birgit (From September 1)
Johannsen, Arne (Temporary from July 1)
Jørgensen, Christian Toftlung (Apprentice from August 1 until November 11)
Kjær, Torben
Kristensen, Eva Tulin (From October 1)
Larsen, Nille Birkebæk (Apprentice until March 5)
Linderholm, Jens (Stationed at ESRF, Grenoble, France until July 1)
Lund, Morits
Nielsen, Steen
Nielsen, Lotte
Nielsen, Anne Bønke
Pedersen, Dorte Juul (Temporary from June 18 until October 31)
Rasmussen, Ove
Saxild, Finn
Stahl, Kim
Theodor, Keld
Top, John Erik (Temporary until July 14)

Temporary Student Assistants

Astradsson, Martin (From June 21 until September 2)
Larsen, Mogens (From October 1 until October 30)
Laursen, Bo Wegge (From July 4 until August 31)
Lundgaard, Dorte (From July 1 until July 22)
Nielsen, Susanne Quist (From August 1 until September 30)

Secretaries

Becker, Helle (Apprentice until January 31)
Frederiksen, Lajla
Jørgensen, Lene Aarestrup (From April 1 until June 30)
Studinski, Ca Thi
Petersen, Dorte Ørsted (Temporary from September 1)

Guest Scientists, Long Time Visitors and Post Docs

Aeppli, Gabriel, AT&T Bell Laboratories, Murray Hill, NJ 07974, USA
Bouwman, Wim
Casalta, Helene (Until December 1)
Gabriel, Jean-Christophe (From April 1 until November 30)
Hadfield, Richard
Kulinna, Christian (From December 1)
Landemark, Erik (From March 1)
Montfrooij, Wouter (Until December 31)
Müller, Horst-Uwe (From April 1 until May 31)
Schleger, Paul (Until December 1)
Shim, Hae Seop, IAEA fellow from Korea Atomic Research Institute, Taejon, Korea
(Until October 23)
Smilgies, Detlef (From April 1)
Wilkes, Stephen B. (From November 22)

Awards and Degrees

Fiig, Thomas Ph.D., Danish Technical University
Findeisen, Eberhard Ph.D., Danish Technical University
Harris, Pernille Ph.D., University of Copenhagen

4.2 Short Time Visitors

one week or more

Arleth, L.	IMFUFA, Roskilde University Center, Denmark
Bates, F.S.	Dept. of Chem. Eng. & Material Sc., University of Minnesota, USA
Bishop, D.	AT&T Bell Laboratories, Murray Hill, NJ 07974, USA
Böni, P.	Paul Scherrer Institute, Villingen PSI, Switzerland
Borbely, S.	Research Institute for Solid State Research, Budapest, Hungary
Borchers, J.	Reactor Division, Bldg. 235, NIST, Gaithersburg, MD 20899, USA
Bordén, B.	Chalmers Tekniska Högskola, Fysiska Institutionen, Sweden
Börjesson, L.	Chalmers Tekniska Högskola, Fysiska Institutionen, Sweden
Broholm, C.	Department of Physics & Astronomy, The Johns Hopkins University, USA
Brown, W.	Institute of Physical Chemistry, University of Uppsala, Sweden
Bucklow, D.	Harwell Laboratory, NDT Materials Characterization, England
Buslaps, T.	Institut für Experimentalphysik, Universität Hamburg, Germany
Dender, D.	Department of Physics & Astronomy, The Johns Hopkins University, USA
Dixon, P.	Harwell Laboratory, NDT Materials Characterization, England
Erwin, R.	Reactor Division, Bldg. 235, NIST, Gaithersburg, MD 20899, USA
Everitt, B.	Loamis Laboratory, 1110 West Green St., Urbane IL, 61801, USA
Figgis, B.	Institute of Chemistry, University of Aarhus, Denmark
Foss, M.	Institute for Physics & Astronomy, University of Aarhus, Denmark
Gammel, P.	AT&T Bell Laboratories, Murray Hill, NJ 07974, USA
Garamus, V.	Frank Laboratory of Neutron Physics, Joint Institute of Nuclear Reaction, Dubna, Russia

Gibbs, D. Brookhaven National Laboratory, Physics Department, USA
 Gimel, J.C. University of Uppsala, Sweden
 Hayden, S. H.H. Wills Physics Laboratory, University of Bristol, England
 Hayes, B. Clarendon Laboratory, University of Oxford, England
 Hendann, C. University of Essen, Germany
 Hill, R.I. Harwell Laboratory, AEA Technology, Didcot, England
 Hutchings, M. NDT Dept., Technical Services Div., AEA Technology, England
 Käll, M. Chalmers Tekniska Högskola, Sweden
 Kawano, S. Research Reactor Institute, Kyoto University, Japan
 Krebs, F. University of Aberdeen, England
 Lander, G. European Institute for Transuranium Elements, Germany
 Larsen, F.K. Institute of Chemistry, University of Aarhus, Denmark
 Lottemoser, L. Institut für Experimentalphysik, Universität Hamburg, Germany
 Malik, A. Institute of Applied Physics, ETH-Zürich, Switzerland
 Mason, T. Department of Physics, University of Toronto, Canada
 Matsugaki, N. School of Physics & Space Research, University of Birmingham, England
 McGreevy, R. Studsvik Neutron Research Laboratory, Uppsala University, Sweden
 Nielsen, K. Danmarks Tekniske Universitet, Denmark
 Nordén, B. Chalmers Tekniska Högskola, Sweden
 Pickavance, P. NDT Materials Characterisation, Harwell Laboratory, England
 Posselt, D. IMFUFA, Roskilde Universitets Center, Denmark
 Rainford, B. Physics Department, Southampton University, England
 Reich, D. Department of Physics & Astronomy, The Johns Hopkins University, USA
 Sackai, N. University of Toronto, Canada
 Samseth, J. Institutt for Energiteknik, Kjeller, Norway
 Scherrenberg, R. Structure & Morphology of Materials Section, PAC-MC, DSM Research,
 The Netherlands
 Schultz, M. Dept. of Chem. Eng. & Materials Sc., University of Minnesota, USA
 Schurtenberger, P. Institute of Polymers, ETH Zürich, Switzerland
 Sehlstedt, U. Chalmers Tekniska Högskola, Göteborg, Sweden
 Sinclair, R. Harwell Laboratory, AEA Technology, Didcot, England
 Sjöberg, B. Dept. of Medical Biochemistry, University of Göteborg, Sweden
 Smith, G. Los Alamos National Laboratory, New Mexico, USA
 Sowden, B.C. Harwell Laboratory, AEA Technology, Didcot, England
 Stuart, S. Department of Physics & Astronomy, The Johns Hopkins University,
 USA
 Svoboda, P., Charles University, Department of Metal Physics, Praha, Czech Republic
 Takahashi, M. Institut Curie, Université Paris-Sud, France
 Tepe, T. Dept. of Chem.Eng. & Material Sc., University of Minnesota, USA
 Uimin, G. Landau Inst. for Theoretical Physics, Russia
 Welz, D. Hahn-Meitner Institut, Berlin, Germany
 Windsor, C. NDT Dept., Technical Services Div., AEA Technology, England
 Wittung, P. Chalmers Tekniska Högskola, Göteborg, Sweden
 Yaron, U. AT&T Bell Laboratories, Murray Hill, NJ 07974, USA
 Zebger, I. Dept. of Physical Chemistry, University of Essen, Germany
 Zhao, J. Dept. of Chem.Eng. & Materials Sc., University of Minnesota, USA

4.3 Short Time Visitors under the CEC Large Installation Programme

Abetz, V.	Max-Planck-Inst.für Polymerforschung, Mainz, Germany
Achu, W.	Physics Department, University of Salford, England
Al-Kanani, H.	Physics Department, University of Salford, England
Amador, U.	Universidad Complutense, Dept. de Quimicas Inorganica I, Madrid, Spain
Azuah, R.	Department of Physics, Keele University, England
Bartels, V.	Max-Planck-Inst.für Polymerforschung, Mainz, Germany
Berbessou, D.	University of Bordeaux I, Talence, France
Booth, G.	Physics Department, University of Salford, England
Boothroyd, A.	Clarendon Laboratory, University of Oxford, England
Brecht, E.	TH Darmstadt, FB Materialwissenschaft, Germany
Bryn-Jacobsen, C.	Clarendon Laboratory, University of Oxford, England
Bull, M.	Birkbeck College, Physics Dept., London, England
Caciuffo, R.	European Institute for Transuranium Elements, Karlsruhe, Germany
Caruana, D.	Department of Biomedical Sciences, University of Malta, Msida, Malta
Castagna, J.C.	Institut Laue-Langevin, ILL, Grenoble, France
Chakkalaka, T.	Department of Physics, University of Warwick, England
Chang, L.-T.	Department of Physics, University of Warwick, England
Cipriani, F.	Institut Laue-Langevin, ILL, Grenoble, France
Cowley, R.	Clarendon Laboratory, Oxford University, England
Crevecoeur, R.	Delft University of Technology, Interfaculty Reactor Institute, The Netherlands
Cubitt, R.	School of Physics and Space Research, University of Birmingham, England
Currie, D.	Department of Chemistry, University of Southampton, England
da Costa, M.M.	University of Coimbra, Department of Physics, Portugal
de C. Paixão, J.	Dept. Fisica, Fac. Ciencias e Tecnologia, Universidade de Coimbra, Portugal
de Jeu, W.	Institut for Atomic and Molecular Physics, FOM, Amsterdam, Holland
de Wijn, H.	Faculty of Physics and Astronomy, University of Utrecht, The Netherlands
Fernandez, L.	Facultad de Ciencias, Universidad de Cantabria, Spain
Fitzpatrick, M.	Department of Materials Science and Metallurgy, University of Cambridge, England
Forgan, E.	School of Physics and Space Resarch, University of Birmingham, England
Frielinghaus, H.	Institut für Festkörperforschung, Forschungszentrum Jülich GmbH, Germany
Garcia-Hernandez, M.	Instituto de Estructura de la Materia, C.S.I.C, Madrid, Spain
Gazeau, D.	Laboratoire de diffusion des rayons X DRECAM, Saclay, France
Geselle, M.	TH Darmstadt, FB Materialwissenschaft Strukturforschung, Germany
Gibbs, M.	Department of Physics, Keele University, England
Goff, J.	Clarendon Laboratory, Oxford University, England
Gomez-Sal, J.	Facultad de Ciencias, Universidad de Cantabria, Spain

Gonçalves, A. Dept Física, Fac. Ciencias e Tecnologia, Universidade de Coimbra, Portugal

Gormezano, A. Department of Chemistry, University of Southampton, England

Gorria, P. Facultad de Ciencias, Universidad de Cantabria, Spain

Harris, M. Clarendon Laboratory, Oxford University, England

Hassan, A.K. University of Coimbra, Department of Physics, Portugal

Hayden, S. H.H. Wills Physics Laboratory, University of Bristol, England

Hutchings, M. AEA Technology, NDT Department, Harwell Laboratory, England

Janssen, S. Institut für Festkörperforschung, Forschungszentrum Jülich GmbH, Germany

Jehan, D. Clarendon Laboratory, Oxford University, England

Jerke, G. Institute of Polymers, ETH Zürich, Switzerland

Johnston, R. Universität Leipzig, Fakultät f. Physik und Geowissenschaften, Germany

Langridge, S. Department of Physics, Keele University, England

Lehmann, K. Universität Leipzig, Fakultät f. Physik und Geowissenschaften, Germany

Lehmann, M. Institut Laue-Langevin, ILL, Grenoble, France

Loewenhaupt, M. Institut für Festkörperforschung, Forschungszentrum Jülich GmbH, Germany

Longmore, A. Clarendon Laboratory, University of Oxford, England

López, F. University of Bordeaux I, Talence, France

Lösche, M. Universität Leipzig, Fakultät f. Physik und Geowissenschaften, Germany

McEwen, K. Birkbeck College, Physics Dept., London, England

Mischenko, N. Department of Chemistry B, University Leuven, Belgium

Mol, L. Institut for Atomic and Molecular Physics, FOM, Amsterdam, Holland

Mompeán, F. Instituto de Estructura de la Materia, C.S.I.C, Madrid, Spain

Morán, E. Universidad Complutense, Dept. de Químicas Inorganica I, Madrid, Spain

Müller, G. Institut für Festkörperforschung, Forschungszentrum Jülich GmbH, Germany

Müller, P. Institut für Anorg. Chemie, RWTH Aachen, Germany

Neville, A. Physics Department, Southampton University, England

Oettel, H. Institut für Meallkunde, TU Bergakademie Freiberg, Germany

Paolasini, L. European Institute for Transuranium Elements, EITU, Karlsruhe, Germany

Paul, D.M. Department of Physics, University of Warwick, England

Paul, S. Universität Leipzig, Fakultät f. Physik und Geowissenschaften, Germany

Pohl, J. Fakultät für Physik, LS Prof.Dr. E. Bucher, Universität Konstanz, Germany

Rainford, B. Physics Department, Southampton University, England

Reynders, K. Department of Chemistry B, University Leuven, Belgium

Rial López, C. Universidad Complutense, Dept. de Químicas Inorganica I, Madrid, Spain

Ribette, L. University of Bordeaux I, Talence, France

Roser, S. School of Chemistry, University of Bath, England

Schlottke, H. Max-Planck-Inst. für Polymerforschung, Mainz, Germany

Schmackers, T. Institut für Festkörperforschung, Forschungszentrum Jülich GmbH,
Germany

Schmahl, W. TH Darmstadt, FB Materialwissenschaft, Germany

Schmidt, S. Institut für Metallkunde, TU Bergakademie Freiberg, Germany

Schmitt, J. Universität Leipzig, Fakultät f. Physik und Geowissenschaften,
Germany

Schwahn, D. Institut für Festkörperforschung, Forschungszentrum Jülich GmbH,
Germany

Simpson, A. Clarendon Laboratory, Oxford University, England

Smorenburg, H. Delft University of Technology, Interfaculty Reactor Institute,
The Netherlands

Srinivasan, A. Instituto de Estructura de la Materia, C.S.I.C.,
Madrid, Spain

Stamm, M. Max-Planck-Inst.für Polymerforschung, Germany

Steigenberger, U. ISIS Science Division, Rutherford Appleton Laboratory, England

Stirling, W. Department of Physics, Keele University, England

Strauss, R. TH Darmstadt, FB Materialwissenschaft Strukturforchung,
Germany

Swaddling, P. Clarendon Laboratory, Oxford University, England

Valkonet, J. Faculty of Physics and Astronomy, University of Utrecht, Holland

Vogel, S. Freiberg Univ. of Mining and Technology, Inst. of Physical Metallurgy,
Germany

Watmough, M. Birkbeck College, Physics Dept., London, England

Watson, D. School of Physics and Space Research, University of Birmingham,
England

Weller, M. Department of Chemistry, University of Southampton, England

Wilkinson, C. Institut Laue-Langevin, ILL, Grenoble, France

Wilson, C. Institut Laue-Langevin, ILL, Grenoble, France

Winand, H. Department of Materials Science and Metallurgy, University of
Cambridge, England

Wingfield, J. School of Physics and Space Research, University of Birmingham,
England

Wylie, M. School of Physics and Space Research, University of Birmingham,
England

Zink, U. Institut f. Metallkunde, TU Clausthal, GKSS-Forschungszentrum
(Abt.W-TUC), Germany

Zinkin, M. Clarendon Laboratory, Oxford University, England

Title and author(s)

Annual Progress Report of the Department of Solid State Physics
1 January - 31 December 1994

edited by P.-A. Lindgård, K. Bechgaard, K. N. Clausen, R. Feidenhansl, and I. Johannsen

ISBN

87-550-2026-7

ISSN

0106-2840

0907-0249

Dept. or group

Department of Solid State Physics

Date

January 1995

Groups own reg. number(s)

Project/contract No.

Pages

162

Tables

3

Illustrations

116

References

181

Abstract (Max. 2000 char.)

Research in the department is concerned with "Materials with Distinct Physical and Chemical Properties". The principal activities of the department in the period from 1 January to 31 December, 1994, are presented in this Progress Report.

Neutron and x-ray diffraction techniques are used to study a wide variety of problems in condensed matter physics and include: two- and three-dimensional structures, magnetic ordering, heavy fermions, high T_c superconductivity, phase transitions in model systems, precipitation phenomena, and nano-scale structures in various materials. The research in chemistry includes chemical synthesis and physico-chemical investigation of small molecules and polymers, with emphasis on polymers with new optical properties, block copolymers, surface modified polymers, and supramolecular structures. Related to these problems there is work going on in theory, Monte Carlo simulations, and methods of data analysis.

Descriptors INIS/EDB

MAGNETISM; POLYMERS; PROGRESS REPORT; RESEARCH PROGRAMS; RISØ NATIONAL LABORATORY; SOLID STATE PHYSICS; SUPERCONDUCTIVITY

Available on request from:

Risø Library, Risø National Laboratory (Risø Bibliotek, Forskningscenter Risø)

P.O. Box 49, DK-4000 Roskilde, Denmark

Phone (+45) 46 77 46 77, ext. 4004/4005 · Telex 43 116 · Telefax (+45) 46 75 56 27

Some e-mail addresses and direct phone numbers of

The Department of Solid State Physics

Name	Phone no.	Fax no.	E-mail address
Almdal, Kristoffer	+45 4677 4785	+45 4675 5330	almdal@risoe.dk
Als-Nielsen, Jens	+45 4677 4745	+45 4237 0115	
Andersen, Niels Hessel	+45 4677 4711	+45 4237 0115	hessel@risoe.dk
Bechgaard, Klaus	+45 4677 4701	+45 4237 0115	fys-klbe@risoe.dk
Berg, Rolf Henrik	+45 4677 4782	+46 4675 5330	
Bouwman, Wim	+45 4677 4716	+45 4237 0115	bouwman@risoe.dk
Christensen, Morten Jagd	+45 4677 4712	+45 4237 0115	morten@fys-hp-1.risoe.dk
Clausen, Kurt N.	+45 4677 4704	+45 4237 0115	clausen@risoe.dk
Eskildsen, Morten Ring	+45 4677 4722	+45 4237 0115	eskild@risoe.dk
Feidenhans l. Robert	+45 4677 4708	+45 4237 0115	fys-rofe@risoe.dk
Gerstenberg, Michael C.	+45 4677 4741	+45 4237 0115	gerstenberg@risvxl.risoe.dk
Hadfield, Richard	+45 4677 4715	+45 4675 5330	rik@risoe.dk
Hvilsted, Soren	+45 4677 4784	+45 4675 5330	hvilsted@risoe.dk
Johannsen, Ib	+45 4677 4747	+45 4675 5330	ibj@risoe.dk
Jorgensen, Mikkel	+45 4677 4717	+45 4237 0115	fys-mijq@risoe.dk
Kjær, Kristian	+45 4677 4709	+45 4237 0115	kkjaer@risoe.dk
Landemark, Erik	+45 4677 4715	+45 4237 0115	fys-erla@risoe.dk
Lebech, Bente	+45 4677 4705	+45 4237 0115	lebech@risoe.dk
Lefmann, Kim	+45 4677 4741	+45 4237 0115	lefman@risoe.dk
Lindgård, Per-Anker	+45 4677 4706	+45 4237 0115	pal@risoe.dk
McMorrow, Des	+45 4677 4723	+45 4237 0115	memo:row@fys-hp-1.risoe.dk
Mortensen, Kell	+45 4677 4710	+45 4237 0115	mortensen@risoe.dk
Nielsen, Mourits	+45 4677 4703	+45 4237 0115	fys-moun@risoe.dk
Pedersen, Jan Skov	+45 4677 4718	+45 4675 5330	skov@risoe.dk
Pedersen, Marianne	+45 4677 4779	+45 4675 5330	
Pedersen, Walther Batsberg	+45 4677 4783	+45 4675 5330	
Petersen, Klaus	+45 4677 4771	+45 4237 0115	
Petersen, Thomas	+45 4677 4721	+45 4237 0115	petersen@risoe.dk
Smilgies, Detlef	+45 4677 4719	+45 4237 0115	fys-desm@risoe.dk
Sorensen, Steen Aagaard	+45 4677 4722	+45 4237 0115	sqrensen@risvxxq.risoe.dk
Vigild, Martin	+45 4677 4712	+45 4237 0115	martin.vigild@risoe.dk
Winther, Lars	+45 4677 4779	+45 4675 5330	



Objective

The objective of Riso's research is to provide industry and society with new potential in three main areas:

- *Energy technology and energy planning*
- *Environmental aspects of energy, industrial and plant production*
- *Materials and measuring techniques for industry*

As a special obligation Riso maintains and extends the knowledge required to advise the authorities on nuclear matters.

Research Profile

Riso's research is long-term and knowledge-oriented and directed toward areas where there are recognised needs for new solutions in Danish society. The programme areas are:

- *Combustion and gasification*
- *Wind energy*
- *Energy technologies for the future*
- *Energy planning*
- *Environmental aspects of energy and industrial production*
- *Environmental aspects of plant production*
- *Nuclear safety and radiation protection*
- *Materials with new physical and chemical properties*
- *Structural materials*
- *Optical measurement techniques and information processing*

Transfer of Knowledge

The results of Riso's research are transferred to industry and authorities through:

- *Research co-operation*
- *Co-operation in R&D consortia*
- *R&D clubs and exchange of researchers*
- *Centre for Advanced Technology*
- *Patenting and licencing activities*

To the scientific world through:

- *Publication activities*
- *Co-operation in national and international networks*
- *PhD- and Post Doc. education*

Riso-R-779(EN)
ISBN 87-550-2026-7
ISSN 0106-2840
ISSN 0907-0249

Available on request from:
Riso Library
Riso National Laboratory
PO. Box 49, DK-4000 Roskilde, Denmark
Phone +45 46 77 46 77, ext. 4004/4005
Telex 43116, Fax +45 46 75 56 27

Key Figures

Riso has a staff of just over 900, of which more than 300 are scientists and 80 are PhD and Post Doc. students. Riso's 1995 budget totals DKK 476m, of which 45% come from research programmes and commercial contracts, while the remainder is covered by government appropriations.